Durham E-Theses

Vibrational Spectroscopic Studies on the Model Lubricant 2-Ethvlhexvl Benzoate TEHB)

Whitley, Andrew

How to cite:

Whitley, Andrew (1990) *Vibrational Spectroscopic Studies on the Model Lubricant 2-Ethvlhexvl Benzoate TEHB)*, Durham theses, Durham University. Available at Durham E-Theses Online: http://etheses.dur.ac.uk/6252/

Use policy

Vibrational Spectroscopic Studies on the Model Lubricant 2-Ethylhexyl Benzoate (EHB)

by

Andrew Whitley B.Sc. (Hons) Dunelm

A thesis submitted to the University of Durham
for the degree of Doctor of Philosophy

June 1990

DECLARATION

The work described in this thesis was carried out by me in the Chemistry Department of the University of Durham, between October 1986 and June 1990. I declare that this work has not been accepted in substance for any degree, and is not being concurrently submitted in candidature for any other degree. The work is original except where indicated by reference.

Dated   12/06/90

FOR SUE AND MY PARENTS

ACKNOWLEDGEMENTS

ABSTRACT

In an attempt to investigate the relationship between microscopic and macroscopic fluid properties, like viscosity and density, a vibrational spectroscopic study of the model lubricant 2-ethylhexyl benzoate (EHB) was initiated. The variation in frequencies and band shapes of the vibrational modes of the molecule have been studied as a function of concentration, temperature and pressure.

Estimates of correlation times for the reorientational motion of the phenyl ring of EHB, as a function of temperature, have been made from measurements of the Raman bands of the ring v(C-C) deformation mode and ^{13}C N.M.R. spin lattice relaxation times. It has been shown using this data that the viscosity/temperature behaviour of EHB is dependent on the reorientational as opposed to the translational motion of the molecule.

A noncoincidence of the Raman isotropic and anisotropic bands of the v(C=O) stretching mode of EHB has been seen and explained in terms of a resonance energy transfer (RET) process via transition dipole-transition dipole interactions, most probably as a consequence of preferential alignment via dipole-dipole interactions. It appears from dilution experiments that the EHB molecules do not become completely separated until below 2% mole-fraction.

The infrared band of the v(C=O) stretching mode of EHB shows an unusual red shift with increased pressure to 6.5kbar, followed by a blue shift as the pressure is further increased. This has been explained as due to the competing effects of increased alignment of carbonyl dipoles (red shift) and the increase in the repulsive interactions (blue shift). All the other bands exhibit blue shifts, of varying degree, with increased pressure, showing that the repulsive forces dominate the shifts. The spectral changes are consistent with chain extension and increased interchain interactions with increased pressure. The band widths of all the vibrational modes increase with pressure consistent with an increase in vibrational relaxation rate. The fluid appears to exhibit a phase change close to 6.5kbar.

CONTENTS

<u>SECTION II - RESULTS</u>

CHAPTER 4:   RESULTS OF INFRARED HIGH PRESSURE STUDIES   115

CHAPTER 5:   RESULTS OF VARIABLE TEMPERATURE STUDIES   139

SECTION III - INTERPRETATION

CHAPTER 7: PHENOMENOLOGICAL APPROACHES TO INTERPRETING
           EXPERIMENTAL DATA OBTAINED ON EHB   186

SECTION I

CHAPTER 1: INTRODUCTION

CHAPTER 2: VIBRATIONAL SPECTROSCOPY AND MOLECULAR
DYNAMICS IN LIQUIDS

CHAPTER 3: EXPERIMENTAL

CHAPTER 1

INTRODUCTION

1.0 Introduction

The work discussed in this Thesis is part of a project
coordinated and sponsored by Shell Research U.K. designed to
study the relationship between molecular structure and bulk
fluid physical properties, in particularly viscosity and
density. The overall objective is to enable knowledge
gained from this and other similar projects to be used to
design superior lubricants.

The lubrication of machinery in which contacting
surfaces move relative to one another is an essential
ingredient to the efficient operation of any such machine.
This includes the lubrication of plane, journal, rolling or
pivot bearings, gear wheels and pistons.

The primary functions of a lubricant are to reduce
friction and thereby increase mechanical efficiency and
decrease wear of the surfaces. The lubricant also has
secondary functions to perform. It dissipates heat which is
evolved by the moving surfaces, and it carries away any wear
particles or impurities which may otherwise have increased
the wear on the surfaces. Lubrication is generally achieved
by the formation of a film between the mutually opposed
surfaces of the machine. This film bears the load and shear
generated by the surfaces and reduces the friction to a
minimum. The lubricant must possess a long lifetime, it
should not rapidly degrade under the operating conditions,
and it should not corrode any part of the machinery it comes
in to contact with. The suitability of a lubricant depends
upon the viscosity and the response of the viscosity to the
conditions encountered during lubrication, that is, high

2

pressures and temperatures and variable shear rates.

Originally lubricants were tested on their bulk fluid responses alone. Bulk properties such as viscosity and density were measured as a function of temperature, pressure and shear rate. Better lubricants were found on a more or less trial and error basis, by following trends in families of suitable lubricant compounds[1]. The practical significance of viscosity temperature behaviour was recognized many years ago, and numerous viscosity temperature relationships have been advanced[2,3]. It was not until the last two decades that the importance of the viscosity/pressure relationship was appreciated. Expressions to describe the relationship were then more fully proposed[4]. However, until recently[5], these temperature/pressure viscosity expressions offered little hope of predicting a fluids viscosity response, or suggesting ways of modifying a fluid to give it a more desired lubrication performance.

The performance of a lubricant must ultimately depend on the molecular properties of the fluid. The flexibility, size and shape of a lubricant molecule and the interactions with the surrouding molecules determines the bulk fluid properties[3]. As far back as the 1930's attempts were made to connect viscosity with "chemical constitution" and derive theoretical expressions for the viscosity of liquids in terms of the internal structure and thermodynamic properties[1,3]. These tend to be unreliable and still fail to explain fully the dependence of viscosity on true molecular properties such as rotations, translations, interactions, flexibility, size and shape.

More recently various techniques which allow the probing of molecular properties have been used to help discover how these properties control bulk fluid responses as a function of pressure, temperature and shear rate. The techniques used fall into two main categories molecular modelling[6,7] and spectroscopic techniques[8]. Analysis using these methods allows a detailed probing of the molecular dynamics and interactions in the fluid. If this is coupled with measurements of bulk fluid physical properties attempts can be made to qualitatively relate molecular composition to the physical properties of the fluid. This should then indicate which parts of the molecule could be altered to change the molecular and thus macroscopic properties of the fluid. With this knowledge better lubricants can be designed, with physical properties closer to the ideal.

The work in this thesis is concerned with the study of molecular dynamics and interactions of fluids, specifically the model lubricant 2-ethylhexyl benzoate (EHB), shown in Fig.1.1, using the vibrational spectroscopic techniques, Raman and infrared. It also includes the analysis of some of the NMR work carried out on EHB at the University of Illinois as part of this Shell project. There has previously been very little attempt to study the molecular behaviour of lubricant fluids, the bulk of the work and our understanding is limited to small rigid species CH_4, CCl_4, C_6H_6, CH_3I, etc. There are clear reasons to expect very different behaviour for the higher densities accessible with the larger molecules typical of lubricants. The inherent flexibility of most lubricant components also gives them differing dynamic behaviour to the small rigid molecules.

4
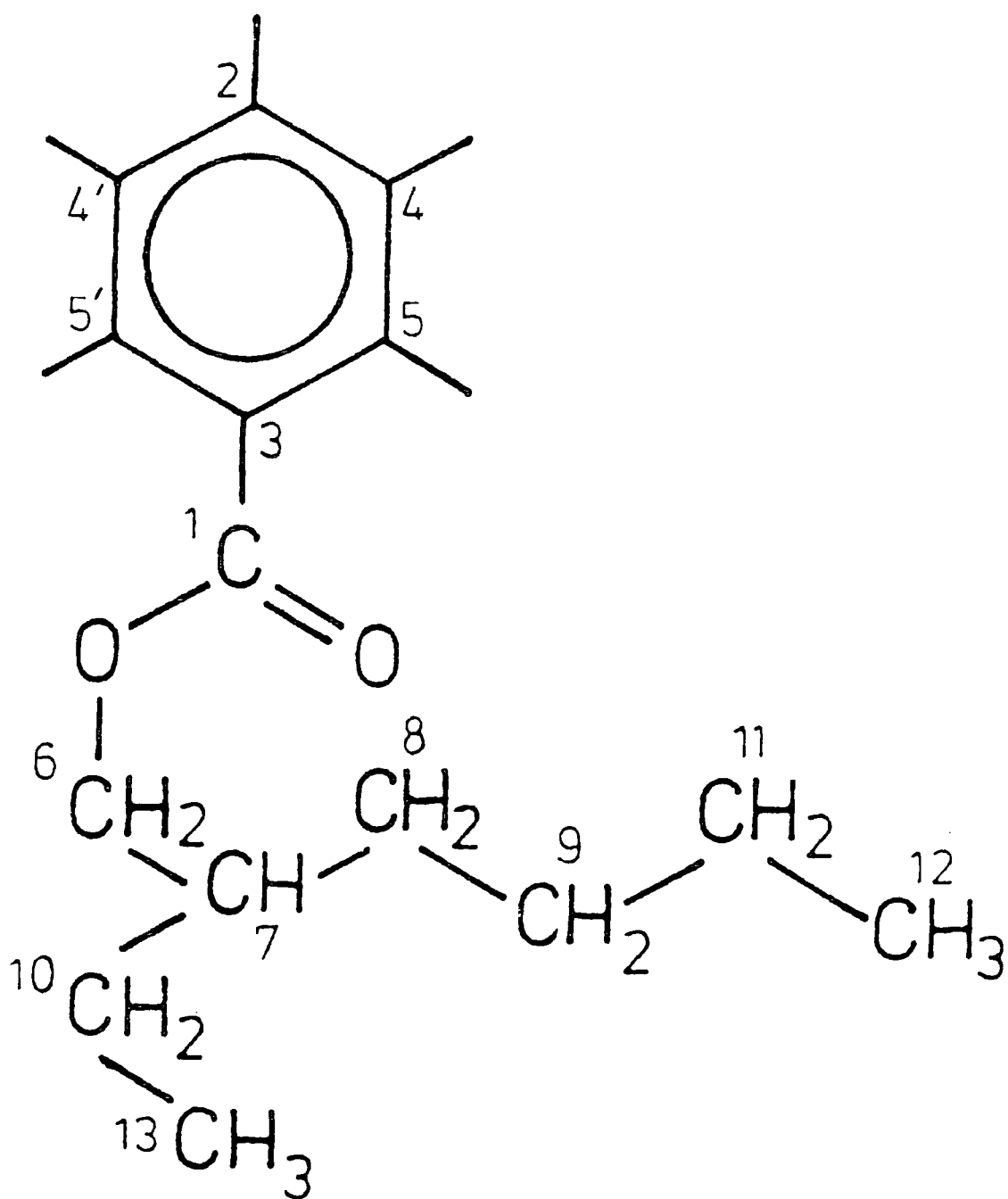
Figure 1.1. The 2-ethylhexyl benzoate (EHB) molecule

1.1 Lubrication

The mechanisms by which lubrication occurs fall into four main categories, hydrodynamic, elastohydrodynamic boundary and extreme pressure lubrication. Each mechanism is distinct, that is they rely on the properties of the lubricant and surfaces to different extents.

1.1.1 Hydrodynamic lubrication

The mechanism of hydrodynamic lubrication relies on the moving surfaces being completely separated by the lubricant. In order for this to occur the surfaces must be moving ("dynamic") relative to one another, the liquid ("hydro") separating them must be viscous and the motion of the surfaces over one another must produce a convergent wedge of fluid. Due to this convergence the inlet region is larger than the outlet and as a result there is an increase in velocity of flow as the liquid passes through the narrowing constriction. Due to the viscosity of the liquid there is a build up of pressure in the wedge of fluid and this, under favorable conditions, is sufficient to keep the surfaces completely separated[9]. An example of hydrodynamic lubrication occurs in journal bearings, Fig.1.2 demonstrates a journal bearing and the build up of pressure close to the contact.

In hydrodynamic lubrication the whole of the friction arises from shearing the lubricant film, so it is determined by the viscosity of the lubricant. The less viscous the

lubricant the lower the friction. There is, however, another factor which places a limit to the lowest viscosity permissible, that is the distance of nearest approach. This distance gets smaller the higher the load on the bearing, the higher the speed or the lower the viscosity. If the viscosity of the lubricant is too low the distance may become smaller than the height of the surface irregularities, the film may then be penetrated with a consequent increase in friction and wear.
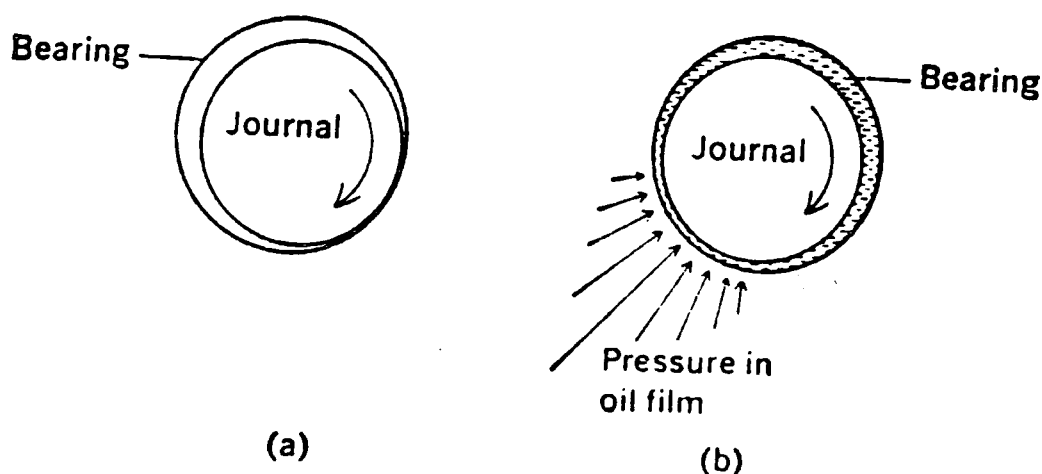
Figure 1.2. Example of hydrodynamic lubrication in a journal bearing. Journal or shaft rotating clockwise in a bearing. (a) Unlubricated, the shaft climbs up to the right. (b) In the presence of a suitable lubricant the shaft moves to the left and drags a wedge of oil with it. Under ideal hydrodynamic conditions the oil pressure can support the load and all the friction arises from the viscous resistance of the oil. Reproduced, by permission, from reference 9 .

The great advantage of hydrodynamic lubrication is that the friction can be very low and in the ideal case there is no wear on the moving parts. The surfaces must be smooth and well aligned, the two surfaces should conform well so that the contacting load is carried over a relatively large area. Allowance should be made for the frictional work heating the lubricant and thus reducing the viscosity. This results in a reduced lubricant thickness, with a danger of oil penetration, upon increased running time. There are two ways of coping with this if it becomes a problem. One is to have a large supply of oil which is continually circulated and cooled in the oil reservoir. The other is to use special additives, known as viscosity index improvers (VII's), these are usually polymers (molecular weights about 200,000) which are added to the lubricant in small amounts (1-5%), VII's make the viscosity, through interaction with the lubricant molecules, far less temperature sensitive.

1.1.2 Elastohydrodynamic lubrication

Elastohydrodynamic (EHD) lubrication occurs when the surfaces do not conform well to one another, so the load is concentrated into a small contact area. Under these circumstances the operating pressures at the point of contact can reach up to 100's of times (up to 40kbar) that in hydrodynamic lubrication. Examples of such EHD systems are ball bearings and mating gears.

Under EHD conditions it would seem that the relatively low hydrodynamic pressures generated in the converging

region are unlikely to be able to separate the surfaces in the high pressure region of the contact, otherwise known as the Hertzian zone. However EHD lubrication works because under this extreme pressure the fluid film becomes extremely thin ($\simeq 10^{-6}$m) and it's viscosity is increased by several orders of magnitude[9].

As the fluid flows into the converging surfaces of the inlet region a reduction in velocity occurs creating hydrodynamic pressure. At the leading edge of the Hertzian region this hydrodynamic pressure is sufficient to separate the two surfaces. Once this is achieved the fluid cannot escape from the Hertzian region, as the viscosity is too great and the film too thin for escape of the fluid in the short time in which the surfaces pass through the contact. The fluid entering the contact becomes trapped between the surfaces, and at the high pressures in the Hertzian region, behaves like a solid separating layer. This layer prevents any surface-surface contact. The friction involved with the extreme pressure in EHD lubrication can be up to a hundred times greater than in hydrodynamic lubrication. Even so, this is still considerably less than if the contacts were unlubricated. This type of lubrication is known as elasto-hydrodynamic as in the Hertzian region the extreme pressures developed in the fluid cause the surfaces to deform elastically. Unlike with hydrodynamic lubrication EHD lubrication is dependent on the properties of both the fluid and the surface material.

The fluid pressure profile in EHD lubrication is shown in Fig.1.3, the presence of a pressure spike at the trailing edge is a result of secondary elastic deformation of the

contact which forms a lip in order to constrict the outflow
of fluid from the contact zone and maintain continuity of
flow across the system.

As in hydrodynamic lubrication, it is of vital
importance in EHD lubrication that the film thickness in the
contact zone is greater than the height of the surface
asperities. This is much more of a problem with EHD
lubrication due to the high pressure and thin films
involved. If the film is not thick enough increased
friction and wear will occur as the asperities run into each
other. If EHD lubrication is to be exploited successfully
it requires that the surfaces are very smooth and carefully
aligned.
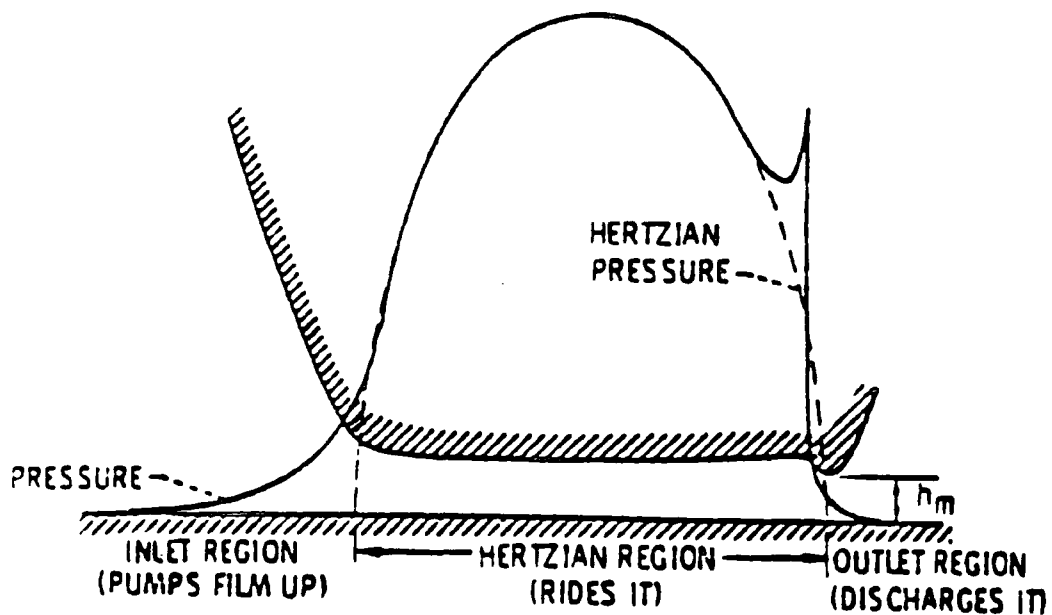
Figure 1.3. Elastohydrodynamic pressure profile.
Reproduced, by permission, from reference 9 .

10

The success of EHD lubrication depends heavily on the film thickness. It has been shown[9] that film thickness depends primarily on the mean relative velocity of the contacting surfaces, the lubricant viscosity and the pressure viscosity coefficient. Increase in any of these parameters results in increasing the film thickness.

The effect of pressure on viscosity is counteracted to some extent by a decrease in viscosity due to local heating which is a result of the friction inherent in all EHD contacts. This effect is usually more of a problem with EHD lubrication than hydrodynamic lubrication due to greater friction and thinner films involved. It can in extreme situations cause a breakdown in effective EHD lubrication, in some cases temperatures can reach 473K or higher. This problem can be lessened as with hydrodynamic lubrication by incorporating VII polymers into the lubricant. Generally it is the pressure/viscosity relationship that dominates the picture.

Obviously an understanding of what controls fluid viscosity and the pressure and temperature dependence, at molecular level, is of vital importance to help design better EHD lubricants. The strategy is to probe the molecular properties which determine the viscosity temperature and pressure relationships for a range of fluids. Armed with this knowledge molecular structures that minimise the viscosity/temperature coefficient, and at the same time optimise the viscosity/pressure behaviour, can be proposed and physically tested. The work in this thesis is part of such a strategy, the study is mainly concerned with the effect of conditions appropriate to EHD lubrication.

1.1.3 Boundary lubrication

If the pressures are too high, the running speeds too low or the surface roughness too great, "penetration" of the lubricant film will occur. Contact will take place between the asperities, the friction will rise and wear will take place. If conditions are severe the lubricant breakdown will become so bad that the system scores or seizes and the system can no longer operate successfully. The viability of the lubricant can be extended by incorporating small quantities (less than 1%) of active organic compounds in to the fluid. These additives do not effect the viscosity of the lubricant, they function because they form surface films which are strongly attached to the metal surfaces. Although they are generally only one or two molecules thick, these films are able to prevent metal to metal contact, this type of lubrication is known as boundary lubrication.

It is found that the best boundary lubricants are long chain hydrocarbons with active end groups, typically an alcohol, an amine or a fatty acid. Representative molecules of this type are shown in Fig.1.4. When such a material, dissolved in the lubricant, meets a metal or other solid surface the active end group attaches itself to the material and gradually builds up a surface layer, it becomes physisorbed, as is shown in Fig.1.4. The film is strongly attached to the surface. In addition because the attraction between the chains is very strong it is difficult to penetrate the film. If two surfaces covered with such a film come into contact they tend to slide over their outermost faces, and the friction is reduced. Some

12

penetration may occur but it is far less than would occur if only the fluid were present on the surface.

Boundary lubrication is a purely physical phenomenon where the adsorption process is thermodynamically reversible with respect to surfactant concentration and temperature. As the temperature is increased the strength of the surface attachment is weakened and the rate of pickup/transfer of surfactant increases. As this happens a marked increase in friction and surface damage occurs. The best boundary lubricants cease to be effective above 200 - 250°C.
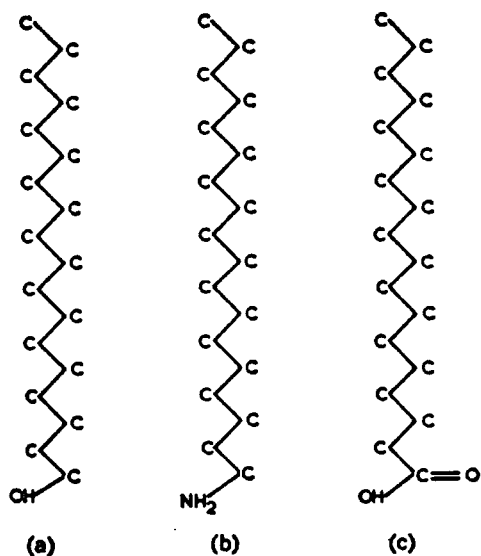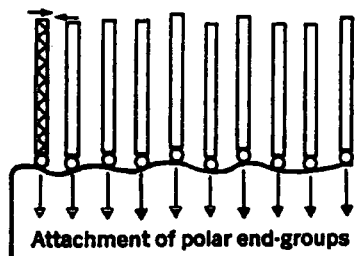
Figure 1.4. Boundary lubrication: the molecules consist of a long backbone of carbon atoms with an active polar end group. With alcohols (a) the polar group is OH, with amines (b) it is NH2 and with (c) fatty acids it is COOH. The polar groups attach themselves to the surface. Reproduced, by permission, from reference 10 .

1.1.4 Extreme pressure lubrication

If machines are to operate under severe conditions where boundary lubrication breaks down other types of lubrication are required. These are called extreme pressure (EP) lubricants, they are in some ways similar to boundary lubricants but operate under different conditions. The name EP lubrication is a slight misnomer as it is not the pressure, but the temperature reached between the sliding surfaces that controls EP lubrication.

The EP additive is present in the fluid in only a small amount (less than 1%), the commonest additives used for this purpose contain phosphorous, chlorine or sulphur. They function by reacting with the metal surface, the molecules become chemisorbed, to form a surface film which prevents metal to metal contact. The EP additives usually only react at high temperatures, they are incorporated with boundary lubricants in the fluid, so that at high temperature, when boundary lubricant desorption rate is high, the EP additive reacts with suitable surface sites that have become uncovered. This ensures protection even under high temperature conditions. The behaviour is shown schematically in Fig.1.5, the coefficient of friction is plotted against temperature. Curve I is for paraffin oil (base oil) and shows that the friction is initially high and increases as the temperature becomes raised. Curve II is for fatty acid dissolved in base oil, it becomes physisorbed on the surface to provide good lubrication from room temperature up to the temperature at which desorption becomes dominant. Curve III is for is for a typical EP

additive dissolved in the base oil, this reacts very slowly at temperatures below T_r so that in this range the lubrication is poor, while above T_r the protective film is formed and effective lubrication is provided up to a very high temperature. Curve IV is the result obtained when both fatty acid and EP additive are present in the base oil, good lubrication is provided by the fatty acid below T_r while above this temperature the greater part of the lubrication is provided by the EP additive. At still higher temperatures a deterioration in lubricating properties will also occur for both curves III and IV.
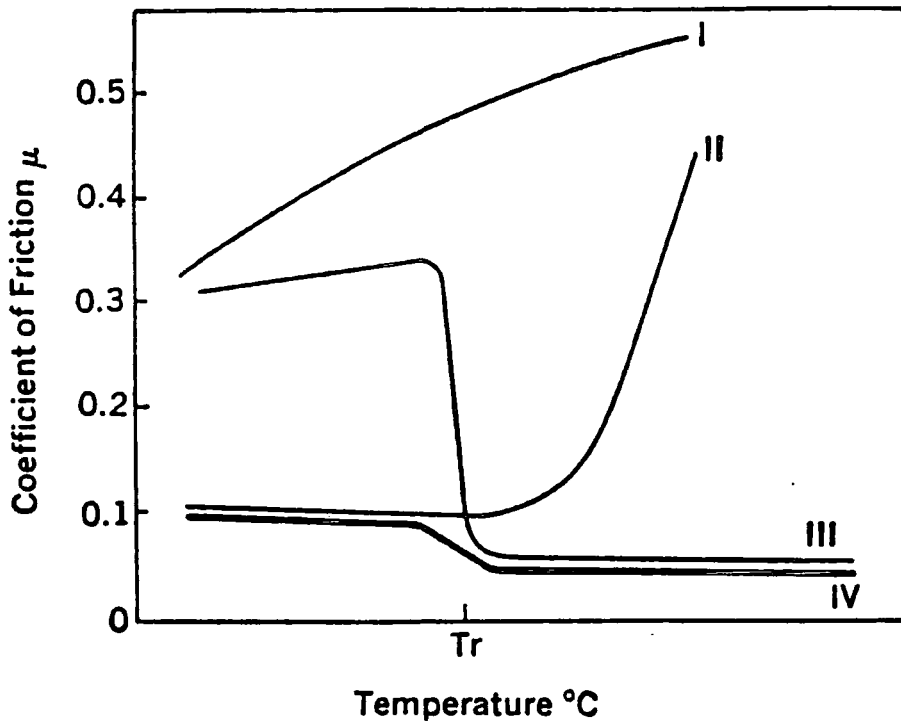
Figure 1.5. Graph showing in a schematic way the frictional behaviour of metal surfaces in the presence of various types of lubricant. Reproduced, by permission, from reference 10 .

15

1.2 Viscosity and the relationship with temperature and pressure

For most applications the ideal lubricant would be one with a large pressure-viscosity coefficient, but a small temperature-viscosity coefficient. This means that the viscosity should increase markedly with pressure but should not decrease very much with an increase of temperature. Unfortunately the experimental evidence[11] suggests that there is an overall broad correlation between pressure and temperature-viscosity coefficients for all liquids. This is demonstrated by Fig.1.6, the large "cross" indicates the kind of behaviour that is desirable. This correlation imposes limits on the scope for design of the ideal lubricant. However within Fig.1.6 there is sufficient scatter to suggest that the goal of optimum combination of high pressure-viscosity and low temperature-viscosity coefficients is worth pursuing, with a factor of at least 3 separating the highest pressure to temperature-viscosity coefficient ratio from the lowest. The position of a lubricant in the correlation of Fig.1.6 is dependent upon the molecular structure. A better understanding of this dependence is what this project and similar projects are trying to achieve.
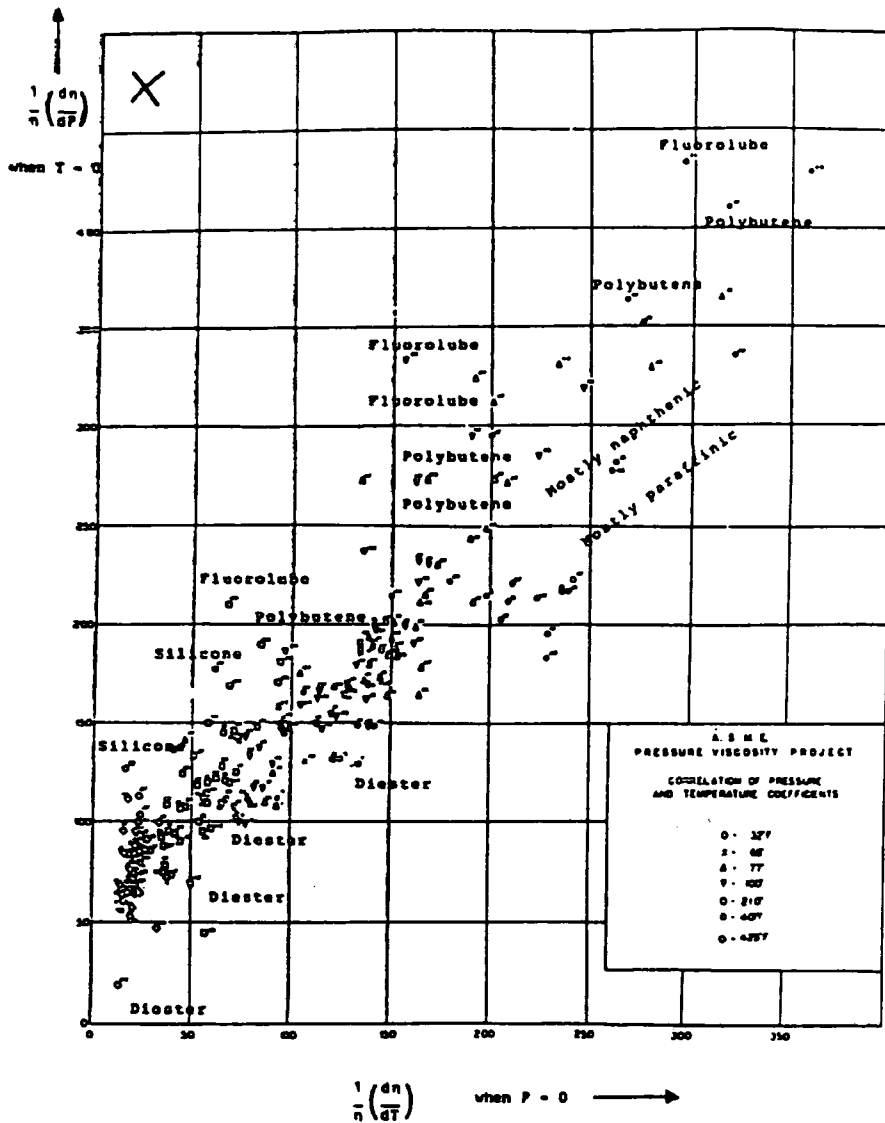
Figure 1.6. Correlation of viscosity-pressure behaviour with viscosity-temperature behaviour. The large cross is the desired response for the ideal lubricant. Reproduced, by permission, from reference 11 .

17

1.2.1 Viscosity

Imagine a body of fluid contained between two parallel surfaces, see Fig.1.7, the viscosity of the fluid can be considered to be the resistance of the fluid molecules to flow past one another. Viscosity is therefore a consequence of the intermolecular interactions in the fluid. If the two surfaces move relative to one another, with a relative velocity U, the surfaces will be subjected to tangential forces f for each unit area of contact, due to the viscosity of the liquid. It is these forces which allow hydrodynamic and EHD lubrication. The size of this force is dependent on the viscosity and the shear rate. The shear rate is equal to the relative surface velocity U divided by the film thickness. The force per unit area is known as the shear stress. At low pressures the fluid is Newtonian, the viscosity varies exponentially with pressure and temperature, the shear stress in these conditions can be shown to be[12]

$$f = \eta.(U/h) \qquad\qquad \text{Eqn.1.1}$$

and so viscosity is equal to the shear stress divided by the shear rate, with the dimensions $ML^{-1}T^{-1}$.

Under the conditions of elastohydrodynamic lubrication the high pressure causes the stress/shear rate relationship to breakdown. This occurs when the shear stress reaches a critical value of f_0, either due to increased viscosity and decrease in h, at high pressure, or because of a high shear rate. Johnson and Evans[13] have observed four distinct

regimes of rheological behaviour of typical lubricants. with
increasing pressure. under conditions of EHD lubrication.
They have shown that the behaviour in each regime can be
modeled in terms of four equations containing the fluid
parameters of viscosity. shear stress and shear strain.
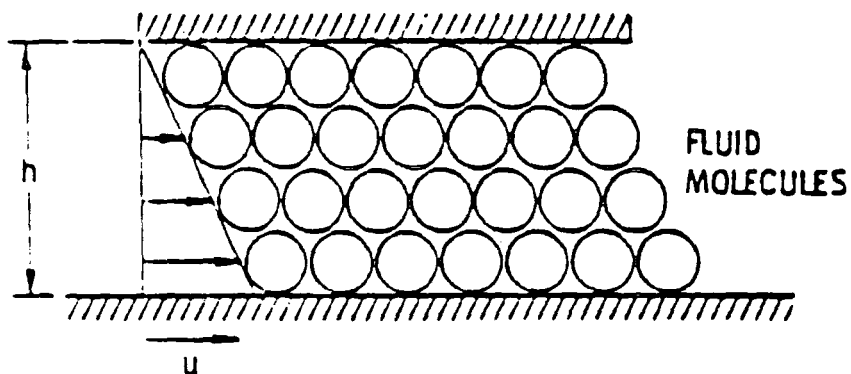
Figure 1.7. Viscous flow between parallel surfaces.
Reproduced, by permission, from reference 9 .

1.2.2 Measurement of the viscosity of fluids

The measurement of the viscosity of fluids is usually made using methods which employ Poiseuille's laws of viscous flow of fluids[12]. For example the time it takes for a known mass of fluid to pass through a set length of capillary tubing is measured. The other absolute methods employ Stoke's laws for the motion of a sphere in a viscous fluid[12]. For example the time it takes for a sphere or needle to fall under gravity a set distance in the fluid is measured. There are also secondary viscometers which require calibrating using the results of the first two methods, i.e. using fluids of known viscosity, these are usually easier to use but involve more severe errors[12].

The measurement of viscosity as a function of shear or temperature are relatively easy to make, for conditions representative of EHD lubrication. Measurements of the effect of pressure on viscocity is not easily made for pressures representative of EHD conditions. The reason for this is that the inherent high viscosity occurring under such high pressures hinders the method of measurement[14].

1.2.3 Viscosity-temperature equations

There have been a considerable number of viscosity temperature laws proposed for lubricating oils since the publication of work by Reynolds, in the late 1800's, on olive oil[15]. He showed, empirically, that viscosity can be described in terms of

$$\eta = R.e^{-\alpha T} \qquad \text{Eqn.1.2}$$

where R and α are constants. However this is only valid over a very limited temperature range, when the viscosity variation must also be small. The most accurate equation of the many[2] proposed to describe the variation of viscosity with temperature has been shown to be Vogel's equation. This is a three constant formula

$$\eta = K.e^{b/(T+\theta)} \qquad \text{Eqn.1.3}$$

each constant has a definite physical significance. The exponential term is dimensionless, so K is related to the fluid viscosity and has the units of viscosity. The parameter b has the units of temperature and expresses the inherent viscosity-temperature variation of the fluid. The constant θ expresses the temperature at which the oil would have infinite viscosity if it did not freeze to a solid, since when T equals $-\theta$ the term $e^{b/(T+\theta)}$ becomes infinite. In order to use the Vogel equation the three constants have to be found and for this the viscosity has to be known at three temperatures. The equation does not have any real

predictive value about it until some measurement of the
viscosity has been made.

None of the above viscosity temperature equations have
proven satisfactory over extended ranges of temperature for
all types of fluid. This is not surprising as temperature
is probably not a primary variable upon which viscosity of
liquids depends. It is more likely that viscosity varies in
a regular manner with other liquid properties, like density
or free volume available to a molecule (See 1.2.4 and
1.2.5), such properties are effected in a more obscure way
by changes in temperature.

1.2.4 Viscosity analysed using a flow-rate model

Eyring and his co-workers supposed that as the flow of
a liquid is a rate process the theory of absolute reaction
rates could be applied to the problem of viscosity[16]. The
moving of a molecule from one equilibrium position to the
next is regarded as equivalent to the passage of the system
over a potential energy barrier. Such movement from one
position of a molecule to another requires the expenditure
of energy since work must be done in pushing back other
molecules, this energy is dependent on the viscosity.

Combining the theories of viscosity (section 1.2.1) and
reaction rates they proposed that viscosity could be
expressed in terms of $\Delta F^{\ddagger}$ the standard free energy of
activation per mole, the molar volume V, Avagadro's number
N, the gas constant R, Planck's constant h and temperature T

$$\eta = (hN/V).e^{\Delta F^{\ddagger}/RT} \qquad\qquad \text{Eqn.1.4}$$

Since $\Delta F^{\ddagger}$ can be replaced by $\Delta H^{\ddagger} - T\Delta S^{\ddagger}$, where $\Delta H^{\ddagger}$ is the standard enthalpy of activation and $\Delta S^{\ddagger}$ is the standard entropy of activation Eqn.1.4 becomes

$$\eta = [(hN/V).e^{-\Delta S^{\ddagger}/R}].e^{\Delta H^{\ddagger}/RT} \qquad\qquad \text{Eqn.1.5}$$

Since the molar volume of a liquid does not vary greatly with the temperature, and $\Delta S^{\ddagger}$ being taken as a constant[16], Eqn.1.5 takes the form

$$\eta = B.e^{E_{vis}/RT} \qquad\qquad \text{Eqn.1.6}$$

E_{vis} is the activation energy per mole for viscous flow. This relationship had previously been suggested empirically by both Arrhenius[17] and by Reynolds[15]. What exactly E_{vis} measures at the molecular level cannot be certain without probing of the molecular interactions over the same temperature range that the viscosity is measured.

This model works for many liquids and has been widely used to describe the behaviour of lower molecular weight liquids[18,19]. However, it is not satisfactory for many other liquids except perhaps at high temperature and low pressures. The break-down of the model is possibly a consequence of the molecules moving in sections rather than as a whole, as the chain lengths increase, and also as the molecules increase in size they cannot be treated as single units, as they become more associated due to entanglements.

The association could also be due to attractive interactions like hydrogen-bonding. In these cases it may not be possible to describe the motion of the molecules by a simple flow rate model.

1.2.5 Viscosity and free volume

Various early workers attempted to establish a relationship between viscosity and free volume. Fox and Florey[20] introduced the concept that the molecular mobility at low temperatures depends mainly on the free volume (v_f). They proposed that the probability of a molecular jump is governed by the probability that sufficient free volume is available in the region surrounding the molecule, thereby providing the space into which the molecule can move, rather than by the rate at which a molecule can overcome an energy barrier.

Doolittle[21] was the first to develop an empirical free volume equation which accurately represents precise viscosity measurements over a wide temperature range. This is expressed by Eqn.1.7,

$$\ln(\eta) \; = \; A \; + \; B(v_o/v_f) \qquad\qquad \text{Eqn.1.7}$$

where v_o was defined as the limiting specific volume of the liquid at 0 K, A and B are constants and v_f is the free volume per gram of liquid.

Fulcher[22], and Tammann and Hess[23] constructed an empirical equation to describe the temperature dependence of

$$\ln(\eta) = A' + B'/(T-T_0) \qquad\qquad \text{Eqn.1.8}$$

where A' and B' are constants and T_0 is a constant which indicates the temperature at which the viscosity of a liquid would be infinite. Barlow and co-workers[24] pointed out that Eqn.1.7 and 1.8 are identical for liquids whose density varies linearly with temperature, as has seen to be the case for most liquids. They referred to Eqn.1.8 as the modified free volume equation. T_0 is said to be the temperature at which free volume disappears ($v_f=0$), it has been stated that T_0 defines a thermodynamic transition of fundamental importance to the liquid phase[24].

Barlow et al[24] came to a number of conclusions following extensive work studying the viscosity of a number of hydrocarbon liquids. They concluded that at temperatures which are sufficiently high for a liquid to have more than 10 to 16% free volume, the Arrhenius equation adequately describes the temperature dependence of the liquid. The viscosity of the liquid is dependent principally on the energy required to jump from one site in a liquid to another. At lower temperatures the decrease in free volume means that the available free volume is the chief factor determining viscous flow. Under these circumstances the modified free volume equation (Eqn.1.8) accurately describes the temperature and pressure dependence of the viscosity.

1.2.6 Viscosity-pressure equations

As long ago as 1893 Barus[25] proposed the following formula describing the isothermal viscosity-pressure dependence of liquids

$$\ln(\eta/\eta_0) = \alpha.p \qquad\qquad \text{Eqn.1.9}$$

where η is the viscosity of the liquid at a pressure p, η_0 is the viscosity at atmospheric pressure and α is the viscosity-pressure coefficient which is characteristic of the fluid. The larger the value of α the greater the dependence of viscosity on pressure. The value of α is dependent on the temperature of the fluid.

The Barus equation is only valid to a reasonable approximation at low pressures and over a moderate pressure range. In fact, although according to the equation, plotting $\log(\eta)$ against pressure, for a fluid at constant temperature, should give a straight line, this is generally not the case. The plots are perceptively curved, usually concave towards the pressure axis, see Fig.1.8, in a few cases they curve away from the pressure axis. At very high pressures 5,000 to 20,000 bars the plots which are initially straight or concave show a point of inflection such that they become convex[26,27]. Attempts to find more satisfactory expressions to describe this pressure-viscosity relationship of fluids have been made. One example is

$$\eta = \eta_0 (1 + C.p)^n \qquad \qquad \text{Eqn.1.10}$$

where n and C are constants with values that depend on the class of fluid being considered. This and other relationships[3,26] give a better viscosity-pressure correlation, but as with the viscosity-temperature equations are only satisfactory over a limited range and cannot be successfully applied to all families of fluids. This is because. as with temperature, pressure is not a primary variable upon which viscosity depends.
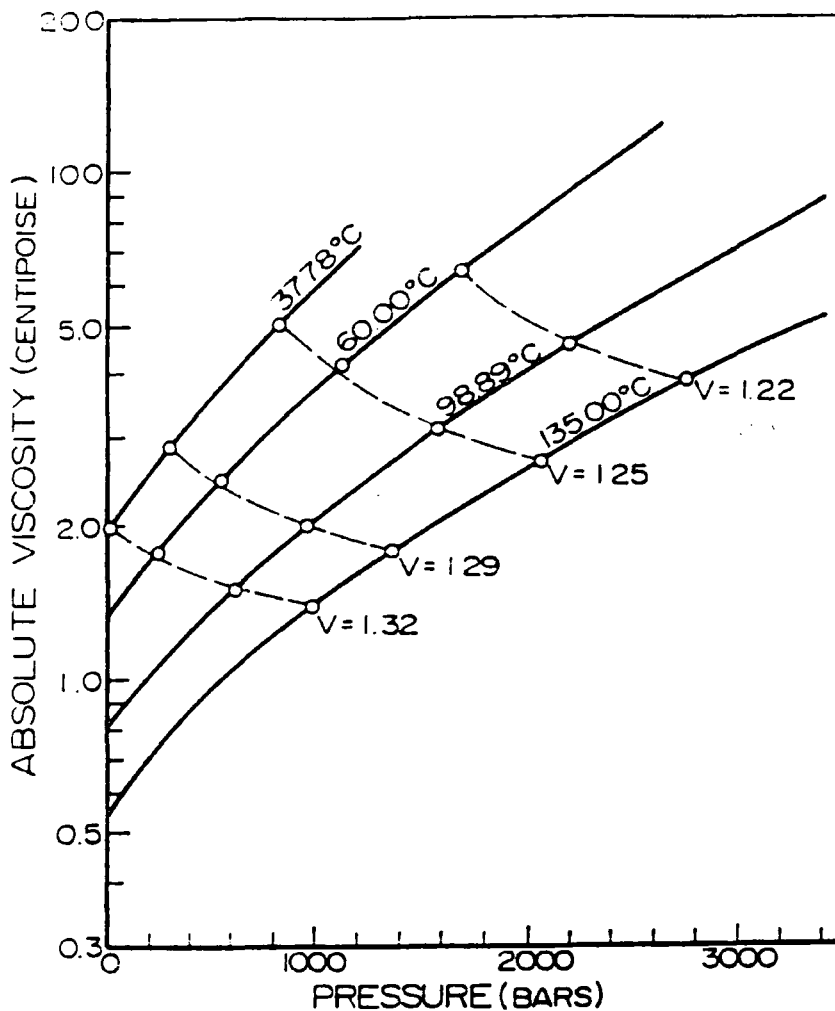
Figure 1.8. Viscosity-Pressure Isotherms for n-C_{15}.
Reproduced, by permission, from reference 26 .

To achieve a more detailed understanding of the viscosity-pressure/viscosity-temperature relationships, and therefore have the ability to predict fluid behaviour more closely it is necessary to probe the molecular interactions as a function of temperature and pressure and the effect these interactions have on viscosity. This is being attempted with projects such as the one described in this thesis. The theories of viscosity are also being developed to incorporate fluid properties on a more molecular basis, such as the volume of free space available to a molecule in the fluid[3,26]. These theories will however always be limited in their applicability, as they require the estimation of molecular quantities from the physical parameters of the fluid. A true understanding of the effect of temperature and pressure on viscosity can only be approached by use of both theoretical studies and methods able to study molecular interactions as a function of both of these variables.

1.3 Effects of molecular structure on viscometric behaviour

The intermolecular interactions that control the viscosity of a fluid and the viscosity behaviour depend on the molecular structure of the fluid. A number of observations about the variation of viscosity and the temperature/pressure dependence have been made from systematic variations of molecular structure across a family of molecules.

Increases in the chain length of a homologous series increases the isobaric viscosity, as well as the viscosity pressure coefficient[28]. Chain branching results in an increase in the viscosity and a much greater pressure dependence, compared with linear molecules of the same family having the same number of carbon atoms[26].
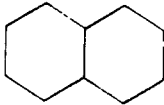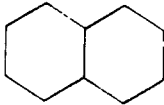
Johari has shown[29] on a series of isomeric C_8 alcohols that the viscosity and the viscosity pressure coefficient depend markedly on the position of the hydroxyl group and the proximity of any neighbouring methyl groups. The dependence of viscosity on pressure is greatest for those isomers whose hydroxyl group is most sterically hindered. This effect is most pronounced at low temperatures and becomes negligible at high temperatures.

The effect of ring substituents has been shown to increase viscosity, relative to alkyl molecules of similar molecular weight, and also to increase the pressure dependence of viscosity[30]. Pressure-viscosity coefficients of compounds with cyclohexyl rings were found to be greater than those of the analogous phenyl substituted molecules[30].

Hogenboom and co-workers[26] have found that cis ring

structures experience greater changes in relative viscosity than do the corresponding trans structures, with increasing pressure. Table 1.1 compares the isochoric, ambient pressure viscosities with those at a pressure of 3.5kbars for a number of linear, branched and cyclic alkanes.

Table 1.1. The effect of structure on viscosity.

COMPOUND	STRUCTURE	$\eta(\text{atm})$	$\eta(3.5\ \text{kBAR})$	$\dfrac{\eta(3.5)}{\eta(\text{atm})}$
n-pentane	$n\text{-}C_5$	0.22	1.28	5.93
cyclopentane	[ring structure]	0.39	2.69	6.90
n-hexane	$n\text{-}C_6$	0.29	1.84	6.47
2-2,Dimethyl-butane	$CH_3\text{-}\underset{\underset{CH_3}{\textstyle|}}{\overset{\overset{CH_3}{\textstyle|}}{C}}\text{-}CH_2\text{-}CH_3$	0.33	5.47	16.57
methylcyclo-hexane	$CH_3\text{-}$[hexagon]	0.64	9.12	14.23
n-decane	$n\text{-}C_{10}$	0.80	—	—
decan-1-ol	$C_{10}H_{21}OH$	7.85	—	—
cis-DHN (353K)[+]	[fused ring structure]	1.17	24.5	20.9
trans-DHN(353K)		0.86	13.1	15.2
7-n-hexyl-tridecane(308K)	$C[\text{-}C_6]_3$	3.53	85.6*	24.2*
EHB (310K)	see Fig.1.1	3.62	128.0	35.4
1,1-diphenyl-ethane (308K)	$C\text{-}C[\text{-}Ph]_2$	7.98	139.0	48.8

+ DHN is decahydronaphthalene

* at 3.0kBAR

Highly branched molecules, or those with cyclic structures show a greater ambient viscosity with a relatively large temperature dependence on viscosity, whereas linear chain molecules of similar molecular weight have a much lower viscosity-temperature coefficient[26]. Molecules that have strong attractive interactions, e.g. by hydrogen bonding, or are said to associate, maybe through entanglements of long chains, show a much greater ambient viscosity than the corresponding non-associated compound. An example of this can be seen comparing decan-1-ol with decane[31]. Fluids consisting of associated molecules also show a greater viscosity temperature coefficient, as when the temperature is increased the interactions are removed. With decan-1-ol and decane the viscosities are almost the same at 100°C whereas at 20°C decan-1-ol had a viscosity fifteen times greater than decane. This is demonstrated by Fig.1.9.

Viscosity measures the ease with which molecules can flow past each other. If the fluid contains molecules of a rigid structure the whole of a molecule has to reorientate itself, if there is a hindrance to flow, to be able to pass another. The more chain branching a molecule contains the more steric hindrance to flow is likely to occur. Flexible molecules will more readily reorientate, possibly only part of the molecule is required to move to allow flow, this results in a lower viscosity. These difficulties encountered by rigid and/or branched molecules become more pronounced as the pressure is increased forcing the molecules closer together, so these molecules also have a greater viscosity-pressure coefficient. When the

31

temperature is increased there is more energy available to the molecules, so they have a greater flexibility compared with at lower temperatures. The molecules can more easily reorientate to flow past each other, with a resultant decrease in viscosity. This temperature effect is more pronounced for molecules which were rigid and/or had steric hindrance to motion at the lower temperatures, and so these molecules have a greater viscosity-temperature coefficient.
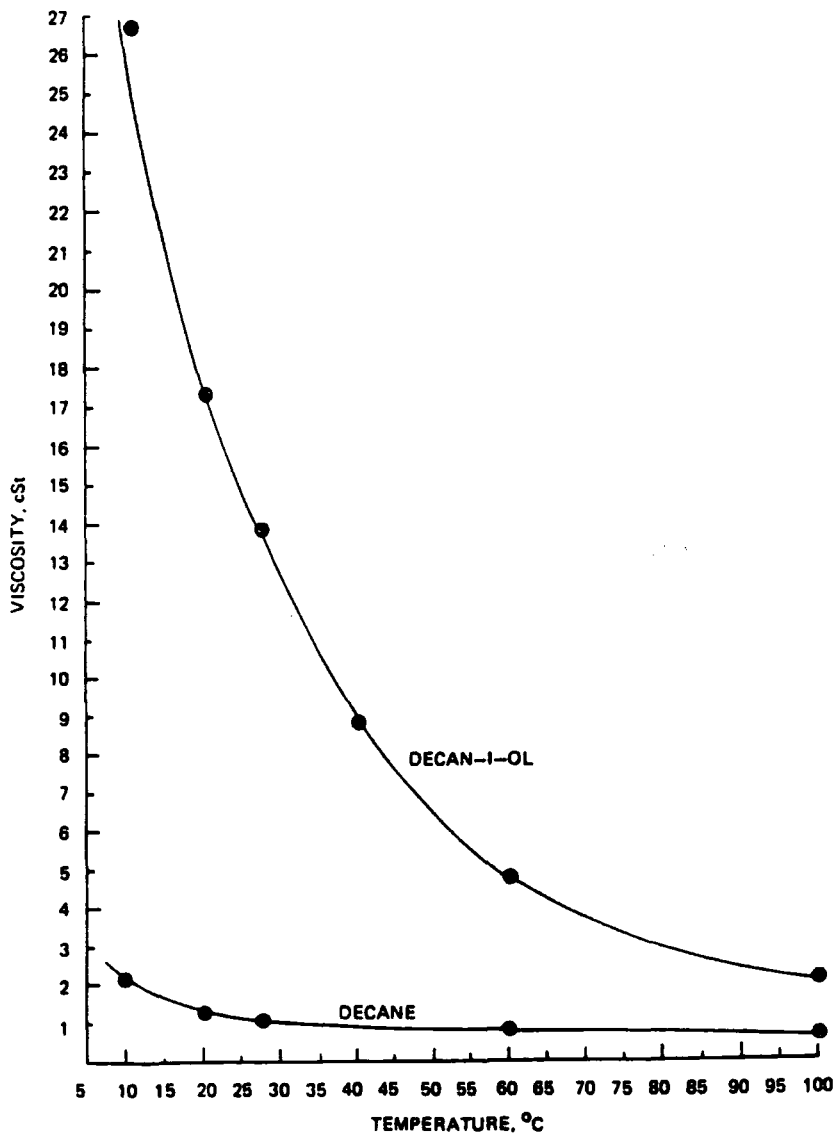
Figure 1.9. Temperature Dependence of Viscosity for Decane and Decanol. Reproduced, by permission, from reference 31 .

1.4 Vibrational spectroscopic studies of the liquid phase as a function of macroscopic fluid properties

As has been stressed throughout this chapter, in order to fully understand how pressure, temperature and shear rate affect the viscosity of a fluid it is necessary to probe the intermolecular potential and molecular dynamics, in the liquid, as a function of these three variables. This thesis demonstrates how vibrational spectroscopy can be used to probe molecular interactions and motions of a complicated flexible molecule, 2-ethylhexyl benzoate, by the analysis of vibrational frequencies, band intensities and band shapes or the associated correlation function. If this is carried out as a function of temperature, pressure and concentration, observed changes can be linked to macroscopic changes such as viscosity and density.

Although the analysis and interpretation (see Chapter 2) of vibrational spectra, especially for more complicated flexible molecules, may be of some difficulty, it is essential to study "functional fluids"[32] to allow a better understanding of the processes which are controlling the macroscopic properties such as viscosity. This will then help improve fluid design. Such information on a microscopic level is of vital importance not only to the lubricant industry but to many other areas of industry[32] including the manufacture of surfactants, plastics and paints. It is therefore sensible to choose molecules which are similar to those present in industrially useful fluids, so that any knowledge gained will be immediately applicable. The molecules should not however be too complicated so as to

to make interpretation of the observed results impossible.
Chapter 2 includes a brief discussion of some of the
vibrational spectroscopic studies on flexible molecules
which have already been carried out.

1.5   2-ethylhexyl benzoate

To be able to use the spectroscopic techniques of
Raman, infrared and NMR to probe the molecular dynamics and
interactions of a fluid, and then to be able to use this
information to relate molecular composition to fluid
physical properties, the fluid has to adhere to certain
criteria. If the effect of molecular flexibility on fluid
viscosity is to be investigated, the fluid has to consist of
non-rigid molecules. However, as explained above, the
molecule should not be so complicated that interpretation of
spectra becomes impossible.

The molecule 2-ethylhexyl benzoate (EHB), see Fig.1.1,
was chosen for this study, it was synthesized by Palmer
Research Ltd (UK) with a purity $\geq$ 99.8%. EHB is
sufficiently complex so that it relates closely to a range
of simple one-component lubricant base stocks (diesters are
commonly used as turbine lubricants) whilst remaining simple
enough to allow study of it's molecular dynamics by the
Raman, infrared and NMR techniques. EHB satisfies the
diverse requirements of these spectroscopic techniques. The
molecule contains saturated and aromatic components, and an
ester group, as well as a branch point. EHB thus
facilitates probing along it's whole length, and information

is therefore available about the interactions at different points of the molecule. The ester grouping also allows for more ready synthesis of isotopically substituted materials which will facilitate the monitoring of local (internal) dynamics whilst not substantially altering the bulk fluid properties. The fluid is a clear colourless liquid. It has a wide range of fluid viscosities (see Chapter 7), with a liquid temperature range at ambient pressures from 250°C (BPt) to -65°C where it either forms a glass or a crystalline solid depending on the rate at which it is cooled down.

EHB is therefore a suitable fluid to use to study the effect that molecular dynamics and interactions have on macroscopic properties, as a function of temperature, pressure, and concentration. These molecular properties depend on the size, shape and flexibility of the molecule and it should be possible to try to relate this to the physical properties of the fluid.

The work in this thesis is an attempt to probe the microscopic properties of the "functional fluid" EHB. Various bands arising from groups along the whole length of the molecule have been studied, as a function of one or more of solvent, concentration, temperature and pressure.

CHAPTER 2

VIBRATIONAL SPECTROSCOPY AND MOLECULAR DYNAMICS IN LIQUIDS

2.0 Introduction

In order to use vibrational spectroscopy to study the relationship between molecular structure and bulk fluid physical properties, it is necessary to be able to extract information about molecular dynamics in fluids. This needs to be done over a wide range of concentrations, temperatures and pressures. To obtain this information it is important to understand how infrared and Raman spectral bands arise from the molecular vibrations of a condensed system, how the intermolecular potential is modified by molecular motions and how the interactions with the potential affect the frequency and relaxation processes of a vibration. With this knowledge and the observed spectral changes it may be possible to postulate which molecular motions control particular physical properties. From this a link between microscopic and macroscopic fluid properties may be obtained. Having obtained this information one will have a better idea of how to modify a molecular structure to improve macroscopic behaviour.

2.1 Vibrational spectroscopy

2.1.1 Molecular vibrations

Consider a non-linear molecule containing N atoms the positions of which are described by three coordinates. It can be shown that as each atom possesses 3 independent degrees of freedom (in the x, y and z directions) the molecule possesses 3N-6 vibrational degrees of freedom. Each of these vibrational degrees of freedom corresponds to a normal vibrational mode of that molecule. A normal vibrational mode is a combination of movements of atoms that retains the centre of gravity of the molecule. In such a mode all the contributing atoms oscillate with the same frequency, the vibrational frequency of that mode, distorting the equilibrium geometry of the molecular framework, but in such a manner that the molecule does not rotate or translate. Each normal mode has a characteristic frequency which is a consequence of the masses of the atoms and the force constants involved in the mode. Each normal mode is also characterised by a normal coordinate (Q) which oscillates periodically. Normal modes are said to occur independently of one another and can therefore be treated separately, each makes a separate contribution to the vibrational energy of the molecule.

2.1.2 Infrared absorption

When a molecule is irradiated with an infrared beam the oscillating electromagnetic field of the beam and the molecule interact. For the molecule to be able to interact with the electromagnetic field and absorb or emit a photon of frequency v it must possess, at least transiently, a dipole oscillating at that frequency. If this condition is met there is the possibility of the vibrational mode, corresponding to the energy $E = hv$, absorbing or emitting a photon, see Fig.2.1.
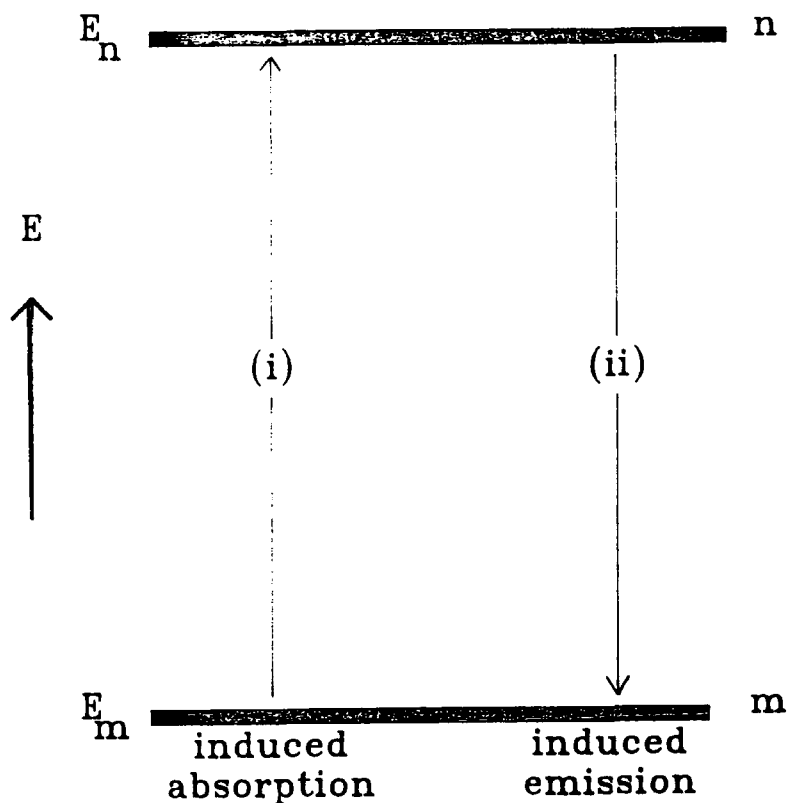
Figure 2.1. (i) Absorption ($M + hcv \longrightarrow M^*$) and (ii) emission ($M^* + hcv \longrightarrow M + 2hcv$) of photons by a vibrational mode through interaction with electromagnetic radiation.

With absorption (and emission) spectra this transient dipole is expressed in terms of the transition dipole moment[33], R_v , which for a transition between lower and upper vibrational energy states v'' and v', described by the wave functions $\Psi_{v''}$ and $\Psi_{v'}$ is defined as

$$R^{v'v''} = \int \Psi_{v'}^* \hat{\mu} \, \Psi_{v''} \, \delta Q \qquad \text{Eqn.2.1}$$

where $\hat{\mu}$ is the total dipole moment operator and Q represents the displacement coordinate $Q = r - r_e$. R_v can be thought of as the oscillating electric dipole moment due to the transition. The dipole moment may be expressed as a Taylor series

$$\hat{\mu} = (\vec{\mu})_e + (\delta\mu/\delta Q)_e Q + (\delta^2\mu/\delta Q^2)(Q^2/2!) + \ldots \qquad \text{Eqn.2.2}$$

where the subscript "e" refers to the equilibrium configuration.

For a harmonic oscillator $\hat{\mu}$ can then be taken to be

$$\hat{\mu} = (\vec{\mu})_e + (\delta\mu/\delta Q)_e Q \qquad \text{Eqn.2.3}$$

and so

$$R^{v'v''} = (\vec{\mu})_e \int \Psi_{v'}^* \Psi_{v''} \delta Q + (\delta\mu/\delta Q)_e \int \Psi_{v'}^* Q \Psi_{v''} \delta Q \qquad \text{Eqn.2.4}$$

Since $\Psi_{v'}$ and $\Psi_{v''}$ are eigenfunctions of the same Hamiltonian they are orthogonal which means that when $v' \neq v''$ then $\int \Psi_{v'}^* \Psi_{v''} \delta Q = 0$ therefore the transition dipole moment becomes

$$R^{v'v''} = (\delta\mu/\delta Q)_e \int \Psi_{v'}^* Q \Psi_{v''} \, \delta Q \qquad \text{Eqn.2.5}$$

The intensity of a particular absorption band is proportional to the square of the transition dipole moment $(I \propto |R_v|^2)$[33], so only if a transition gives rise to a non zero transition dipole moment will it contribute any intensity to the spectrum. The first term in Eqn.2.5 is only non zero if $\Delta v = \pm 1$, and since we are considering absorption, $\Delta v = +1$, is the selection rule for infrared spectroscopy in the harmonic oscillator approximation. Note that, from Eqn.2.5, the molecule need not have a permanent dipole, the rule for absorption requires only a change in the dipole, possibly from zero. Some vibrations do not affect the molecular dipole moment (e.g. the stretching motion of a homonuclear diatomic molecule) and so they neither absorb nor generate radiation, such vibrations are inactive. It can be seen, from Eqn.2.5 that the intensity is proportional to $|\delta\mu/\delta Q|^2$.

When a normal mode goes up two or more vibrational energy levels (e.g. transition from v=0 to v=2, see Fig.2.2), absorbing radiation at a frequency almost but not necessarily exactly twice the fundamental frequency (i.e. for transition from v=0 to v=1 level), this absorption gives rise to an overtone band[33], see Fig.2.2. It is a consequence of anharmonicity of vibrations, which requires that the terms higher than $(\delta\mu/\delta Q)_e Q$ in Eqn.2.2 have to be included in the expression for the total dipole moment operator, Eqn.2.3. This results in non-zero terms in Eqn.2.5 for values of $\Delta v = \pm 1, \pm 2, \pm 3$ etc, the overtone transitions then become allowed. There is also the

possibility of combination bands, when two normal modes are
excited to a higher vibrational energy level together
absorbing a photon equal to the sum of the energies of the
transitions, see Fig.2.2. These overtone and combination
bands are usually no more than 10% of the intensity of their
fundamentals, due to the reduced probability of their
occurrence.
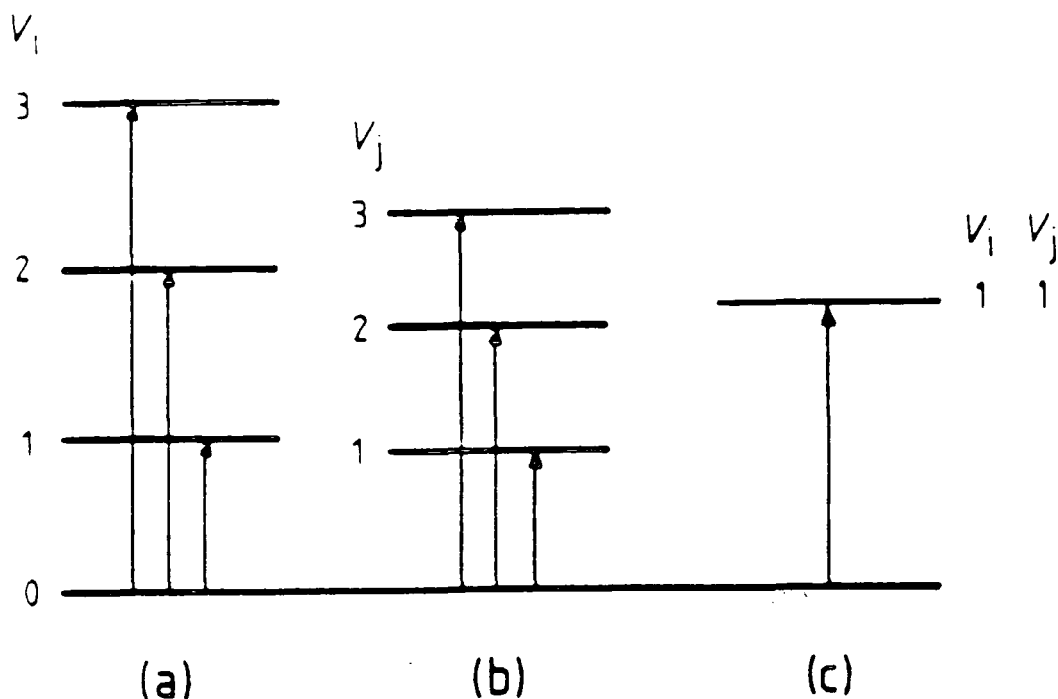
Figure 2.2. Overtone and combination bands involving
vibrations v_i and v_j. (a,b) Fundamental and overtone, and
(c) combination transitions. Reproduced, by permission,
from reference 33 .

The intensity of absorption bands depends on the difference between the population of the initial and excited states, as well as upon $(\delta\mu/\delta Q)^2$. The greater the population of the initial state the greater the probability of a transition occurring, and the more intense a band will be. The Boltzmann distribution law gives

$$N_f/N_i = (g_f/g_i)\exp(-\Delta E/k_b T) \qquad \text{Eqn.2.6}$$

where g_i and g_f are the degeneracies of the states. When $\Delta E > k_b T$ ($k_b T = 208\text{cm}^{-1}$ at 300K) $N_f/N_i \ll 1$, as the temperature is increased or for a smaller value of ΔE the value of N_f/N_i increases.

2.1.3 Raman scattering

If a molecule is placed in an electric field then the electron cloud will be distorted inducing a dipole in the molecule regardless of whether there is a permanent molecular dipole moment or not. The magnitude of this induced dipole, the dipole moment (μ') depends on the strength of electric field and the molecular polarizability (α) according to

$$\mu' = \alpha E \qquad \qquad \text{Eqn.2.7}$$

If the electric field oscillates at frequency v_0 then the dipole will also oscillate at that frequency scattering light of that frequency, hence

$$E = E_0 \cos 2\pi v_0 t \qquad \qquad \text{Eqn.2.8}$$

In such a field the induced dipole will oscillate according to

$$\mu' = \alpha E_0 \cos 2\pi v_0 t \qquad \qquad \text{Eqn.2.9}$$

This oscillating dipole can now radiate electromagnetic radiation of frequency v_0. This process is known as Rayleigh scattering. If a normal vibration causes the polarizability of the molecule to change then the vibration can interact with the oscillating dipole. For a harmonic oscillator the normal coordinate Q of a vibration is a function of time and oscillates according to

44

$$\mathbf{Q} = \mathbf{Q}_0 \cos 2\pi v_i t \qquad \text{Eqn.2.10}$$

where v_i is the frequency of the ith vibration. If the polarizability of the molecule changes during the vibration it's value for small vibrational amplitudes can be expressed as a Taylor series, as with the dipole moment in Eqn.2.2,

$$\alpha = \alpha_e + (\delta\alpha/\delta\mathbf{Q})_e \mathbf{Q} + (\delta^2\alpha/\delta\mathbf{Q}^2)_e (\mathbf{Q}^2/2!) + \ldots \qquad \text{Eqn.2.11}$$

and thus for a harmonic oscillator

$$\alpha = \alpha_e + (\delta\alpha/\delta\mathbf{Q})(\mathbf{Q}_0 \cos 2\pi v_i t) \qquad \text{Eqn.2.12}$$

substituting into Eqn.2.9 gives

$$\mu' = \alpha_e E_0 \cos 2\pi v_0 t + (\delta\alpha/\delta\mathbf{Q})_e [\mathbf{Q}_0 E_0 (\cos 2\pi v_i t)(\cos 2\pi v_0 t)$$

$$\text{Eqn.2.13}$$

using a trigonometric identity

$$\mu' = \alpha_e E_0 \cos 2\pi v_0 t +$$
$$(\delta\alpha/\delta\mathbf{Q})_e (\mathbf{Q}_0 E_0)/2 [\cos 2\pi(v_0 - v_i)t - \cos 2\pi(v_0 + v_i)t]$$

$$\text{Eqn.2.14}$$

The first term in Eqn.2.14 describes a classically oscillating dipole radiating at frequency v_0, i.e. Rayleigh scattering. The second term of Eqn.2.14 describes dipoles oscillating at frequencies $(v_0 + v_i)$ and $(v_0 - v_i)$, corresponding to anti-Stokes and Stokes scattering respectively. It is the scattering of these frequencies

that is known as Raman scattering[34], the radiated frequencies differ from the incident frequency by the frequencies of the normal vibrational modes of the molecules.

Eqn.2.14 also contains the selection rule for Raman activity, that is Raman scattering will not occur unless the derivative term $(\delta\alpha/\delta Q)$ is non zero, in other words, in order for Raman scattering to arise from a vibration it must give rise to a change in the polarizability of the molecule.

The quantum treatment of the Raman effect considers a molecule colliding with the incident photon and being raised from the v=0 level to an unstable "virtual" energy level much higher than v=1. The molecule immediately returns to the v=0 level emitting a photon of the same energy of the incident photon, Rayleigh scattering. Raman scattering occurs when a small proportion of the the excited molecules return not to their original state but to a higher or lower vibrational energy level, see Fig.2.3. In these cases the scattered photon has a different energy from the exciting photon. Molecules making transitions from the v=0 to the v=1 levels, give Stokes scattering, emitting a photon of energy $E = h(v_0 - v_i)$. Molecules making transitions from the v=1 to v=0 levels, give anti-Stokes scattering, emitting a photon of energy $E = h(v_0 + v_i)$.

The Raman transition moment is $R^{v'v''} = \int \Psi_{v'}^* \mu' \Psi_{v''} \delta Q$, employing Eqns.2.7 and 2.11 the vibrational Raman transition moment $R^{v'v''}$ is given by

$$R^{v'v''} = \alpha_e E \int \Psi_{v'}^* \Psi_{v''} \delta Q + (\delta\alpha/\delta Q)_e E \int \Psi_{v'}^* Q \Psi_{v''} \delta Q \qquad \text{Eqn.2.15}$$

as in Eqn.2.4 the first term is equal to zero when $v' \neq v''$, and the first term is only non zero if $\Delta v = \pm 1$, which contributes the vibrational Raman selection rule. Intensities of Raman transitions are proportional to $|R_v|^2$ and therefore $(\delta\alpha/\delta Q)_e^2$.

According to a Boltzmann distribution, the relative populations of the $v=0$ and $v=1$ levels, at room temperature, is such that the Stokes Raman intensity is always greater than the anti-Stokes intensities. As with infrared absorption bands there is the possibility for overtone bands due to the modification of the selection rules to $\Delta v = \pm 1$, ± 2 . ± 3...., because of the anharmonicity of a vibration. Combination bands are also present in Raman spectra. Again the overtone and combination bands are at a much lower intensity than the fundamental bands.
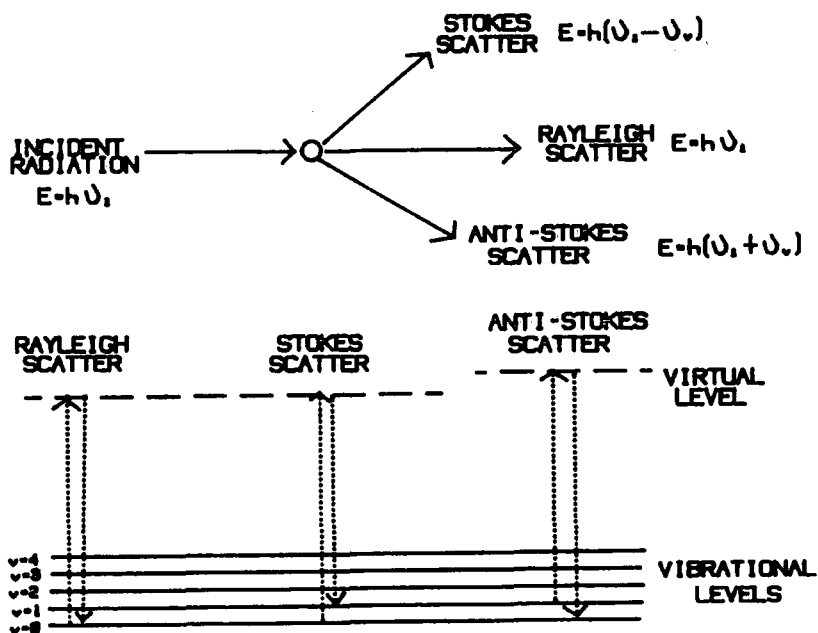
Figure 2.3. Stokes and anti-Stokes scattering

2.2 The study of molecular dynamics using vibrational spectroscopy

The use of infrared and Raman spectroscopy has come a long way since their first introduction for the identification of compounds. These techniques are now extensively used to study dynamic processes in liquids by studying band shapes and calculating correlation functions from infrared and Raman spectral profiles.

The advance from simple compound recognition to the study of liquid dynamics has only been allowed by significant developments in experimental technique. These include, with infrared the developments of FTIR with better resolution instruments and more sensitive detectors, and in Raman spectroscopy the introduction of laser sources, high quality photo multiplier tubes and better resolution. The study of molecular dynamics has also depended on the development of computer systems to enable relatively quick and easy data sampling, storage and processing.

2.2.1 Peak frequencies and band shapes.

Peak frequencies of vibrational bands of liquid-phase molecules depend on static parameters, force constants, atomic masses, bond distances and angles, and electric charges, which are modified by molecular interactions with the surrounding potential. Band profiles and bandwidths depend on dynamic parameters from atomic and molecular motions.

If only the theory for infrared absorption and Raman scattering for isolated molecules, considered in the previous section, is taken into account, then for each vibrational mode one would expect to find an infinitely narrow delta function, corresponding to transitions of the type $E = h\upsilon$, found at the corresponding frequency υ. This is not observed, one sees bands of various width and shape, due to molecular motion and interactions, see Fig.2.4.

The vibrational band shape is dependent on the "lifetime" of the molecule in the excited vibrational state. When an oscillator is instantaneously excited to an upper oscillator level it only has a finite lifetime in this level before oscillator-medium interactions return it to the ground level. This "lifetime" leads to a bandwidth increment $\Delta\omega$, (this can be estimated by the energy-time uncertainty relation[35] ($\tau\Delta E \simeq h$ or $\tau\Delta\omega \simeq 1$)). Consequently, the radiation induced transitions between ground and upper system levels show a frequency distribution, a band profile, around the unperturbed oscillator frequency. The band shape is also dependent on the "spread" of the vibrational transition frequency of a particular mode due to an

49

environmentally induced distribution of energy for the
vibrational levels. An explanation of both these processes
is given in section 2.3.
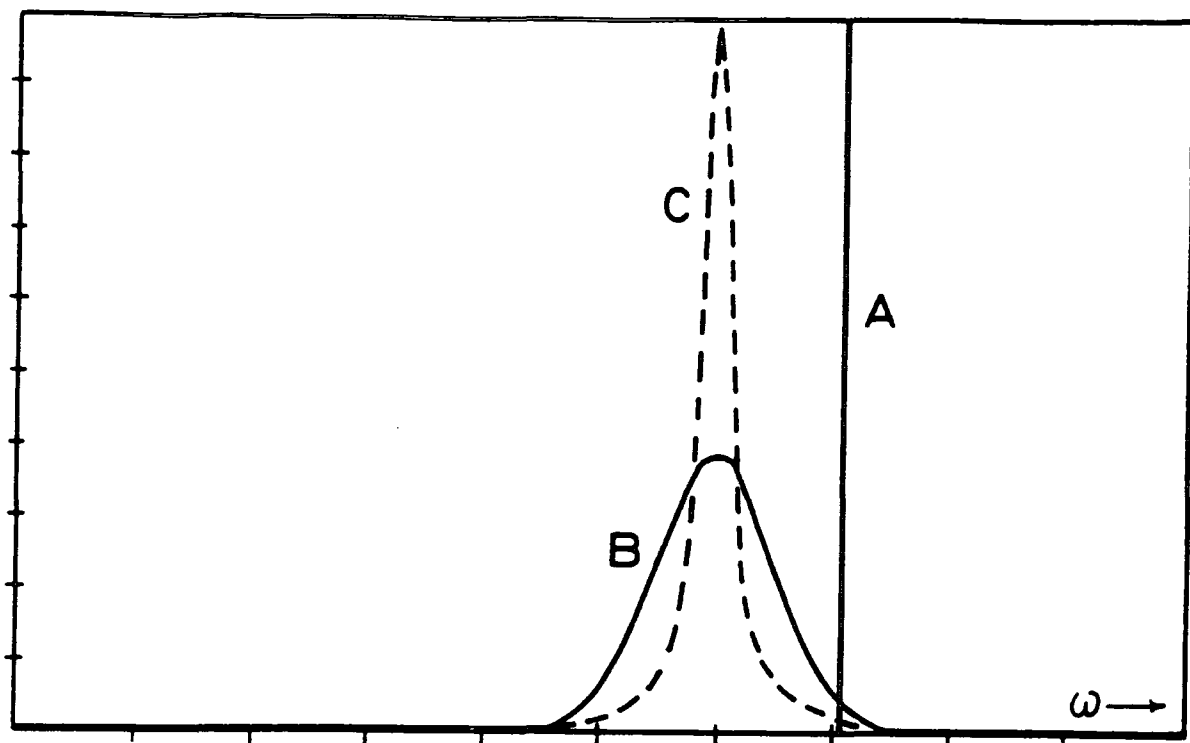
Figure 2.4. The effect of environment on the broadening of a
given vibrational mode. A) dilute gas, B) liquid with slow
molecular motions - (little motional narrowing, for example
at low temperature), C) liquid with more rapid molecular
motions and significant motional narrowing. Reproduced, by
permission, from reference 38 .

2.2.2 Band shapes and correlation functions

Experimental analysis of relaxation mechanisms and molecular motions using Raman and/or IR spectroscopy can be carried out by direct analysis of the band shape, or on the corresponding correlation function obtained by direct Fourier transformation. Early work and a lot of research being carried out now probes intermolecular potentials and molecular dynamics[36] by studying their effect on band shape parameters (width and shift). This includes much of the work discussed in this thesis (see Chapter 7). Any consideration of whether to use band shape or correlation function analysis to study molecular dynamics, has to consider which method shows the effects most clearly and can be interpreted most easily. One also has to consider the quality and reliability of the correlation function obtained. This will be discussed in this section. Often one has to compare experimental results with theories which describe molecular motions as a function of time, with these it is better to use correlation functions. However many of the theories and models attempt to predict the shape of bands from molecular and macroscopic parameters, in these cases it is obviously better to remain in the frequency domain.

2.2.3 Correlation functions

The Fourier transform

$$F(p) = \int \delta q . \exp(ipq) . f(q) \qquad \text{Eqn.2.16}$$

decomposes a function of independent variable p into an integral sum over a continuous range of an associated variable q. Identifying p with ω and q with t, the experimental spectral profile $I(\omega)$ can be transformed into the time domain by

$$f(t) = \int \delta\omega . I(\omega) . \exp(-i\omega t) \qquad \text{Eqn.2.17}$$

where $\omega = 2\pi\bar{v}c$ (for $\bar{v}$ in cm^{-1})

The time range available to vibrational spectroscopy is about 0.1ps to 100ps, this being a function of the inverse frequency of the radiation. This is ideal for the study of rapid molecular motions and interaction fluctuations in fluids.

Infrared and Raman band shapes may be conveniently considered to be the Fourier transforms of certain time autocorrelation functions $\phi(t)$. Within the limits of experimental error, and if selection rules allow, three band profiles can be obtained for a particular mode between the frequencies ω_1 and ω_2 and centred at ω_0. Measurement of the polarization characteristics of $90°$ Raman scattered light allows one to separate the isotropic $[I_{iso}(\omega) = I_{VV}(\omega) - 4/3.I_{VH}(\omega)]$ and anisotropic $[I_{aniso}(\omega) = I_{VH}(\omega)]$ parts of the scattered light, see Appendix 2. The infrared band

profile measurement $[I_{ir}(\omega)]$ is more straight forward. These components are modulated by different relaxation processes. The isotropic part gives information about vibrational relaxation, whereas the anisotropic and IR part contains contributions from both vibrational relaxation and reorientational relaxation. For an infrared band with normalised intensity $I_{ir}(\omega)$[37,38].

$$\phi_v(t)\phi_{1R}(t) =$$
$$\langle Q_i(0).Q_i(t)\rangle\langle P_1[\vec{\mu}_i(0).\vec{\mu}_i(t)]\rangle = \int_{band} I_{ir}(\omega)\exp(i\omega t)\delta\omega$$

Eqn.2.18

where $\langle Q_i(0).Q_i(t)\rangle$ is the vibrational relaxation function and $\langle P_1[\vec{\mu}_i(0).\vec{\mu}(t)]\rangle$ is the first Legendre polynomial pure rotational (or reorientational) correlation function ($P_1 = \cos\theta_i(t)$ where $\theta_i(t)$ is the angle of the transition dipole of the ith molecule at time t=t) and where $\vec{\mu}$ is a unit vector along the direction of the transition moment corresponding to the normal coordinate Q_i of the ith molecule. The IR reorientational correlation function describes the reorientation of a vector lying in the direction of the permanent dipole moment.

For Raman spectra things are more complicated because we are dealing with polarizability components and their derivatives, which have tensorial properties. For normalised intensities it can be shown[38] that

53

$$\phi_v(t) = <Q_i(0) \cdot Q_i(t)> = \int_{band} I_{iso}(\omega)\exp(i\omega t)\,\delta\omega \qquad \text{Eqn.2.19}$$

and

$$\phi_v(t)\phi_{2R}(t) =$$
$$<Q_i(0) \cdot Q_i(t)><P_2[\vec{\mu}_i(0) \cdot \vec{\mu}_i(t)]> = \int_{band} I_{aniso}(\omega)\exp(i\omega t)\,\delta\omega$$
$$\text{Eqn.2.20}$$

Thus one measures the vibrational relaxation function directly by an isotropic scattering experiment. The 2nd order Legendre polynomial P_2 (equal to $1/2(3\cos^2\theta_i(t) - 1)$ is present in Eqn.2.20 as a consequence of the Raman experiment measuring the reorientation of a tensor[38]. In Eqns.2.18 to 2.20 the autocorrelation function $<Q_i(0) \cdot Q_i(t)>$ (vibrational relaxation function) includes <u>all</u> non-reorientational contributions to the decay of the total $\phi(t)$ function, see section 2.3.

The instrument resolution function is characterised by a function whose Fourier inversion leads in the time domain, to $\phi_S(t)$, so that the autocorrelation functions become

$$\phi_{ir}(t) = \phi_v{}^{ir}(t)\phi_{1R}(t)\phi_S(t) \qquad \text{Eqn.2.21}$$

$$\phi_{iso}(t) = \phi_v{}^{iso}(t)\phi_S(t) \qquad \text{Eqn.2.22}$$

and $\qquad \phi_{aniso}(t) = \phi_v{}^{aniso}(t)\phi_{2R}(t)\phi_S(t) \qquad \text{Eqn.2.23}$

So that

$$\phi_v{}^{iso}(t) = \phi_{iso}(t)/\phi_S(t) \qquad \text{Eqn.2.24}$$

$$\phi_{1R}(t) = \phi_{1R}(t)/\phi_{iso}(t) \qquad \text{Eqn.2.25}$$

$$\phi_{2R}(t) = \phi_{aniso}(t)/\phi iso(t) \qquad \text{Eqn.2.26}$$

Thus for the determination of $\phi_v(t)$ it is necessary to correct for finite slit width. This is usually done by assuming the slit profile to be a pure Gaussian function with width equivalent to the slit, and obtaining ϕ_S as the Fourier transform of this profile. It should be noted that Eqn.2.25 is only valid if ϕ_S is the same for infrared and Raman experiments.

Separation of the three correlation functions is only feasible if $\phi_v{}^{iso}(t) = \phi_v{}^{ir}(t) = \phi_v{}^{aniso}(t)$. Eqns.2.25 and 2.26 only hold if the vibrational and reorientational relaxation processes are statistically independent[38]. For statistical independence it is generally thought that it is necessary for the two processes to be occurring on different time scales. For EHB it was thought, and experiment has provided supporting evidence, that the size of the molecule would ensure reorientational relaxation occurs much slower than vibrational relaxation, hopefully ensuring statistical independence. An added advantage for fluids with much slower reorientational relaxation than vibrational relaxation, is that for some bands it may be possible to assume that the band width arises entirely from vibrational relaxation. This is useful when for any reason calculation

and separation of two correlation functions is not possible
e.g. weak and noisy $I_{VH}(\omega)$ component.

The correlation functions contain both self and
distinct terms[37-39], for example the dipole reorientation
function in Eqn.2.18 can be written as

$$\sum_{i,j} <\vec{\mu}(0).\vec{\mu}(t)> = \underset{\text{self}}{\sum_{i} <\vec{\mu}_i(0).\vec{\mu}_i(t)>} + \underset{\text{distinct}}{\sum_{i \neq j} <\vec{\mu}_i(0).\vec{\mu}_j(t)>}$$

<div align="right">Eqn.2.27</div>

where i and j label different molecules. For I.R. and Raman
spectra it is usually assumed[37,40] that the reorientational
CF's obtained contain only the "self" (single particle)
terms. However experimental evidence[37,39,41] shows that
intermolecular coupling of vibrational motions of molecules
i and j can be significant, resulting in the need for
non-zero "distinct" terms in the expression for the
vibrational correlation function. Unless vibrational and
rotational motions are totally uncorrelated then non-zero
"distinct" contributions also emerge in the reorientational
CF's[39].

When calculating CF's one might also have to consider
the effects of local electrical fields[42,43] on the spectral
intensity or dynamics the result of which means that the
molecules in the fluid do not experience the same electric
field as that propagated into the medium. The contribution
of interaction-induced intensity[44,45] should also be
considered. This results from the transient dipole moment
which arises from the distortion of the charge distribution
due to interacting molecules or atoms. The resulting

induced dipole moment is varying within the time scale of collision/motions that is much faster than the molecular motions themselves, so that it contributes mostly to the higher frequency absorption and will mainly affect the short time part of the CF's. A detailed study and simulation of the interaction induced intensity has only been carried out for very simple molecules[44,45]. There is a need to accurately know the pair potentials and induced dipole functions for the system. Even then the results show that there is the need to be able to consider many particle effects, and not just two particle[46], which at present is only possible for far infrared work, and even this is limited to relatively simple systems. It is impossible therefore to take into account interaction induced intensity when looking at molecular fluids on the scale of lubricant fluids, and there appears to be no answer to this problem in the near future.

Provided that the complications mentioned above are not too severe, then expressions for the desired correlation functions can be obtained. EHB has some advantages over smaller molecules, including the probability that vibrational and reorientational motions can be considered separately, due to the molecular size and the fluid density. EHB has many spectral bands enabling motions and interactions of the whole molecule and parts of the molecule to be investigated. However this has disadvantages, it is difficult to model the motion of such a complicated molecule and there are problems with obtaining CF's of molecules with many vibrational modes as will be explained in the next section.

2.2.4 Problems involved in obtaining correlation functions

To be sure that the digitized band intensity is correct there are a number of experimental problems to be overcome. With Raman it is necessary to pass the laser light through a Glan-Thompson prism or a polarizer placed in front of the sample to ensure that the incoming laser beam is fully vertically polarized. For highly polarized bands there may also be a problem with leakage from the $I_{VV}(\omega)$ spectrum into that of $I_{VH}(\omega)$, giving

$$I_{VH}^{obs}(\omega) \quad = \quad I_{VH}^{true}(\omega) \quad + \quad CI_{VV}(\omega) \qquad \text{Eqn.2.28}$$

Bartoli and Litovitz[47] found values of C of about 0.2% for some typical polarised bands. This can be overcome by using measurements on the 459 cm^{-1} band of CCl_4, which has a well known[48] depolarization ratio, to calculate $I_{VH}^{true}(\omega)$ from $I_{VH}^{obs}(\omega)$.

The most serious difficulties arise with achieving an accurate base line and good S/N ratio (especially in the wings of the band). If S/N is poor, as with weak bands, the resulting correlation functions are very noisy with imprecise correlation time determination[49]. At the expense of longer experimental time these problems can usually be overcome. The baseline problem is more serious, due to the difficulty in recording a meaningful background, especially for the IR spectra of pure liquids. Computational procedures have been devised to help overcome difficulties arising from optical problems, like interference fringes.

On top of these problems with sampling the data there

58

are a number of factors which limit the accuracy of a determined CF. It is essential that the band centre is found accurately[50]. Collecting data at smaller frequency intervals is often the answer, but this again requires longer experimental times. The effects of overlapping bands be it hot bands, overtones or simply the presence of another vibrational mode of similar frequency, make it difficult to determine the band centre, thus hampering the calculation of reliable CF's. The removal of the first two effects can sometimes be achieved by isotopic substitution, also in certain cases by calculation[51], but for this one needs to know the frequency shifts and fractional intensity of the various species present and assume that the relaxation processes effects each isotopic band in the same way. For two different bands close together there is no reliable solution to the problem of finding the band centre. Such difficulties become particularly acute with complicated molecules like EHB.

Overlapping bands also restrict the maximum frequency range over which a band may be measured. If it is only possible to measure the spectrum between certain limits ω_i and ω_f, this restricts the time resolution which may be achieved[52].

$$\Delta t = \pi/2\pi c \ (\bar{v}_o - \bar{v}_i) \approx \frac{16 \times 10^{-12} \ sec}{(\bar{v}_o - \bar{v}_i)} \qquad Eqn.2.29$$

where v_o and v_i are in cm^{-1}. This limitation can be quite serious. If $v_o - v_i$ is 100 cm^{-1} then the corresponding time resolution is 0.2 psec. Clearly it might be difficult to

properly define the short time part of C(t) if the time resolution is insufficient and the relaxation time is short i.e. for a broad band. (To adequately describe the short time part one should always aim for $\bar{v}_0 - \bar{v}_i$ to be 10 x FWHM). Therefore with molecular fluids like lubricants there can be difficulties in obtaining accurate CF's because of limits imposed on the analysis due to the presence of many vibrational modes contributing to the spectra. Often it is just not possible to calculate a CF for a band because it is too close to other bands. Inaccuracies in measurement of the wings of a band will result in a CF which does not accurately describe the short time part of molecular dynamics[47].

Since C(t) measures an ensemble average, it should measure a correlation between individual molecules of the ensemble. However the radiation is of a wavelength much larger than the molecular size and so C(t) measured corresponds to domains of molecules. In these circumstances, strictly, interference terms need to be included in the expression for C(t).

The requirement of sampling at interval $\Delta\omega$ leads[52] to a periodic C(t) function with period $\tau = 2\pi/\Delta\omega$. The calculated correlation function is therefore only reliable up to a time $\pi/\Delta\omega$. $\Delta\omega$ is usually controlled by the instrumental slit width δ_S such that $\Delta\omega \leq \delta_S$. The range is thus given by

$$t = \pi/2\pi c \delta\bar{v} \approx (16 \times 10^{-12}/\delta\bar{v}) \text{ sec} \qquad \text{Eqn.2.30}$$

Where δv is the slit width in cm^{-1}. For example for a slit

of 1cm^{-1} the CF is valid out to 16psec. Except for very narrow bands (ie long correlation times) obtained with poor resolution this is not normally a limiting factor.

There are a number of effects which necessitate corrections to the observed data in order to provide a more accurate representation of the true band profile. The effects of overlapping bands has already been discussed. With the far-infrared data it is not possible to experimentally measure the whole of the band profile down to zero wave numbers due to the limits of the detectors. In order to be able to calculate a correlation function it is necessary to measure the rest of the spectrum using microwave data. In some IR bands errors can arise in the computed CF if the band profile is seriously distorted by rapid variation in the refractive index $\eta(\omega)$ through the band and can be corrected for if $\eta(\omega)$ and the absorption coefficient can be measured separately[38].

2.2.5 Correlation times

If possible, and after making a number of assumptions, separation of the various correlation functions has been achieved, it is often convenient to characterise the function by obtaining the corresponding correlation time, τ_x where

$$<\tau_x> = \int_0^{t_1} \phi_x(t)\,\delta t \qquad \text{Eqn.2.31}$$

61

and t_1 is the expected time limit, controlled by the spectral resolution. If, as is often found for models[38,52,54] describing relaxation functions, the $\phi_x(t)$ function can be written as $\phi_x = \exp(-t/\tau_x)$ then the integrated value $\langle\tau_x\rangle$ is equivalent[55] to the "decay" time $\tau_x^{\,e}$ measured directly from the $\phi_x(t)$ vs t curve, see Fig.2.5, (i.e. the time required for $\phi_x(t)$ to fall from 1 to 1/e). If due to experimental uncertainties discussed above it is not possible to calculate $\phi_x(t)$ accurately then, assuming $\phi_x(t) = \exp(-t/\tau_x)$ holds, one can calculate τ_x from $(\pi c \Delta\bar{v}_{1/2})^{-1}$ where $\Delta\bar{v}_{1/2}$ is the apparent full-width at half-maximum height (FWHM) in cm^{-1}. If ϕ_x can be obtained
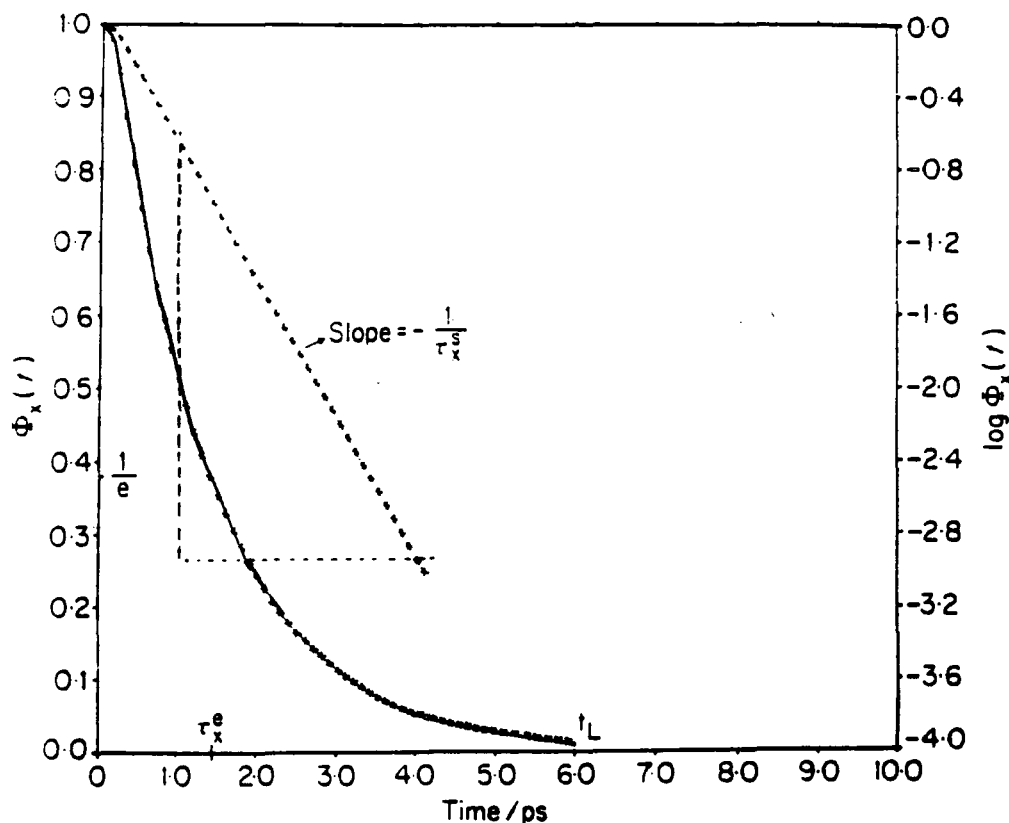
Figure 2.5. Correlation function for pure Lorentzian band of half-width (FWHM) = $7cm^{-1}$, showing the various correlation times that can be produced. Reproduced, by permission, from reference 37 .

but integration is not possible it is often possible to calculate τ_x from the slope of the plot of $\ln\phi_x(t)$ against t at long times when $\phi_x(t)$ becomes exponential regardless of the details of the band shape, (see section 2.3).

Considering correlation times estimated from bandwidths entails a loss of information, since the time development of the correlation function is no longer observed, but only the average. The advantage of infrared and Raman spectroscopy over nuclear magnetic or dielectric relaxation, namely the observation and evaluation of this time development of the correlation function, is thus lost. However possessing the correlation time, for the vibrational or reorientational relaxation of a mode, can still help with the understanding of molecular dynamics and interactions, through models and theoretical calculations of the relaxation processes from which an estimate for the correlation time can be obtained.

2.2.6 Summary

Assuming one can obtain a reliable set of CF's for a molecule under various conditions they contain useful information on molecular motions and are currently used for a wide variety of purposes.

(i) To provide information on the rates of (a) rotational and translational motions and (b) energy and phase relaxation in molecular liquids.

(ii) To probe the effects of environment (in particular intermolecular torques or intermolecular interactions) on the motions and relaxation modes of fluid phase molecules.

63

(iii) To allow a check to be made on the intermolecular potentials used for MD simulations.

(iv) To aid theoreticians developing models for molecular rotation or vibrational relaxation - since the essential features of the correlation function (especially at short times) must eventually be reproduced by such models. Clearly this can be applied to lubricant molecules to gain a better understanding of the microscopic properties controlling macroscopic properties

(v) To compare with correlation times obtained using other spectroscopic techniques on the same fluid, e.g. using NMR or Depolarized light scattering, in order to gain a more detailed knowledge of all motions of the molecule.

2.3 Relaxation Processes

In a liquid there are usually many different relaxation processes contributing to the overall relaxation of a particular vibrational mode. The type of processes which occur are determined by the molecular motions and interactions in the fluid.

For a rapid relaxation rate the corresponding correlation function will decay rapidly, with the result that the correlation time will be small, see Fig.2.5. In the frequency domain this is seen as a relatively broad band. If the relaxation is slow then the opposite is seen. By comparing the shape of vibrational bands and/or correlation functions for a system, as a function of concentration, temperature and pressure, it may be possible to evaluate the predominant relaxation processes and gain an insight into the molecular motions and interactions.

2.3.1 Vibrational Relaxation

Vibrational relaxation is essentially a measure of the efficiency with which molecules can interact with one another. For a given mode of a given molecule there are a number of processes which contribute to the vibrational relaxation of that mode, and which consequently contribute to the band shape and the decay of $\phi_V(t)$. These may include one or more of the following[53].

(a) The energy can be transferred into the translations, rotations or other vibrations close in frequency. This type of process is known as vibrational energy relaxation (or transfer), the population difference is reduced by dissipation of energy into the surrounding lattice molecules.

(b) Intramolecular vibrational relaxation, a process whereby vibrational energy moves from the originally excited mode to a different mode in the same molecule.

(c) Resonance vibrational energy transfer. The energy loss of an upper oscillator level is the subsequent energy gain to the same oscillator level but on an adjacent molecule. The relatively strong interactions between the molecules in a liquid sometime cause part of the excitation energy to shift to other molecules by resonant transfer. During the transfer process neighbouring molecules are performing vibrational motions simultaneously. The vibrational energy in this situation is different from the single molecule vibrational energy. As the transfer process starts during the excitation process, the excitation energy will be influenced by this intermolecular vibrational

66

coupling. The disordered liquid results in different pairs of molecules being coupled with different coupling strengths, because of this the resonance effect causes a distribution of excitation energies. This causes band broadening, see below, which is is a type of "inhomogeneous broadening".

(d) Vibrational dephasing, band broadening effects occurring because of loss of phase coherence of the excited vibrations in a particular mode[53,56]. There are two ways for this to occur, either "inhomogeneous" or "homogeneous" broadening . In a disordered condensed phase the sharp transition frequency ω_0 of a two level oscillator system is "smeared" out into a continuous, non-resolvable distribution of vibrational transition frequencies. The interactions between the oscillator and the surrounding molecules in their various positions and orientations have caused perturbative "instantaneous" shifts of the lower and upper oscillator energy levels. This is often referred to as "inhomogeneous" broadening. The band broadening occurs because of the spread of (inhomogeneity in) oscillator frequencies which the electromagnetic field of the beam effectively samples, see Fig.2.6. The interactions which cause inhomogeneous broadening fluctuate rapidly due to fast translational and rotational motions. This causes partial averaging of all possible energy levels because spectroscopy has a limited time resolution, it cannot show the instantaneous situation of the liquid state. This averaging is called "motional narrowing" because it narrows the inhomogeneously broadened band, see Fig.2.4.

There is a second type of vibrational dephasing, which

is a "homogeneous" broadening process. this arises from loss of phase due to phase shifts caused by molecular collisions. this is illustrated in Fig.2.7.

molecule

1 -
2 -
3 -
4 -
5 -
6 -
7 -
8 -
⋮
n -

$\longrightarrow$ t

sum function
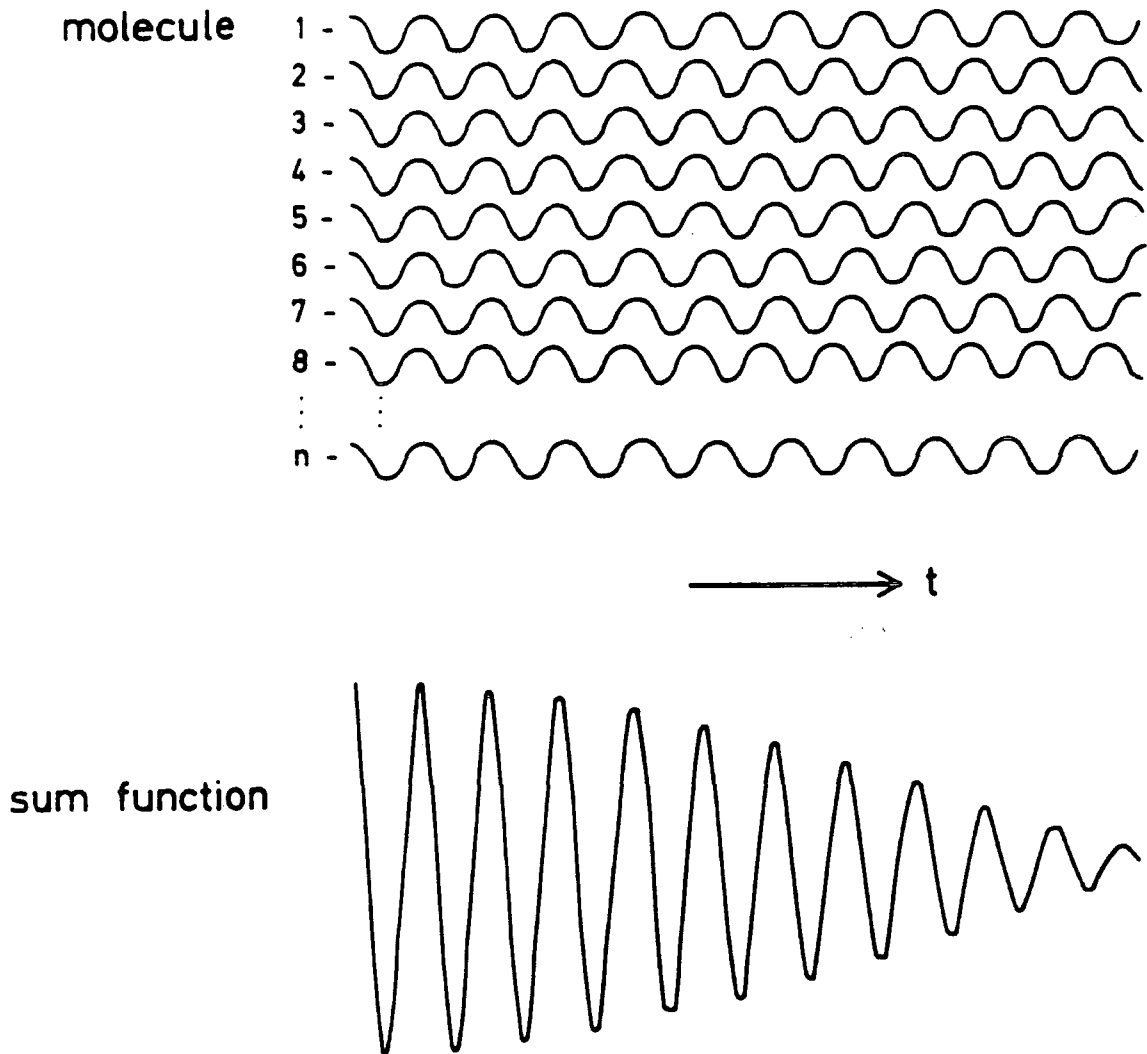
Figure 2.6. Inhomogeneous broadening. Reproduced, by permission, from reference 38 .

The first two effects, (a) and (b) are essentially vibrational depopulation effects and as such are known as energy relaxation processes. The bandwidth increment is dependent on the lifetime of the oscillator in the excited state, as explained in 2.2.1. Effects (c) and both mechanisms of relaxation in (d) are phase relaxation processes and are known as broadening effects. Resonance vibrational energy transfer is an inhomogeneous effect caused by loss of oscillator phase arising from the coupling of the oscillators involved in the energy transfer.
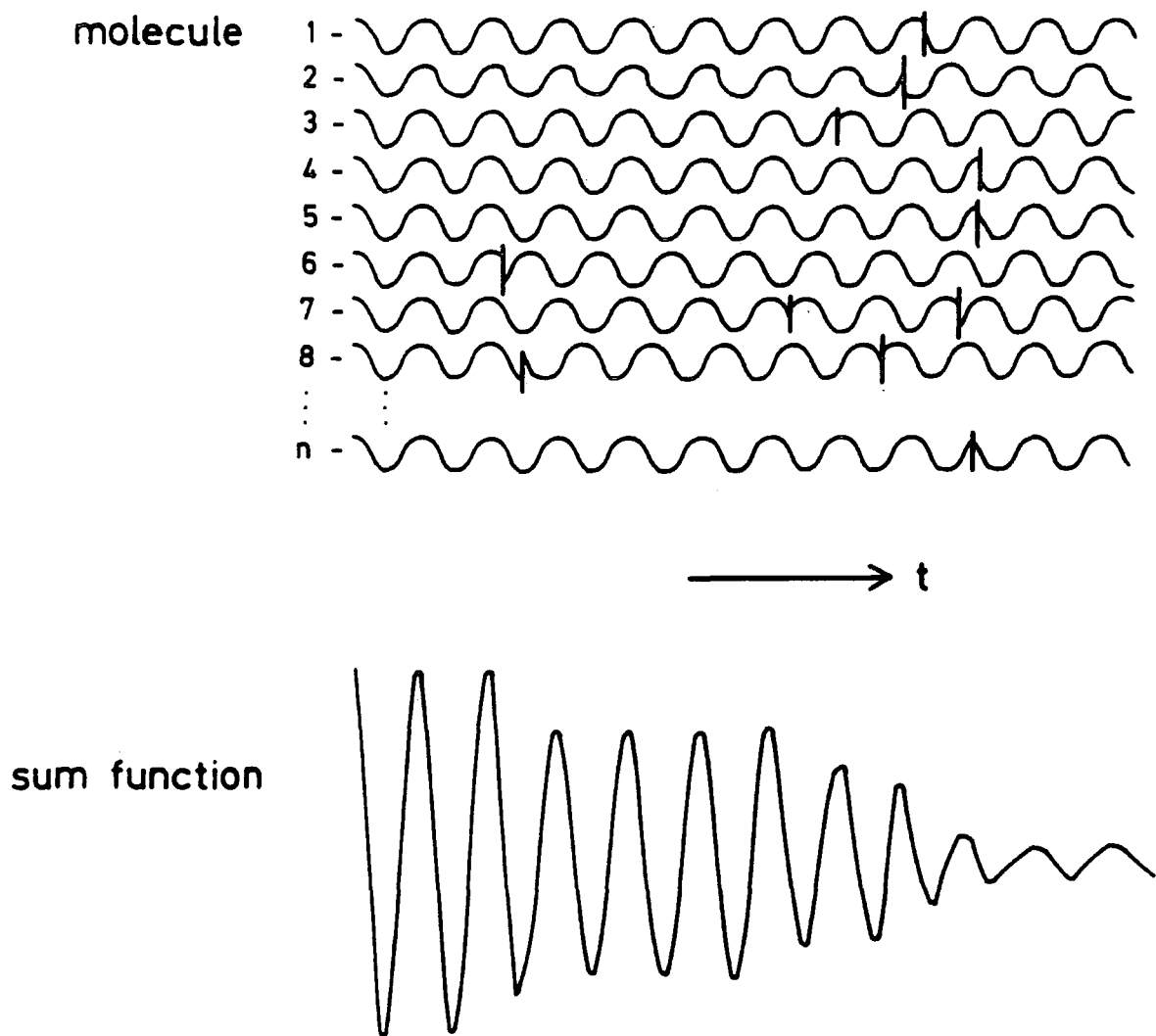
Figure 2.7. Phase relaxation by hard collisions, homogeneous broadening. Reproduced, by permission, from reference 38.

Assuming statistical independence of the two types of processes then

$$\phi_V(t) = \phi_E(t)\phi_{pp}(t)$$ Eqn.2.32

where the subscripts "E" and "pp" refer to energy and phase relaxation respectively. It is generally found that broadening by phase relaxation processes are the dominant contributions to bandwidths, as energy relaxation processes tend to be much slower, because the vibrational energy is in most cases much higher than rotational or translational energies and therefore dissipation of energy is only possible by complicated processes. Inhomogeneous broadening processes depend on the spread of different vibrational frequencies of the active molecule. Hence the rate of vibrational relaxation via these processes is a result of the extent of frequency distribution caused by the surrounding intermolecular potential. Thus, in principal, measurement of vibrational relaxation functions allow the study of such potentials. The major difficulty is that the loss of phase coherence may occur through many different types of interaction. These may be due to dipole-dipole, dipole-quadrupole (etc) types or due to repulsive potentials. Fortunately these different types of interaction may sometimes be distinguished experimentally[37] and sometimes it can be shown that one type is predominant for a particular vibrational mode. In these favorable cases the variation of concentration, temperature and pressure will enable the nature and behaviour of the interaction to be studied in detail.

In order to be able to achieve the above it is necessary for a detailed description of the mechanism of vibrational relaxation. To do this there is the need for the use of fully descriptive models[37] for each type of interaction. This enables an understanding of when and why a particular process will predominate, and how this should manifest itself in the correlation functions.

For phase relaxation, which as explained, tends to be the dominant vibrational relaxation mechanism, the Kubo model for vibrational dephasing is frequently employed[37,57], the relaxation function $\phi_{pp}(t)$ is expressed as

$$\phi_{pp}(t) = \exp\{-<\Delta\omega^2>[t\tau_m + \tau_m^2[\exp(-t/\tau_m) - 1]]\} \qquad \text{Eqn.2.33}$$

where $<\Delta\omega^2>$ is the mean square frequency fluctuations (shift) due to the different interactions of a particular mode with the surrounding "potentials" (equivalent to the vibrational second moment $M2_v$), τ_m is the modulation (or correlation) time which is related to the time scale of these "bath" fluctuations. It can be shown[37] that for $t<<\tau_m$ the slow modulation time limit,

$$\phi_{pp}(t) \simeq \exp[-(1/2)<\omega^2>t^2] \qquad \text{Eqn.2.34}$$

the oscillators vibrate with random phase in a "quasi-static" environment which has not had time to change. In this case the decay of $\phi_{pp}(t)$ and the corresponding band profile are expected[37] to follow a Gaussian distribution, and the half width (or equivalent dephasing rate τ_{pp}^{-1}) gives $<\omega^2>$ directly as,

$$\tau_{pp}^{-1} = 2(2\ln 2)^{1/2} . <\Delta\omega^2>^{1/2} \qquad \text{Eqn.2.35}$$

For $t \gg \tau_m$, times much longer than the correlation time of the perturbation, the fast modulation limit, the phase relaxation function $\phi_{pp}(t)$ decays more slowly and the band shape becomes Lorentzian[57] (the motionally narrowed situation). Now, $\phi_{pp}(t)$ is represented by a single exponential,

$$\phi_{pp}(t) \simeq \exp(-<\omega^2>\tau_m t) = \exp(-t/\tau_p) \qquad \text{Eqn.2.36}$$

the corresponding rate of dephasing is

$$\tau_{pp}^{-1} = <\omega^2>\tau_m \qquad \text{Eqn.2.37}$$

The decay of $\phi_{pp}(t)$ in the slow and fast modulation regimes are shown in Fig.2.8. The situation encountered for a particular fluid depends on the rate of modulation due to fluctuations of the intermolecular potentials. It should be noted that τ_m may have different interpretations depending on the nature of the potentials giving rise to the frequency shift fluctuations, this will be discussed in Chapter.7.

In the slow modulation limit ($\tau_m <\omega^2>^{1/2} \gg 1$) the perturbation effectively lasts for a long time and the dephasing process is rapid, the resulting $\phi_{pp}(t)$ function decays rapidly with a small long time exponential tail. For rapid modulation ($\tau_m <\omega^2>^{1/2} \ll 1$) the perturbation due to fluctuations in the intermolecular potentials decays rapidly and phase relaxation is much slower. $\phi_{pp}(t)$ decays more slowly and the band profile significantly narrows. For

times $t > \tau_m$ an exponential decay of $\phi_{pp}(t)$ is observed. In the fast modulation limit essentially motional narrowing is observed.
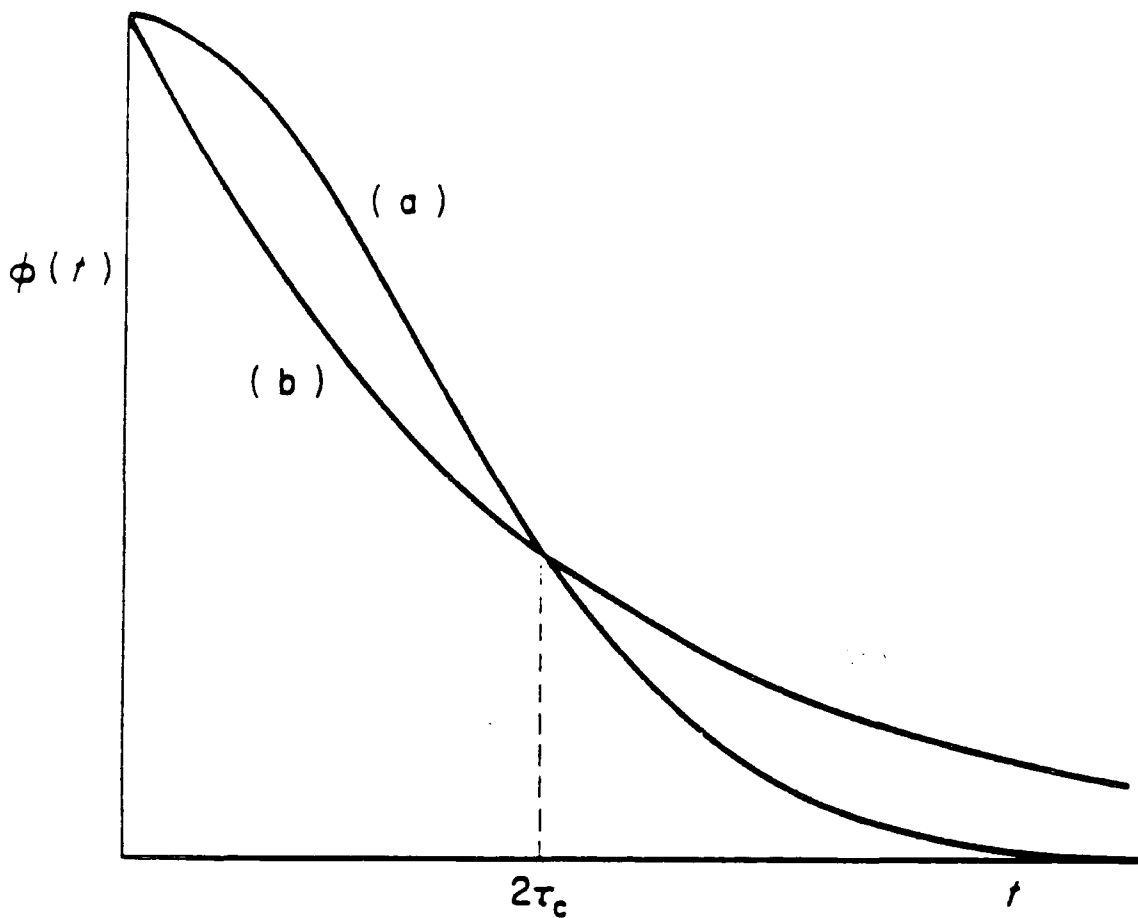
Figure 2.8. The behaviour of $\phi(t)$ in (a) the slow modulation $(\tau_m \langle \omega^2 \rangle^{1/2} \gg 1)$ and (b) rapid modulation $(\tau_m \langle \omega^2 \rangle^{1/2} \ll 1)$ limits. Reproduced, by permission, from reference 37 .

If it is possible to obtain reliable second-moments from integration of the isotropic Raman band profile or by calculating $(d\ln\phi_{pp}(t)/dt)_{t=0}$ [see Eqn.2.34] then both τ_m and $<\omega^2>$ can be obtained experimentally. Both contain valuable information about the intermolecular potential[37].

2.3.2 Reorientational relaxation

The reorientational correlation function describes the time development of the angular dependent part of the transition moment, which depends on the rank of the transition moment tensor, and the molecular fixed direction which is dependent on the intramolecular and intermolecular reorientational fluctuations. The decay of the correlation function is known as reorientational relaxation.

As has been shown in this chapter the reorientational correlation function $<P_1[\vec{\mu}(0).\vec{\mu}(t)]>$ can often be obtained from the Raman I_{VH} - I_{VV} experiment, see Appendix 1. It can also be obtained from purely rotational far infrared[58] (l=1) and depolarised Rayleigh[59] (l=2) spectra which depend on autocorrelation functions of the type

$$\sum_i <P_1[\vec{\mu}_i(0).\vec{\mu}_i(t)]> + \sum_{i \neq j} <P_1[\vec{\mu}_i(0).\vec{\mu}_j(t)]> \qquad \text{Eqn.2.38}$$

The second term in Eqn.2.38 involving cross correlations between molecules i and j has usually, but not always[60] been considered unimportant for vibrational-rotational (IR and Raman) spectra. Therefore infrared and Raman spectra usually yield the first term in Eqn.2.38. However (as explained in section 2.2.3) cross correlation terms may be observed in the reorientational correlation function if the vibrational relaxation function contains non-zero distinct terms and the vibrational and reorientational relaxation processes cannot be considered to be independent.

The first term in Eqn.2.38 the single particle correlation function is therefore usually obtainable from infrared (l=1) or from Raman or NMR (l=2). Whereas depolarized Rayleigh and far infrared spectra reflect the inclusion of both the terms in Eqn.2.38. A comparison of reorientational correlation times obtained by the different techniques may therefore give important information about the degree to which motions of different molecules are coupled via intermolecular forces.

The processes which give rise to the reorientational band width increment and lead to the decay of the associated reorientational correlation function are similar to the dephasing processes described in 2.3.1. Rotational transition energies are small compared to vibrational excitation energies encountered in mid-infrared and Raman. An ensemble average over a Boltzmann distribution is observed. This ensemble averaging of rotational energies leads to the loss of the initial coherence of the reorientational correlation function, since the rotational energies are "smeared out". It is the nature and rate of collisions and reorientation which control the rotational energies and thus the observed relaxation. Observation of the reorientational correlation functions therefore allow an insight into the rates of collisions and reorientational motions.

Attempts to model the reorientational relaxation are constructed in terms of orientational (positional) and kinetic (angular momentum) coordinates. The models usually contain parameters such as collision times[61], residence times, jump times, friction/torque parameters[62], and shape

parameters to describe any deviation from "pseudo-free" rotation.

The most frequently used models used to describe reorientational motion are based on Stoke-Einstein-Debye (SED) theory[63]. One of the most extensively used models of this type is the "extended diffusion" model of Gordon[64], applied to the study of rotational processes in liquids by Kivelson and McClung[65,66].

Models proposed for use with spectra arising in the far infrared region are more complicated as it is known that for polar molecules this absorption process is a result of several different and simultaneous phenomena. Of these, the contributions from the short time part of the overall Debye relaxation process[67] and the collision induced enhancement[68] of the transition dipole both provide information about the intermolecular potential. One particularly successful model for dielectric and far infrared spectra of dipolar liquids has been proposed by Coffey and his co-workers[69,70]. It is based on the itinerant oscillator (IO) model in which the librator is surrounded by a "cage" of nearest neighbours which restrict any motion but which do not contribute to the molecular polarizability (ie no induced intensity). Reorientational diffusion of the central molecule is assumed to be restricted by interaction with the surrounding molecules and assumed not to be affected by collisions. The far infrared absorption band can be predicted by solving the (Langevin) equations of motion for the molecules. The equations take into account the dipolar angles, the angular frequency, the moments of inertia of the molecules frictional and torque parameters (the torques on the

molecule are presumed to arise from dipole-dipole coupling),
and a parameter related to the strength of the
intermolecular potential which describes the potential well
depth. The equations are solved in terms of the complex
polarizability which can then be related to the
absorption[69]. This model has been applied successfully to
account for the spectra of simple liquids such as CH_3CN[71]
and CH_3Cl[66]. As of yet no attempt has been made to fit the
IO model to more complex molecules. It is unlikely that
this would be successful as the model assumes that the
surrounding cage is a rigid framework, some account for
flexibility would have to be included in the model.

Reorientational motion for larger molecules becomes
slower, due to size and steric hindrances. They also become
more difficult to describe using theoretical models. The
vibrational relaxation plays an increasingly important role
in determining vibrational band shapes for larger molecules.
It is unlikely for large molecules that mid-infrared and
Raman studies can adequately extract reorientational
correlation functions which arise as a consequence of
overall molecular rotation. However if intramolecular
reorientation is significant then this may contribute an
observable increment to the band width, and reorientational
correlation functions for such motions could be obtained.
Intramolecular motion is extremely difficult to model for
large flexible molecules, however spectroscopic studies can
help to give an idea of how flexible the molecules are and
which interactions are important in controlling this. This
"flexibility" must in some way control the macroscopic

properties of the fluid and hopefully any information obtained could be linked to these properties.

2.4 The use of spectroscopic techniques to study the molecular dynamics, interactions and conformations of non-rigid molecules

Spectroscopic techniques are now used almost routinely, but with care, to probe the molecular interactions and motions of condensed phase molecules, in order to investigate how they effect the macroscopic properties of the fluid. This is achieved through the analysis of vibrational frequencies, band intensities and band shapes or the associated correlation function as a function of concentration, temperature and pressure. Investigations have been limited in the main to fairly small rigid molecules[44,53,73,74] which facilitate a more accessible theoretical approach to interpreting the data. In particular most models for molecular reorientational motion in dense fluids[44,53,74-76] assume a rigid molecular framework. Interpretation of results obtained on more flexible systems is more complicated, due to the increase in internal motions. It has been shown that increased flexibility makes a significant difference to molecular motions and interactions, which consequently alters the values of physical parameters such as diffusion coefficients[77]. Flexibility must be taken into account when attempting to interpret vibrational band shapes and correlation functions of longer chain molecules[78]. Methods of analysis and interpretation of vibrational spectra of flexible molecules are limited, as those developed are designed to deal with simple rigid molecules.

Such fluids need to be studied using a variety of

techniques, under favourable conditions (as discussed in this chapter), and employing the knowledge gained from studies on simpler systems, useful information about the intermolecular potentials and molecular dynamics can be obtained. With a suitable choice of molecular size, shape and environment it ought to be possible to separate vibrational from reorientational effects, and internal from overall reorientational motion. This section is a brief discussion of some of the work of this nature already carried out.

Several studies of the conformational populations and dynamics of normal alkanes and their derivatives have been made. If the molecule is relatively short the number of trans/gauche conformers may be sufficiently small to permit them to be distinguished by vibrational spectroscopy. In addition the normal coordinates and vibrational frequencies of the conformers can be calculated and used in analysing the observed spectrum[79].

Changes in conformational populations as a function of temperature and pressure have been studied by monitoring vibrational spectral intensities[80]. Increasing the temperature has been shown to favour an increased gauche contribution to the molecular structure[81]. It has also been observed[80,82] that an increase in pressure favours the higher energy gauche conformer because these have a smaller associated molecular volume; they are more globular than the purely trans conformer. However, Wong[83,84] reported that in long alkyl chains (e.g. n-hexadecane) the pressure-induced trans/gauche transformation does not occur below about

10kbar because it is prevented by lateral compression which causes a full extension of the alkyl chains, resulting in a reduction of the total volume (of the solid). At very high pressure, the lateral compression reaches a maximum and further reduction in total volume can only be achieved by compression along the chain and thus the formation of gauche bonds. Schoen[85] has commented on the high pressure behaviour of the alkanes comparing it with polyethylene which, as with the long alkyl chains prefers to be in the extended chain form as the pressure is increased. Polyethylene molecules appear to be in an ordered liquid phase at about 5kbar. Wong[82-84] reported that the vibrational bands of alkanes also broaden upon increasing the pressure, the amount of broadening depends on the mode being studied, but in general is a consequence of the pressure-induced conformational disorder. This broadening is in common with observations made by Jonas[86-88] on a number of simpler systems. Vibrational relaxation rates were seen to increase with increasing pressure, reflecting more efficient vibrational dephasing. This increase in vibrational relaxation rate is due[86-88] to an increase in the modulation time τ_m (see Section.2.3.1) which is dependent on the viscosity (see Section 7.5.3), and/or an increase in the mean square frequency fluctuation ($<\Delta\omega^2>$. For flexible molecules $<\Delta\omega^2>$ is inevitably going to depend upon the conformational "disorder".

Schwartz and co-workers[89] have shown, for 1,2-dibromoethane, using Raman spectra of the v(C-Br) mode, that the trans and gauche isomers have different degrees of

vibrational relaxation. They demonstrated that the second moment M_{2V}^{iso}, which is a measure of the mean square frequency distribution $\langle \Delta\omega^2 \rangle$ of a mode, for the trans isomer is much higher than for the gauche. This difference in second moments results in the vibrational relaxation times τ_{iso} being lowest for the trans isomers, as (from Section.2.3.1, $\tau_{iso} = 1/M_{2v}^{iso}\tau_m$), even though the calculated modulation time τ_m for the trans isomer is smaller than that of the gauche. The overriding factor inducing more efficient dephasing of the trans form is the larger observed second moment, although it is uncertain why this is larger for the trans form than the gauche.

Wunder et al[90] studied the Raman spectral width behaviour of deuterated alkanes as function of chain length and temperature. They concluded that the chain length and temperature dependence of the d⁻ bands (antisymmetric CH2 stretching mode), for low molecular weight alkanes, can be explained in terms of end over end rotation of the molecule. However, for this mode of alkanes, with chain lengths longer than propane, hindered internal motions contribute to the band widths. Broadening occurs through the coupling of the antisymmetric stretching modes to backbone torsional motions which hinder the oscillation of the CH2 groups. This mechanism is thought to contribute very slightly to the broadening in butane and pentane, as for these short molecules end over end reorientational motions predominate. However as the chain length increases overall rotation becomes hindered, initially a decrease in band width is observed until overall rotation is too slow to contribute to the observed band width. Broadening is then solely a

consequence of internal motions. the band width is seen to
become independent of chain length. This also indicates
that broadening does not depend on the number of possible
conformations of the molecules. This is demonstrated by
Fig.2.9. as the band width of polyethylene falls on the same
band width vs temperature curve as that for nondecane. The
number of possible conformations is obviously much greater
for polyethylene because of it's increased chain length.
The temperature dependent broadening for relatively long
chain alkanes is simply a consequence of higher order
torsional modes becoming more populated at high
temperatures.
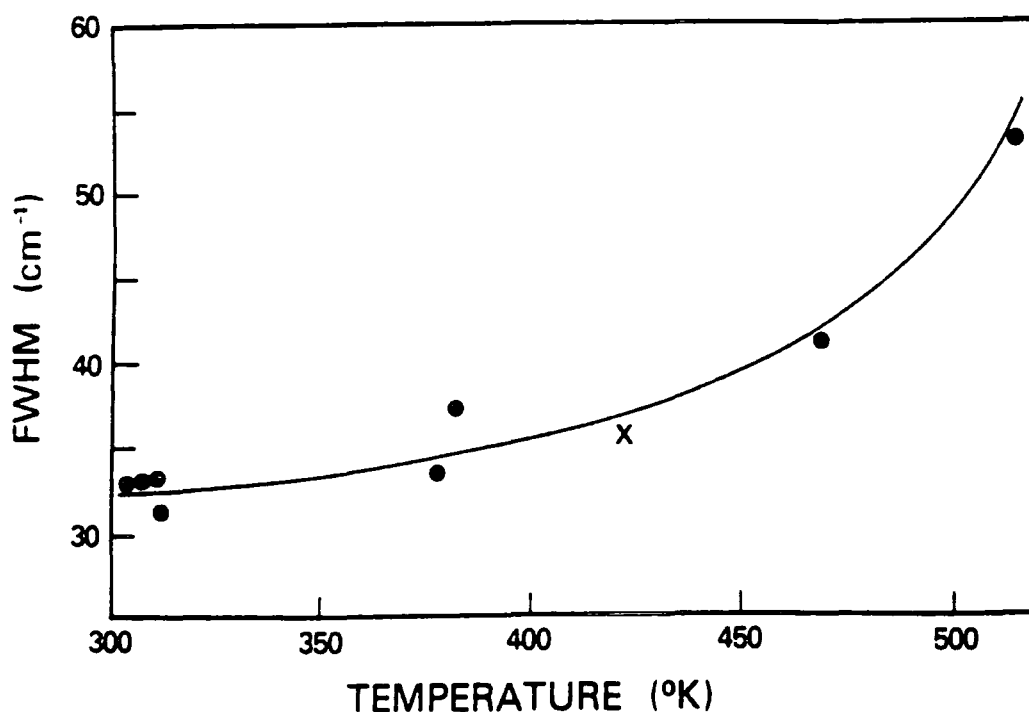
Figure 2.9. Comparison of Raman band half-widths (FWHM) of
the d⁻ bands of nonadecane (●) and polyethylene (x).
Reproduced, by permission, from reference 90 .

84

Goulay and co-workers[91] have attempted to relate the reduced infrared correlation times τ_{1R}^{*} , obtained for the two vibrational modes $\upsilon(\equiv C\text{-}H)$ and $\upsilon(C\equiv C)$ of a series of 1-n-alkynes, to a hydrodynamic model. The values of τ_{1R}^{*}, for the alkynes in n-heptane, showed a very different dependence on temperature and viscosity from the data for the (rigid) acetylene molecule, as is shown in Fig.2.10. The experimental slopes for acetylene indicate that free volume effects are dominant and the results fit a collisional model of Hynes[92]. The results for the larger flexible alkyne molecules are indicative of strong collective effects. These observations may be related to a molecular flexibility affect.
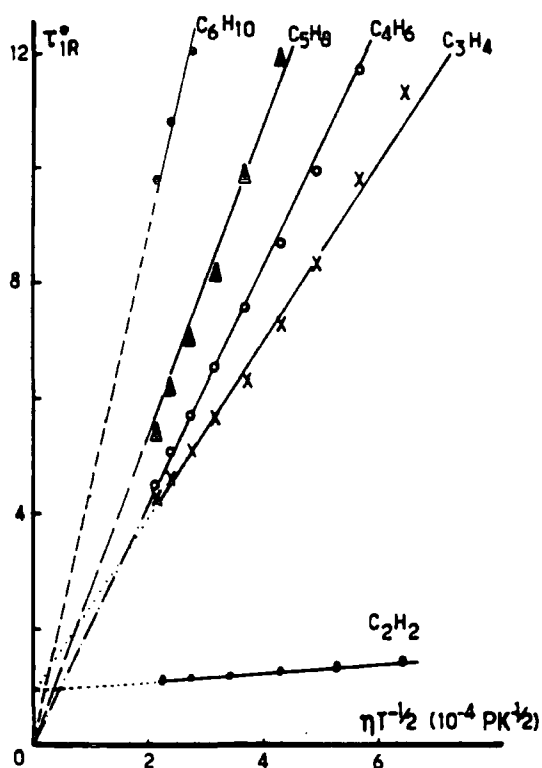
Figure 2.10. Comparison of the viscosity and temperature dependence of the reduced reorientational correlation time of acetylene with those of longer chain n-alkynes.

Reproduced, by permission, from reference 91 .

The spectral response between $1cm^{-1}$ and $300cm^{-1}$ is particularly sensitive to both intramolecular and intermolecular dynamics, and bands in this region are usually purely reorientational in origin. There have been several reports of multiple bands that appear to have multi-process origins[93-95], such phenomenon arise because different parts of the molecule may rotate at different rates, or because the shape of the molecule allows for more than one axis for overall rotation with different rotation rates. Normal hexane has been shown[94] to have a dipole correlation function which decays with two relaxation times of 3 and 8 psec. The short relaxation is said to describe rotations about the long axis, while rotational diffusion about the short axis is said to occur on the longer time scale.

The more polar molecules like the ketones, aldehydes or esters give bands in the 1 to $300cm^{-1}$ region due to both intermolecular rotational motion and internal (librational) rotations. For example Vij and Hufnagel studied a series of non rigid ketone molecules of increasing chain length[95]. They found that in addition to the well known Poley[96] absorption, which is an internal mode found at about $50cm^{-1}$, there appears a secondary absorption profile at about $300cm^{-1}$. This is demonstrated in Fig.2.11, which also shows that the two bands change in relative intensity as the chain lengthens. The secondary absorption band is seen to depend upon the flexibility of the ketone molecule, as such no profile is seen for acetone (which has almost rigid molecules), see Fig.2.11. They assign this secondary band to an intra-librational motion of the $-CO$ and $-CH_3CO$ about

86

the backbone to which they are attached.

Finally in this section it is important to point out the vital role that NMR can play in determining the motions of flexible molecules. The information content of NMR relaxation experiments is high as it is possible to study nuclei along the whole of the molecule. This under favourable conditions allows calculation of correlation times for internal motions and a correlation time for overall molecular tumbling[31,96-100]. However it is not always certain what motions are being observed. NMR can also allow the measurement of self diffusion coefficients[100].
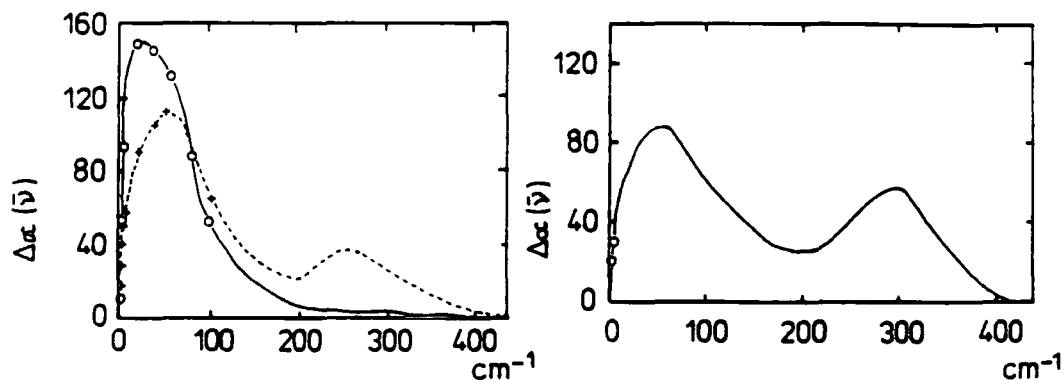
Figure 2.11. Far-infrared spectra of liquid acetone (o) and hexanone (---) at ambient temperature. The right hand spectrum demonstrates (for undecanone-6) that the two bands change in relative intensity as the chain lengthens.

Reproduced, by permission, from reference 95 .

CHAPTER 3

EXPERIMENTAL

3.1 Raman Spectroscopy

Raman spectra were obtained both at Newcastle Polytechnic and Durham University. The variable temperature and initial 10% mole fraction solution studies were recorded at Newcastle on a Spex 1403 double monochromator and Datamate computer, see Fig.3.1. The Raman spectra of EHB at different concentrations in hexane and the ruby fluorescence spectra, required for pressure calibration of the diamond anvil cell for the infrared work, were obtained in Durham using a Cary Model 82 spectrometer linked to a Glen Spectra IBM-SCADAS (Spectrometer Control and Data Aquisition System). Excitation is provided by the green 514.5nm line from a Spectra Physics argon ion laser and a Cambridge Lasers CL-4 argon ion laser in Newcastle and Durham respectively. With both systems the light passes through a premonochromator where it is dispersed by prisms set to allow only the 514.5nm line to pass through. The light is then focused into the 90° scattering compartment and on to the sample. Scattered light from the sample passes through a polarizer, if polarization analysis is required, and then through a light scrambler to remove any polarisation properties from the scattered light. The light is then directed onto the entrance slit of the monochromator. Light detection in the two systems is provided by cooled photomultipliers linked to the photon counting electronics of the respective computer systems. All spectra with the exception of the ruby fluorescence spectra were calibrated against a mercury emission line, from the lights, at $1122.5cm^{-1}$.
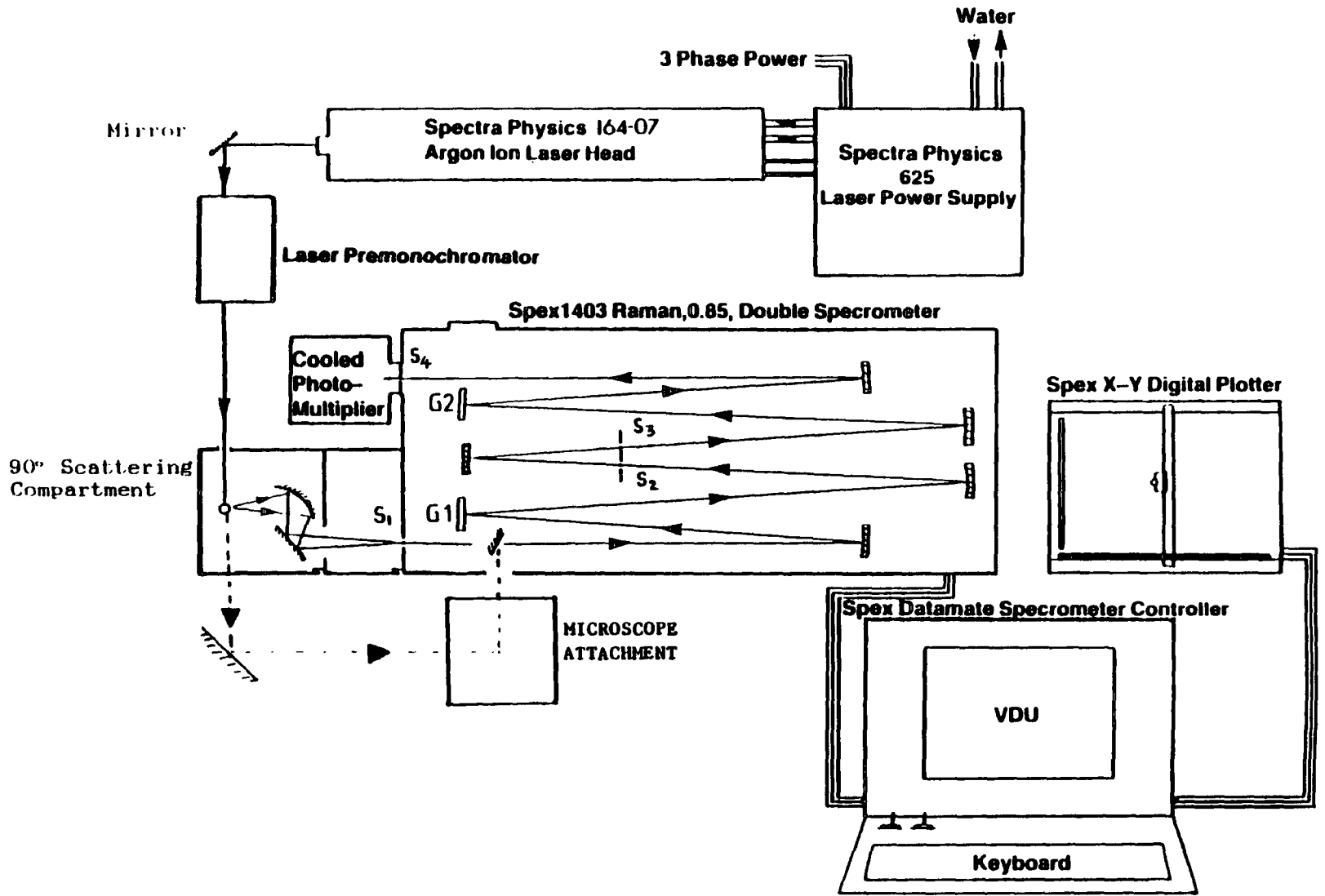
Figure 3.1. The Raman system used at Newcastle Polytechnic.

90

3.1.1 Solution Studies

All the Raman solution work was carried out with the
solutions contained in an optically flat glass cuvette held
in the focal position at the optical axis of the collection
optics. All chemicals used were of 99+ % spectrophotometric
grade purity, and, with the exception of EHB, were obtained
from the "Aldrich Chemical Company Limited" (Gillingham,
England). Solutions were made up by weight to the required
mole fraction.

3.1.2 Temperature Variation

High temperature Raman work was carried out using a
brass block coupled to three heating elements. The sample
is contained in a sealed glass tube within the block.
Temperature measurements can be made using a chromel-alumel
thermocouple attached to the brass block. The arrangement
is shown in Fig.3.2.

For low temperature Raman work a glass Dewar cell was
used, see Fig.3.3. The sample is contained in an evacuated
sealed glass tube held within contact with the required
coolant. To prevent condensation on the windows of the cell
the cell is evacuated and sealed before use. Again
temperature measurement is achieved using a chromel-alumel
thermocouple attached to the copper block.
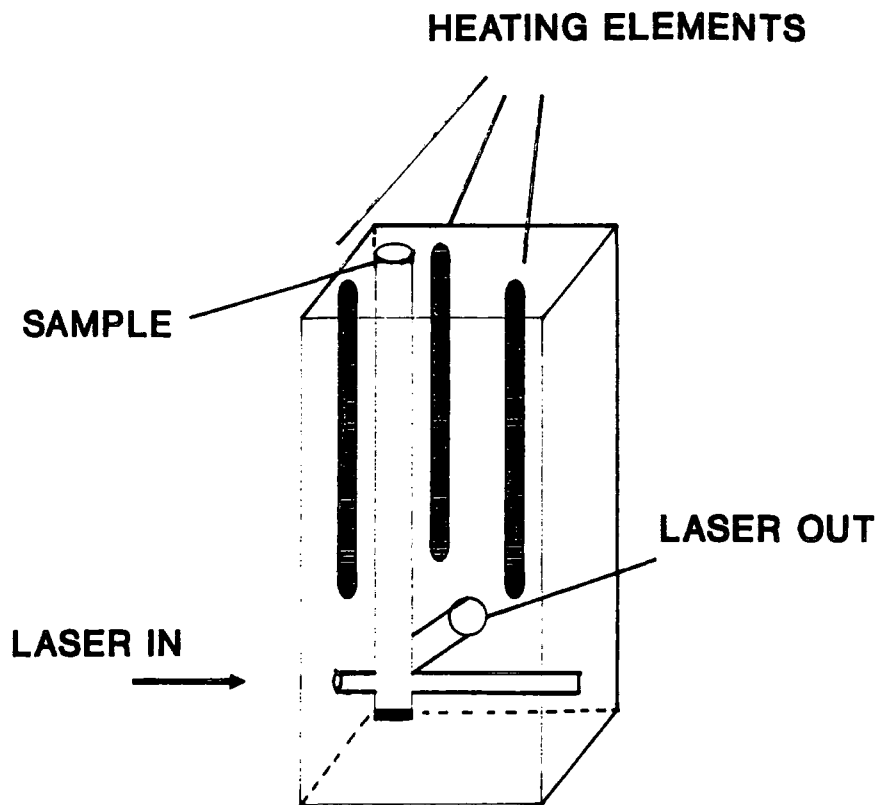
Figure 3.2. High temperature Raman cell.
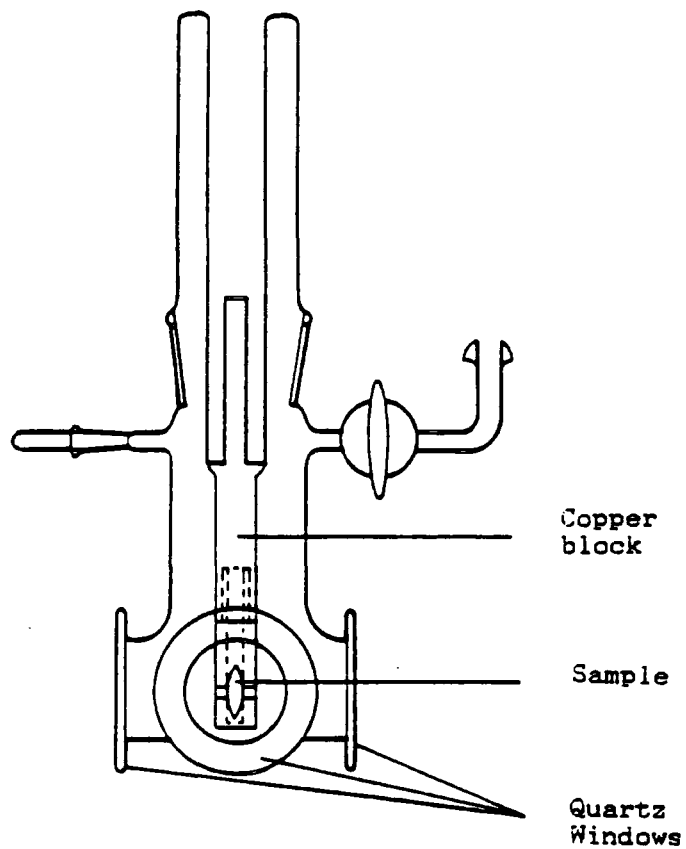
Figure 3.3. Low temperature Raman cell.

3.2 Mid-Infrared Spectroscopy

All the mid-infrared, $400cm^{-1}$ to $4800cm^{-1}$, work was carried out using a Mattson Instruments Sirius 100 Fourier Transform Infrared Spectrometer, see Fig.3.4, linked to the Mattson Starlab computer system. This is a rapid scanning FTIR instrument, the interferometer of which incorporates cube corner retroreflectors for both the moving and fixed interferometer mirrors[101]. It is a single beam instrument, this means that interferograms are recorded for sample and background separately and a ratio is performed in the frequency domain to obtain the absorption spectra. Spectra were obtained with the use of a water-cooled globar source, germanium coated KBr beam-splitter and liquid nitrogen cooled Mercury Cadmium Telluride (MCT) "Bullseye" Detector. Interferograms were processed using a triangular apodization function. Resolutions of $1cm^{-1}$ and $4cm^{-1}$ were used for the solution work and DAC spectra respectively.

3.2.1 Solution studies

Solvents were as described in Section 3.1.1. For the mid-infrared solution studies on EHB $12\mu m$ films between KBr plates were used, apart for the very low concentration solutions where longer pathlengths were employed. Spectra were obtained either by ratioing single beam spectra of solution and solvent or, if the solvent absorbed in a region of interest, both solution and solvent single beam spectra were ratioed against an instrument background single beam
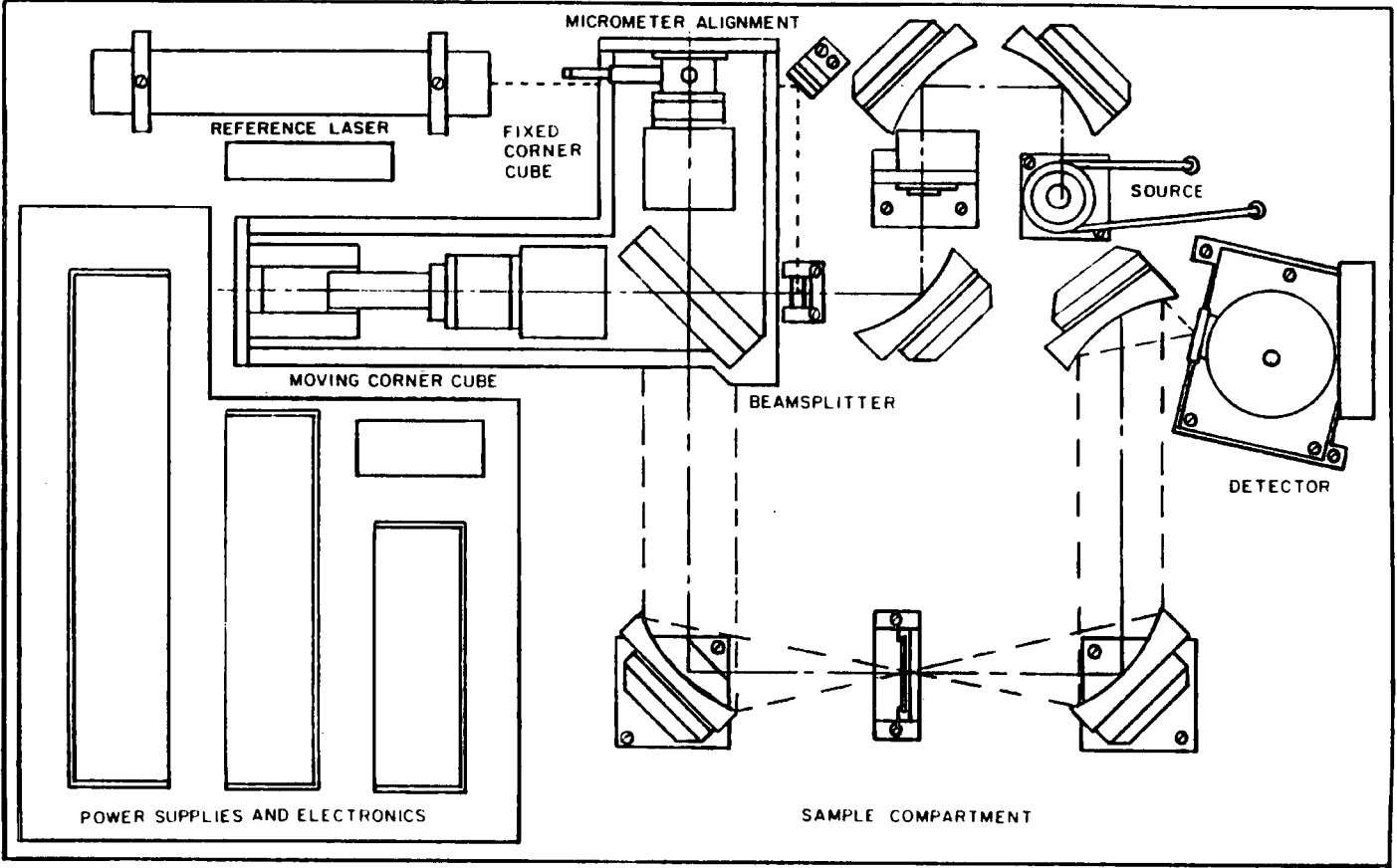
Figure 3.4. The Mattson Sirius 100 FTIR instrument.

MICROMETER ALIGNMENT

REFERENCE LASER

FIXED
CORNER
CUBE

SOURCE

MOVING CORNER CUBE

BEAMSPLITTER

DETECTOR

POWER SUPPLIES AND ELECTRONICS

SAMPLE COMPARTMENT

spectrum. The resulting solution absorption spectra then had the solvent absorption contribution removed by subtraction of a fraction of the solvent absorption spectrum. Due to the presence of water vapour and the intensity and position of some of the EHB bands it was necessary to purge the instrument with nitrogen gas, and in some cases to subtract water vapour from spectra. In the case of the DAC experiments purging was not possible and so water vapour subtraction was usually necessary.

3.2.2 High pressure mid-infrared research

High pressure mid-infrared spectra, were obtained using a diamond anvil cell (DAC)[102], designed and manufactured by Dr David Adams of "Diacell Products"[103]. In this cell high pressure is applied to a sample by forcing two flat faced diamond anvils (of type IIA diamonds) together along a common axis. One diamond is mounted, using Araldite epoxy resin, on a plate of hardened tool steel set into the base of a cylinder. The opposing diamond is mounted, in a similar way, on a piston. also of hardened tool steel, which fits tightly into the cylinder, see Fig.3.5. If the cell is being used with liquids a gasket is required to hold the liquid in place. For the infrared work, using EHB, copper gaskets of a thickness of 0.08mm were used, for Raman spectroscopy it is more usual to use a gasket of 0.2mm. The sample is held in a tiny hole, of approximately 0.5mm diameter, in the gasket, between the two diamond faces, see Fig.3.5. A cradle system holds the diamond cell and
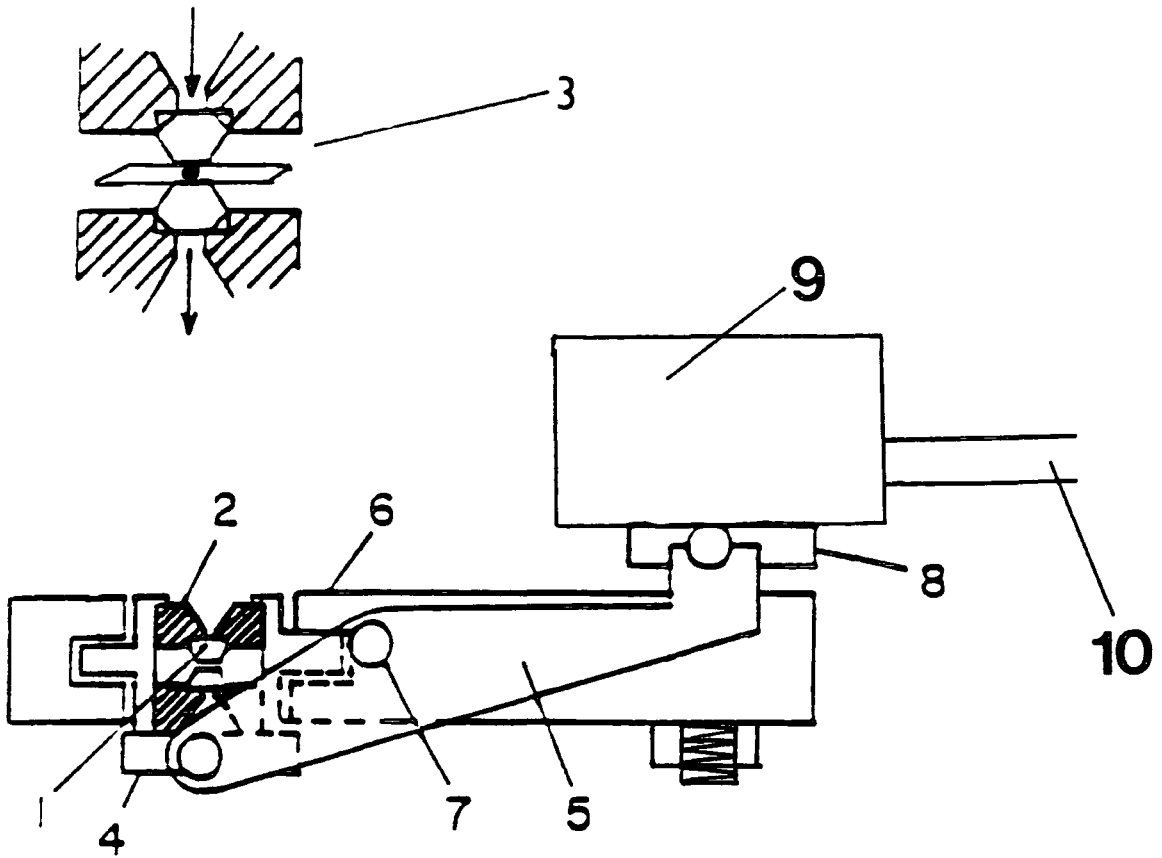
Figure 3.5. The diamond anvil cell and pressurising system;
(1) diamond anvil, (2) pistons, (3) DAC with gasket,
(4)pressure transmitting plate, (5) lever arm, (6)
supporting block, (7) pinion, (8) plate, (9) piston, (10) to
the pump.

facilitates high pressure generation by the lever action of a hydraulically operated piston, see Fig.3.5. The "Hydrapak" pump, manufactured by "Tangye Limited", was employed to generate the pressure for the system. A 50:50 mixture of brake fluid oil and castor oil was found to operate as the best pressure transmitting fluid in the pump.

Pressure determination in the DAC is achieved by use of the pressure related shift of the strong fluorescence emission lines, R1 and R2, of ruby found at 14400 and $14430cm^{-1}$ respectively[104-106], see Fig.3.6. In ruby purely electronic transitions are responsible for the R-lines and there is no Stokes shift present. The transitions take place between the ^2E and $^4A_2$ crystal field split states of the Cr^{3+} ion. The ^2E state is split into two states $\bar{E}$ and $2\bar{A}$ and it is this splitting which is responsible for the two peaks. These lines show a linear frequency shift of 0.77 and $0.86cm^{-1}$/kbar respectively, to at least 50kbar[104-106]. The most reliable procedure for setting up the DAC with gasket, ruby and liquid was found to be; (1) Using a microscope, and illuminating the DAC with a white light source, a small drop of liquid should be placed on to the face of the cylinder diamond, using a syringe needle; (2) The gasket can then be placed on to this diamond, in a way that the gasket hole completely covers the diamond face; (3) A small amount of powdered ruby should then be introduced to the gasket hole. Care must be taken to ensure that the ruby fills no more than 20% of the gasket hole, otherwise, as pressure is applied, this may cause a non hydrostatic environment. Non-hydrostatic pressure in the liquid sample may arise due to a number of reasons, the major ones being;
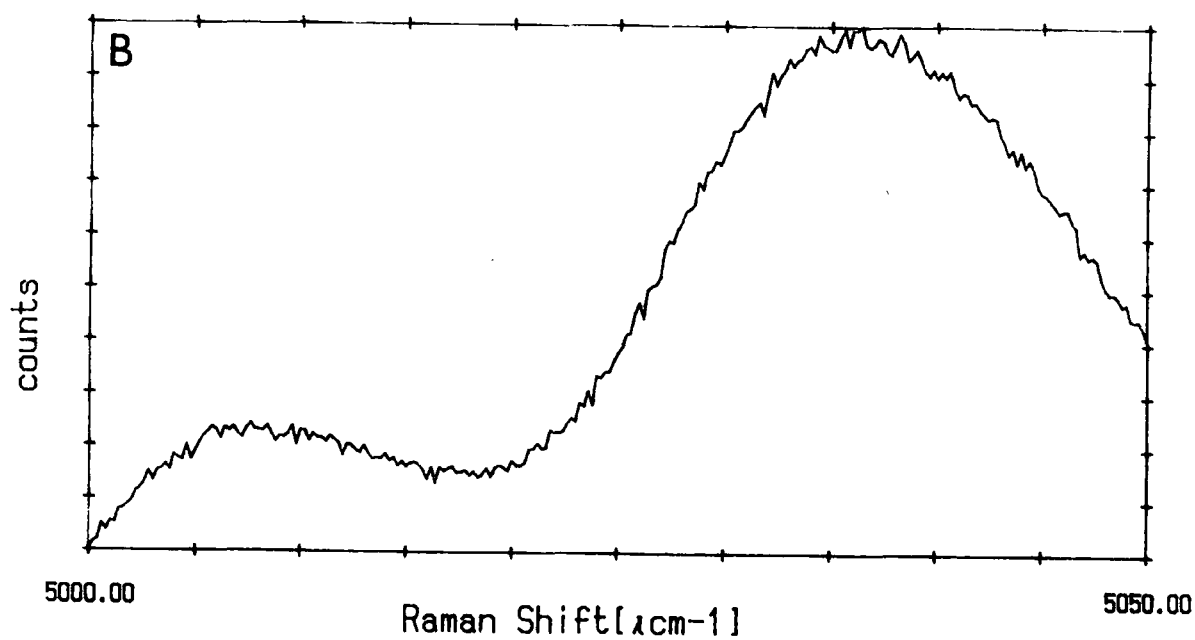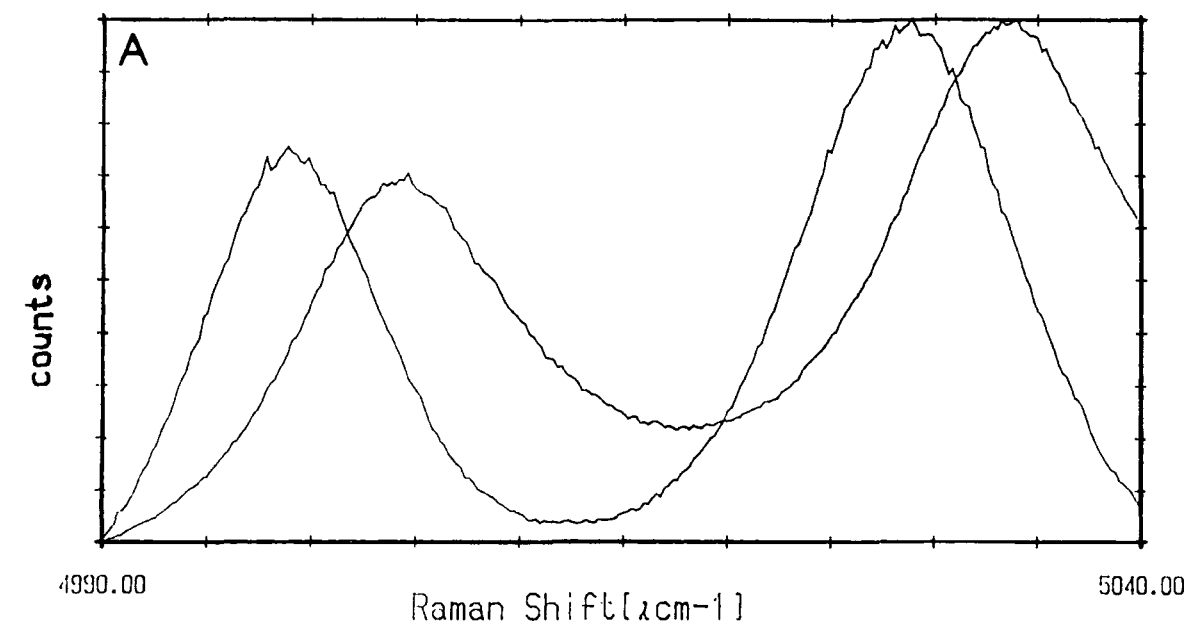
Figure 3.6. Typical ruby fluorescence spectra; (a) At 1bar and 6.5kbar hydrostatic pressure; (b) Under non-hydrostatic pressure.

(a) A poorly drilled gasket hole; (b) The hole is offset from true alignment with the diamond faces; (c) There is too much ruby present (or the pieces of ruby are too big); or (d) The majority of the liquid has been squeezed out from the gasket hole. However non-hydrostatic pressure can be readily observed as the ruby lines tend to broaden considerably and do not retain their $29cm^{-1}$ spacing,[105,106], see Fig.3.6.

For Raman work using the DAC the ruby calibration spectra and sample spectra can be obtained using the same instrument and set up[107]. However with infrared work, the ruby fluorescence cannot be measured using the infrared spectrometer so a separate measurement of the fluorescence spectra is required, this was obtained using the Cary model 82 spectrometer. Due to lack of space between our instrument focal position and collection optics the usual 180° scattering configuration for use with the DAC[102] could not be employed. Therefore, using three flat mirrors the laser is brought into the back of the DAC, effectively employing a 0° scattering configuration. Very little laser power is required to obtain a good fluorescence spectrum, typically 50mW at the sample provides a signal strength of 5 × 10^{4} counts/sec with a slitwidth of $2cm^{-1}$. In both cases the position of the lines were measured relative to a nearby neon emission line at $14431cm^{-1}$.

Infrared spectra through the DAC were obtained by ratioing single beam spectra of EHB in the DAC against single beam spectra of deuterated hexadecane in the DAC. This was found to be necessary to minimise the effects of fringes in the interferograms produced by a small percentage

99

of radiation being reflected by the diamond faces, Fig.3.7
shows the resultant absorption spectra produced by ratioing
DAC with EHB and empty DAC single beam spectra.
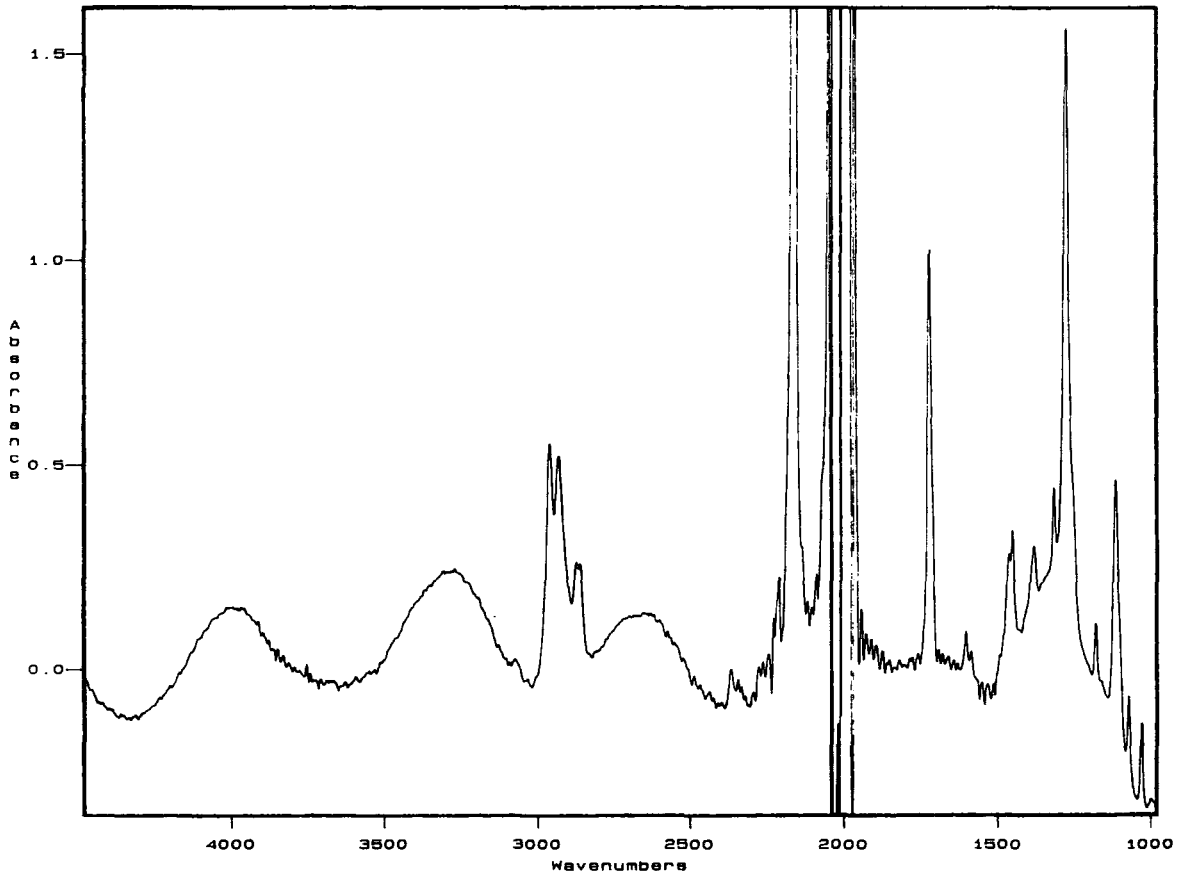
Figure 3.7. Example of effect on absorption spectra,
obtained through DAC, if contribution from interference
fringes is not adequately minimised. Spectrum is of EHB at
1bar.

3.3 Far Infrared Spectroscopy

A Beckman FS720 Michelson interferometer, see Fig 3.8, was used to collect all the far infrared spectra recorded in this work. This is a slow scanning interferometer which employs a moving mirror driven by a stepping motor, the signal at the detector is measured after each step. There is an inherent amount of "slack" in the stepping motor and it is essential to take this up using the inch control on the stepping motor controller before starting to record an interferogram. The sample is placed in the sample container just before the detector. The sample is irradiated by the emission from a mercury arc lamp, which has been through the interferometer optics, of beam splitter stationary mirror and stepping mirror. Phase modulation is achieved by jitter of the stationary mirror. The mirror is attached to a ling vibrator, the jitter is controlled by means of a power oscillator, so that the frequency and amplitude of vibration can be varied. The frequency should be tuned to match the attributes of the detector that is used. The Golay detector operates better with a frequency of between 11 and 15 Hz, whereas the efficiency of the bolometer detectors improves at frequencies up to an order of magnitude higher than this[108], though multiples of 50 HZ should be avoided as mains interference can be a problem.

The waveform from the phase modulator is fed into the reference channel of a lock-in amplifier. The signal from the detector is fed into a preamplifier before the lock in amplifier so that a wider range of sensitivities can be accessed and full dynamic range of the analogue to digital
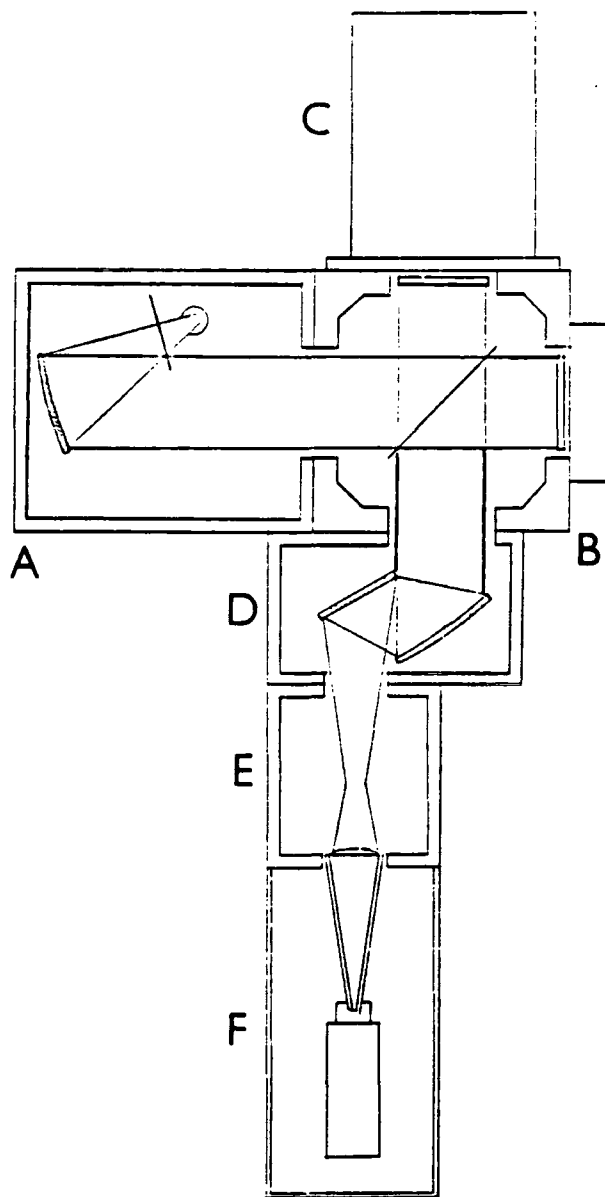
Figure 3.8. Schematic representation of the Beckman FS720 Michelson interferometer. A contains the mercury arc lamp and collimating optics; B contains the beam splitter mounting optics and fixed mirror; C contains the moving mirror and drive; in D is the condensing optics; E is the sample chamber; and F is the detector module.

converter can be achieved. For the collection and analysis
of data, the interferometer is linked to a Duet 16
microcomputer. Fig 3.9 shows the layout of the
interferometer electronics.
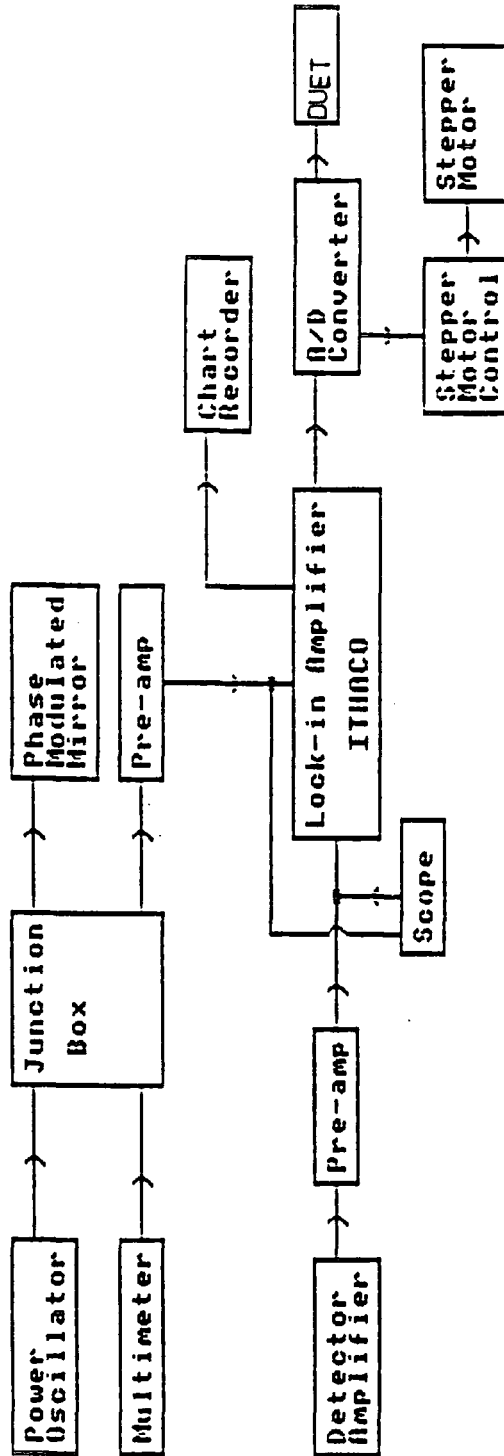
Figure 3.9. Layout of interferometer electronics.

It is necessary to evacuate the interferometer using a rotary pump connected to a vacuum line and to purge the sample compartment using dry nitrogen gas, in order to remove intense bands caused by water vapour.

Unlike the Mattson and Raman spectrometers, a number of scans cannot be rapidly accumulated and averaged before analysis. However the average of a number of absorption spectra can be computed or if necessary a number of modulus spectra may be added together and averaged before computation of the absorption spectra.

3.3.1 Far infrared detectors

Two types of detector are available for use with the Beckman FS720, IR50 Golay detectors[109,110] and helium cooled germanium or indium/antimony bolometers[111,112]. Golay detectors are pneumatic in operation, a gas filled bladder expands when heated by the infrared radiation, expansion is monitored by a photodiode. As such the Golay is sensitive to external vibrations and temperature variations, and the output signal is likely to be noisy. A diamond windowed Golay detector is necessary for work above $120 cm^{-1}$, but below this a quartz windowed detector is sufficient. The germanium bolometer houses a single antimony doped crystal of germanium. The antimony gives rise to donor levels close to the conduction band of germanium. Electrons from the donor levels are excited by infrared radiation into the conduction band and change the resistivity of the crystal. The indium/antimony bolometers work in much the same way.

The signal outputted by the detector is directly related to the resistivity of the crystal and is free from mechanical noise. The efficiency of the bolometers in terms of signal to noise is much greater than that of the Golay detectors. However it is much more difficult to use as it requires cooling to liquid helium temperatures.

By use of a number of bolometers and various thickness beam splitters it is possible to obtain data ranging from $3\text{-}4\text{cm}^{-1}$ to about 200cm^{-1}. The spectra contained in this work were obtained using a germanium bolometer with a range of 15cm^{-1} to 185cm^{-1}, using a sampling interval of $20\mu\text{m}$ and collecting 550 data points to give an effective resolution of 4cm^{-1}.

3.3.2 Solution work

Solvents were as described in Section 3.1.1. The solution spectra were obtained by ratioing 2.5mm thickness' of solution and solvent. The solution was contained in a cell comprising of a gasket, cell windows (backplate and frontplate), a spacer and cell holder. Windows made of poly-4-methylpentene-1 (TPX) were used as they are transparent to visible light and allow careful examination of the cell, as it is being filled, to prevent introduction of air bubbles into the sample. Liquid EHB spectra were obtained by ratioing 1mm and 0.5mm thick films.

3.3.3 High temperature studies

Spectra of EHB at 100°C were obtained by using the Beckman-RIIC variable temperature unit VLT-2, which incorporates a Eurotherm TEM-1C Automatic Temperature Controller with a range from 83 to 523K. The temperature was controlled by simply setting the required temperature on the dial. The cell was mounted in a cell block holder, as shown in Fig.3.10. Heating to maintain the required temperature was provided by two electrical coils mounted on the sides of the cell block. A copper-constantan thermocouple was mounted in a hole in the cell block and this was connected to the temperature control unit. This thermocouple determined the amount of heating necessary. A second thermocouple was mounted in a hole in the liquid cell top plate, this monitored the actual temperature of the cell itself.

For the high temperature experiments the cells were made up using silicon plates, as TPX tended to warp allowing the liquid to run out. At temperatures above 373K, even with silicon windows, there was too much leakage of liquid to obtain spectra. Even below 373K there was some leakage and it was necessary to use a reservoir to replenish the liquid lost.

REFRIGERANT RESERVOIR

THERMOCOUPLE HOLES

ELECTRICAL HEATERS

CELL

CELL-HOLDER BLOCK
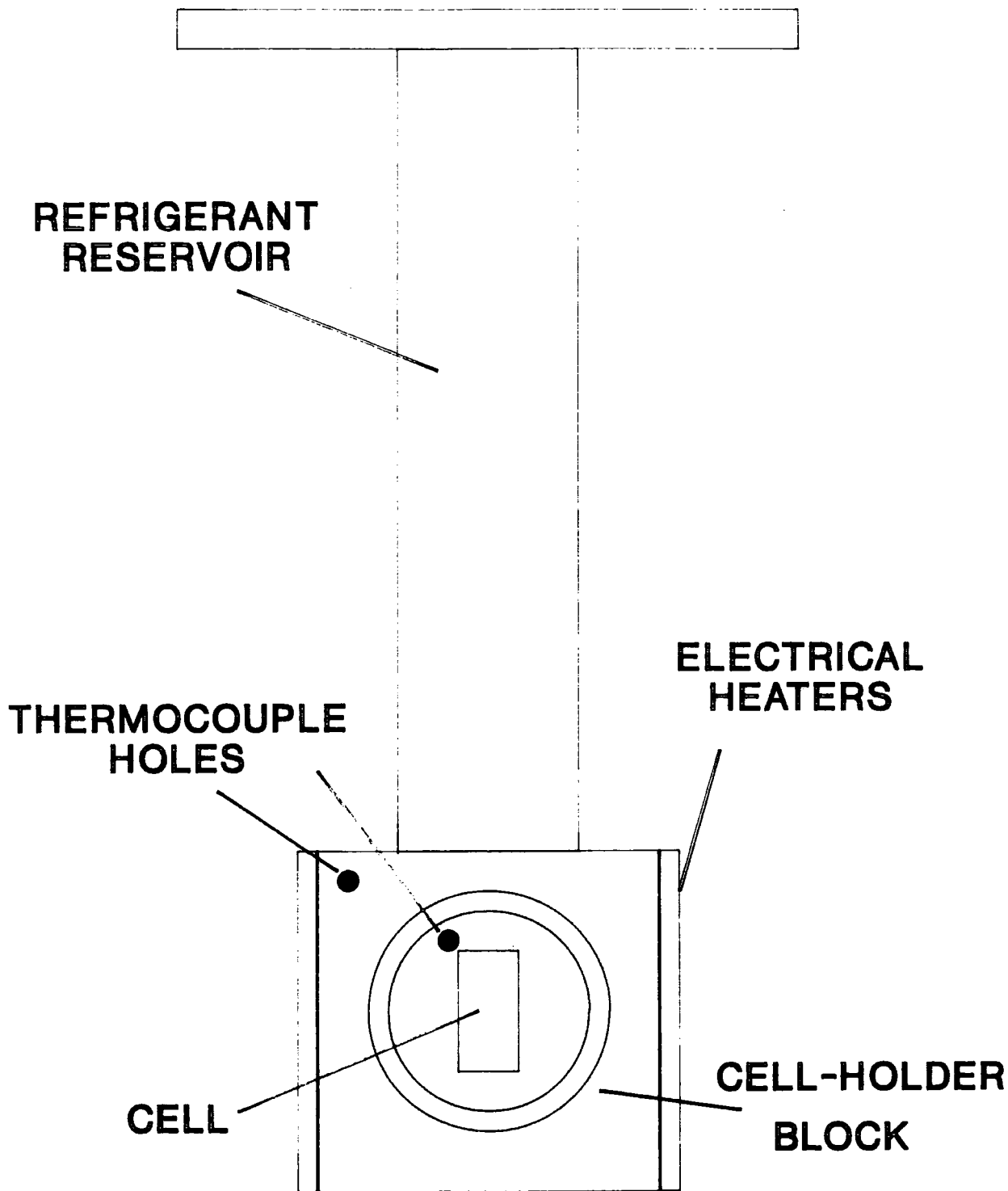
Figure 3.10. Variable temperature cell mounting block

SECTION II

RESULTS

CHAPTER 4: RESULTS OF INFRARED HIGH PRESSURE STUDY

CHAPTER 5: RESULTS OF RAMAN VARIABLE TEMPERATURE STUDY

CHAPTER 6: RESULTS OF SOLUTION STUDIES

II.1 Introduction

The following three chapters summarise all the results obtained for the work in this thesis. For the Raman work spectral bandpasses of approximately one third of the natural band width of the respective peaks were employed to minimise any contribution from the slits, these were $3cm^{-1}$ for all the bands studied except the ring deformation mode, found at $1003cm^{-1}$, for which a bandpass of $0.5cm^{-1}$ and an increment of $0.2cm^{-1}$ were used. For all the other bands increments of $0.5cm^{-1}$ were used. The anisotropic scattering spectra were taken to be the depolarised spectra. The isotropic spectra were computed from the polarised and depolarised spectra in the usual manner using the relationship, $[I_{iso} = I_{VV} - (4/3).I_{aniso}]$, discussed in Appendix I.

For the mid-infrared spectra the Starlab computer subtraction facility, was employed, when necessary, to remove any contributions from water vapour bands.

All peak frequencies and FWHM were measured by hand on plotted out spectra and checked against those given by the computers. Errors were estimated against spectral resolution, noise and reproducibility.

Figs.II.1a and II.1b display the Raman isotropic and anisotropic spectra of liquid EHB, between 2800 and $3150cm^{-1}$ and 700 and $1800cm^{-1}$ respectively. Fig.II.2 gives the full mid-IR spectra of EHB. The position of the major bands are listed in Table II.1, along with tentative assignments from the literature[113-115].
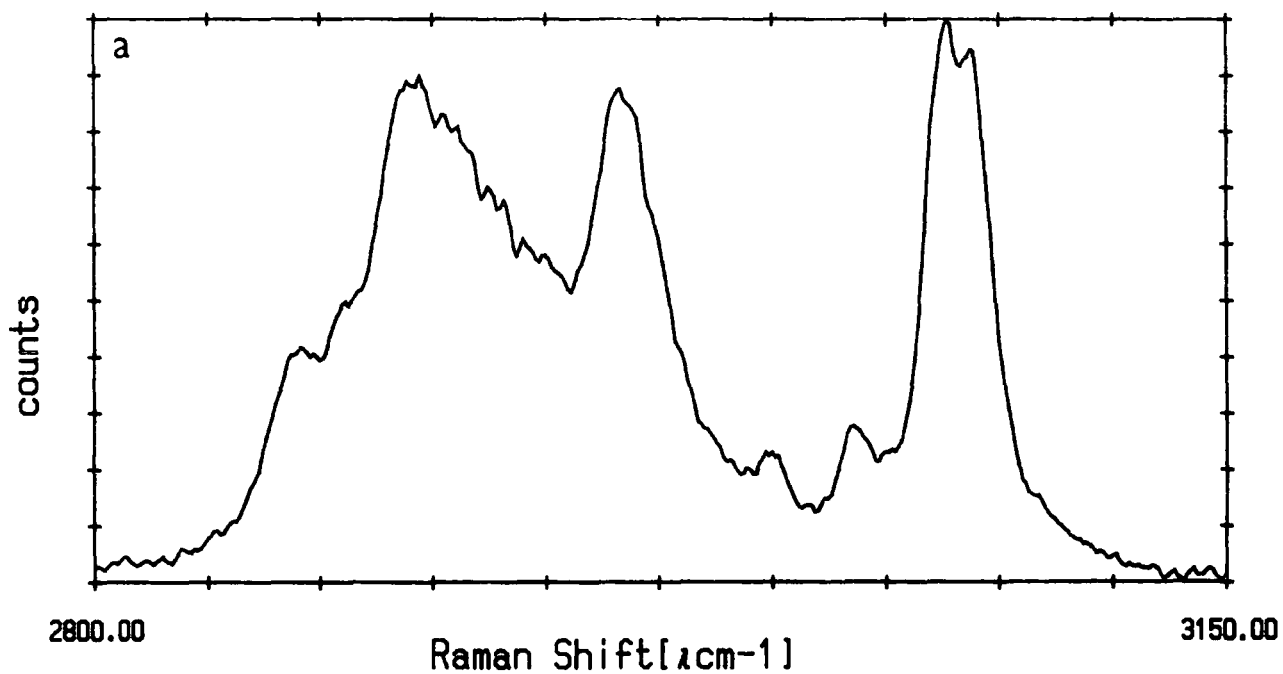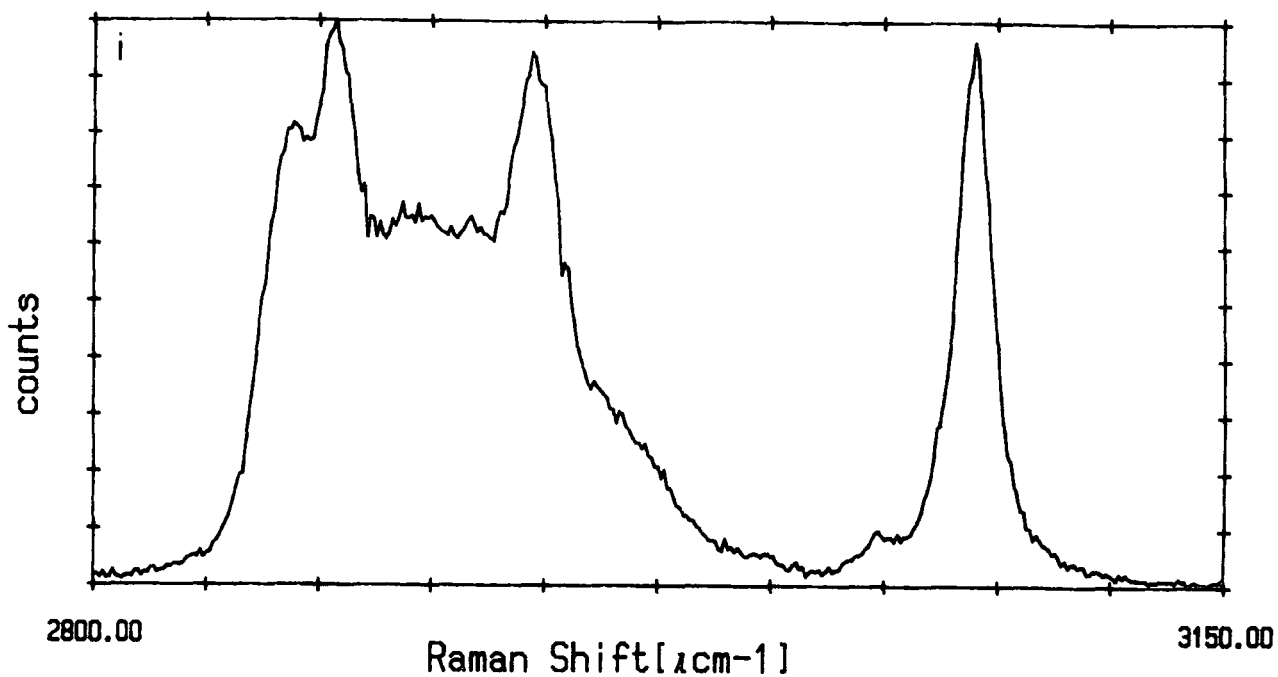
Figure II.1a. Raman isotropic and anisotropic spectra of EIIB, between 2800 and 3150cm^{-1}.

i

counts

700.00   Raman Shift[ιcm-1]   1800.00

a

counts

700.00   Raman Shift[ιcm-1]   1800.00

Figure II.1b. Raman isotropic and anisotropic spectra of EHB, between 700 and 1800cm^{-1}

110

Figure II.2. Mid-infrared spectrum of EHB

111
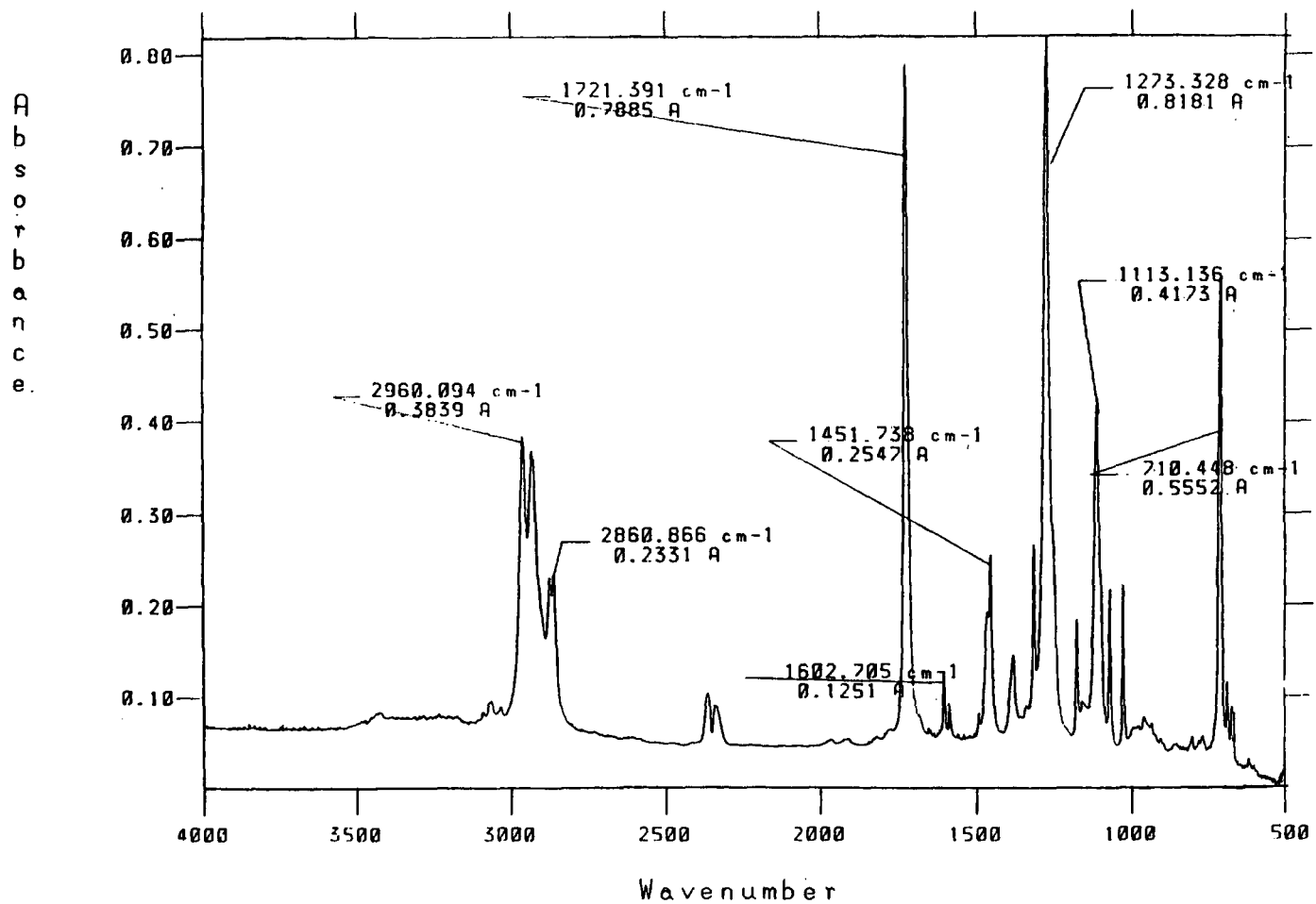
Table II.1. Major bands and assignments for vibrational spectra of EHB.

FREQUENCY RAMAN	IR	FUNCTIONAL GROUP	SYMBOL	DESCRIPTION
3073	—	$=C-H$	$v_s(=C-H)$	aromatic CH str
2962	2960	$-CH_3$	$v_{as}(CH_3)$	antisymm C-H str
2937	2932	$-CH_2-$	$v_{as}(CH_2)$	antisymm C-H str
2875	2874	$-CH_3$	$v_s(CH_3)$	symmetric C-H str
2862	2862	$-CH_2-$	$v_s(CH_2)$	symmetric C-H str
1719	1721	$-C=0$	$v(C=0)$	carbonyl CO str
1603	1603	arom $-C=C-$	$v(C=C)$	i-p C=C ring str
1585	1585	arom $-C=C-$	$v(C=C)$	i-p C=C ring str
1463	1463	$-CH_2-$	$\delta_s(CH_2)$	symm C-H bending
1452	1452	$-CH_3$	$\delta_{as}(CH_3)$	antisym C-H bending
1380	1380	$-CH_3$	$\delta_s(CH_3)$	symm C-H bending
1273	1273	$-C-0-$	$v(C-0)$	skeletal C-0 str
1175	1175	$-C-0-$	$v(C-0)$	skeletal C-0 str
1003	—	arom $-C=C-$	$v(C=C)$	ring deformation
712	712	see text	see text	see text

In liquid EHB the band at $1720 cm^{-1}$, corresponding to the carbonyl $v(C=0)$ stretching mode, shows a non-coincidence of the Raman isotropic and anisotropic peak frequency, see Fig.II.3. This can be explained in terms of a resonance energy transfer (RET) process via transition dipole - dipole coupling, this is explained in greater detail in Chapter 7.
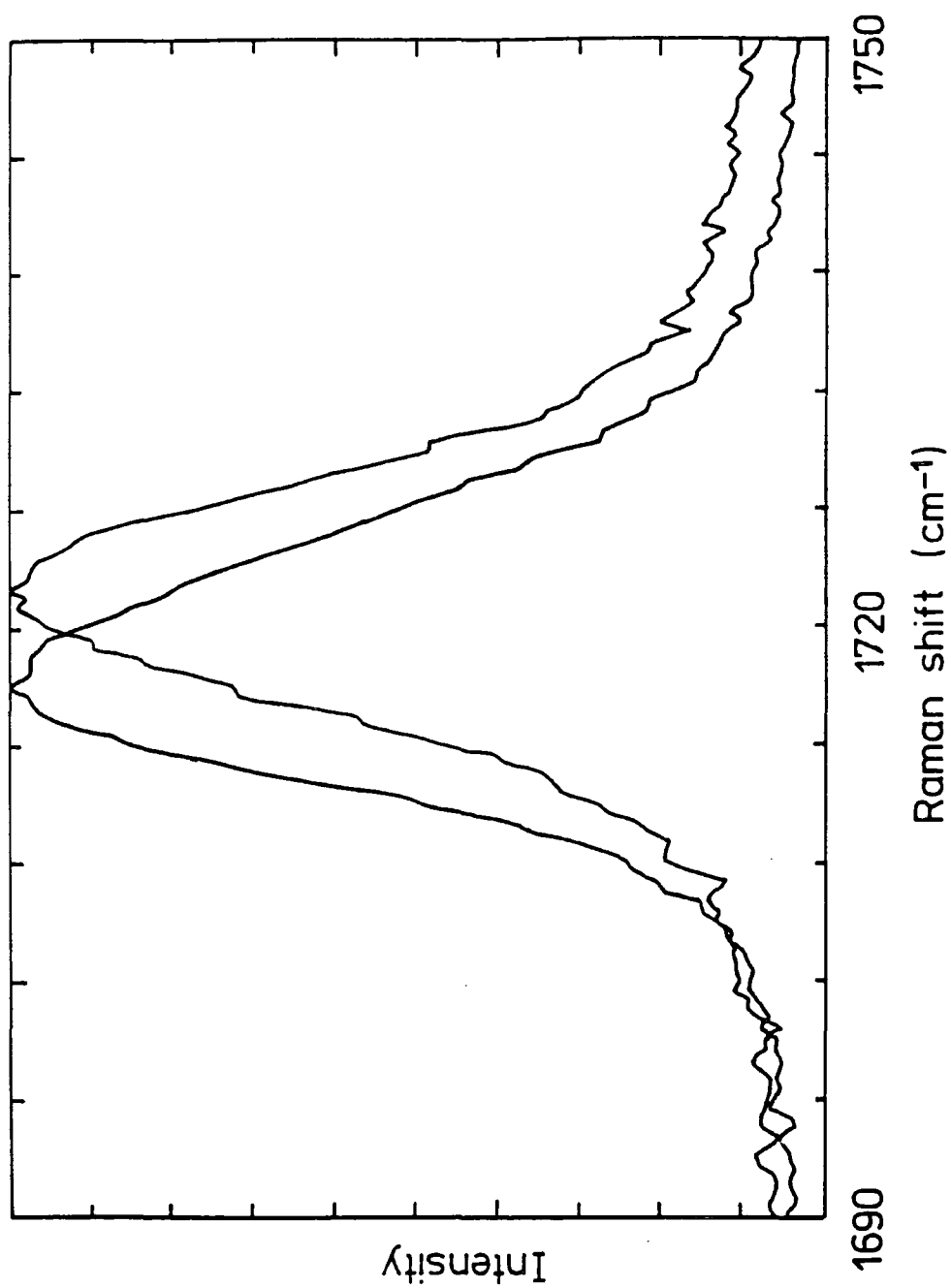
Figure II.3. The non-coincidence effect shown by the Raman
polarised and depolarised spectra of the v(C=O) stretching
mode of EHB

The far infrared spectra, between $15cm^{-1}$ and $185cm^{-1}$, have also been obtained. Figure II.4 shows the FIR spectra of EHB. There can be seen a broad band centred at $74cm^{-1}$ with a maximum absorption coefficient of about $29cm^{-1}$. This is probably a measure of some kind of C=O librational motion relative to the rest of the molecule, see Section 7.4. There is also a band at about $150cm^{-1}$ which has about half the intensity of the lower frequency band. The origin of this band is debatable and is also discussed in Section 7.4.
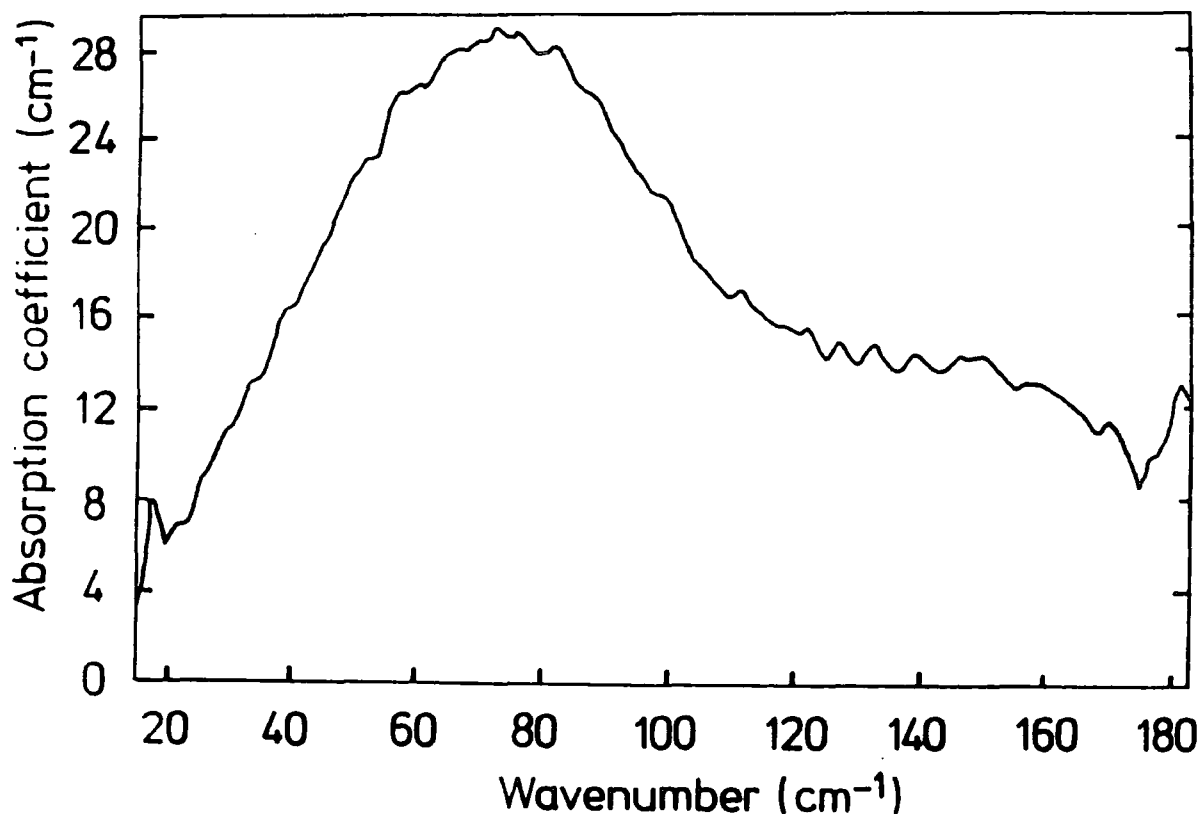
Figure II.4. The far infrared spectra of EHB

CHAPTER 4

RESULTS OF INFRARED HIGH PRESSURE STUDIES

4.1 Introduction

High pressure infrared spectra were obtained using the DAC, as described in 3.2.2. A resolution of $4cm^{-1}$ was employed for all the spectra, the spectra of EHB at normal pressure in the DAC and at 30.3kbar can be seen in Fig.4.1, the lines of high intensity between 2250 and 1950 are due to absorbance at these frequencies from the diamond lattice. A complete summary of the spectral changes with increasing pressure, for EHB, are given in Tables.4.1 to 4.3.

VIBRATION	$v(C=0)$	ring $v(C-C)$ stretch	ring $v(C-C)$ stretch	$v(C-0)$
PRESSURE (kBAR)				
10^{-3}	1723.1	1603.1	1585.0	1274.8
0.7	1722.7	1603.5	1585.5	1275.3
2.5	1721.8	1604.1	1585.8	1276.6
3.6	1720.9	1604.6	1586.4	1277.6
6.5	1720.5	1605.2	1587.4	1277.9
22.7	1721.7	1612.0	1594.8	1286.9
30.3	1723.4	1614.6	1598.3	1291.0
$\delta v/\delta P$ cm^{-1}/kBAR	non-linr	0.38	0.44	0.6

Estimated errors, based on reproducibility, are $\pm 0.5cm^{-1}$, except for the $v(C-C)$ stretching modes were the error is $\pm 1.0cm^{-1}$.

Table 4.1. The frequency shifts (cm^{-1}) of the infrared bands for EHB (other than those related to C-H vibrational modes) as a function of pressure.

VIBRATION	$\nu_{as}(CH_3)$	$\nu_{as}(CH_2)$	$\nu_s(CH_3)$	$\nu_s(CH_2)$
PRESSURE (kBAR)				
10^{-3}	2962.5	2932.3	2875.3	2858.1
0.7	2962.9	2932.6	2875.3	2859.2
2.5	2964.1	2934.1	2874.2	2859.8
3.6	2965.5	2935.6	2874.1	2861.0
6.5	2967.3	2935.4	2875.3	2861.0
22.7	2982.0	2950.0	2878.0*	—
30.3	2987.3	2954.9.	2890.0*	—
$\delta\bar{\nu}/\delta P$ cm^{-1}/kBAR	0.85	0.75	—	—

* - $\nu_s(CH_3)$ and $\nu_s(CH_2)$ bands have become indistinguishable Estimated errors, based on reproducibility are $\pm$ 2.5cm^{-1} for all frequencies, except those of the $\nu_s(CH3)$ mode at the two highest pressures, where the error is about $\pm$ 5cm^{-1},because it has become convolved with the $\nu_s(CH2)$ band.

Table 4.2a. The frequency shifts (cm^{-1}) of the infrared bands arising from C-H vibrational modes, for EHB, as a function of pressure.

VIBRATION	$\delta_s(CH_2)$	$\delta_{as}(CH_3)$	$\delta_s(CH_3)$	712cm^{-1} BAND
PRESSURE (kBAR)				
10^{-3}	1462.5	1453.8	1382.6	712.1
0.7	1462.5	1454.6	1382.8	712.4
2.5	1462.5	1454.6	1382.8	713.0
3.6	1462.5	1454.7	1382.9	713.6
6.5	ǂ	1455.4	1382.8	714.0
22.7	ǂ	1460.7	1386.9	718.6
30.3	ǂ	1462.4	1389.1	720.6
$\delta\bar{v}/\delta P$ cm^{-1}/kBAR	____	0.28	non-linr	0.28

ǂ lost within the adjacent band of the $\delta_{as}(CH_3)$ bending mode

Estimated errors, based on reproducibility, are ± 0.5cm^{-1}, except for the $\delta_{as}(CH3)$ mode (± 1.0cm^{-1}) due to it being partially convolved with the $\delta_s(CH2)$ mode.

Table 4.2b. The frequency shifts (cm^{-1}) of the infrared bands arising from C-H vibrational modes, for EHB, as a function of pressure.

Table 4.3. Variation of the band widths (FWHM), for the resolvable peaks, of EHB as a function of pressure.

VIBRATION PRESSURE (kBAR)	$v(C=O)$	$v(C-O)$	$712cm^{-1}$ BAND	CH stretch envelope[‡]
10^{-3}	16.7	21.3	11.5	131.8
0.7	17.4	23.2	11.7	132.6
2.5	18.9	24.4	12.8	133.3
3.6	20.5	25.5	13.3	137.9
6.5	21.2	24.7	14.2	156.2
22.7	24.4	30.5	18.2	176.0
30.3	25.9	32.4	20.4	183.2

[‡] CH stretching envelope measured at 1/4 maximum height Estimated errors, based on reproducibilty, are $\pm$ 0.5cm^{-1}, except for measurements on the CH stretching envelope which are subject to errors of about $\pm$ 2.5cm^{-1}.

The frequency positions of the five bands of the aliphatic $v(C-H)$ stretching modes between 3055 and 3085cm^{-1} were obtained, where possible, after deconvolution. This procedure carries out a reverse fourier transform on the spectra the result is then multiplied by an apodization function, when the data is transformed forward into the frequency domain this has the effect of resolution enhancement[116]. The program requires an approximation of the FWHM of the bands, the percentage Lorentzian, an enhancement factor, and the apodization function required. Fig.4.2 shows typical spectra of the C-H region and the deconvoluted form.
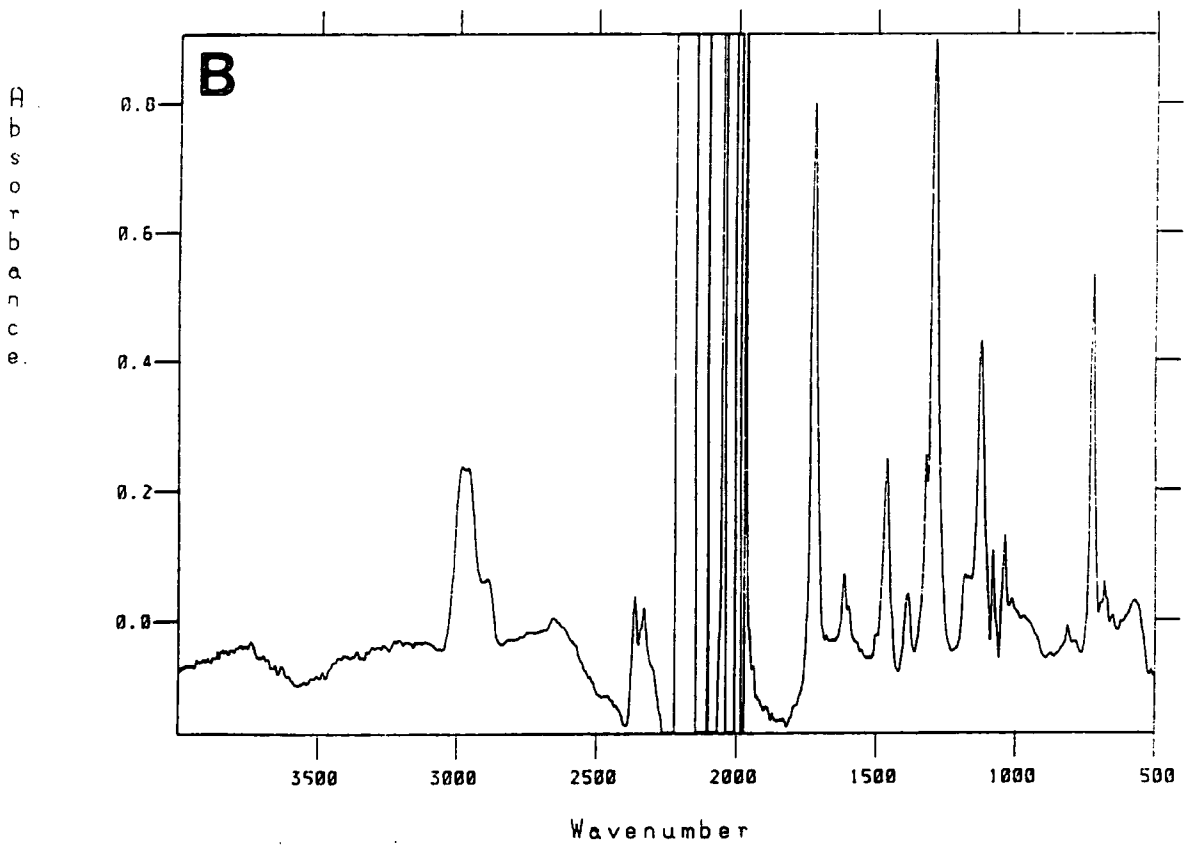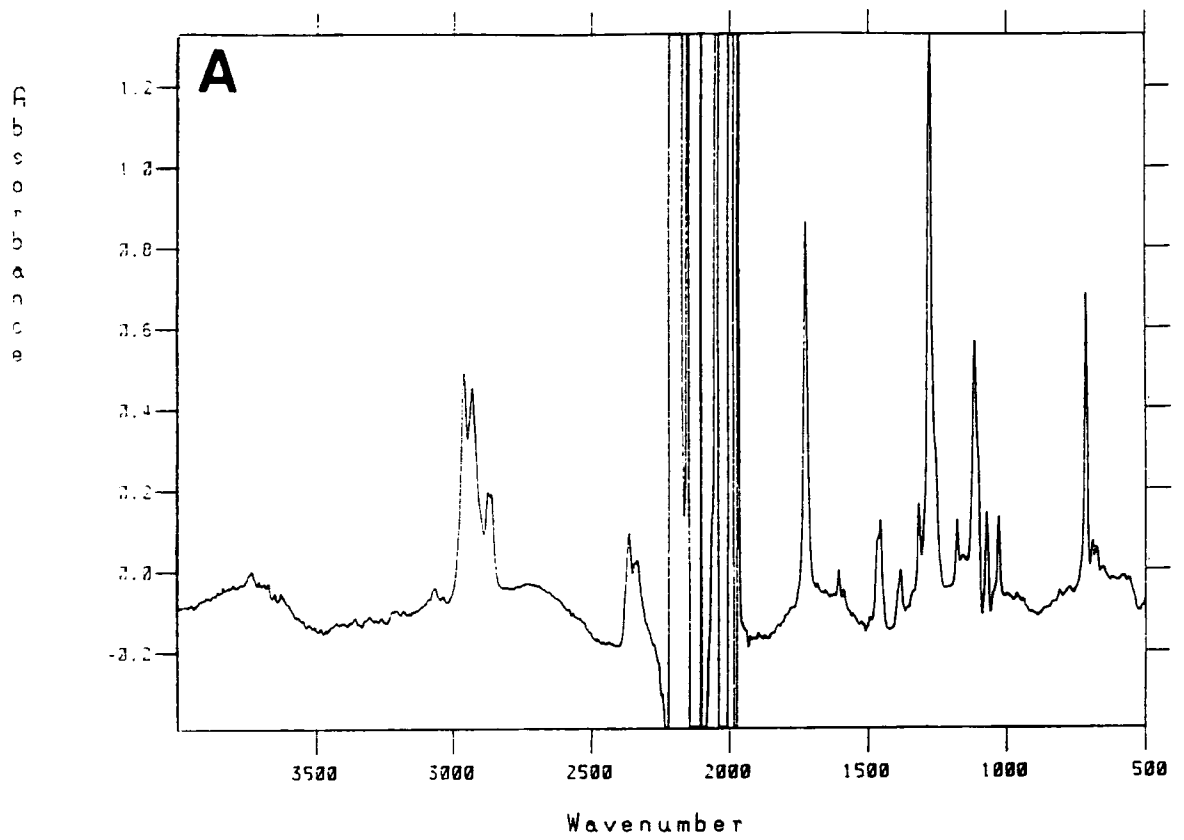
Figure 4.1. The infrared spectra of EHB in the DAC at A:1bar and B:30.3kbar.

120
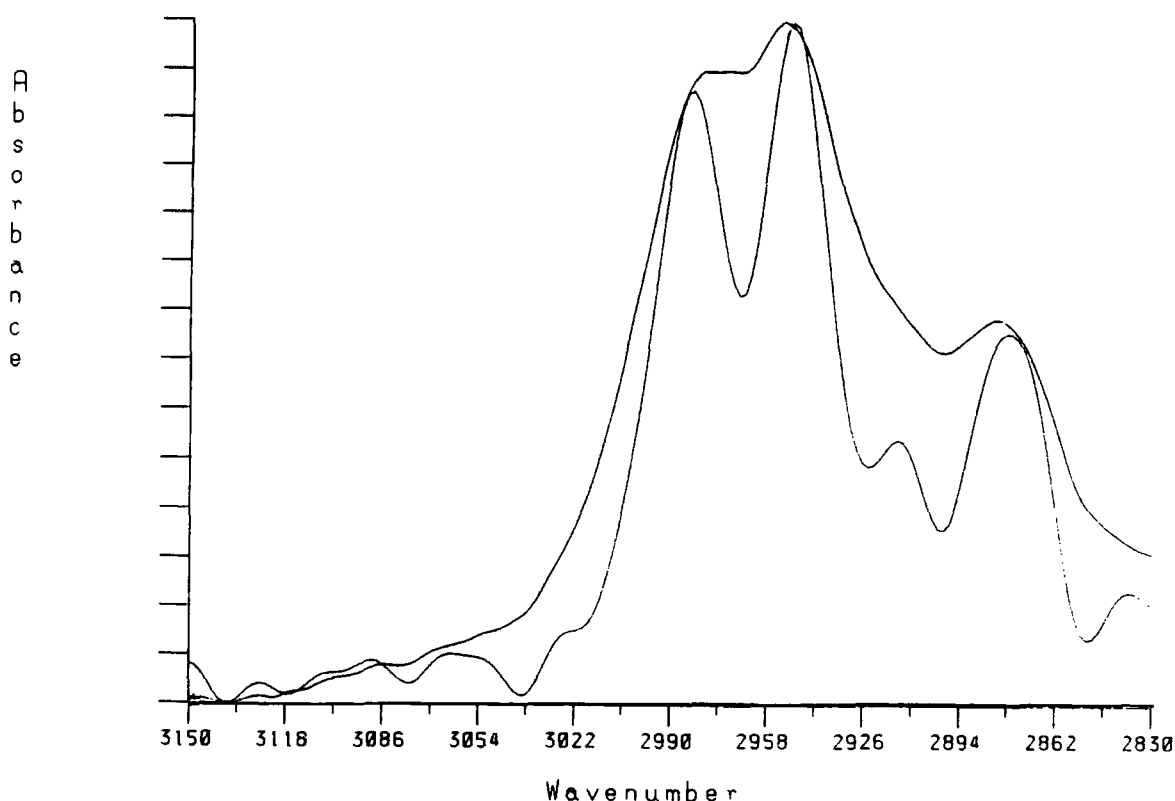
Figure 4.2. The CH envelope of EHB at 22.7kbar, with the deconvoluted bands beneath. (Pure Lorentzian and 30cm^{-1} FWHM assumed for all bands).

4.1.1 Carbonyl stretching mode

The spectra of the $v(C=O)$ stretching mode of EHB at 1bar, 6.5kbar and 30.3kbar are shown in Fig.4.3. The frequency shift as a function of pressure, Fig.4.4, shows an initial decrease, possibly indicating an increase in attractive interaction at the carbonyl groups, however by 22.7kbar the frequency has started to increase, suggesting the repulsive part of the potential is now dominating the frequency shift.
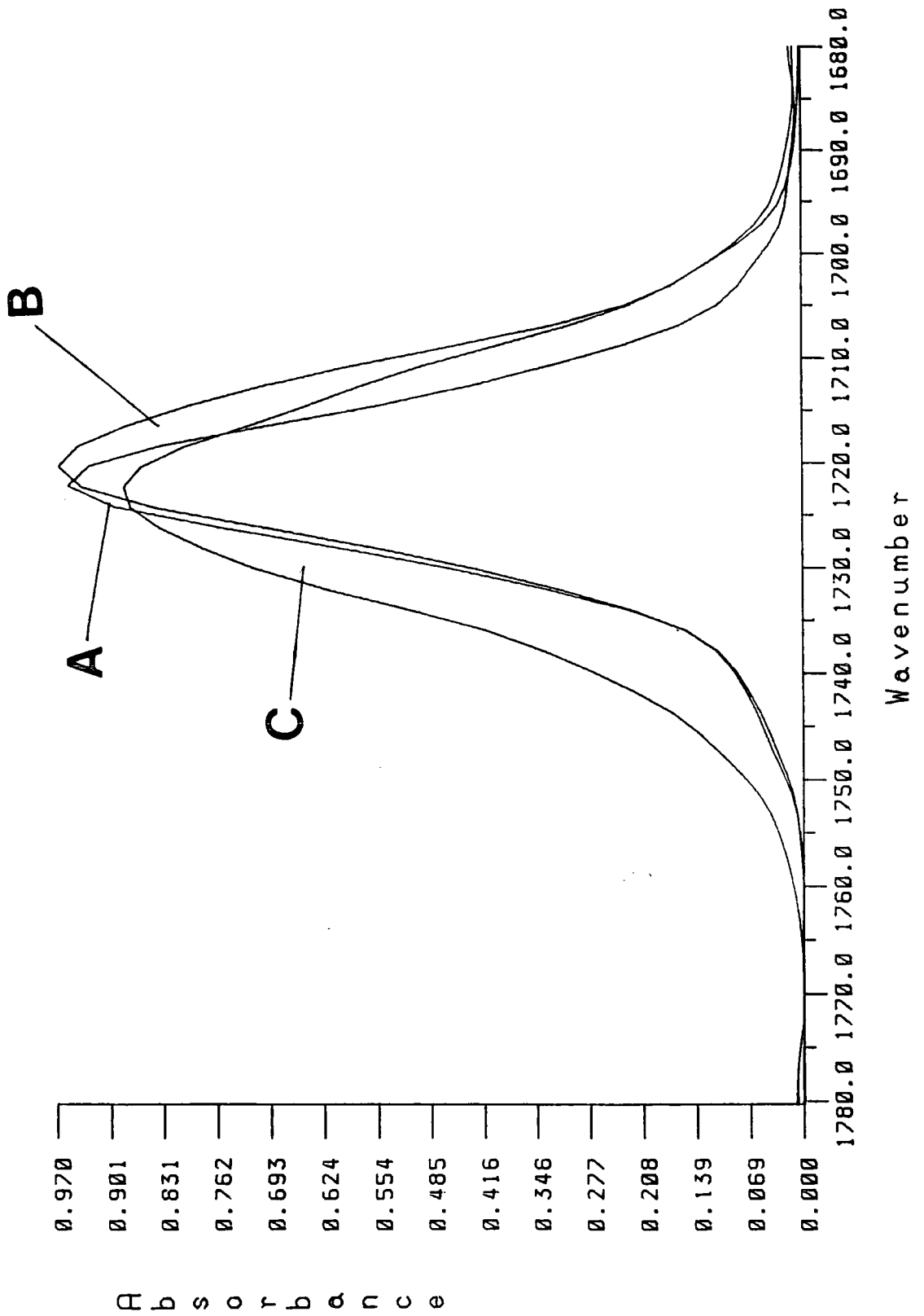
Figure 4.3 The infrared spectra of the $v(C=O)$ stretching mode of EHB at A:1bar, B:6.5kbar, C:30.3kbar.
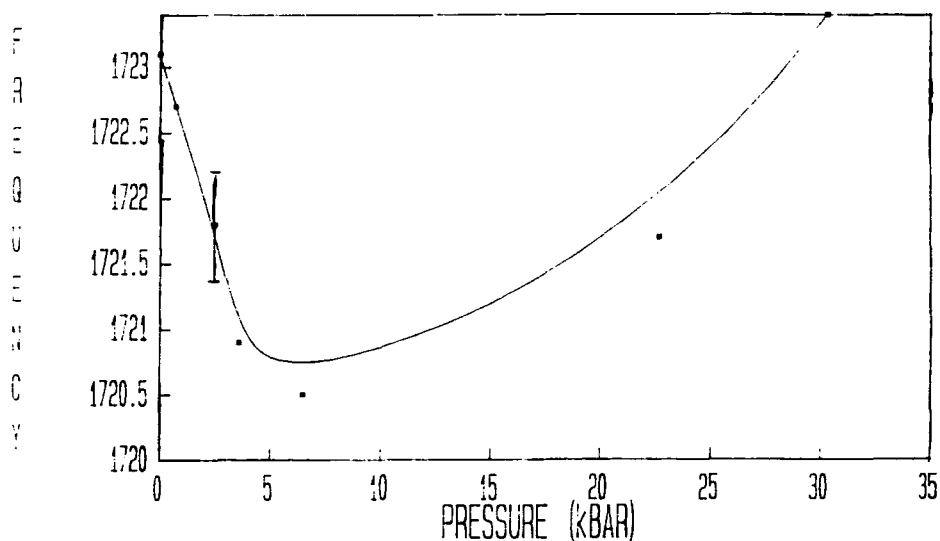
Figure 4.4. The frequency (cm^{-1}) of the $v(C=O)$ stretching mode of EHB as function of pressure.

It can be seen that, for this mode, there is considerable band broadening as the pressure is increased, Fig.4.5 shows that there is initially a very rapid increase in FWHM of about $0.8cm^{-1}kbar^{-1}$, this then levels off, from about 5kbar, to a steady increase of $0.2cm^{-1}kbar^{-1}$. This behaviour is possibly a consequence of the competing effects of an increase in the environmental modulation time and the alignment of the carbonyl groups. A decrease in the rate of modulation of a vibration will effectively increase the vibrational relaxation rate (in the case of this vibration there is the additional effect of RET, see later), and thus the band width. Whilst the relaxation rate and FWHM will

123

decrease with increased alignment, due to the fewer environments for the vibrational mode. These phenomena will be discussed further in Section 7.5.
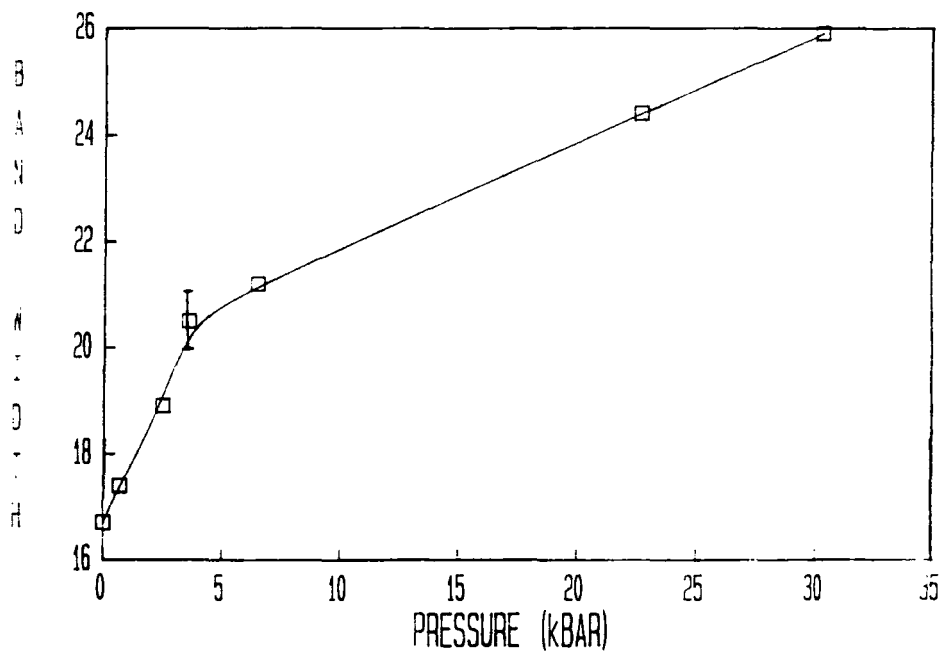
Figure 4.5. The FWHM (cm^{-1}) of the $v(C=O)$ stretching mode of EHB as function of pressure.

4.1.2 The $v(C\text{-}O)$ stretching mode

The spectra of the $v(C\text{-}O)$ stretching mode at $1274cm^{-1}$, see Fig.4.6, and the plot of frequency as a function of pressure for this band, see Fig.4.7, show a large linear increase in frequency of $0.6cm^{-1}kbar^{-1}$. This indicates that the interactions that are controlling the frequency of this band, as the pressure is increased, are localized on the repulsive part of the potential. Apart for the $v(C\text{-}H)$ stretching modes this band easily shows the greatest frequency shift with pressure of all the bands studied. This may be linked in some way with the interactions occurring at the carbonyl groups, this possibility will be discussed in Section 7.5.

This band shows a significant increase in FWHM of $12cm^{-1}$ on going from 1bar to 30.3kbar, see Fig.4.8, the largest change in FWHM for the bands measured. This increase indicates an increase in vibrational relaxation rate.

The relative peak height of this band also drops, see Fig.4.6, consistent with inhomogeneous broadening or a suppression of the dipole moment of the bond.

125
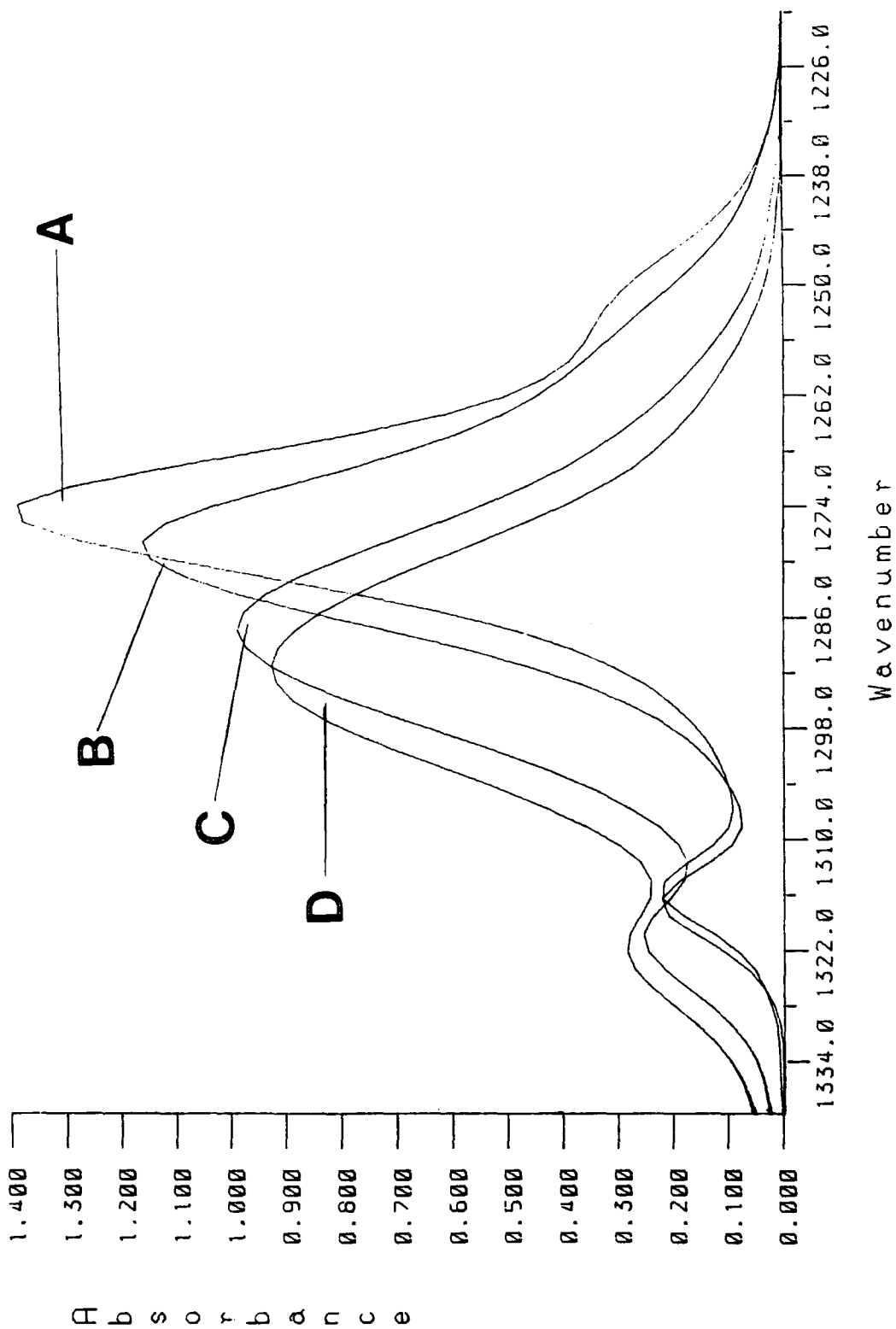
Figure 4.6. The infrared spectra of the v(C-O) stretching mode of EHB at A:1bar, B:6.5kbar, C:22.7kbar, D:30.3kbar.
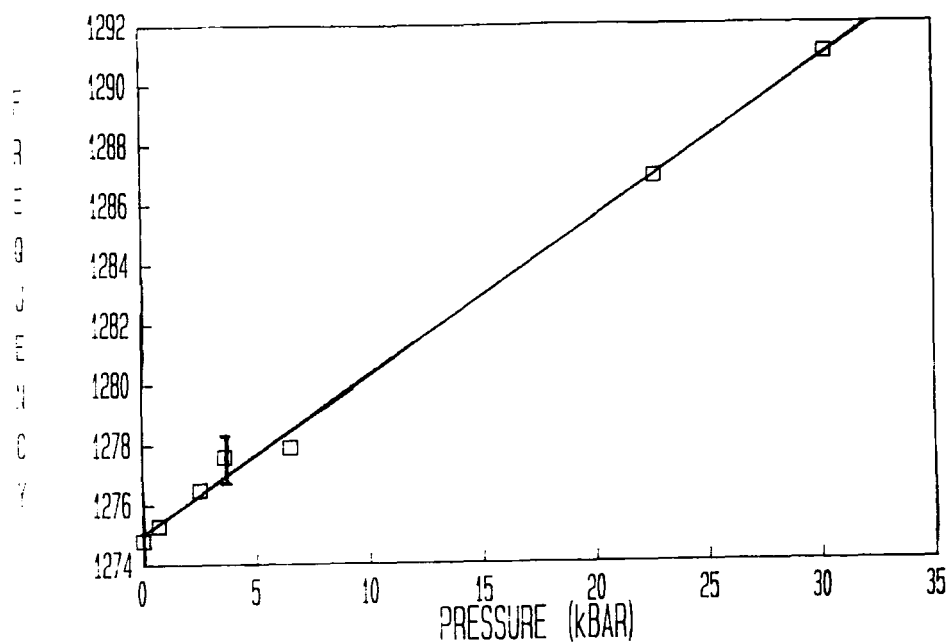
Figure 4.7. The frequency (cm^{-1}) of the $v(C\text{-}O)$ stretching mode of EHB as a function of pressure.
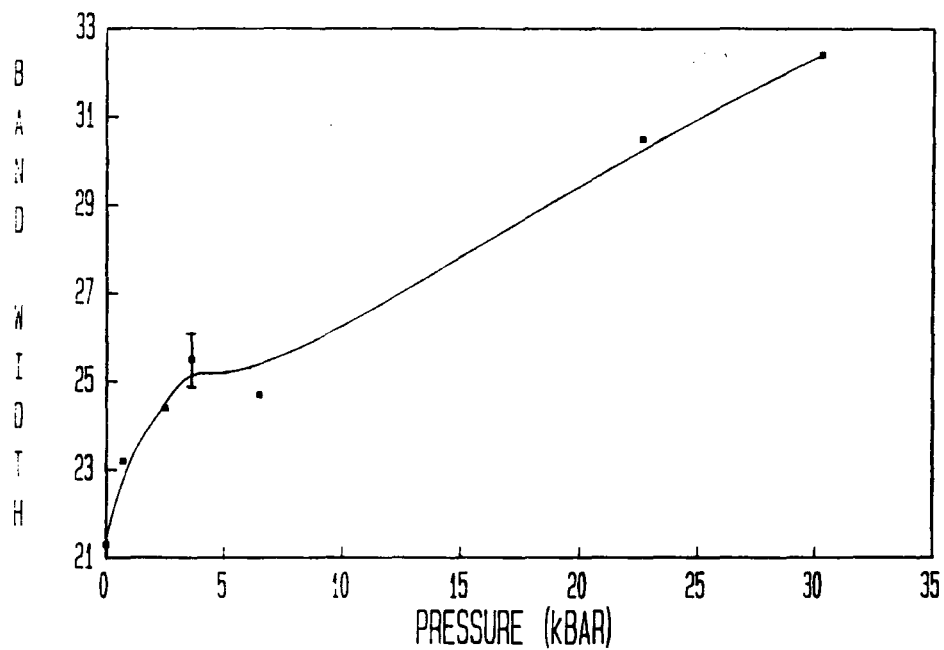
Figure 4.8. The FWHM (cm^{-1}) of the $v(C\text{-}O)$ stretching mode of EHB as a function of pressure.

127

4.1.3 The C-H vibrational modes

It can be seen from Figs.4.9 and 4.10, and Table 4.2, that, as the pressure is increased, the ν_{as}(CH3) and ν_{as}(CH2) stretching modes exhibit considerable linear frequency shifts, of 0.85 and 0.75cm^{-1}kbar^{-1} respectively. This shift is much larger than that of the symmetric CH stretching modes, see Fig.4.11 and Table 4.2, and the corresponding bending modes, see Figs.4.12-4.14 and Table 4.2. There appears to be little change in the positions of the symmetric CH stretching bands up to 6.5kbar, by 22.7kbar the two bands have merged and separation, even by deconvolution, was not possible. It is therefore difficult to assess any frequency shift of these bands after 6.5kbar. It does appear that the ν_s(CH2) band is effected the most. Possible reasons for the above observations, and a comparison with the spectra of other molecules containing alkyl chains, are discussed in Section 7.5.2.1. The increase in frequency arises because of the effect of hard core repulsive forces which increase rapidly with density.

The spectra in Fig.4.9 demonstrate that the C-H stretching envelope of EHB exhibits a large pressure induced broadening. However due to the complex structure of these envelopes quantification of the observed broadening was not a straight forward exercise, it was found that it was only possible to measure the full width of the envelope at 1/4 maximum height, see Table 4.3 and Fig.4.15. There can also be seen a suppression of the peak heights for both the methyl and methylene bands, and a relative decrease in

128
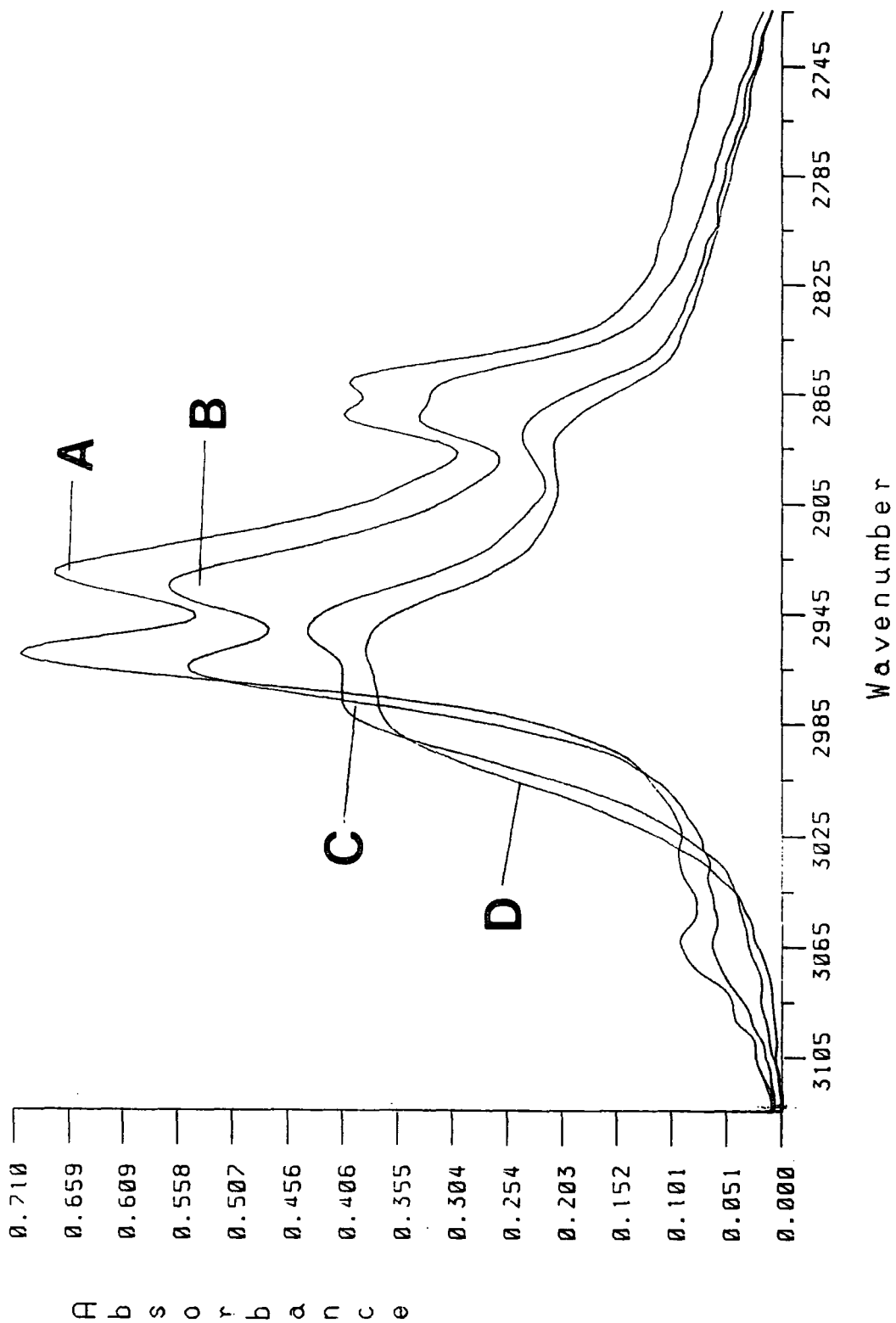
Fig 4.9. The infrared spectra of the v(C-H) stretching modes of EHB at A:1bar, B:6.5kbar, C:22.7kbar, D:30.3kbar.
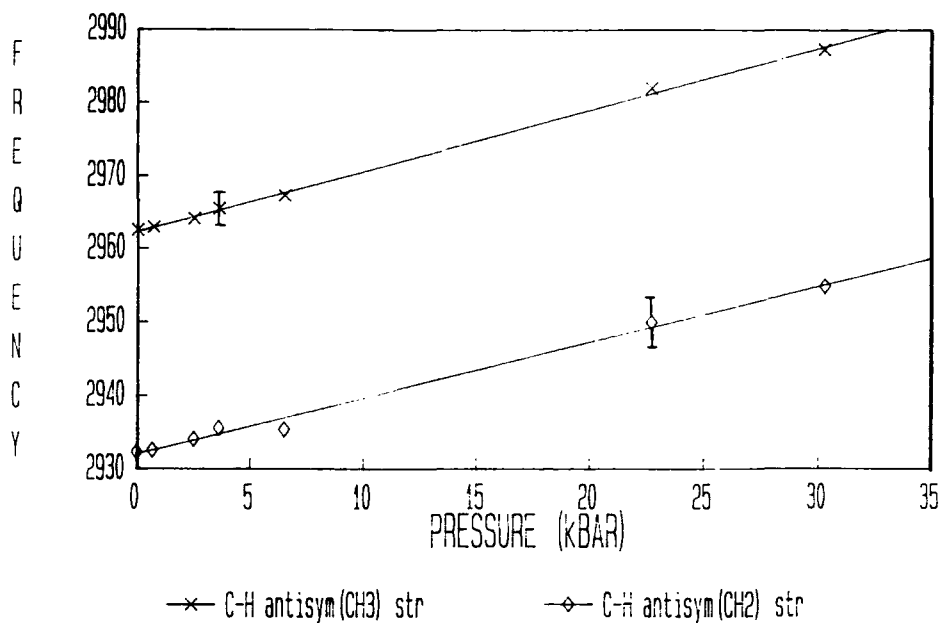
Figure 4.10. The frequency (cm^{-1}) of the ν_{as}(CH3) and ν_{as}(CH2) stretching modes of EHB as a function of pressure.
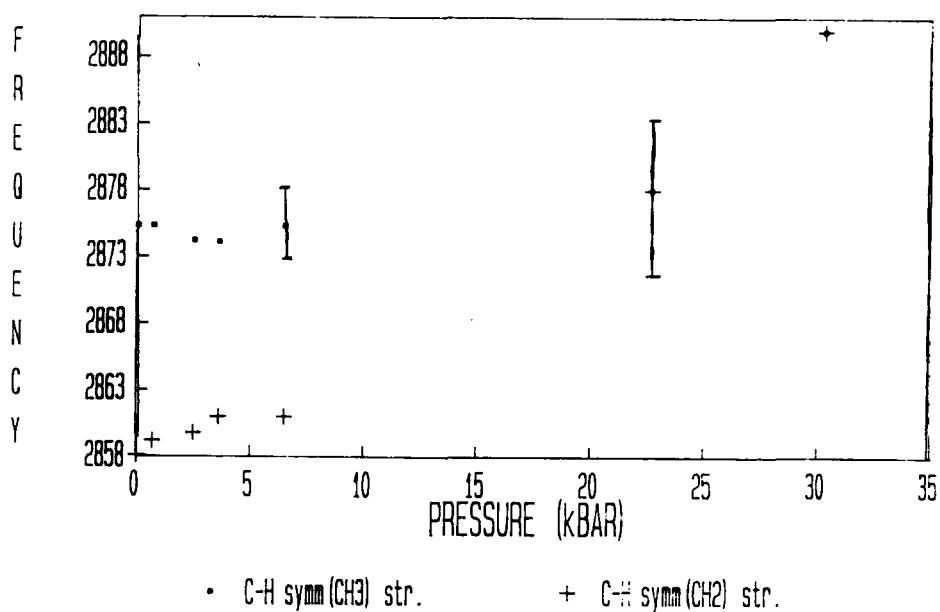
Figure 4.11. The frequency (cm^{-1}) of the ν_{s}(CH3) and ν_{s}(CH2) stretching modes of EHB as a function of pressure.
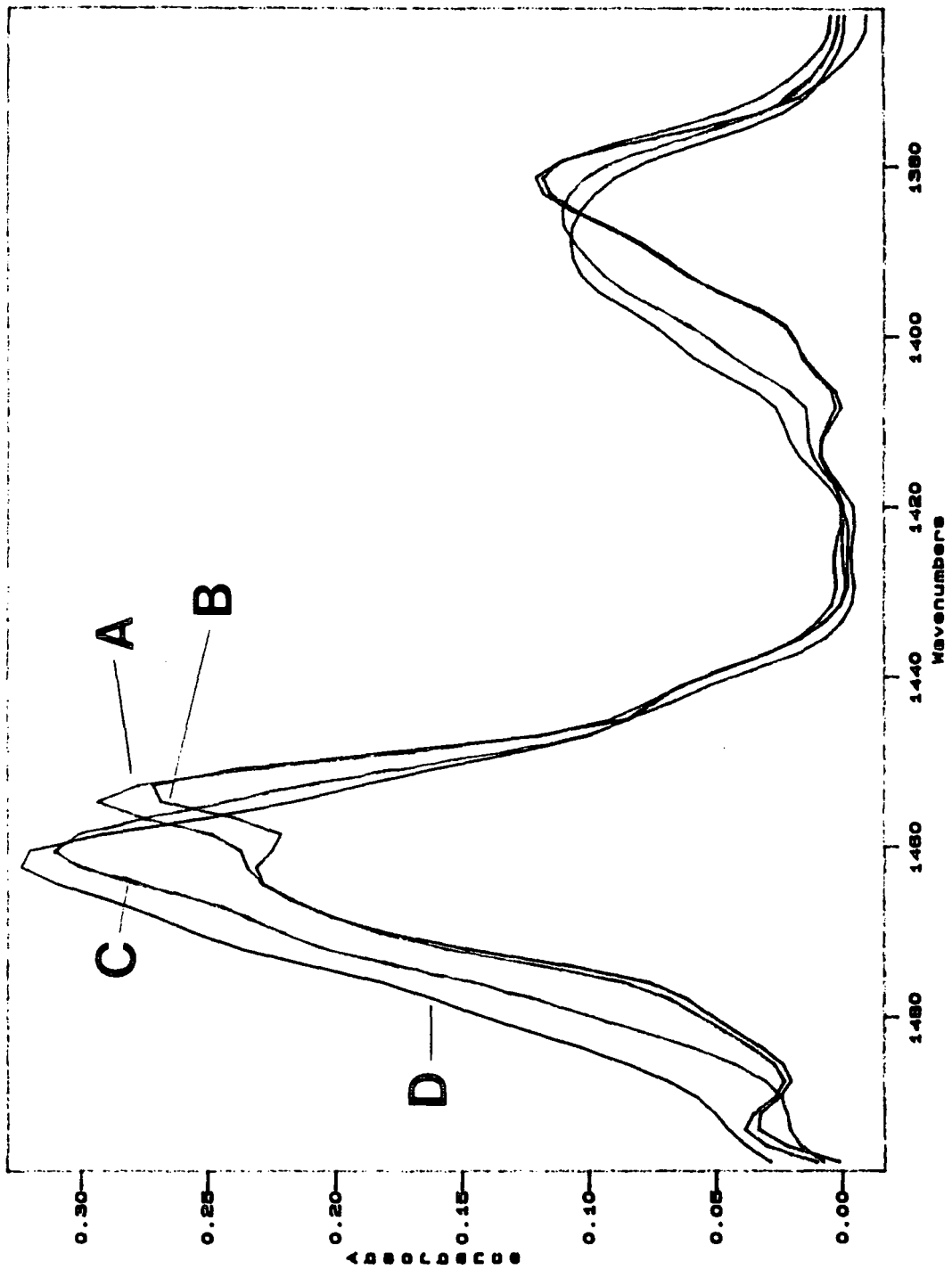
Figure 4.12. The infrared spectra of the δ(CH) bending modes
of EHB at A:1bar, B:6.5kbar, C:22.7kbar, D:30.3kbar.
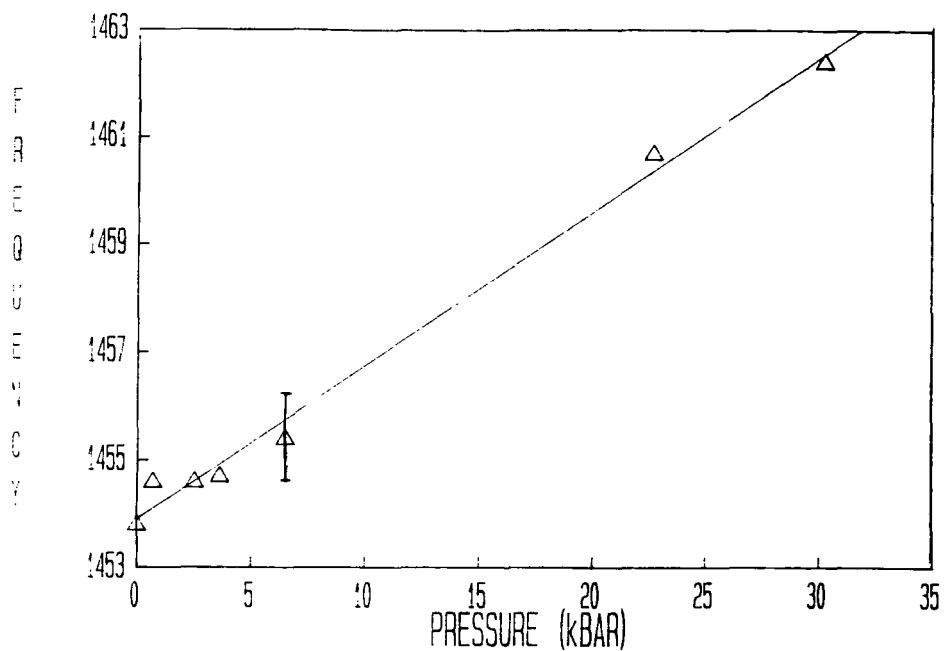
Figure 4.13. The frequency (cm^{-1}) of the δ_{as}(CH3) stretching mode of EHB as a function of pressure.
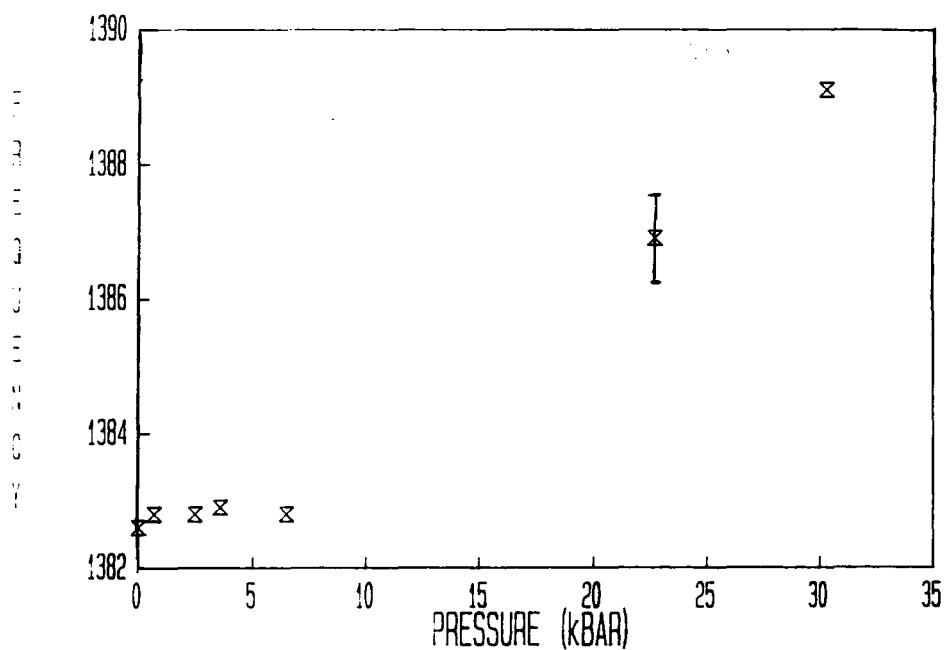
Figure 4.14. The frequency (cm^{-1}) of the δ_s(CH3) stretching mode of EHB as a function of pressure.
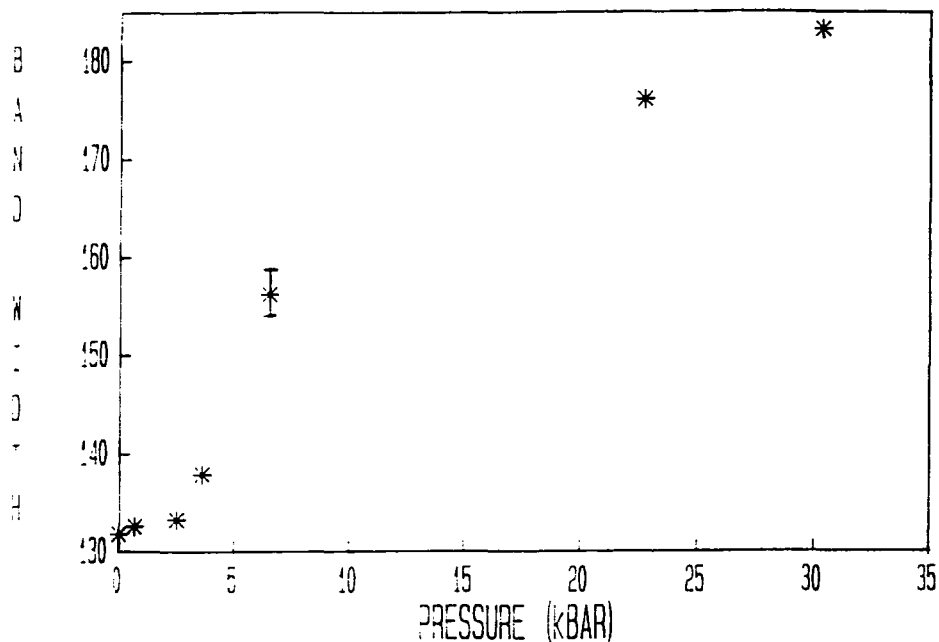
Figure 4.15. The variation of the band width (cm^{-1}) of the CH stretching envelope, measured at 1/4 height, as a function of pressure.

height of the v_s(CH3) compared with the v_{as}(CH3). This broadening and decrease in peak height is consistent with an increase in vibrational environments for the C-H modes with increased pressure. The relative suppression of the v_s(CH3) band is explained in 7.5.2.1, the contributions to the change in the envelope shape are also discussed.

4.1.4 Other Bands

All the other infrared bands of EHB show a linear frequency shift with increasing pressure, of varying degree up to a maximum of about $0.4 cm^{-1} kbar^{-1}$ for the v(C-C) ring stretching modes at $1585 cm^{-1}$ and $1603 cm^{-1}$, see Figs.4.16 and 4.18. It can be seen, see Fig.4.1, that with increasing pressure all the bands broaden and most diminish in height, except the v(C-C) ring stretching modes which appear to increase in height, see Fig.4.16. The infrared band found at $712 cm^{-1}$ may be due to one of two modes, this will be discussed in Section 7.5.2.4. The linear frequency shift of this band and the observed broadening are illustrated in Figs.4.17 and 4.19-4.20.

The high pressure behaviour of the infrared bands of EHB is further discussed in Section 7.5.
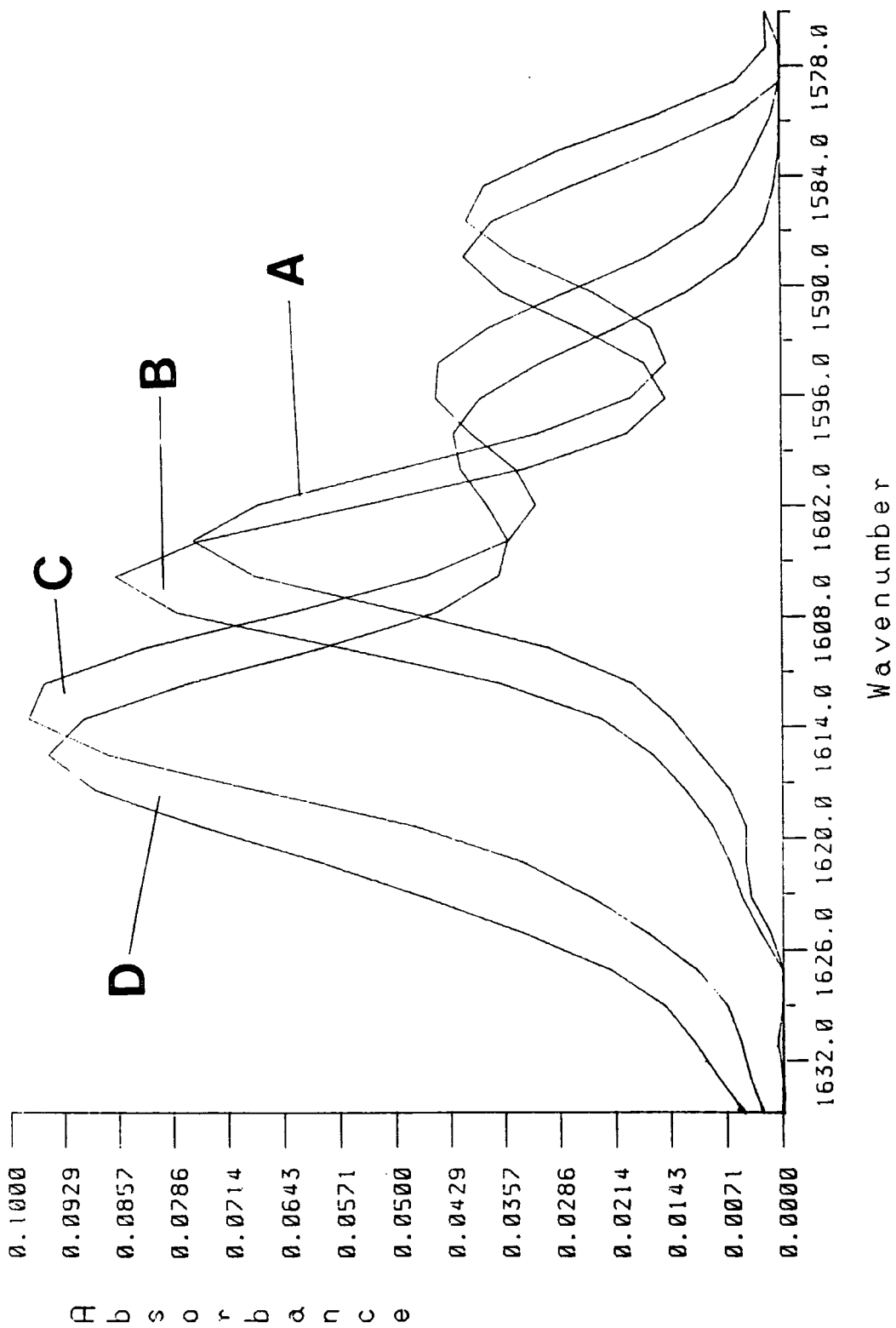
Figure 4.16. The infrared spectra of the v(C-C) ring stretching modes of EIIB at A:1bar, B:6.5kbar, C:22.7kbar, D:30.3kbar.
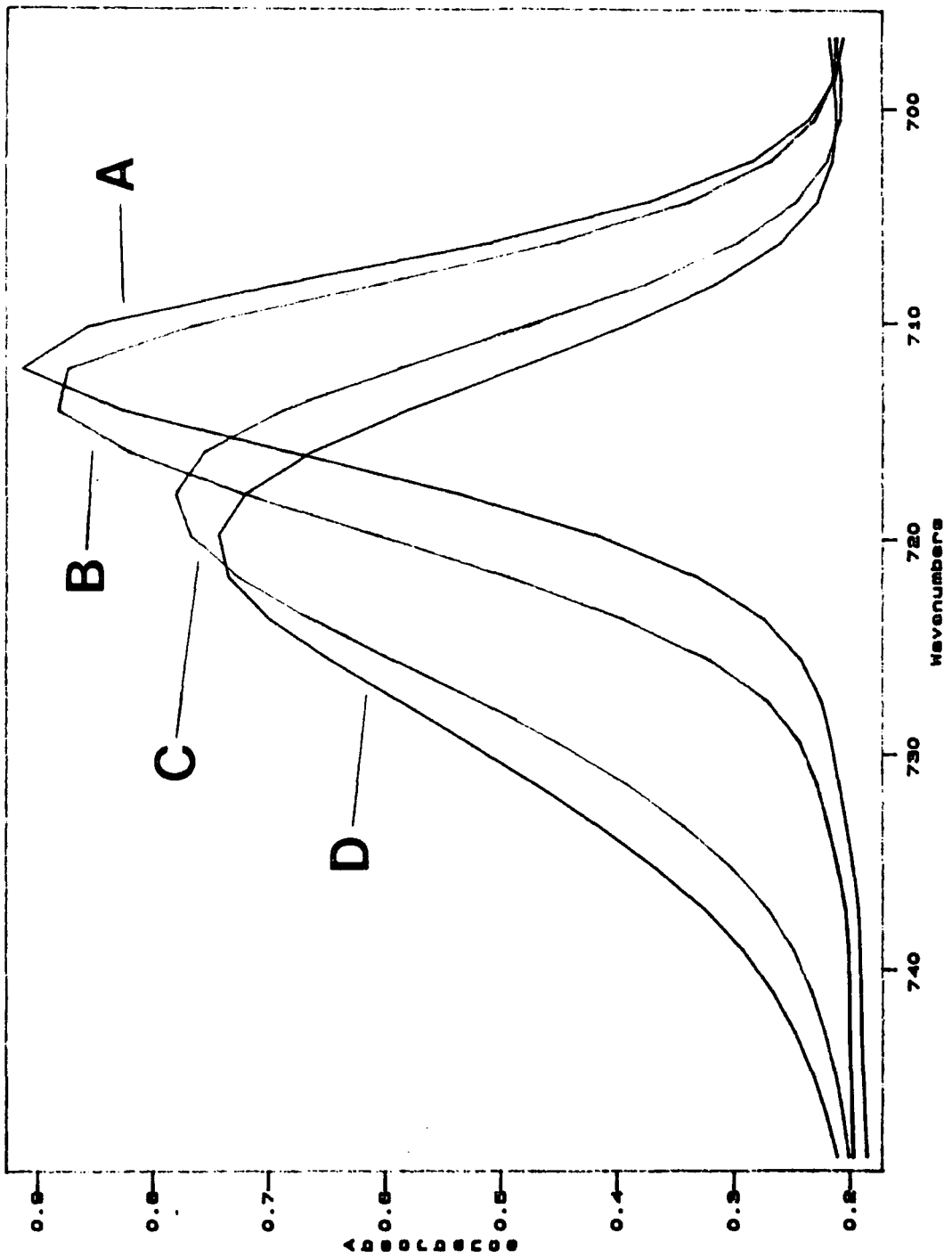
Figure 4.17. The infrared band of EHB found at 712cm^{-1}, for EHB at A:1bar, B:6.5kbar, C:22.7kbar, D:30.3kbar.
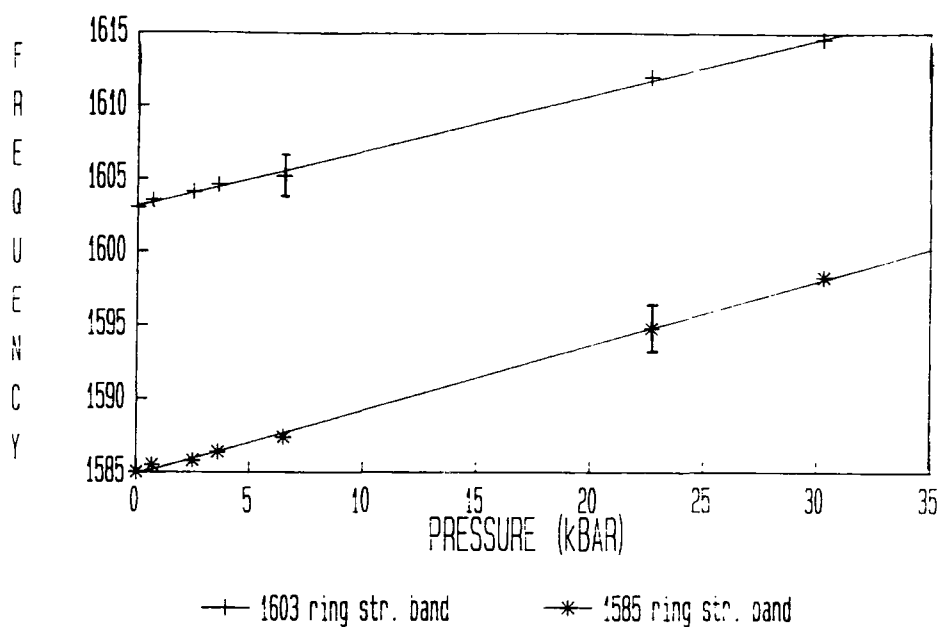
Figure 4.18. The frequency (cm^{-1}) of the v(C-C) ring stretching modes of EHB as a function of pressure.
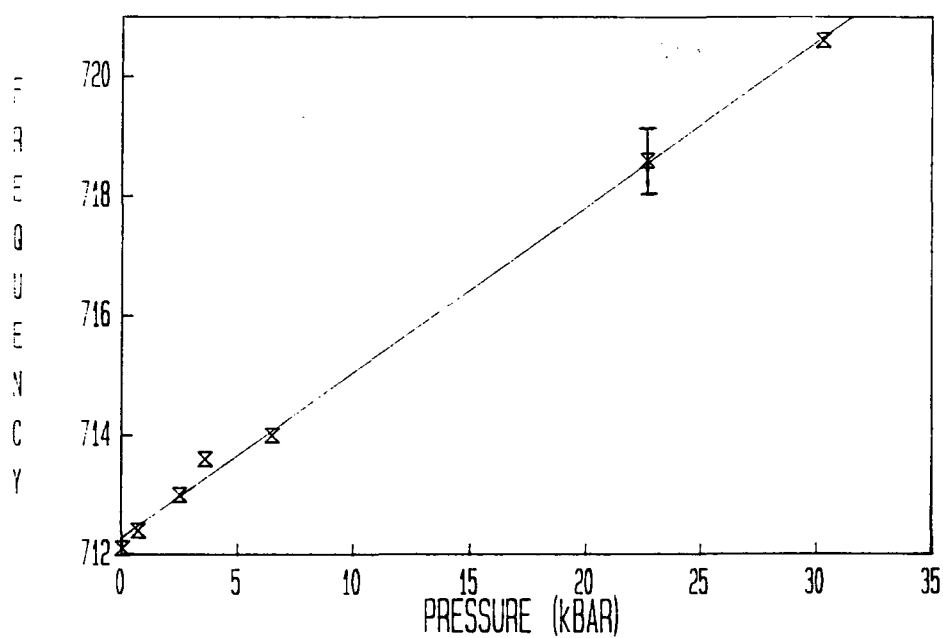
Figure 4.19. The frequency (cm^{-1}) of the $712cm^{-1}$ band of EHB as a function of pressure.
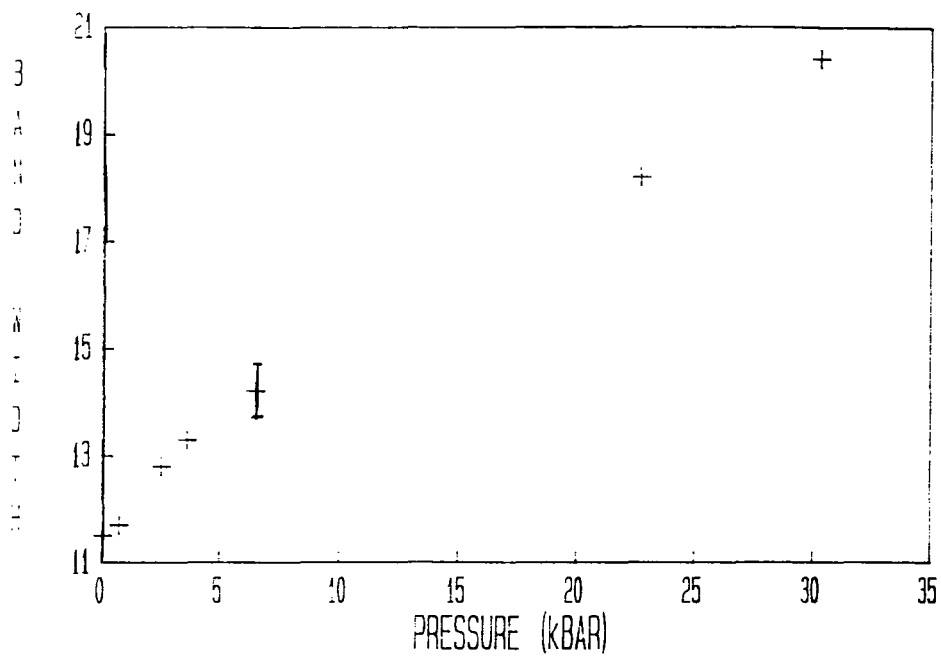
Figure 4.20. The FWHM (cm^{-1}) of the 712cm^{-1} band of EHB as a function of pressure.

CHAPTER 5

RESULTS OF VARIABLE TEMPERATURE STUDIES

5.1 Introduction

High temperature Raman spectra of EHB were recorded with the sample in the brass block, the low temperature spectra were obtained using the low temperature glass Dewar cell. Both are described in Section.3.1.2. Using this apparatus Raman I(VV) and I(VH) spectra of the ring v(C-C) deformation mode (1003cm^{-1}) and carbonyl v(C=O) stretching mode (1720cm^{-1}) were recorded at temperatures of 77K, 190K, 298K, 373K and 443K. The corresponding I_{iso} bands were then computed. Table.5.1 and 5.2 summarise the spectral details.

TEMP (K)	BAND	FREQUENCY (CM^{-1})	FWHM (CM^{-1})
77	I_{iso}	1003.5	3.4
77	I_{aniso}	1003.5	3.4
198	I_{iso}	1003.3	3.0
198	I_{aniso}	1003.3	3.0
298	I_{iso}	1003.4	2.8
298	I_{aniso}	1003.4	2.9
373	I_{iso}	1003.2	2.8
373	I_{aniso}	1003.2	3.3
443	I_{iso}	1002.6	3.1
443	I_{aniso}	1002.6	4.0

Estimated errors, based on reproducibility, are ± 0.1 cm^{-1}.

Table 5.1. Frequency shifts and FWHM for the Raman I_{iso} and I_{aniso} bands of the v(C-C) ring deformation mode of EHB as a function of temperature.

TEMP (K)	BAND	FREQUENCY (CM^{-1})	FWHM (CM^{-1})
77	I_{iso}	1713.8	15.9
77	I_{aniso}	1717.1	15.4
198	I_{iso}	1714.6	15.9
198	I_{aniso}	1717.9	15.3
298	I_{iso}	1718.8	15.8
298	I_{aniso}	1722.1	14.6
373	I_{iso}	1720.2	15.4
373	I_{aniso}	1722.1	14.4
443	I_{iso}	1722.0	15.4
443	I_{aniso}	1723.0	14.7

Estimated errors, based on reproducibility, are $\pm$ 0.3 cm^{-1}.

Table 5.2. Frequency shifts and FWHM for the Raman I_{iso} and I_{aniso} bands of the $v(\text{C=O})$ stretching mode of EHB as a function of temperature.

5.1.1 Ring Deformation Mode

The isotropic and anisotropic Raman spectra of the ring deformation mode at 298K and 443K are shown in Fig.5.1. It can be seen that by 443K the anisotropic band has broadened significantly with respect to the isotropic band. Fig.5.2 shows how the FWHM of the two bands vary with temperature. The isotropic FWHM can be taken to be proportional to the vibrational relaxation rate and in the limit of a Lorentzian band shape[53]:
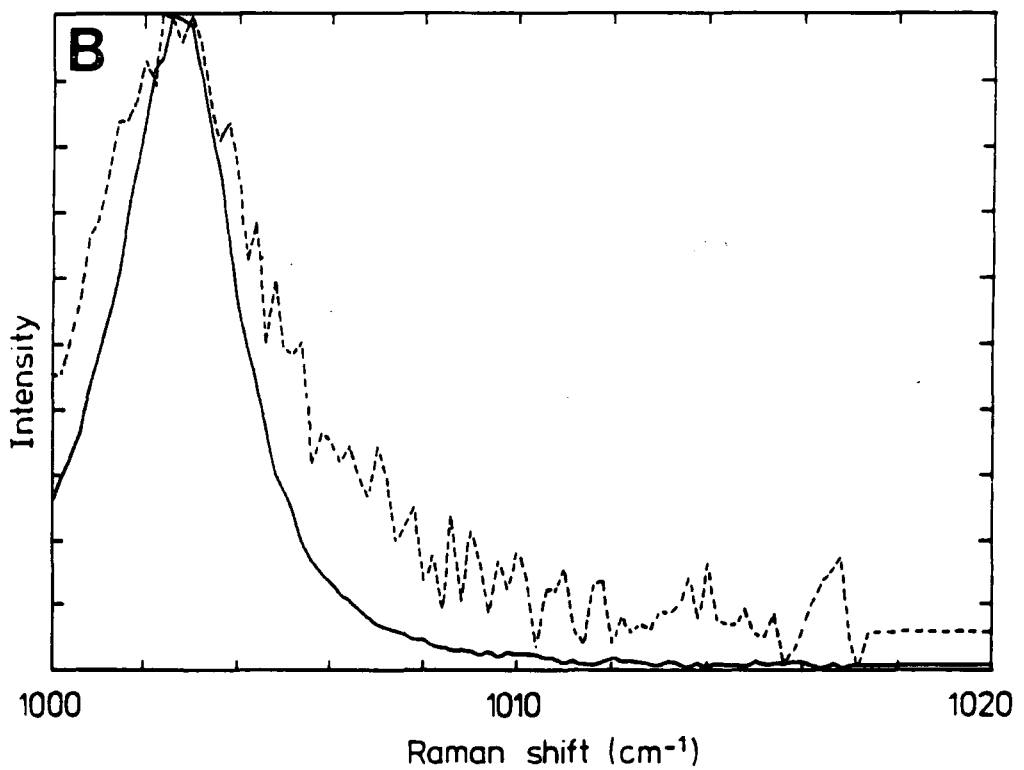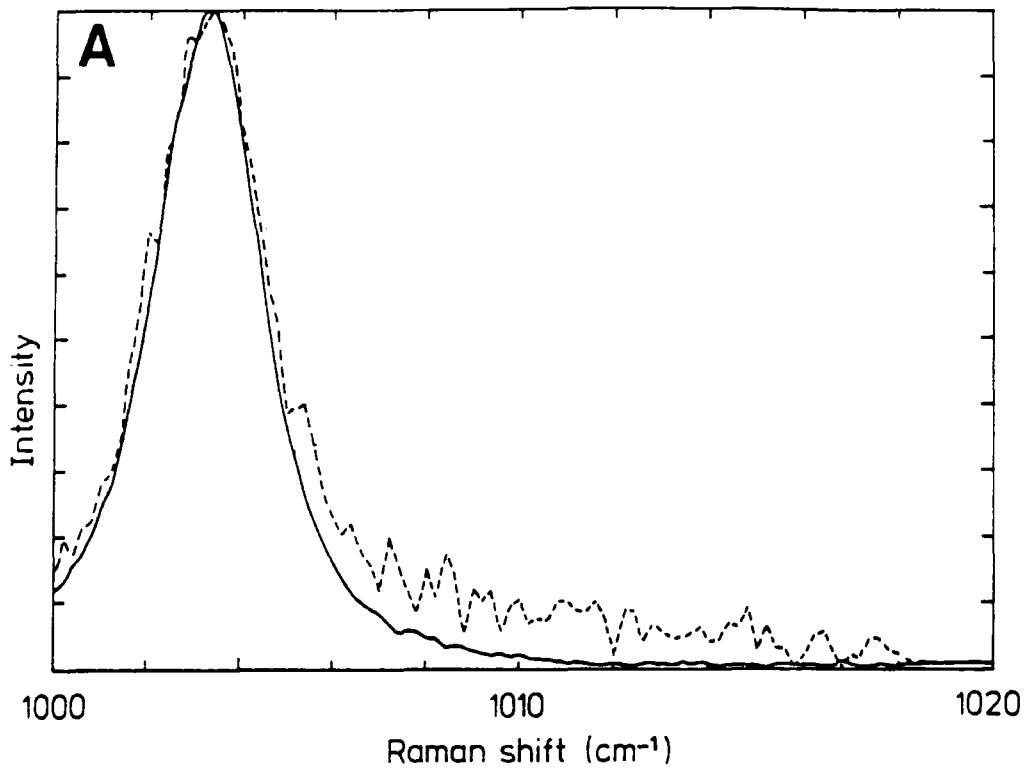
Figure 5.1. The isotropic and anisotropic Raman spectra of the ring v(C-C) deformation mode for EHB at A:298K and B:443K.
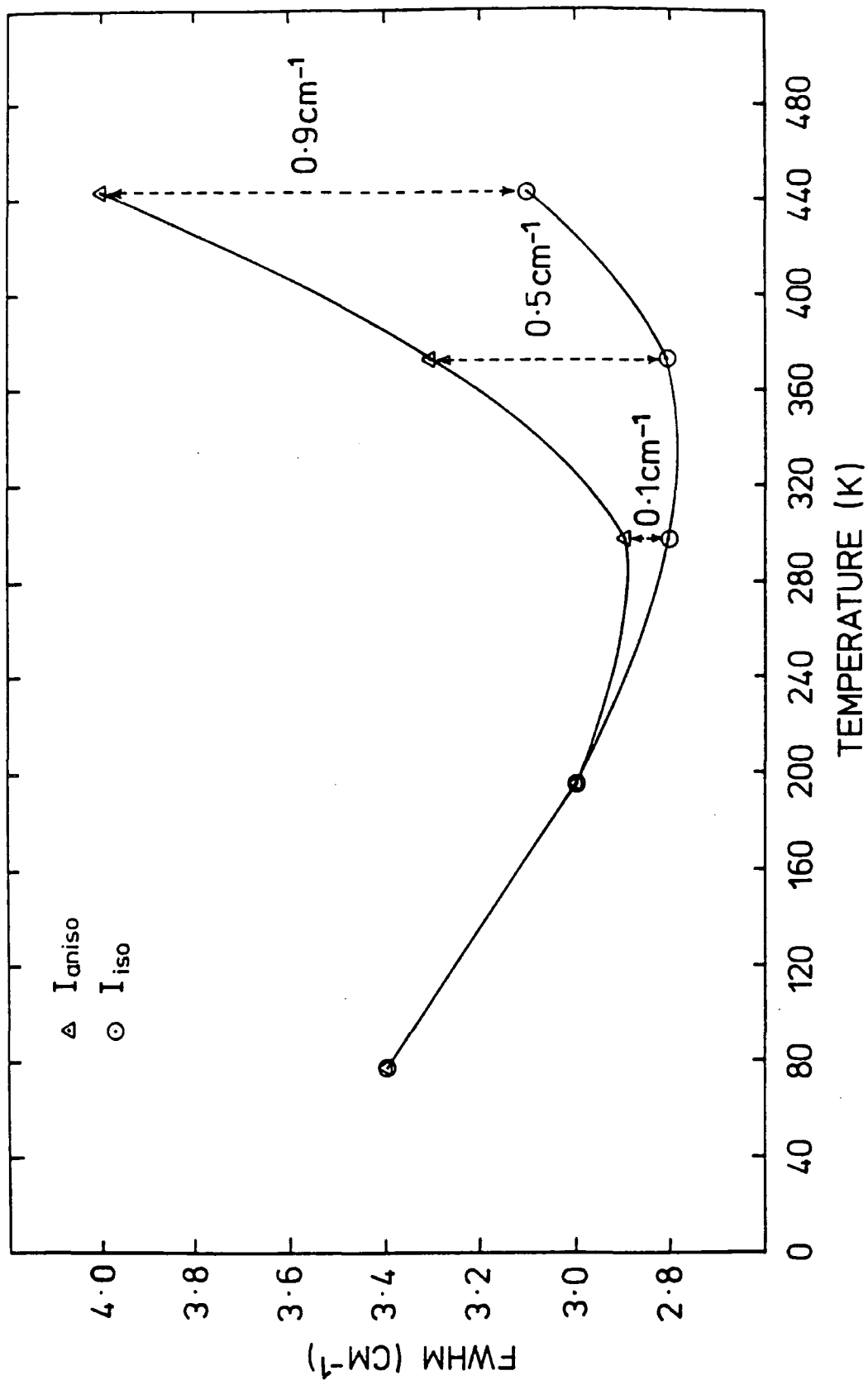
Figure 5.2. Variation of the band width (FWHM) of the
isotropic and anisotropic Raman spectra of the ring v(C-C)
deformation mode for EHB as a function of temperature.

$$\tau_{vib} = [\pi c \Delta v_{1/2}(ISO)]^{-1} \qquad \text{Eqn.5.1}$$

The difference in FWHM between the anisotropic and isotropic bands is proportional to the rotational/reorientational relaxation rate and

$$\tau_{rot} = [\pi c \{\Delta v_{1/2}(ANISO) - \Delta v_{1/2}(ISO)\}]^{-1} \qquad \text{Eqn.5.2}$$

it can be seen that there is little change in the vibrational relaxation rate of the ring deformation mode with temperature. However there is a significant increase in the reorientational relaxation rate with increasing temperature, corresponding to an increase in rate of "rotation" of the ring. NMR C-13 spin lattice relaxation measurements have been made for all the carbon atoms of EHB at a number of temperatures between 270 and 376K[117], see Table.5.3. The NOE values for all carbons but that of the carbonyl carbon were full, relaxation of the nuclei were therefore assumed to be in the motionally narrowed region. Values for τ_{rot}, for all the carbons of EHB, were therefore obtained using Eqn.7.3, see Section.7.1.2. Table.5.3 summarises the results of the NMR measurements.

Fig.5.3 shows the excellent agreement between the Raman estimates for the rotational correlation times (τ_{rot}) at various temperatures, obtained using the FWHM of the Raman bands of the ring v(C-C) deformation mode, and the NMR C-13 spin lattice relaxation times obtained for the para-carbon of the ring[117]. From Fig.5.2 it appears that below 298K there is no reorientation of the ring on the picosecond time scale. These results and a comparison with the

144

T(K)	CORRELATION TIMES (PICOSECONDS)										
	C2	C4	C5	C6	C7	C8	C9	C10	C11	C12	C13
270.7	173	117	119	107	129	82.0	54.6	79.3	36.1	12.1	14.1
296.0	111	63.0	64.7	70.3	78.0	48.2	33.6	47.3	20.5	7.25	9.53
310.3	74.0	38.8	42.3	44.7	51.2	28.6	19.6	30.0	13.2	4.96	6.56
326.6	55.5	34.5	31.9	27.3	37.8	17.5	16.0	23.2	9.11	4.43	5.85
343.0	39.2	20.3	20.0	19.5	22.9	13.8	9.01	12.6	6.22	2.77	3.64
360.5	26.6	14.0	14.4	13.7	16.6	10.3	6.77	9.95	4.94	2.27	2.85
376.6	20.2	10.8	10.8	11.3	14.3	8.14	6.05	8.45	4.19	2.05	2.57

Table 5.3. Results of C-13 spin lattice relaxation measurements for EHB as function of temperature.
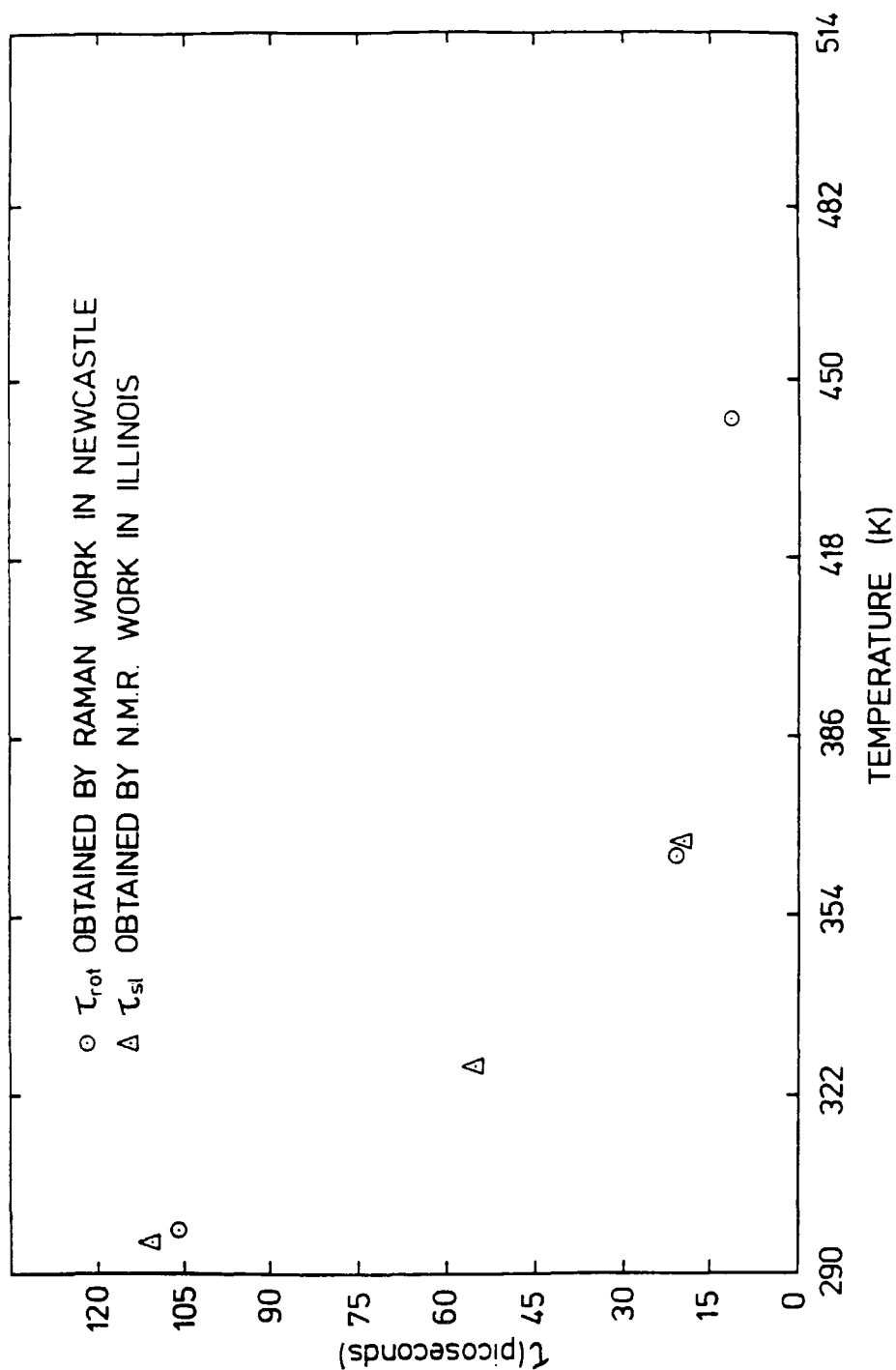
Figure 5.3. Comparison of reorientational correlation times, as a function of temperature, obtained for the ring of EHB from Raman measurements of the ring v(C-C) deformation mode and NMR C13 spin lattice relaxation measurements on the para-carbon of the ring.

viscometric-temperature behaviour of EHB will be discussed
further in Section 7.1.

5.1.2 Carbonyl stretching mode

The isotropic and anisotropic Raman spectra of the
carbonyl stretching mode of EHB at 77K, 298K and 443K are
shown in Figs.5.4a-c. The variation in the frequency of the
two bands as a function of temperature are shown in Fig.5.5.
The noncoincidence of the bands diminishes as the
temperature is increased, suggesting a loss of RET with
temperature, but does not appear to have changed on going
from 298K to 190K or 77K. There is an approximately linear
increase in frequency with increasing temperature for both
the bands. However, there is very little change in the FWHM
of the two bands across the whole temperature range
measured, see Fig.5.6, indicating very little change in
vibrational relaxation rates. Reasons for the observed
changes are considered in Section 7.2.
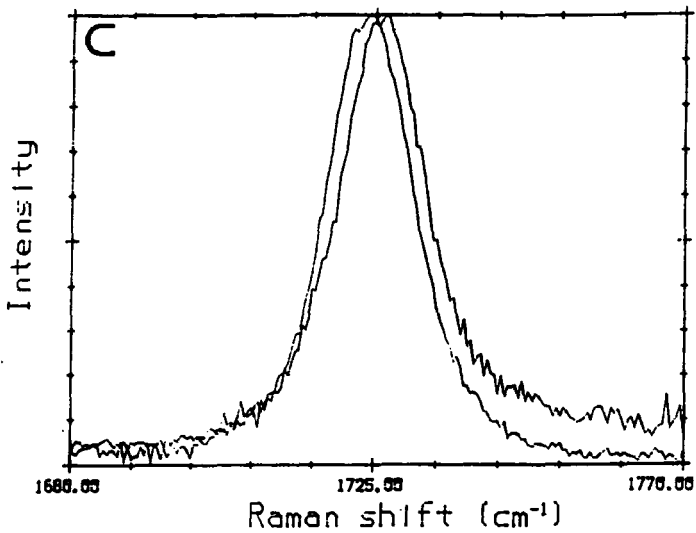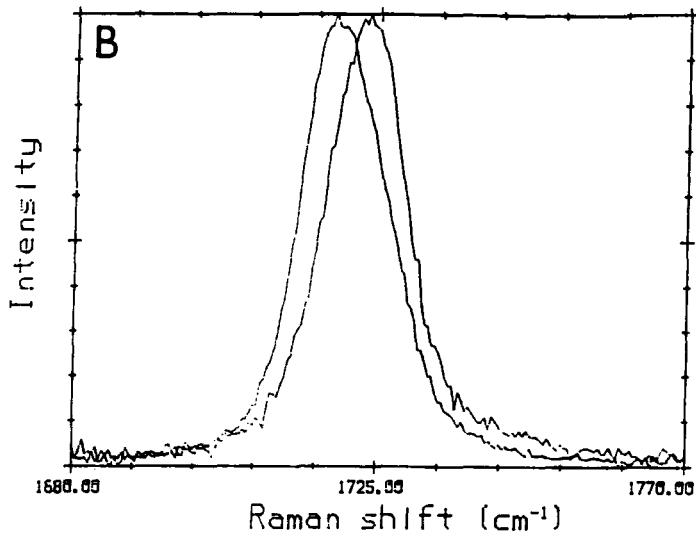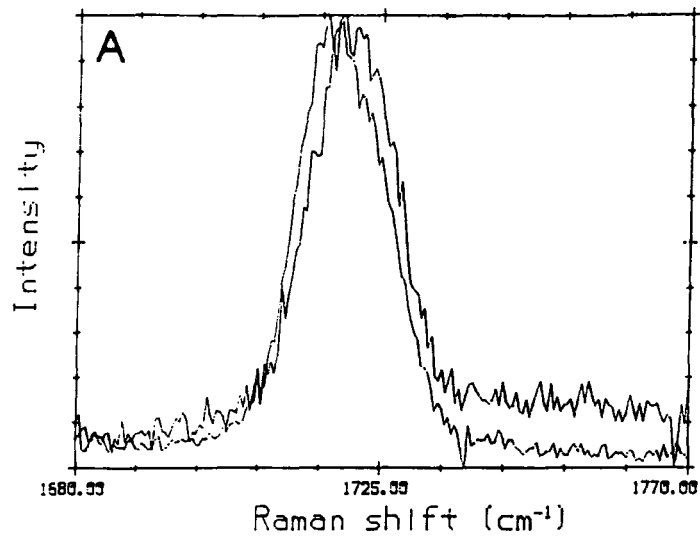
Fig 5.4. Raman I_{iso} and I_{aniso} bands of the v(C=O) stretching mode of EHB at A:77K, B:298K, C:443K.
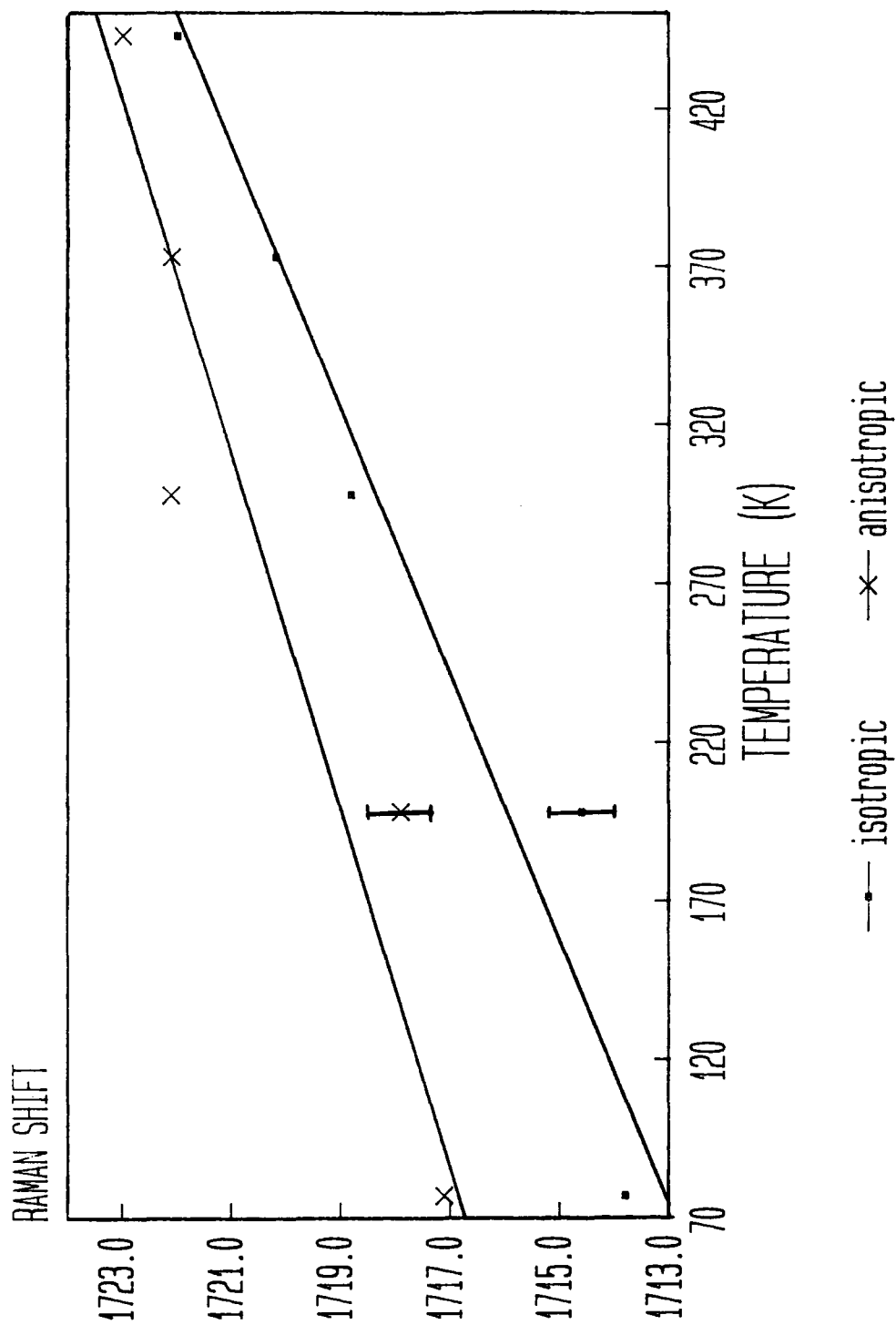
Figure 5.5. Variation of the frequency (cm^{-1}) of the Raman isotropic and anisotropic bands of the v(C=O) stretching mode for EHB as a function of temperature.
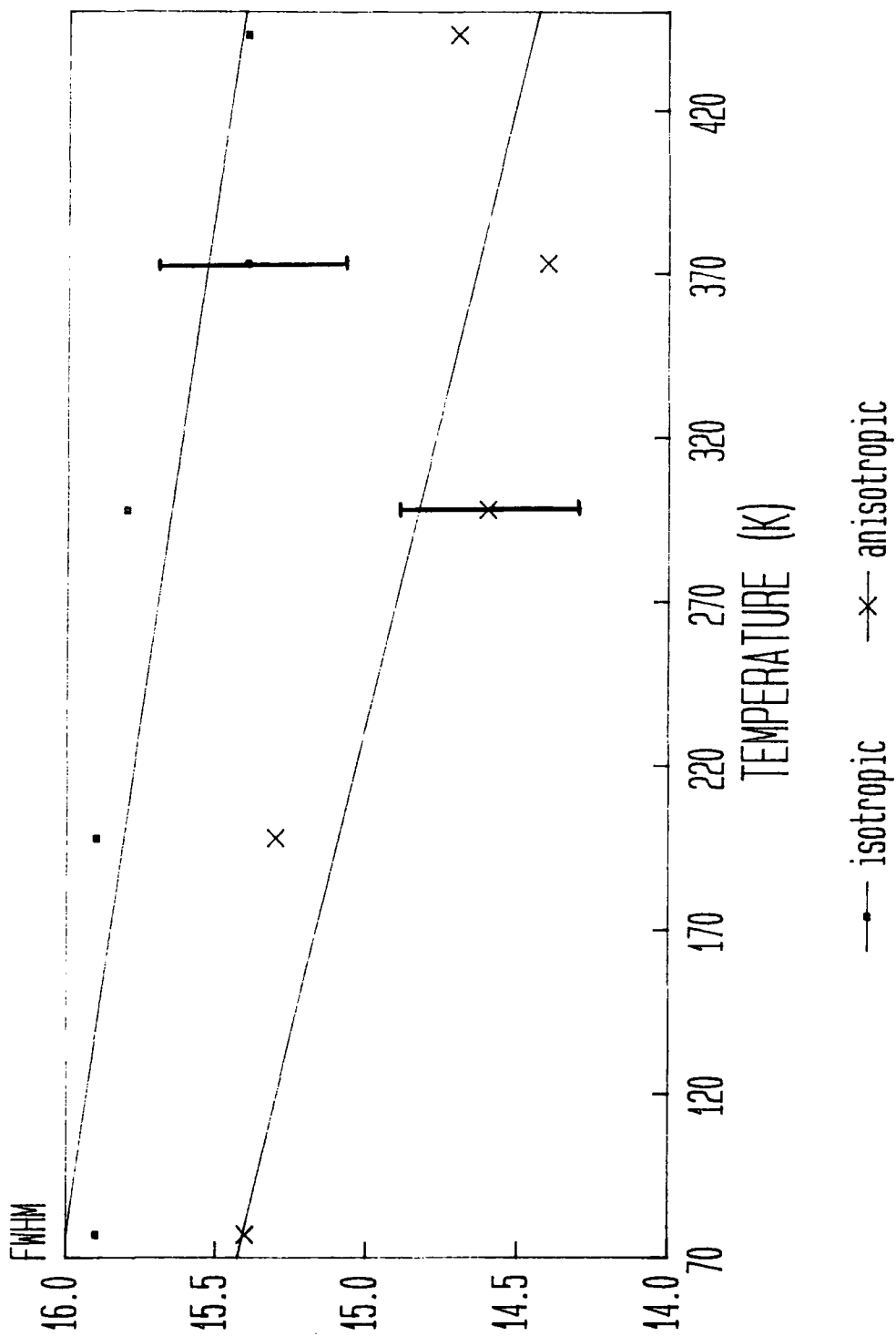
Figure 5.6. Variation of the FWHM (cm^{-1}) of the Raman
isotropic and anisotropic bands of the v(C=O) stretching
mode for EHB as a function of temperature.

5.2 Far infrared

The FIR spectra of EHB at 298 and 373K are shown in Fig.5.7. There is a decrease in frequency from $74cm^{-1}$ to $70.5cm^{-1}$, a difference of $3.5cm^{-1}$, on increasing the temperature from 298 to 373K. However neither the band width, intensity nor shape appear to change with increased temperature.
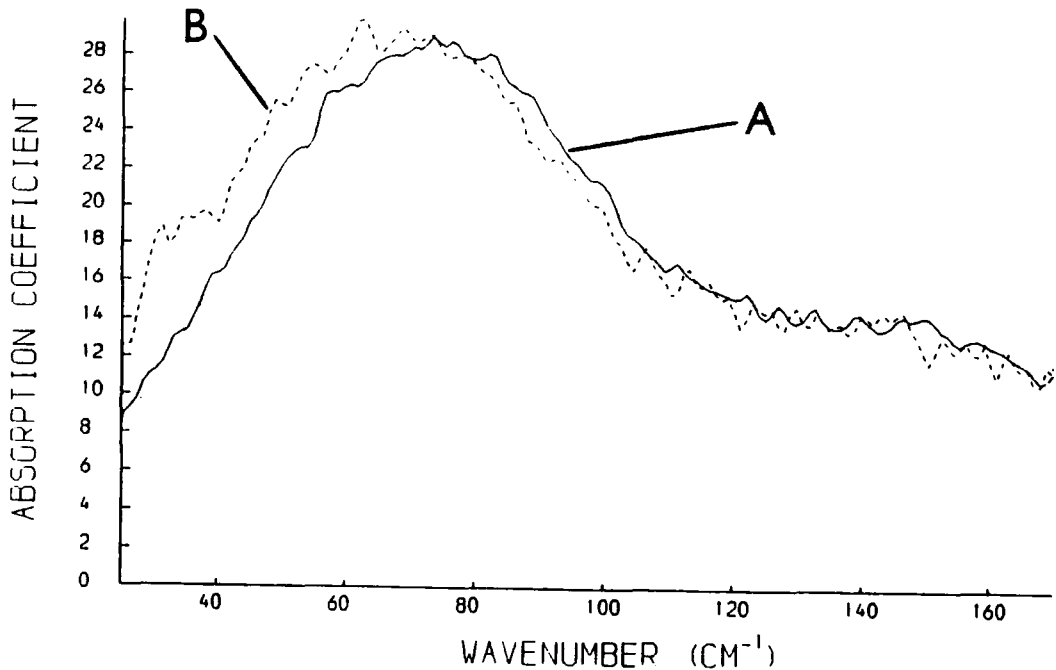
Figure 5.7. The far infrared spectra of EHB at A;298K and B;373K.

CHAPTER 6

RESULTS OF SOLUTION STUDIES

6.1 Raman

All Raman solution spectra were obtained as described in Section 3.1.1. Typical laser power at the sample was 300mw.

6.1.1 EHB in various solvents

Raman I(VV) and I(VH) spectra of the ring v(C-C) deformation mode (1003cm^{-1}), ring v(C-C) stretching mode (1605cm^{-1}), carbonyl v(C=O) stretching mode (1720cm^{-1}), the aliphatic v(C-H) stretching modes (3055-3085cm^{-1}) and aromatic v(C-H) stretching modes (3070cm^{-1}) were recorded, where possible, for liquid EHB and 10% mole fraction solutions of EHB in hexane, benzene and carbon disulphide.

Tables 6.1 to 6.6 summarise the frequency and FWHM of the corresponding anisotropic and isotropic bands computed from the spectra described above. Figs.6.1 to 6.11 show the relevant spectra. It can be seen that for EHB in hexane, in general all the bands studied show a blue frequency shift of varying degree, relative to their position in liquid EHB. Whilst in the more polarisable solvents carbon disulphide and benzene there is seen either no frequency shift or a very small red shift. The FWHM of all the bands decrease when in solution, the effect is greatest with the hexane solutions.

153

Tables 6.1 to 6.6. Variation of the Raman, I_{iso} and I_{aniso} , and infrared, I_{IR} , vibrational frequencies and band widths (FWHM) of the vibrational modes described in the text. For EHB and EHB at 10% mole fraction in hexane, benzene and CS2.

Table 6.1. Ring v(C-C) deformation mode

SOLUTION	FREQUENCY (CM^{-1})			FWHM (CM^{-1})		
	I_{iso}	I_{aniso}	I_{IR}	I_{iso}	I_{aniso}	I_{IR}
EHB	1003.4	1003.4	—	2.8	2.9	—
EHB/HEXANE	1003.4	1003.4	—	2.4	3.2	—
EHB/Bz	1003.5	—	—	2.6	—	—
EHB/CS$_2$	1003.5	1003.7	—	2.3	2.7	—

Estimated errors, based on reproducibility, are ± 0.1 cm^{-1}, for liquid EHB and ± 0.2 cm^{-1} for EHB in solution.

Table 6.2. Ring v(C-C) stretching mode

SOLUTION	FREQUENCY (CM^{-1})			FWHM (CM^{-1})		
	I_{iso}	I_{aniso}	I_{IR}	I_{iso}	I_{aniso}	I_{IR}
EHB	1603.0	1603.0	1603.0	6.5	6.6	8.0
EHB/HEXANE	1605.0	1605.0	1603.5	6.4	6.3	6.0
EHB/Bz	—	—	1602.5	—	—	6.0
EHB/CS$_2$	1603.0	1603.0	1602.5	6.5	6.5	6.0

Estimated errors, based on reproducibility, are ± 0.3 cm^{-1}, for liquid EHB and ± 0.5 cm^{-1} for EHB in solution.

Table 6.3. Carbonyl $v(C=O)$ stretching mode

SOLUTION	FREQUENCY (CM^{-1})			FWHM (CM^{-1})		
	I_{iso}	I_{aniso}	I_{IR}	I_{iso}	I_{aniso}	I_{IR}
EHB	1718.8	1722.1	1721.0	15.8	14.6	17.0
EHB/HEXANE	1727.9	1728.3	1727.0	10.7	10.9	10.0
EHB/Bz	1721.6	1721.6	1720.5	11.3	12.5	12.0
EHB/CS_2	1720.0	1720.0	1720.0	11.7	12.2	12.0

Estimated errors, based on reproducibility, are $\pm$ 0.3 cm^{-1}, for liquid EHB and $\pm$ 0.5 cm^{-1} for EHB in solution.

155

Tables 6.4. The aliphatic v(C-H) stretching modes; (a) $v_{as}(CH_3)$; (b) $v_{as}(CH_2)$; (c) $v_s(CH_3)$; (d) $v_s(CH_2)$

SOLUTION	(a) FREQUENCY (CM^{-1})			(b) FREQUENCY (CM^{-1})		
	I_{iso}	I_{aniso}	I_{IR}	I_{iso}	I_{aniso}	I_{IR}
EHB	2962.0	2962.0	2960.5	2937.0	—	2931.0
EHB/HEXANE	—	—	—	—	—	—
EHB/Bz	—	2964.0	2959.5	2938.0	—	2928.0
EHB/CS_2	2962.0	2962.0	2958.0	2935.0	—	2928.0

SOLUTION	(c) FREQUENCY (CM^{-1})			(d) FREQUENCY (CM^{-1})		
	I_{iso}	I_{aniso}	I_{IR}	I_{iso}	I_{aniso}	I_{IR}
EHB	2875.0	2875.0	2874.0	2862.0	2862.0	2862.5
EHB/HEXANE	—	—	—	—	—	—
EHB/Bz	2877.0	—	2874.0	2864.0	—	2862.5
EHB/CS_2	2875.0	2876.0	2871.5	2860.0	2860.0	2858.5

Estimated errors, based on reproducibility, are ± 1.0 cm^{-1}, for liquid EHB and ± 2.0 cm^{-1} for EHB in solution.

Table 6.5. Frequencies of the aromatic v(C-H) stretching modes

SOLUTION	FREQUENCY (CM^{-1})			FREQUENCY (CM^{-1})		
	I_{iso}	I_{aniso}	I_{IR}	I_{iso}	I_{aniso}	I_{IR}
EHB	3073.0	3073.0	—	—	3063.0	—
EHB/HEXANE	3076.0	3075.0	—	—	3065.0	—
EHB/Bz	—	—	—	—	—	—
EHB/CS_2	3072.0	3072.0	—	—	3063.0	—

Estimated errors, based on reproducibility, are $\pm$ 0.5 cm^{-1}, for liquid EHB and $\pm$ 1.0 cm^{-1} for EHB in solution.

Table 6.6. Widths of the Raman and infrared envelopes of the aliphatic and aromatic v(C-H) stretching modes; (a) aliphatic C-H stretching envelope; (b) aromatic C-H stretching envelope

SOLUTION	(a) BAND WIDTH AT 1/4 MAXIMUM HEIGHT			(b) FWHM (CM^{-1})		
	I_{iso}	I_{aniso}	I_{IR}	I_{iso}	I_{aniso}	I_{IR}
EHB	131.0	141.0	132.0	14.0	24.0	—
EHB/HEXANE	—	—	—	—	—	—
EHB/Bz	—	—	132.0	—	—	—
EHB/CS_2	125.0	133.0	132.0	10.0	21.0	—

Estimated errors, based on reproducibility, are $\pm$ 1.0 cm^{-1}, for liquid EHB and $\pm$ 2.0 cm^{-1} for EHB in solution.
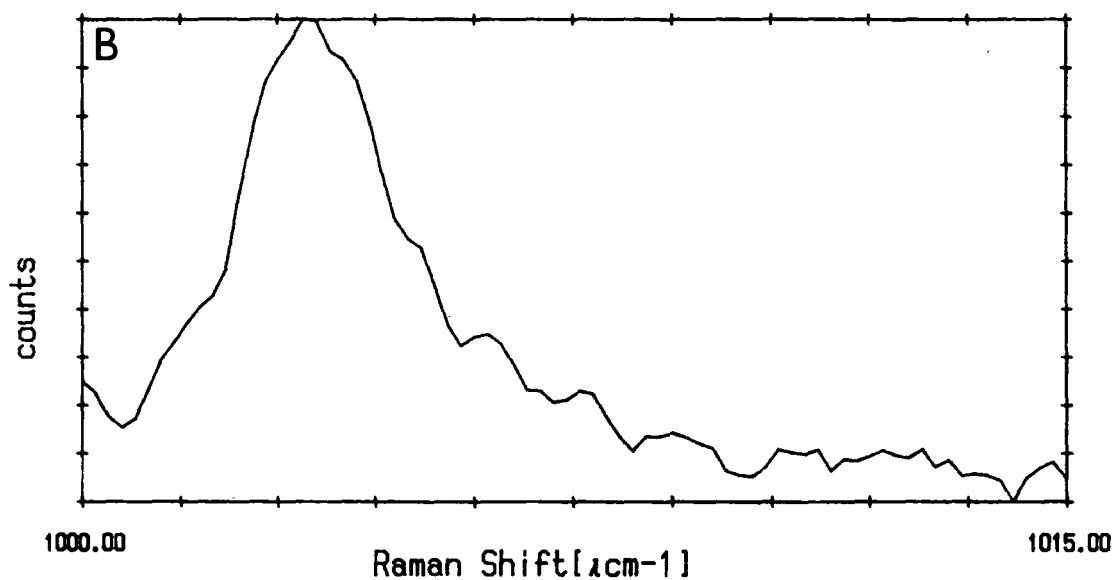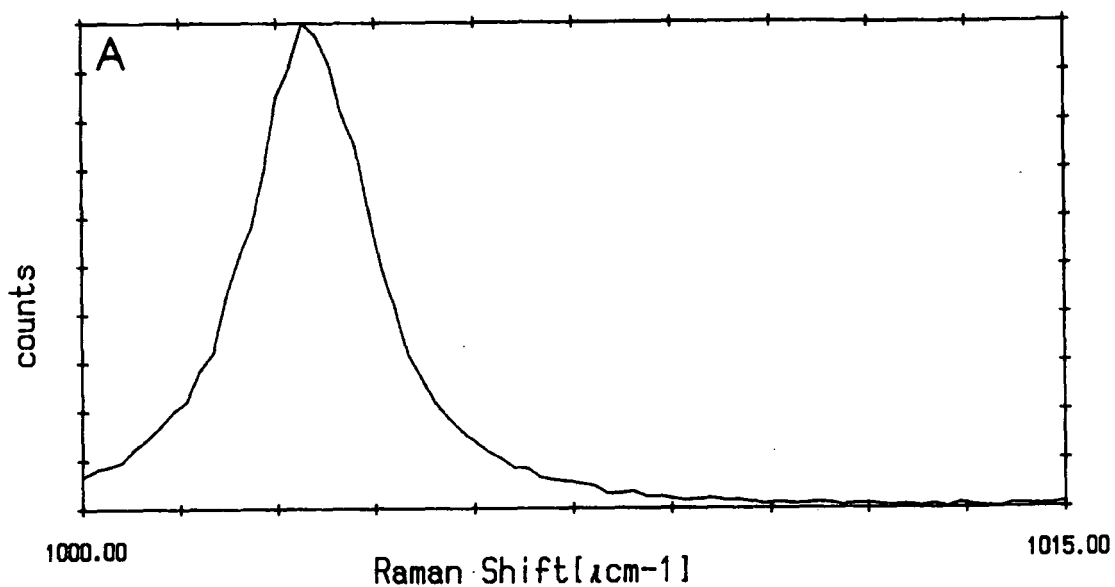
Figure 6.1. Raman, A;isotropic and B;anisotropic bands of
the ring v(C-C) deformation mode, for EHB at 10% mole
fraction in hexane. The anisotropic band has been smoothed
(9 point) to help obtain the peak frequency.
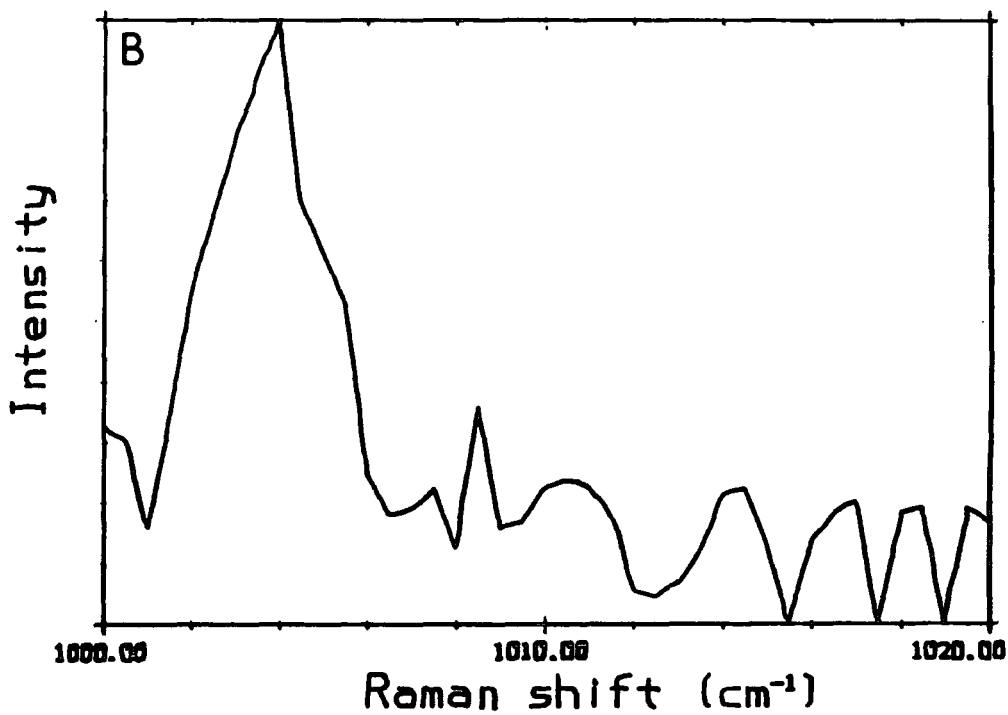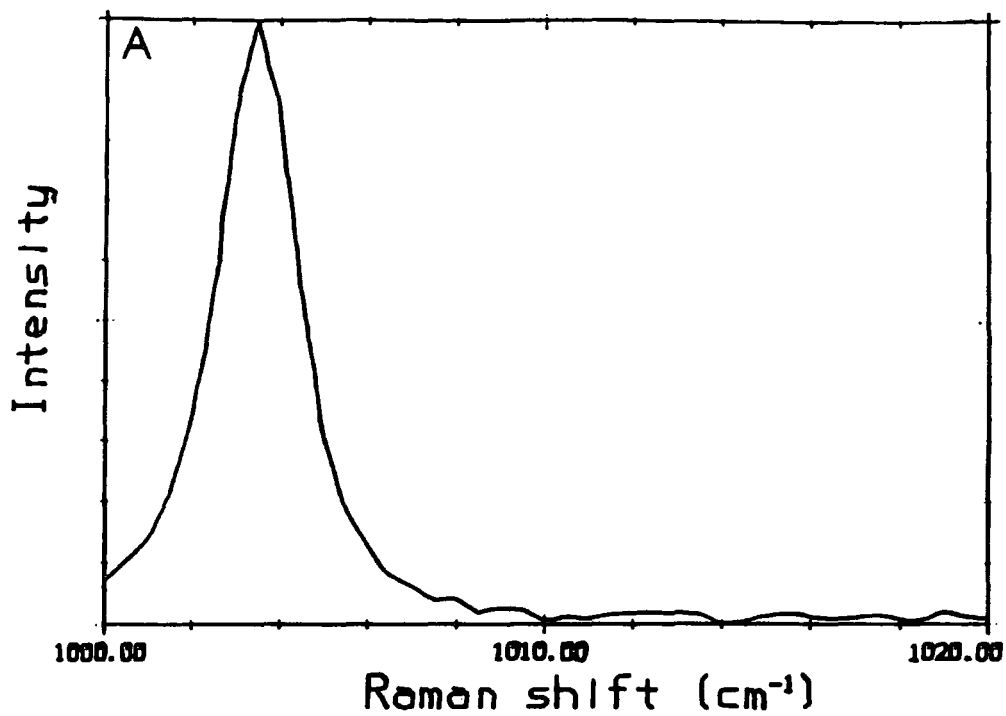
Figure 6.2. Raman, A;isotropic and B;anisotropic bands of
the ring v(C-C) deformation mode, for EHB at 10% mole
fraction in CS_2.

159
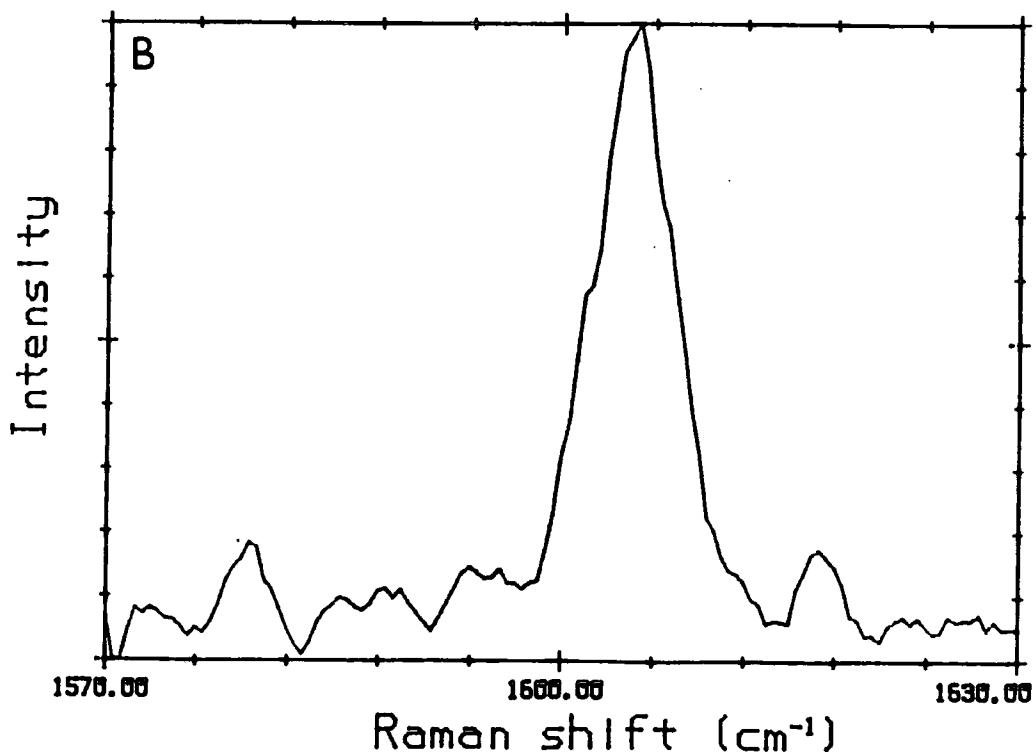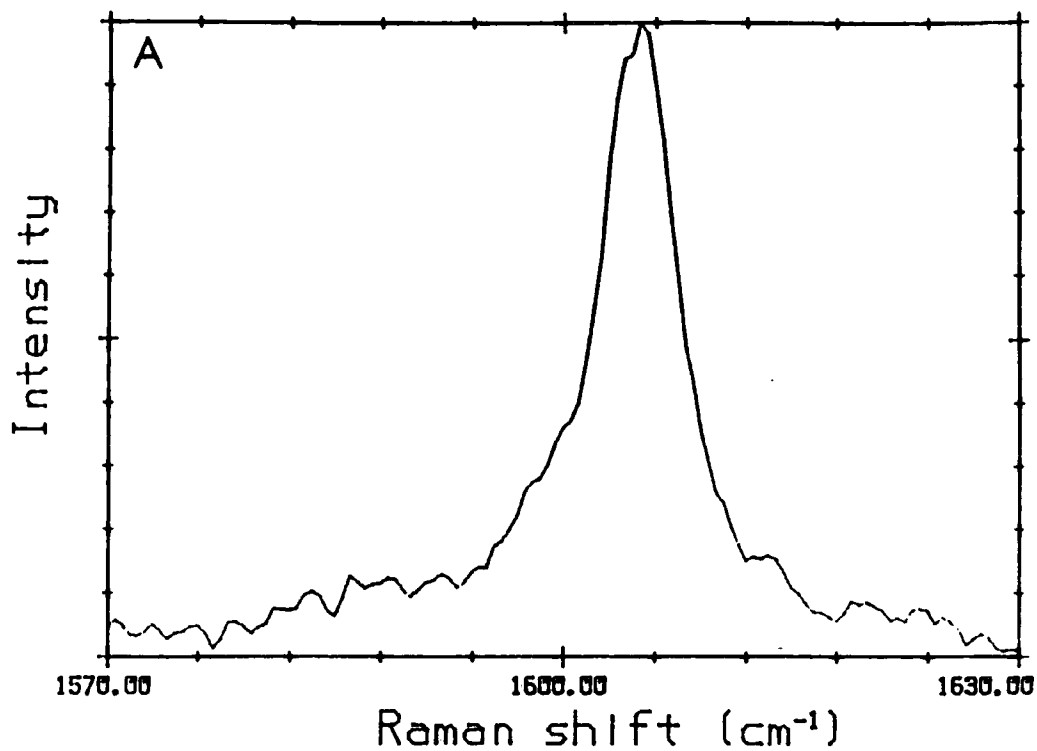
Figure 6.3. Raman, A;isotropic and B;anisotropic, bands of
the ring v(C-C) stretching mode, for EHB at 10% mole
fraction in hexane.
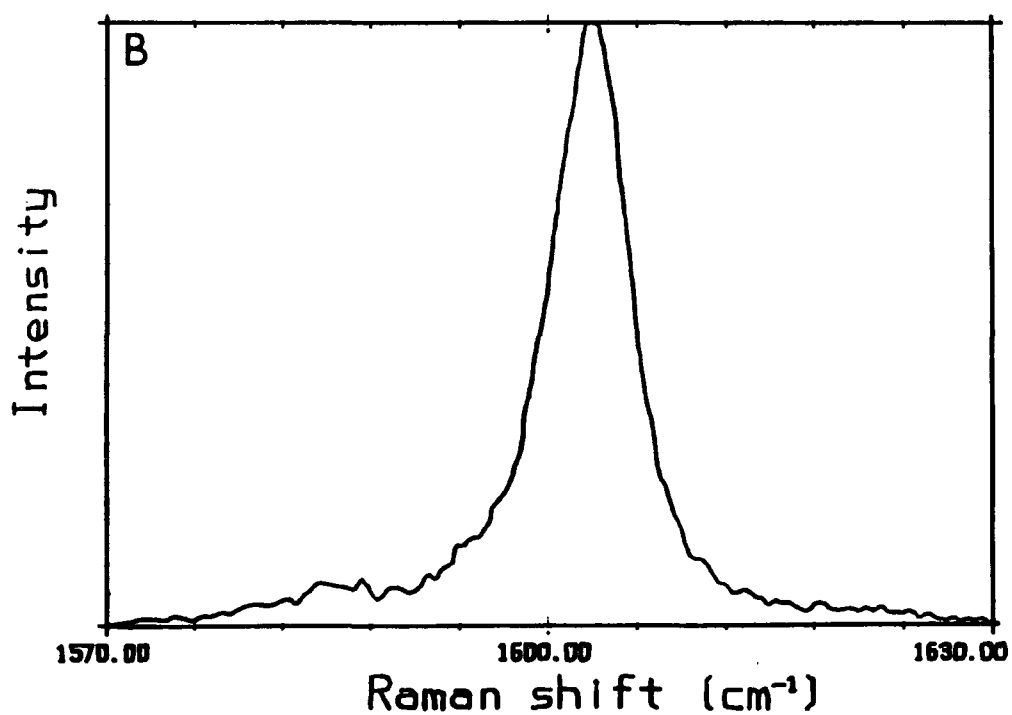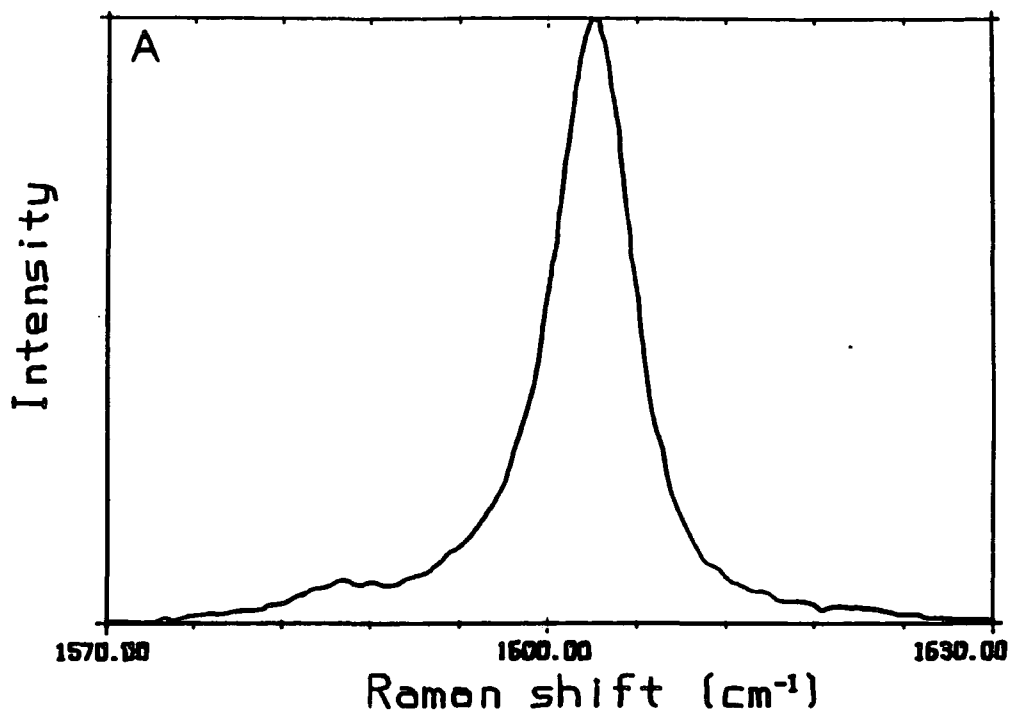
Figure 6.4. Raman, A;isotropic and B;anisotropic, bands of
the ring v(C-C) stretching mode, for EHB at 10% mole
fraction in CS2.
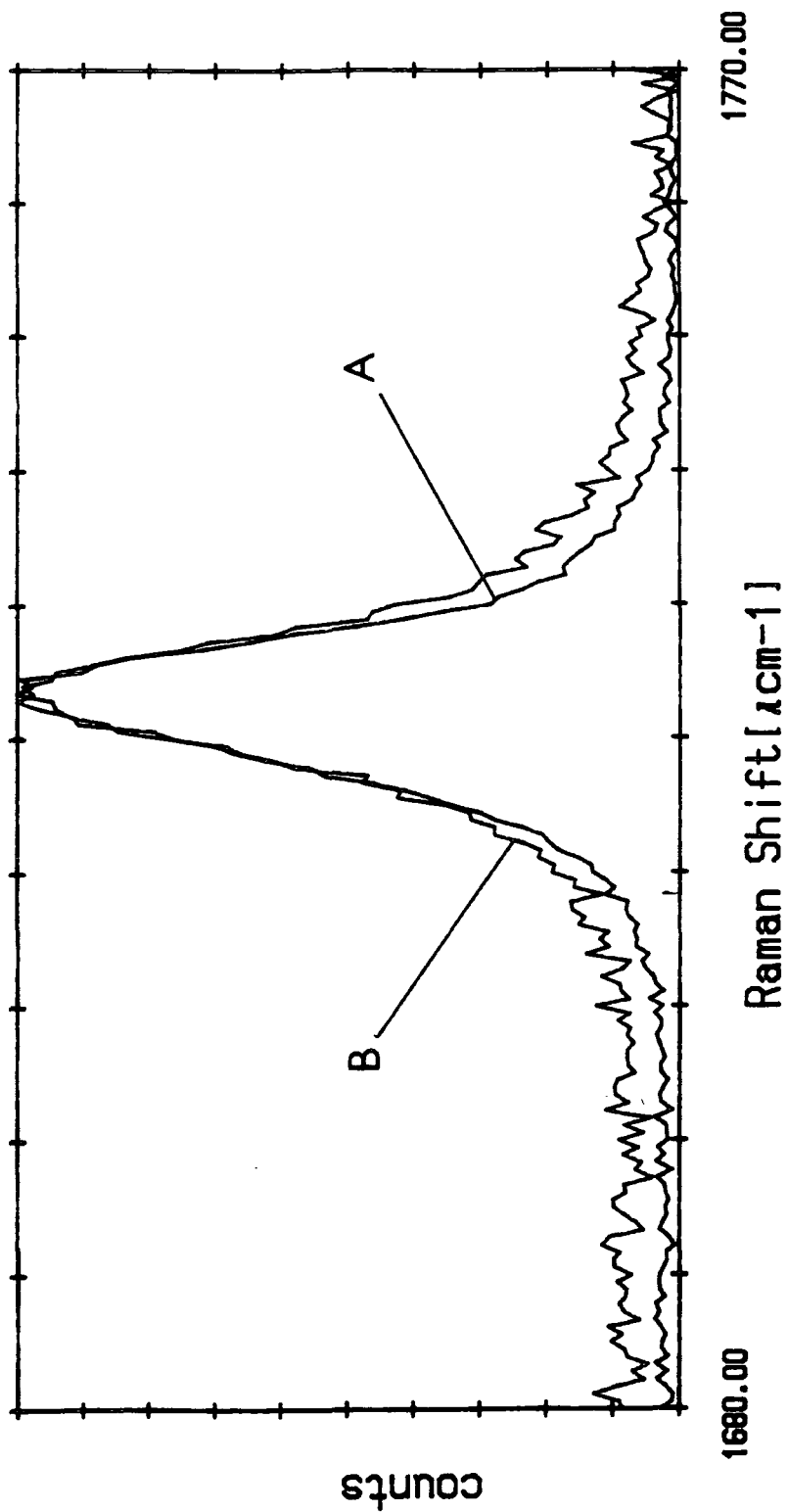
Figure 6.5. Raman, A;isotropic and B;anisotropic, bands of
the carbonyl v(C=O) stretching mode, for EHB at 10% mole
fraction in hexane.
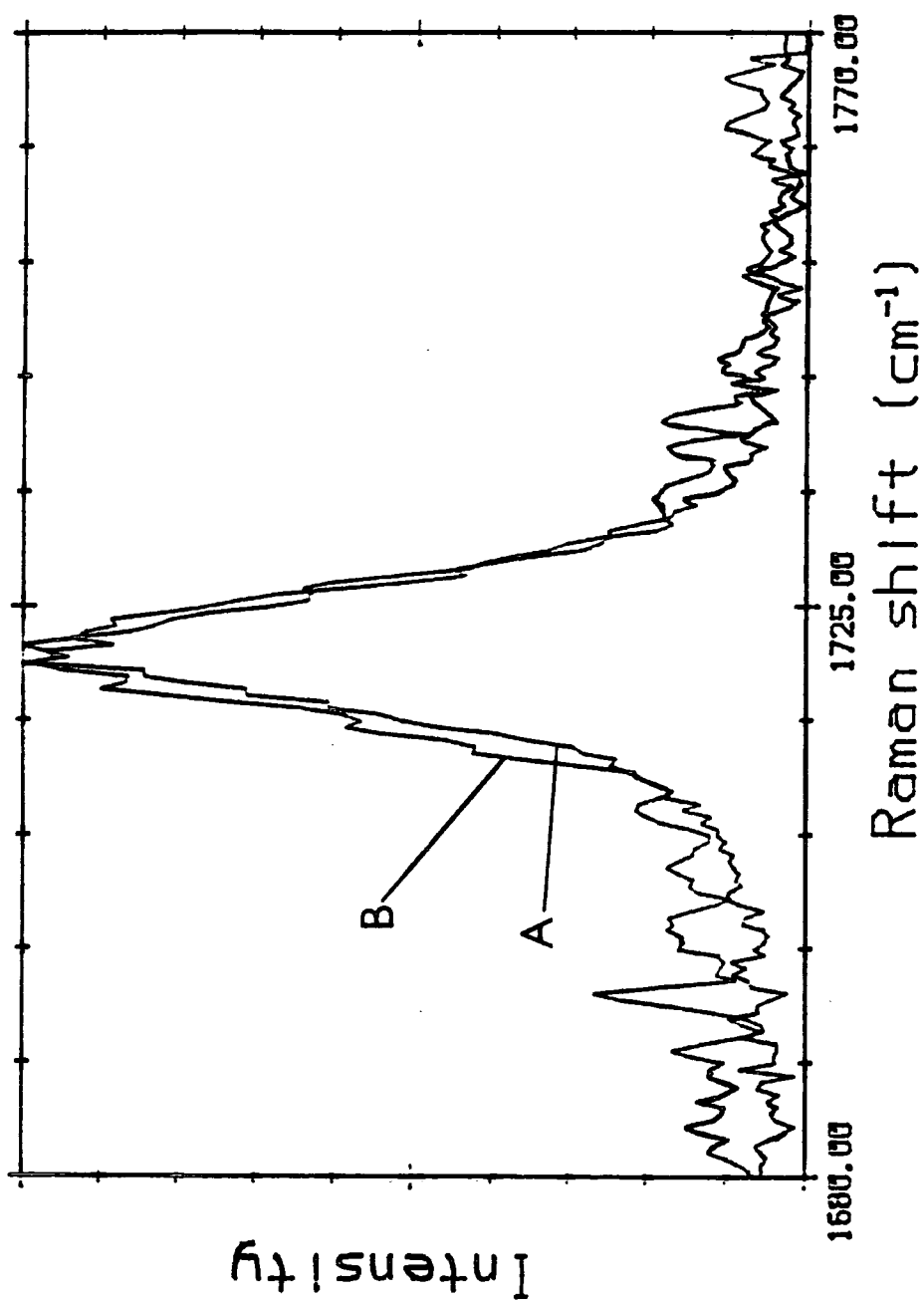
Figure 6.6. Raman, A;isotropic and B;anisotropic, bands of
the carbonyl v(C=O) stretching mode, for EHB at 10% mole
fraction in benzene.
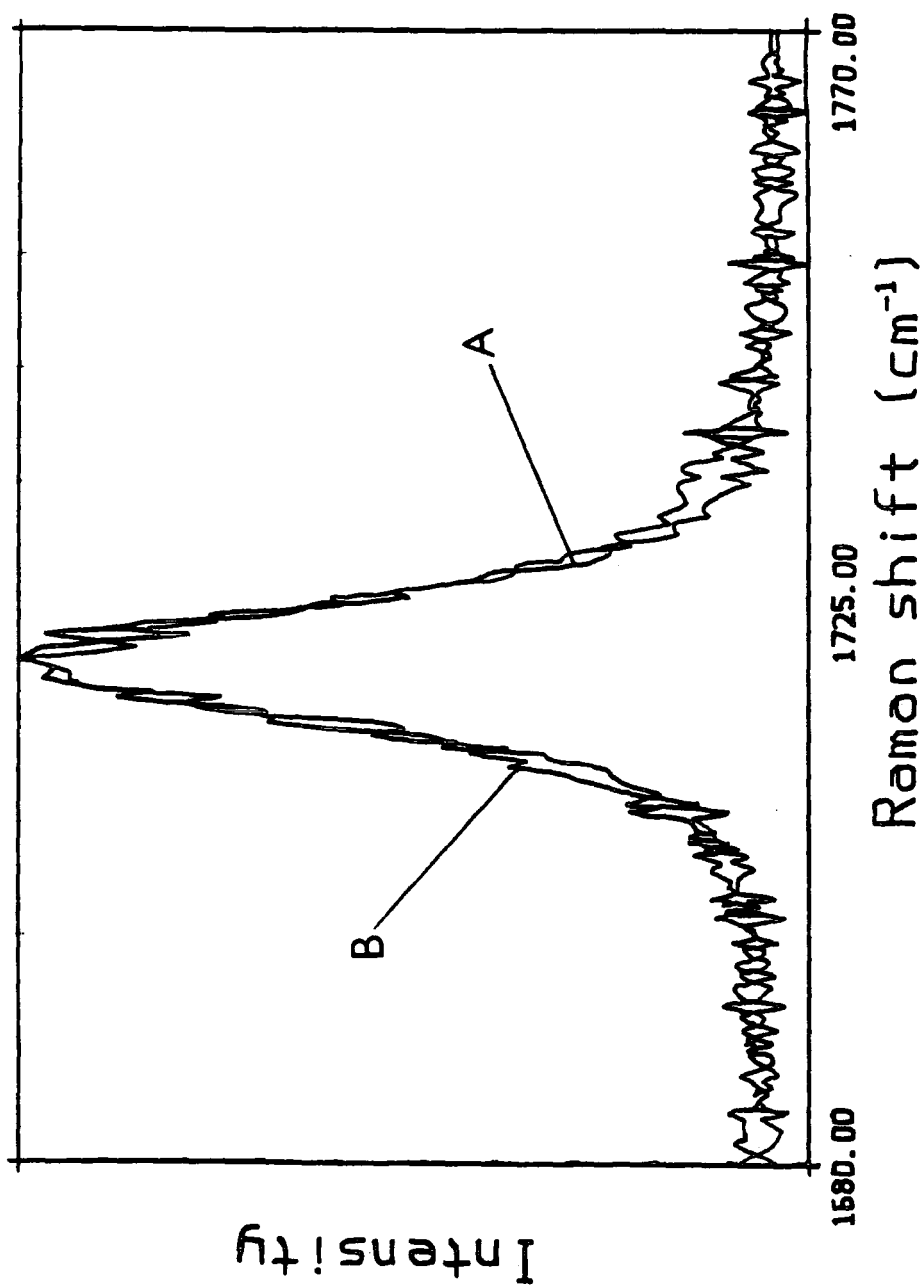
Figure 6.7. Raman, A;isotropic and B;anisotropic, bands of the carbonyl v(C=O) stretching mode, for EHB at 10% mole fraction in CS2.
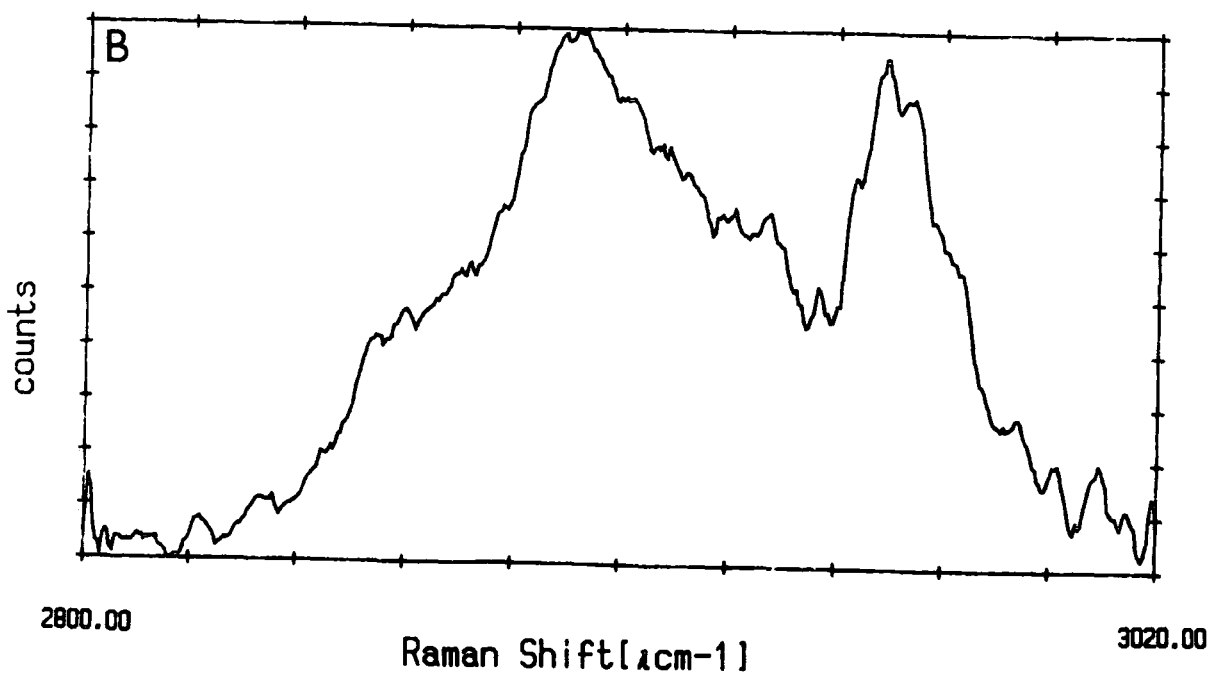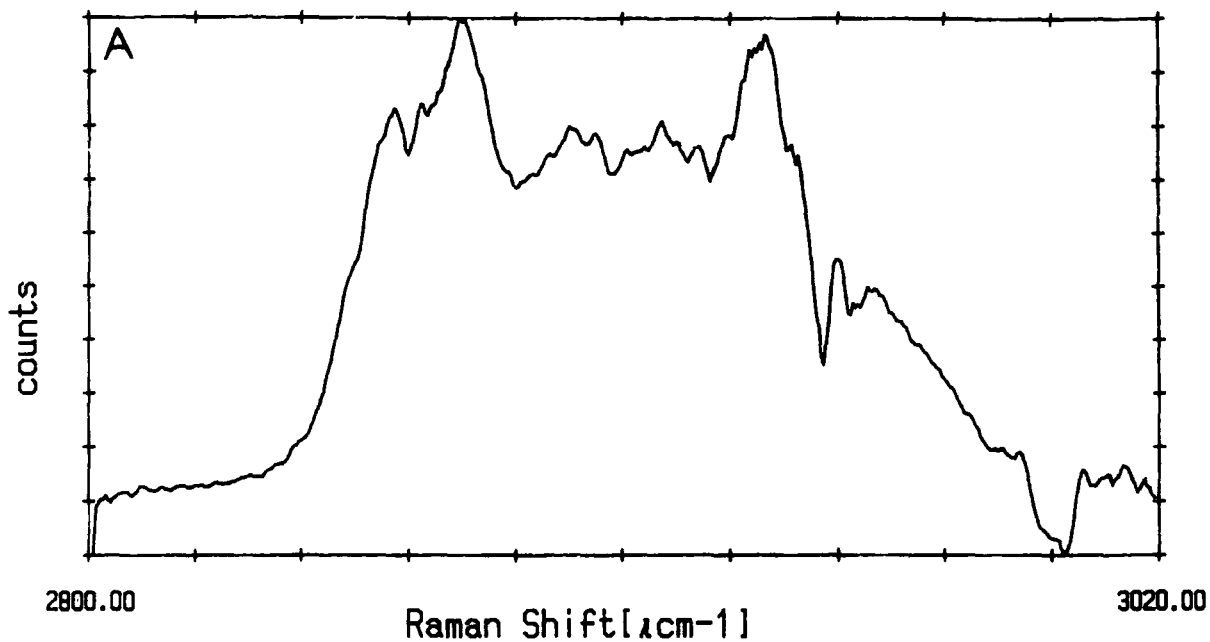
Figure 6.8. Raman, A;isotropic and B;anisotropic, envelope of the aliphatic v(C-H) stretching modes, for EHB at 10% mole fraction in benzene.

165
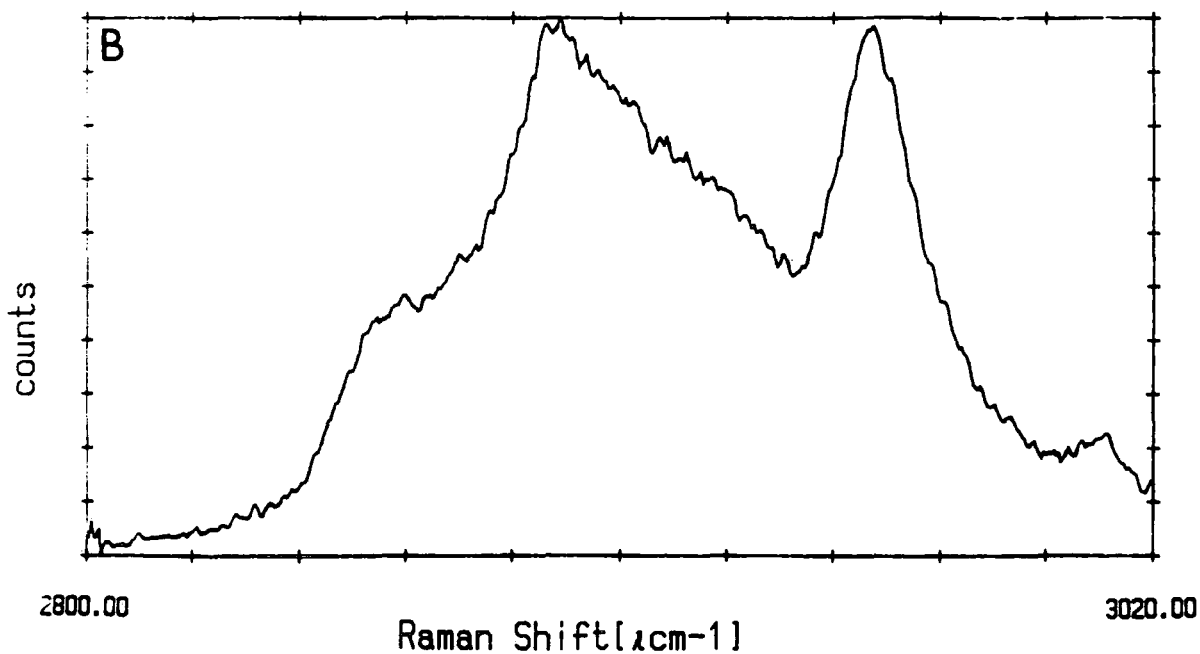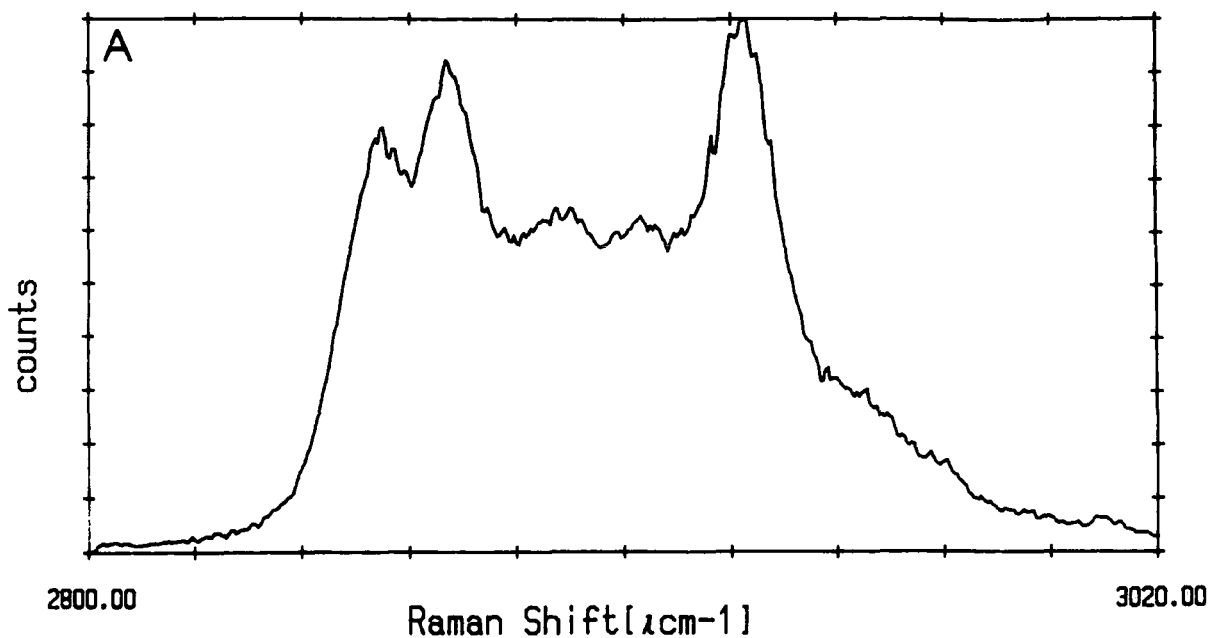
Figure 6.9. Raman, A;isotropic and B;anisotropic, envelope of the aliphatic v(C-H) stretching modes, for EHB at 10% mole fraction in CS2.
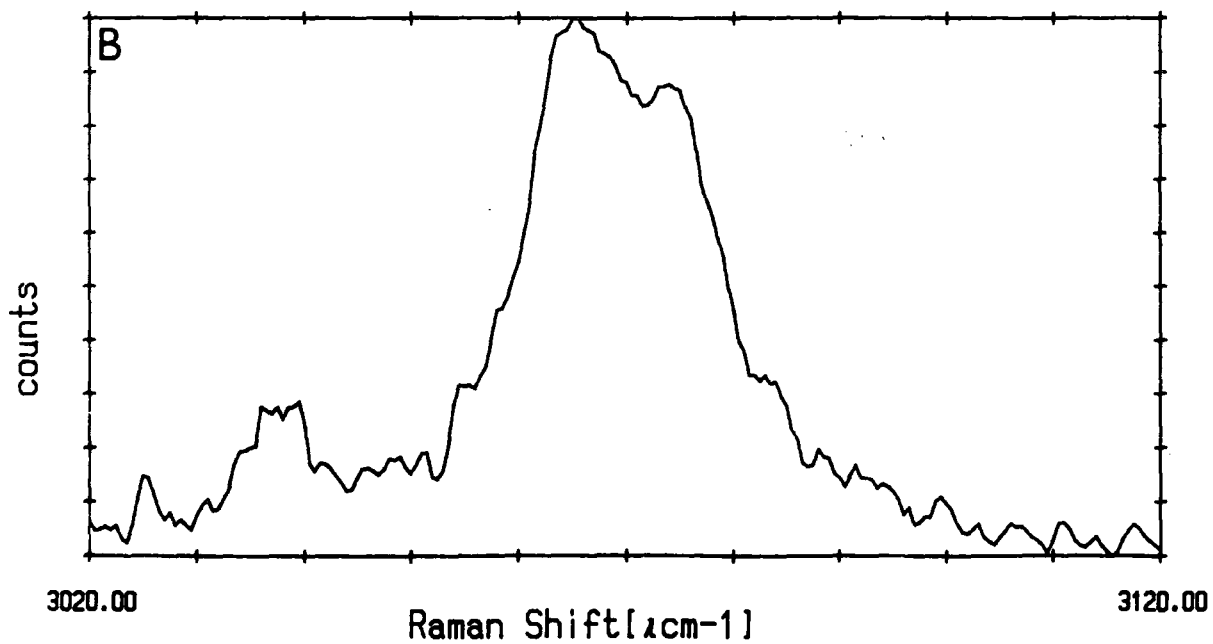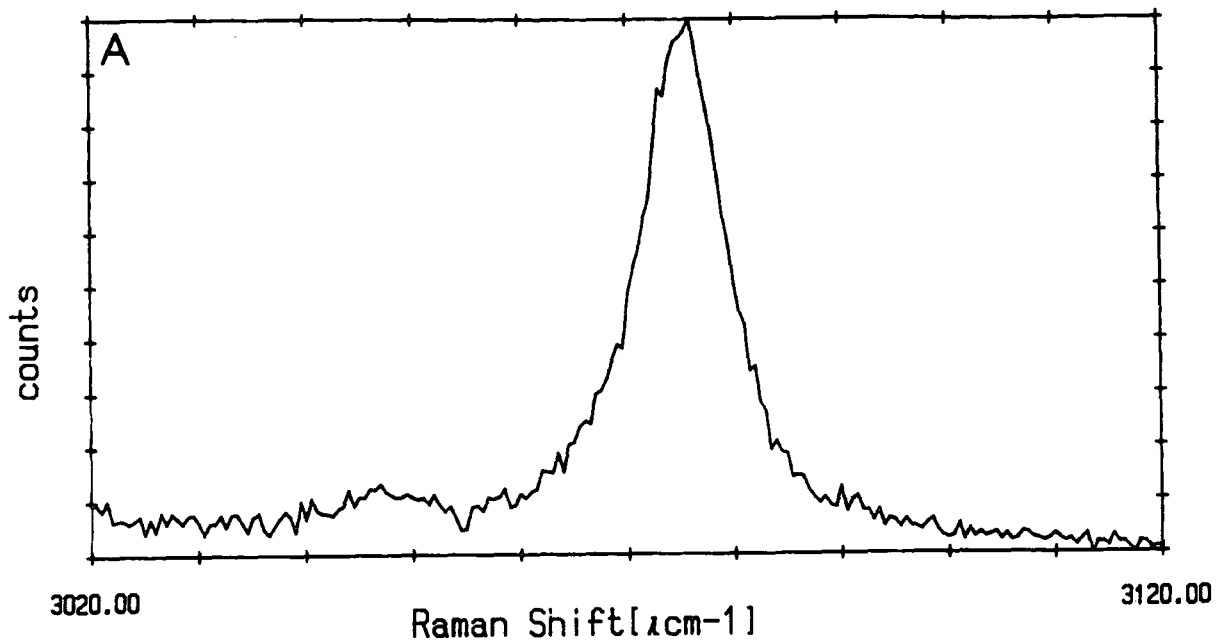
Figure 6.10. Raman, A;isotropic and B;anisotropic, envelope of the aromatic v(C-H) stretching modes, for EHB at 10% mole fraction in hexane.

167
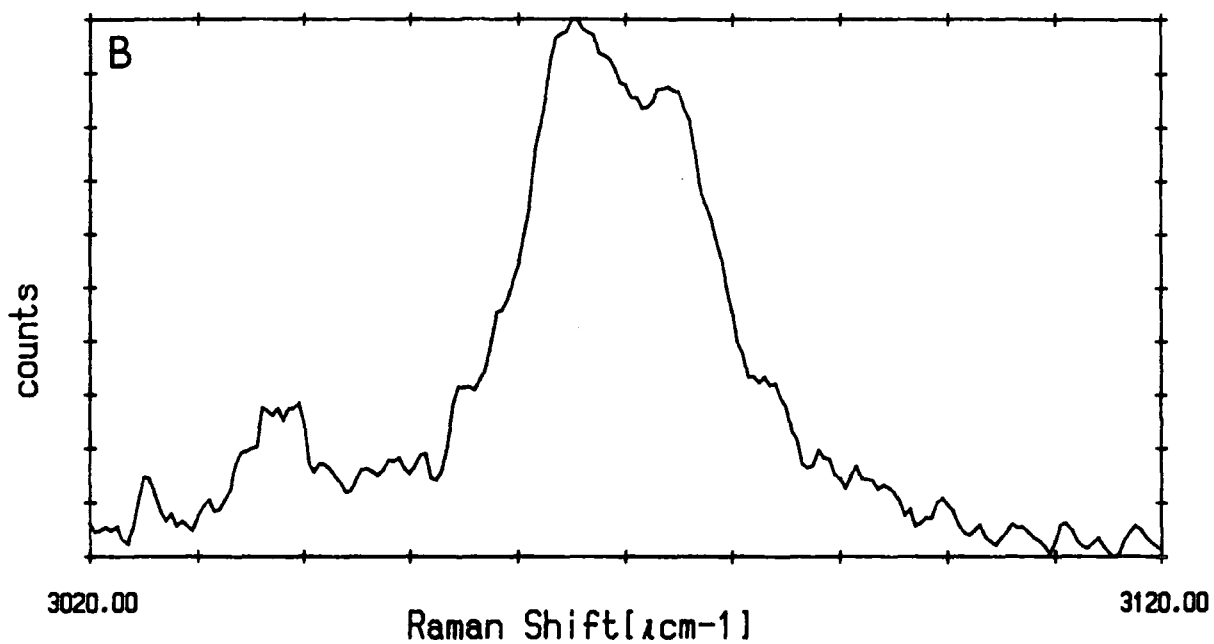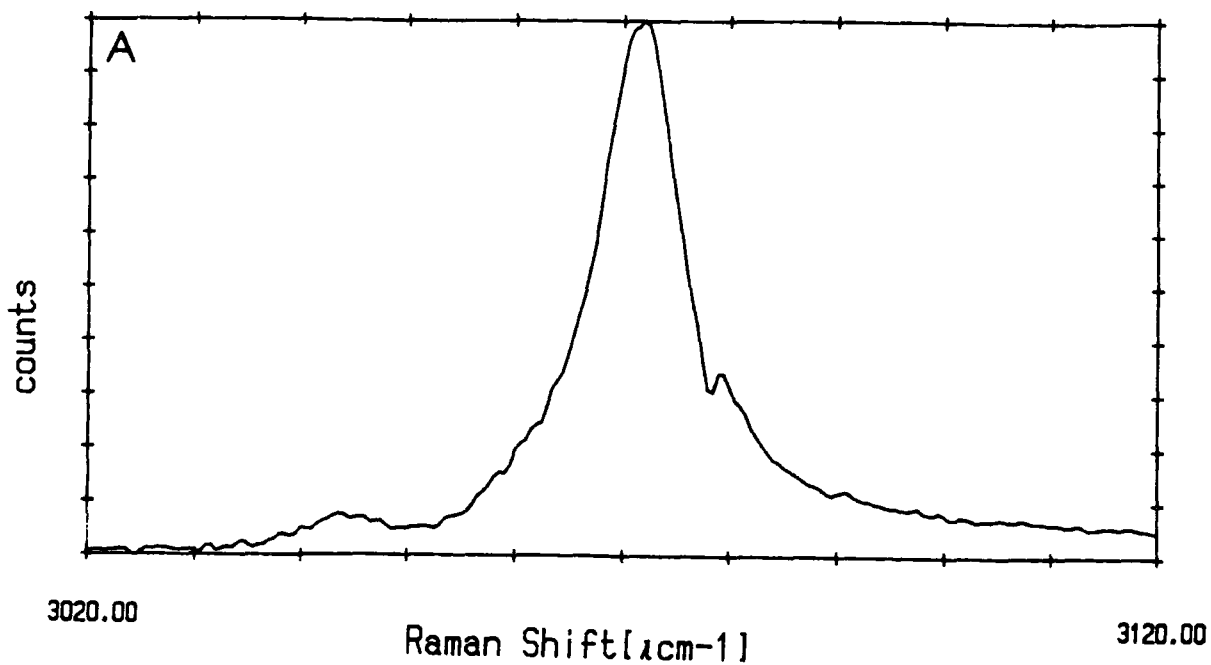
Figure 6.11. Raman, A;isotropic and B;anisotropic, envelope of the aromatic v(C-H) stretching modes, for EHB at 10% mole fraction in CS2.

The greater change in frequency and FWHM, on going from
EHB liquid to EHB in solution, for the $v(C=O)$ stretching
mode compared to the other modes is in part related to the
RET effect, see Section.7.2. The non-coincidence of the
isotropic and anisotropic bands, caused by the RET is no
longer present at 10% mole fraction in all three solvents,
see Figs.6.5-6.7.

6.1.2 Hexane dilution of EHB

The depolarised and polarised Raman spectra of the ring
$v(C-C)$ deformation and $v(C=O)$ stretching modes of EHB were
measured as a function of concentration in hexane, the
spectral details are summarised in Tables.6.7 and 6.8. The
variation of peak frequency and FWHM for the isotropic
$v(C=O)$ stretching mode are illustrated in Fig.6.12. The
ring deformation band shows no change in peak frequency nor
FWHM down to 5% mole fraction. Figs.6.13 and 6.14 show the
non-linear frequency shift and band narrowing of the $v(C=O)$
stretching band with decreasing concentration. It can also
be seen from Fig.6.13 that the noncoincidence of the
isotropic and anisotropic peaks disappears with decreasing
concentration until the two peaks come together at about 10%
mole fraction EHB in hexane.

CONCN (m.f.)	FREQUENCY (CM^{-1})			FWHM (CM^{-1})		
	I_{iso}	I_{aniso}	I_{IR}	I_{iso}	I_{aniso}	I_{IR}
100%	1003.4	1003.4	—	2.8	2.9	—
80%	1003.4	1003.4	—	2.7	3.0	—
60%	1003.4	1003.4	—	2.5	2.9	—
40%	1003.4	1003.4	—	2.4	2.9	—
30%	1003.4	1003.4	—	2.4	3.3	—
20%	1003.4	1003.4	—	2.4	3.2	—
10%	1003.4	1003.4	—	2.4	3.2	—
5%	1003.4	1003.4	—	2.4	—	—

Estimated errors. based on reproducibility, range from ± 0.1 cm^{-1} for the highest concentration solutions to ± 0.2 cm^{-1} for the lowest concentrations.

Table 6.7. Spectral details of the Raman bands of the ring v(C-C) deformation mode of EIIB, as a function of concentration in hexane.

	FREQUENCY (CM^{-1})			FWHM (CM^{-1})		
CONCN (m.f.)	I_{iso}	I_{aniso}	I_{IR}	I_{iso}	I_{aniso}	I_{IR}
100%	1718.8	1722.1	1721.0	15.8	14.6	17.0
80%	1719.9	1723.0	1721.5	15.6	14.6	16.0
70%	—	—	1722.0	—	—	15.5
60%	1721.5	1724.0	1722.5	15.4	14.0	15.0
50%	—	—	1722.5	—	—	14.0
40%	1723.1	1725.3	1724.0	14.5	13.3	13.5
30%	1724.6	1726.1	1725.0	14.0	12.9	13.0
20%	1726.3	1727.0	1725.5	12.9	12.4	12.0
10%	1727.9	1728.3	1727.0	10.7	10.9	10.0
5%	1728.7	1728.6	1728.0	9.0	11.5	9.5
2%	1729.6	1729.1	1728.5	7.8	11.2	8.5
1%	1729.6	1729.4	1728.5	—	—	7.5
0.5%	—	—	1728.5	—	—	7.5
0.2%	—	—	1728.5	—	—	—
0.1%	—	—	1728.5	—	—	—

Estimated errors, based on reproducibility, range from ± 0.3 cm^{-1} for the highest concentration solutions to ± 1.0 cm^{-1} for the lowest concentrations.

Table 6.8. Spectral details of the infrared and Raman bands of the v(C=O) stretching mode of EHB, as a function of concentration in hexane.
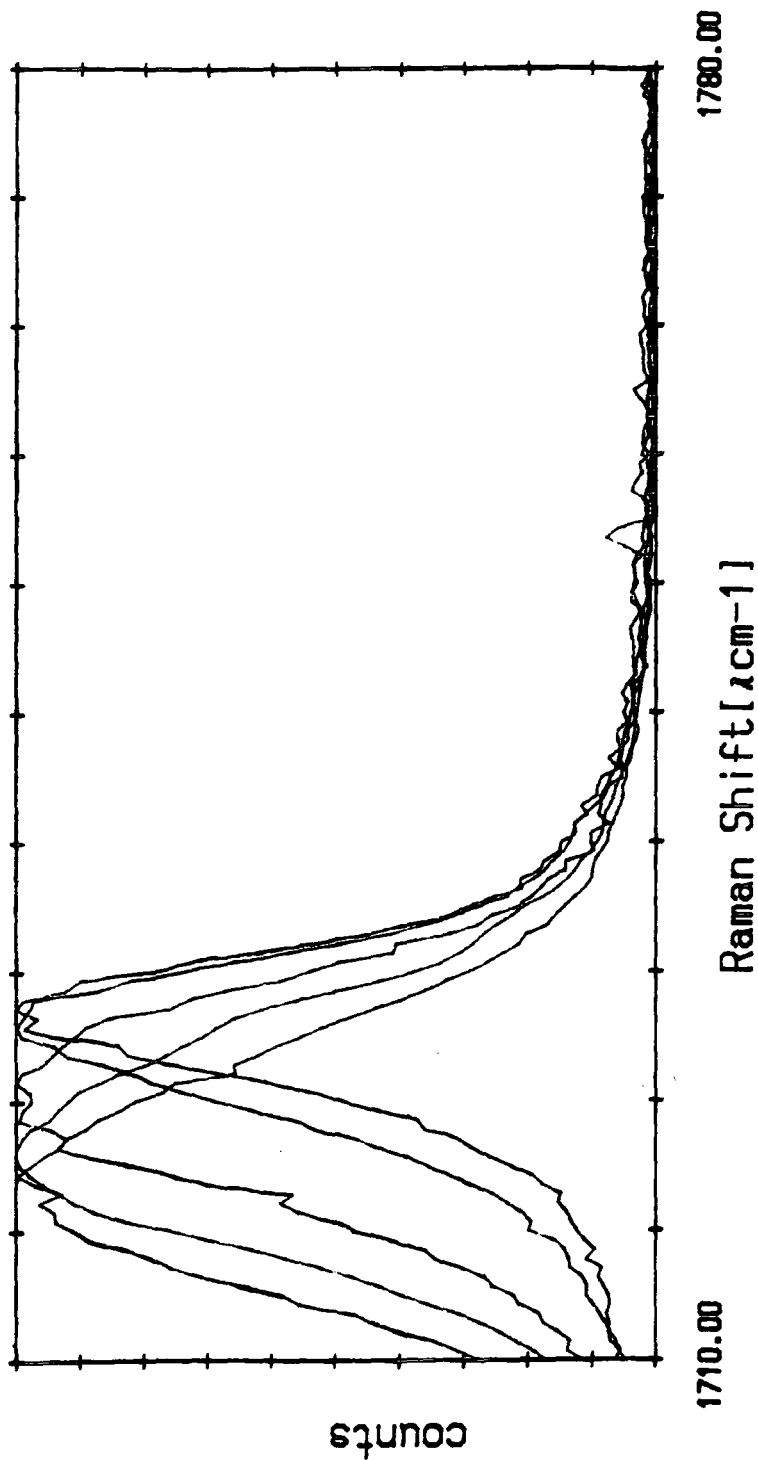
Figure 6.12. The variation of the Raman isotropic band of
the v(C=O) stretching mode of EHB as a function of
concentration in hexane. From left to right the bands are
for EHB at 100, 60, 30, 10 and 5% mole fraction
concentration respectively.

172
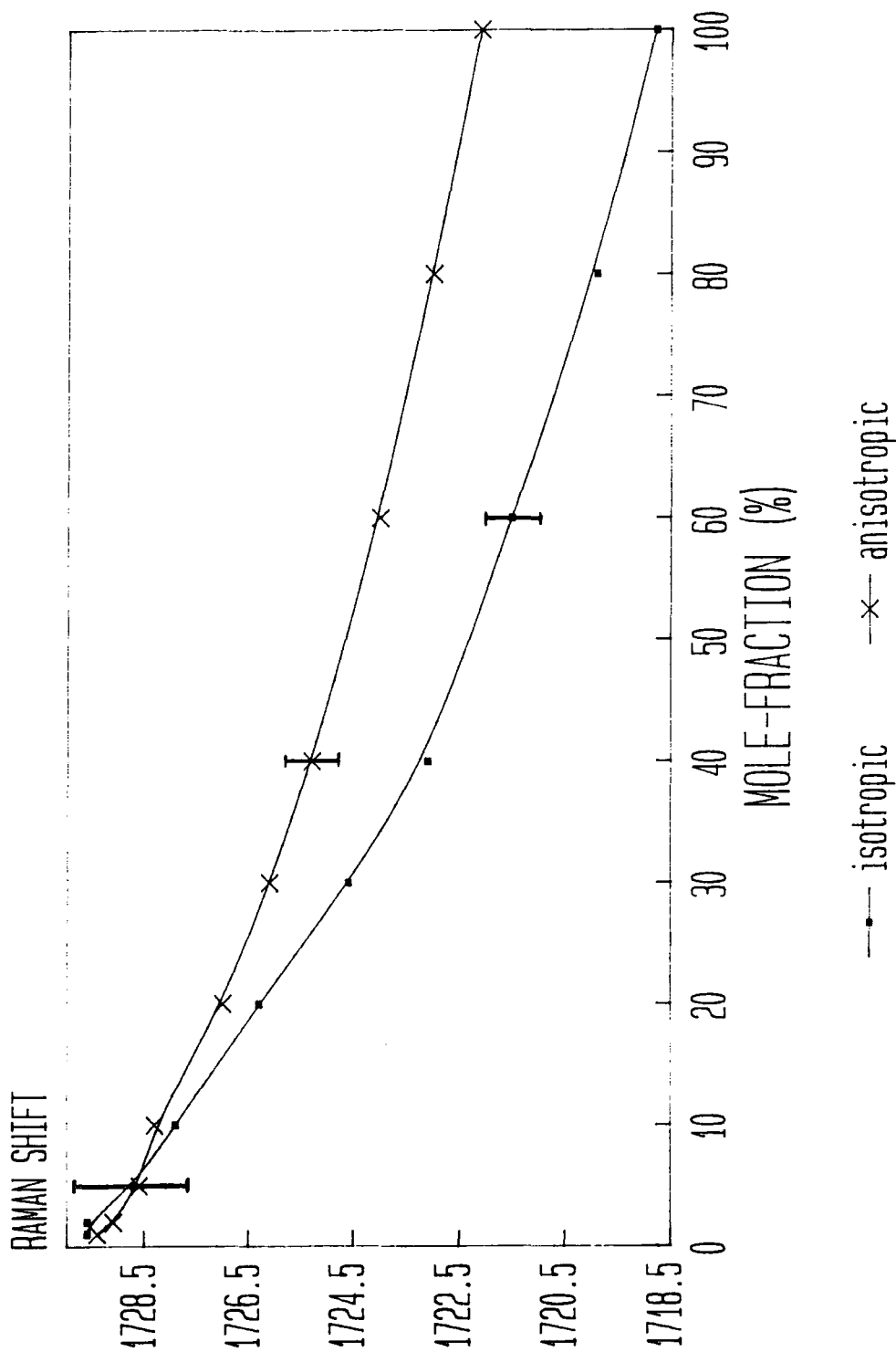
Figure 6.13. The frequency (cm^{-1}) of the Raman isotropic and anisotropic bands of the $v(C=O)$ stretching mode of EHB as a function of concentration in hexane.
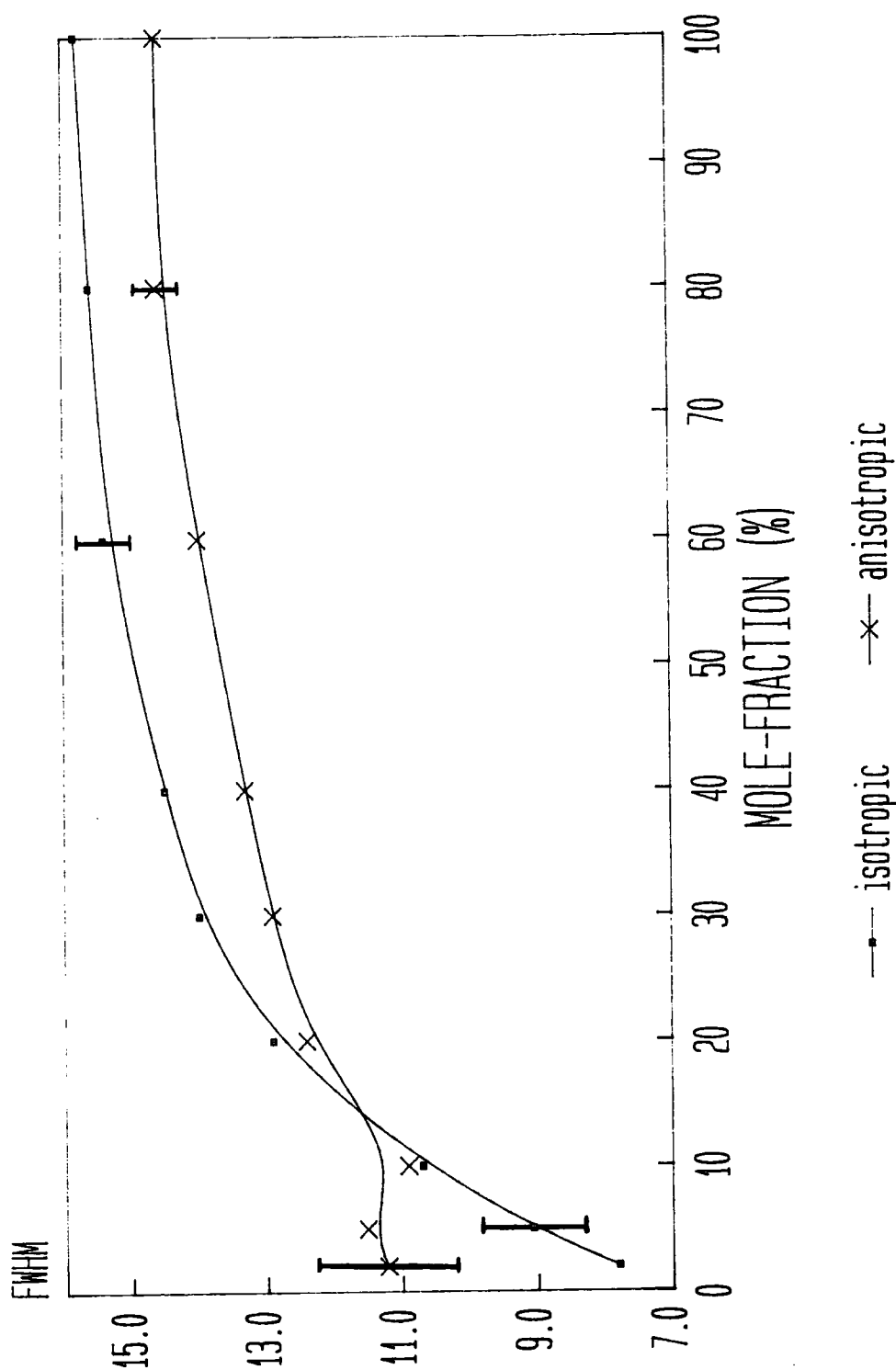
Figure 6.14. The band width (FWHM, cm^{-1}) of the Raman isotropic and anisotropic bands of the $v(C=O)$ stretching mode of EHB as a function of concentration in hexane.

6.2 Mid-infrared

A resolution of $0.96cm^{-1}$ was employed for all the solution studies. For the very low concentration solutions (5% to 0.5% m.f.) $50\mu m$ and 0.1mm thick films were used.

6.2.1 EHB in various solvents

The solutions and modes studied were the same as for the Raman solution work, the only difference being that the v(C-C) ring deformation mode and the aromatic v(C-H) stretching mode are very weak in the infrared, and were therefore not studied. Tables.6.2 to 6.6 show the peak frequencies and FWHM of the bands studied for the 10% mole fraction EHB solutions. Figs.6.15 to 6.17 show the relevant spectra. As with the Raman work there is little if any change in the frequency positions of the bands in the the polarisable solvents carbon disulphide and benzene, whilst in hexane there is a blue frequency shift, for all the bands, which is much greater for the v(C=O) stretching mode. The FWHM of all the bands show a similar decrease to those seen in the Raman solution spectra.
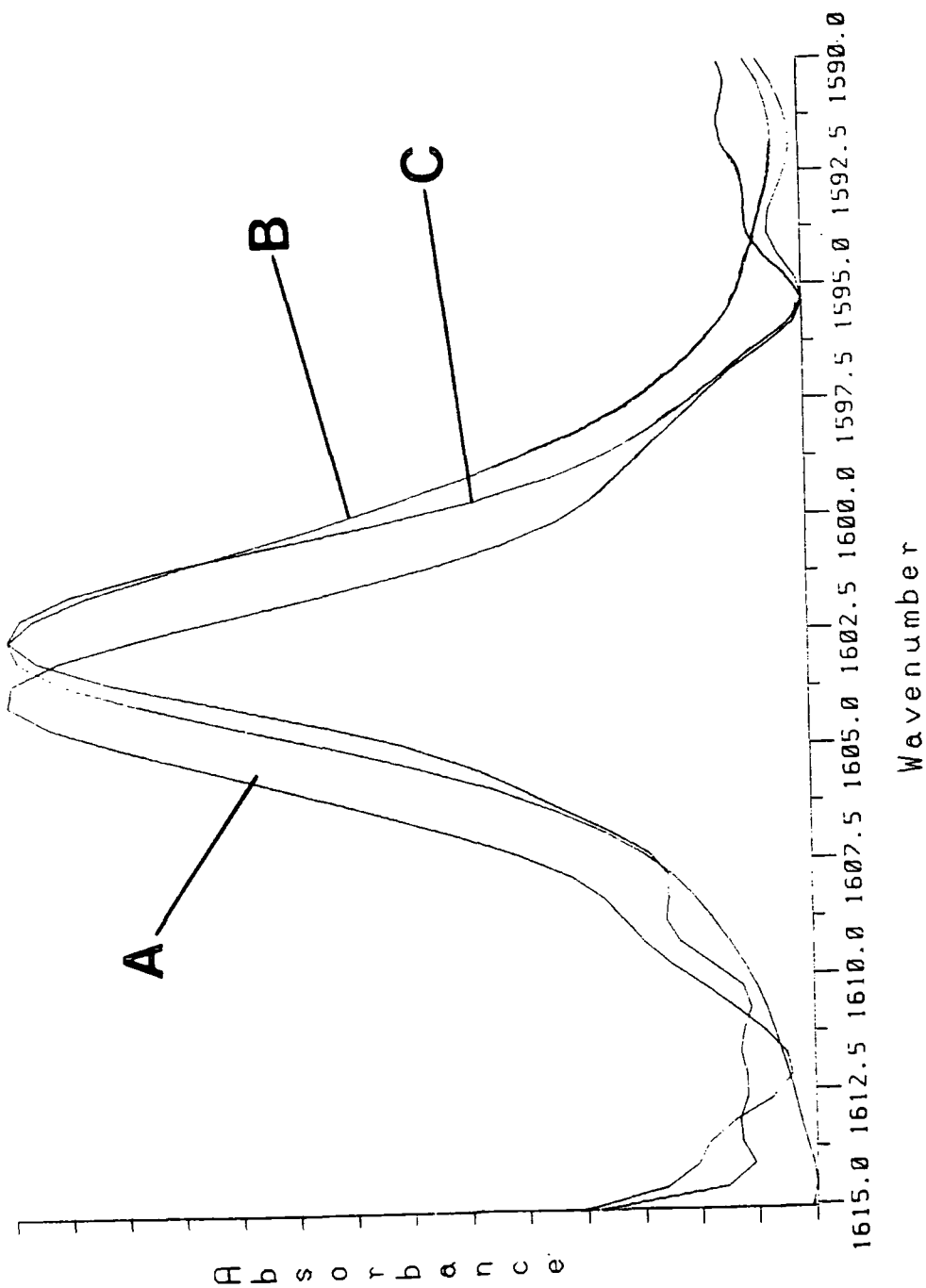
Figure 6.15. The infrared band of the ring v(C-C) stretching mode for EHB at 10% mole fraction concentration in A;hexane, B;CS2, and C;benzene.
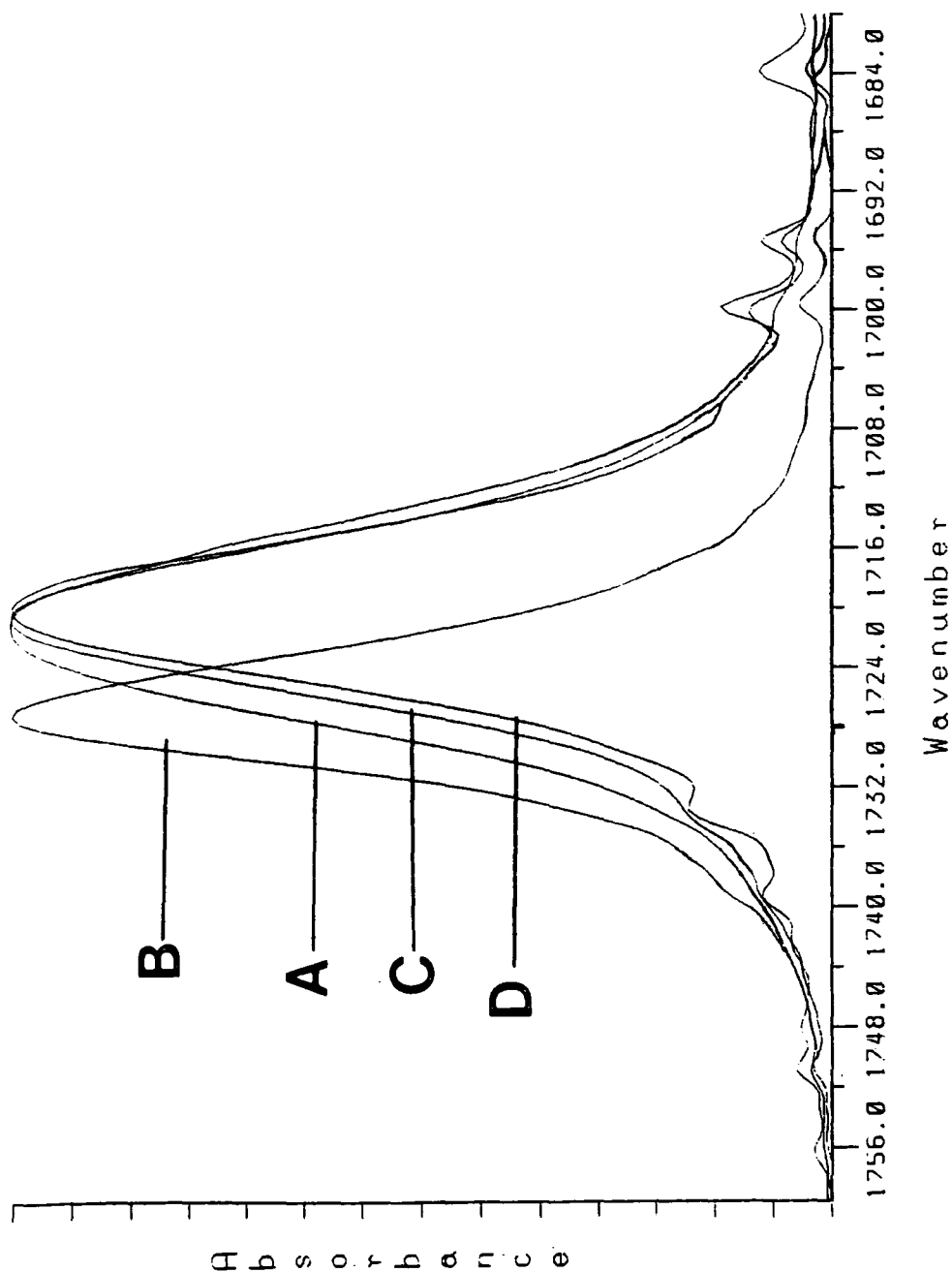
Figure 6.16. The infrared band of the carbonyl $v(C=O)$ stretching mode for A;EHB liquid, and EHB at 10% mole fraction concentration in B;hexane, C;CS2, and D;benzene.
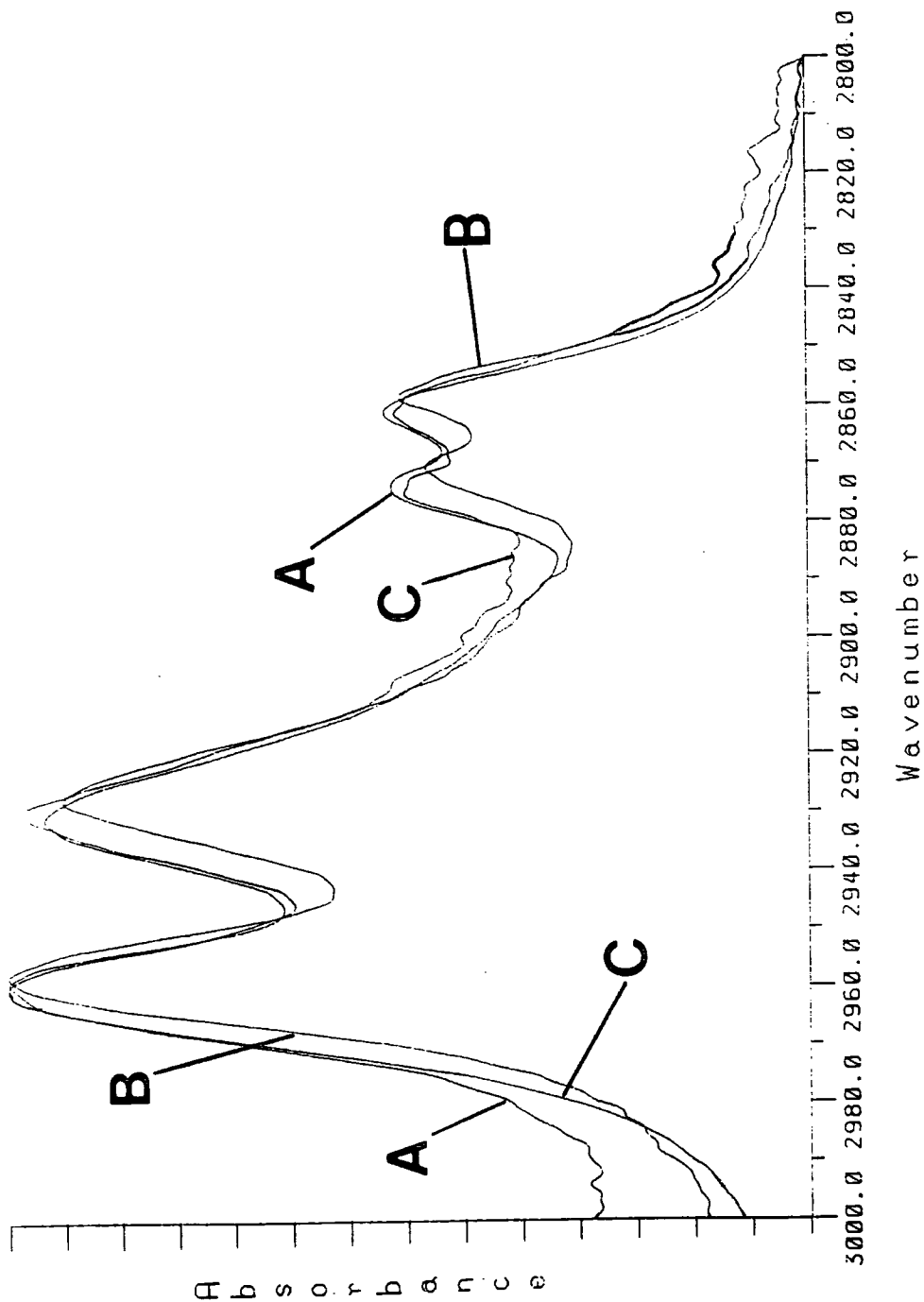
Figure 6.17. The infrared envelope of the aliphatic v(C-H) stretching modes for A;EHB liquid, and EHB at 10% mole fraction concentration in B;CS2, and C;benzene.

6.2.2 Hexane dilution of EHB

The infrared spectra of the $\upsilon(C=O)$ stretching mode of EHB was measured as a function of concentration in hexane, down to 0.5% mole fraction. Table.6.7 provides a summary of peak positions and band widths, Fig.6.18 shows how the band changes with EHB concentration. There is a non-linear increase in peak frequency and decrease in FWHM with decreasing EHB concentration, see Fig.6.19. There also appears to be a concentration threshold, at about 2% mole fraction beyond which further dilution does not affect the frequency nor FWHM of the band.
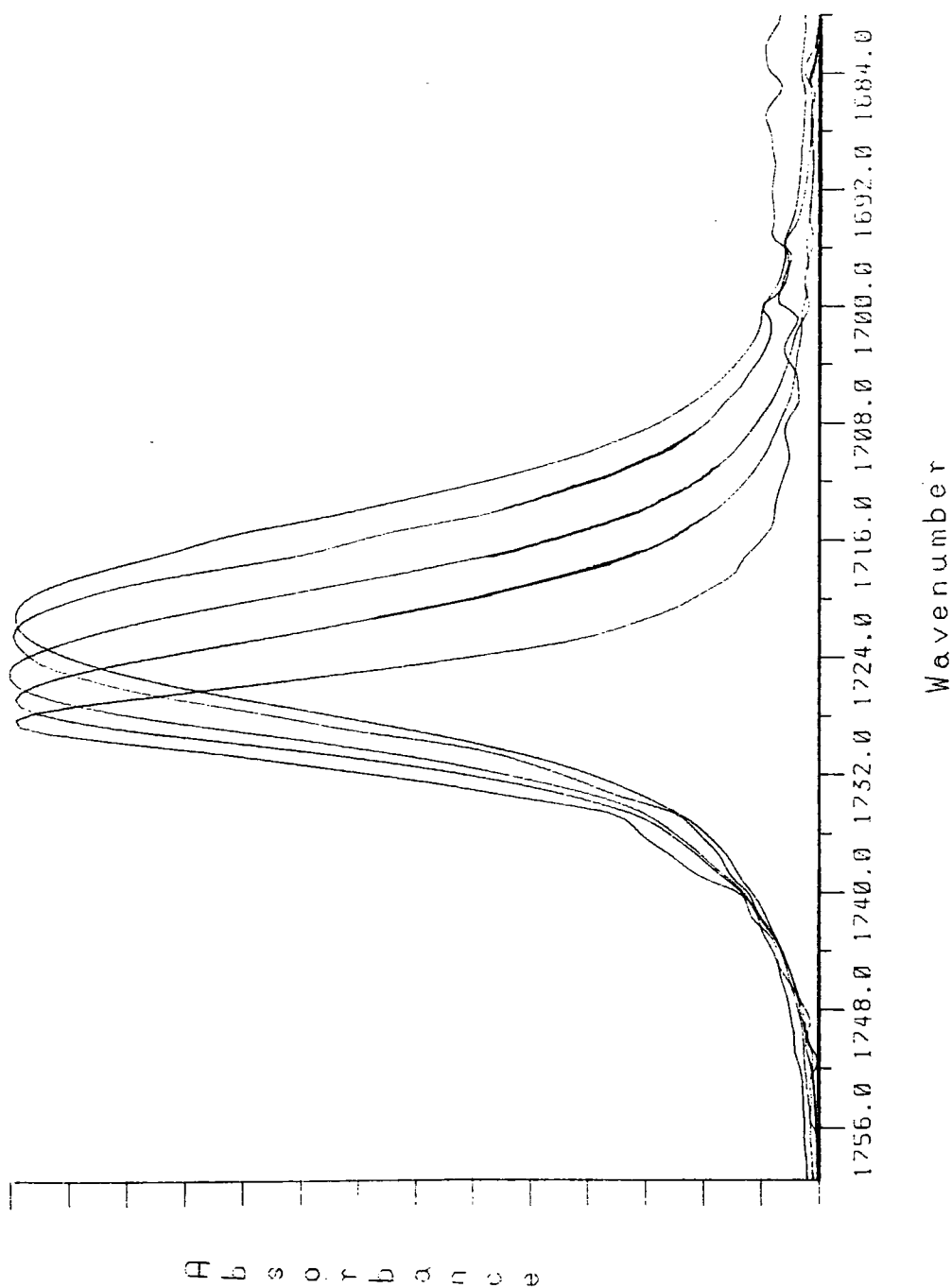
Figure 6.18. The variation of the infrared band of the $v(C=O)$ stretching mode of EHB as a function of concentration in hexane. From right to left the bands are for EHB at 100, 60, 30, 10 and 5% mole fraction concentration respectively.
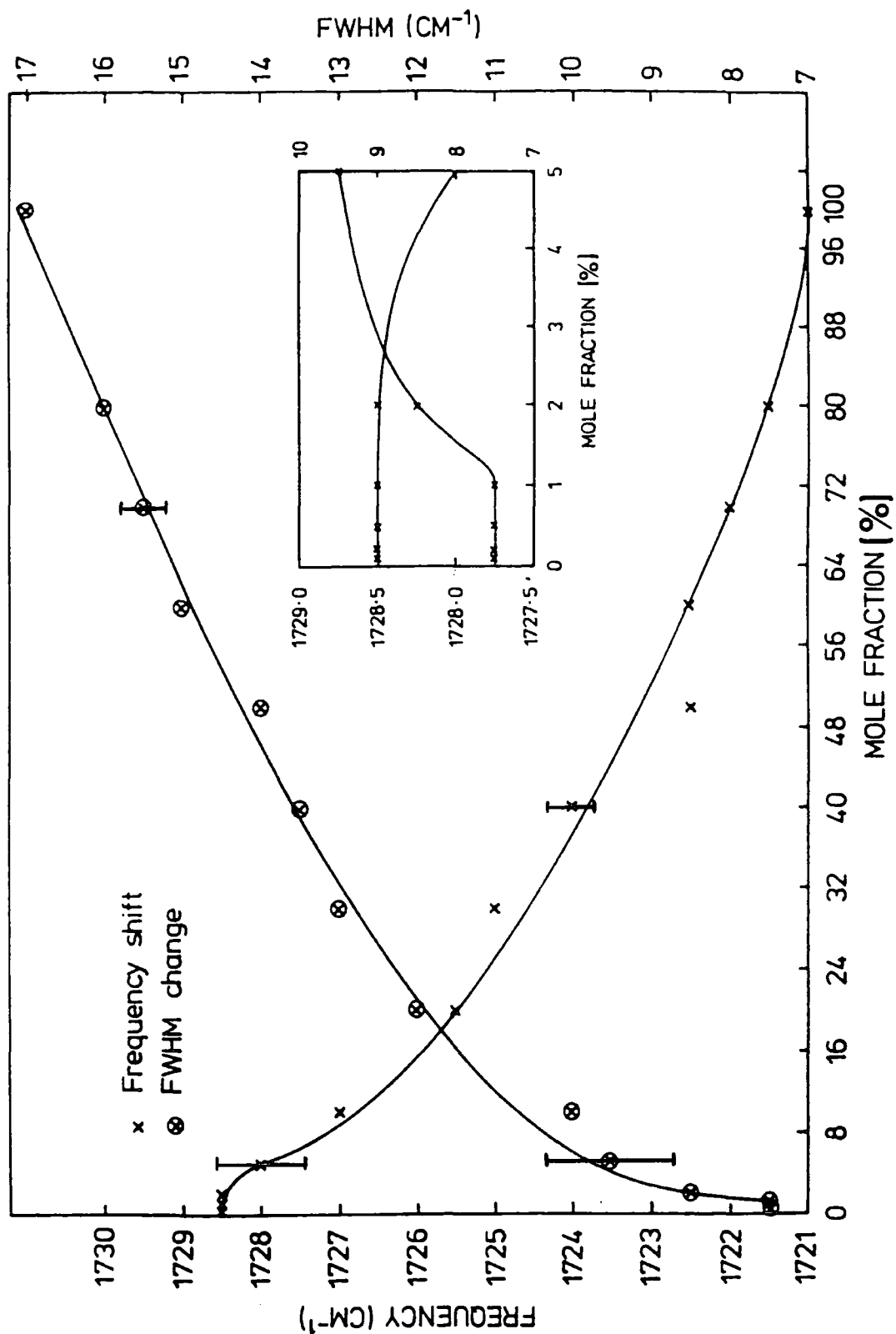
Figure 6.19. The frequency and band width (FWHM) of the infrared band of the $v(C=O)$ stretching mode of EHB as a function of concentration in hexane.

6.3 Far infrared

The far infrared spectra, between 15cm^{-1} and 185cm^{-1}, of the 10% mole fraction solutions of EHB in hexane, carbon disulphide and benzene were measured and compared with that of liquid EHB, see Fig.6.20. In hexane the main band is shifted to 67cm^{-1}, but there is no change of band position in the other two solvents.
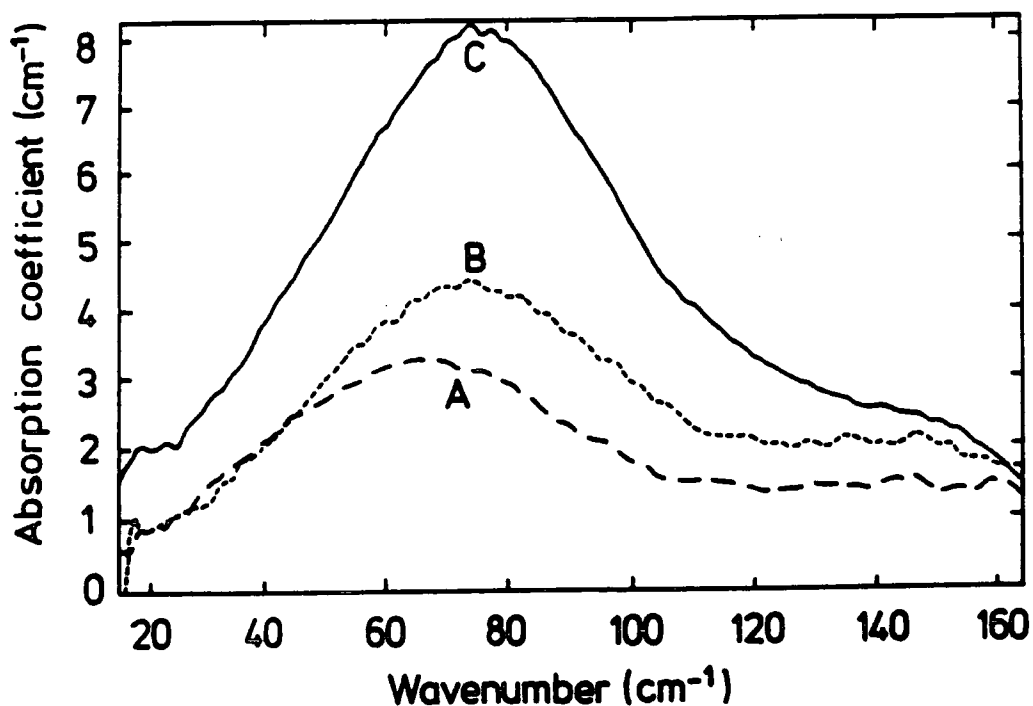
Figure 6.20. The far infrared spectra of EHB at 10% mole fraction concentration in A;hexane, B;benzene, and C; CS2.

6.4 An investigation of the heats of solution generated during the addition of EHB to n-hexane at 298K

The heats of solution generated during the addition of EHB to n-hexane at 298K were investigated by titration calorimetry. The work was carried out at the Thornton Centre, Shell Research, Chester. The LKB 2277 microcalorimeter and Digitam software package were employed for the study.

Four experiments were performed in order to probe the concentration range in sufficient detail. In three of these experiments EHB and EHB/hexane solutions were added to pure n-hexane. In the fourth experiment pure hexane was titrated into pure EHB, to investigate the heats of solution at higher concentation. In each case before the experiment was begun a period of at least seven hours was allowed for equilibration of the system. This was necessary to ensure that the vapour pressure above the titrand was saturated prior to addition of titrant. Following this the system was calibrated to ensure accurate data collection. During the titration 10 microlitre additions of titrant were made at intervals of one hour. The experiment was terminated when sufficient data had been collected. Integration of the data was then carried out using the Digitam software programme.

The results show that a transition occurs on increasing the concentration of EHB in hexane. As can be seen from Table 6.9 and Fig.6.21, the transition occurs between 0.20 and 0.40% mole fraction of EHB. The results are displayed as incremental heats of solution. The observed transition

in Fig.6.21 was repeatable and the only one found over the whole concentration range. The results of this study are discussed in Section 7.3.
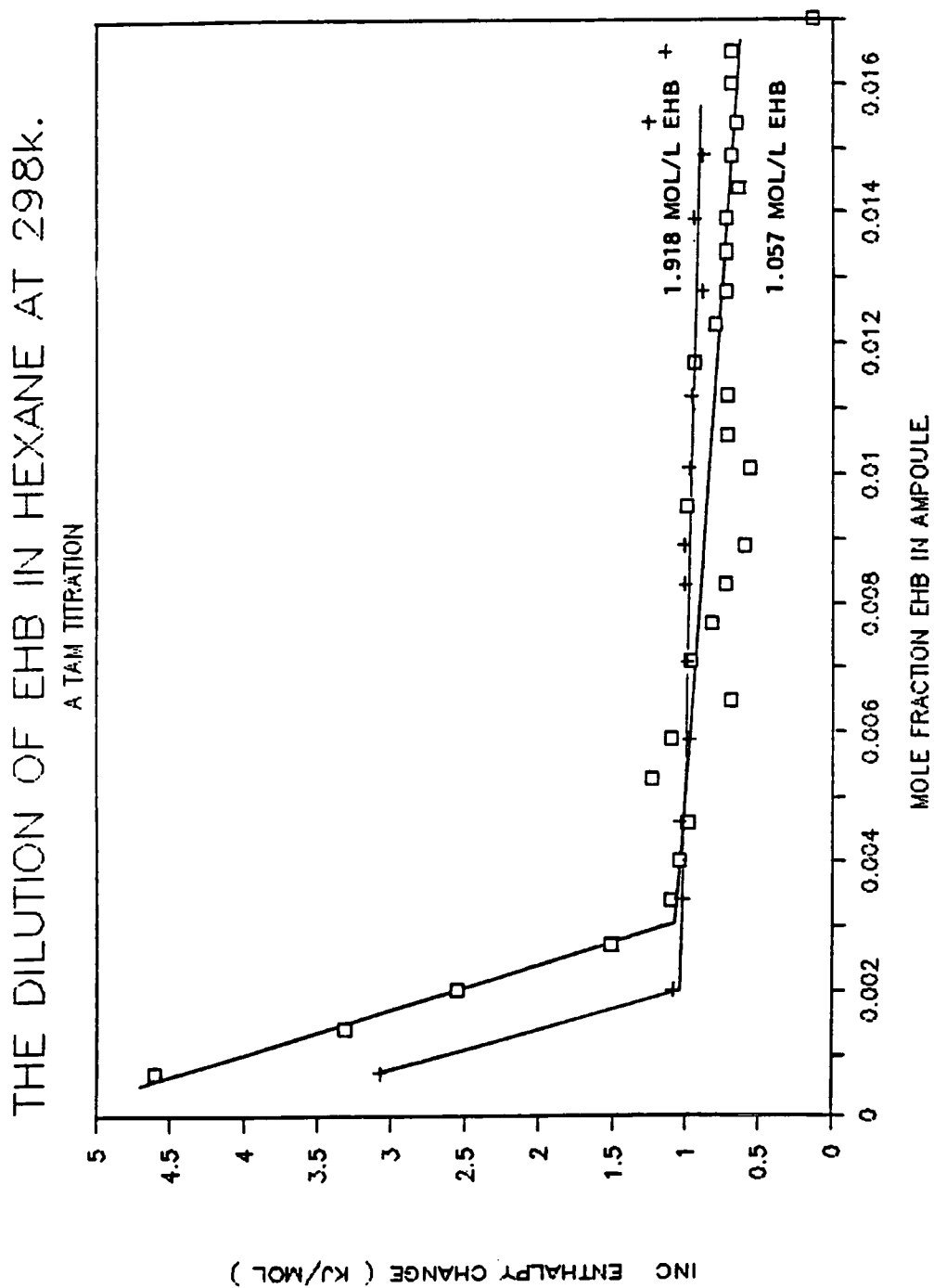
Figure 6.21. Incremental heats of solution for addition of EHB/hexane solutions to pure n-hexane at 298K.

Tables 6.9. Incremental heats of solution for addition of EHB/hexane solutions to pure n-hexane at 298K.

TITRATION OF 1.057 MOL/L EHB INTO HEXANE.

MOLE FRACTION EHB	ENTHALPY CHANGE INC. KJ/MOL
0.0007	4.60
0.0014	3.31
0.0020	2.55
0.0027	1.51
0.0034	1.10
0.0040	1.04
0.0046	0.98
0.0053	1.24
0.0059	1.10
0.0065	0.70
0.0071	0.97
0.0077	0.83
0.0083	0.73
0.0089	0.60
0.0095	1.00
0.0101	0.57
0.0106	0.72
0.0112	0.72
0.0117	0.95
0.0123	0.81
0.0128	0.73
0.0134	0.74
0.0139	0.74
0.0144	0.65
0.0149	0.70
0.0154	0.66
0.0160	0.70
0.0165	0.70
0.0170	0.13
0.0175	-0.08

TITRATION OF 1.918 MOL/L EHB INTO HEXANE.

MOLE FRACTION EHB	ENTHALPY CHANGE INC. KJ/MOL
0.0012	3.80
0.0025	1.09
0.0037	1.03
0.0049	1.04
0.0060	0.99
0.0072	1.00
0.0085	1.01
0.0095	1.02
0.0106	0.98
0.0117	0.97
0.0130	0.90
0.0140	0.95
0.0151	0.89
0.0160	1.26
0.0170	1.15
0.0181	0.91
0.0191	0.85
0.0201	0.81
0.0211	0.82
0.0220	0.81
0.0230	0.83
0.0240	0.84
0.0249	0.84
0.0258	0.78

SECTION III

INTERPRETATION

CHAPTER 7: PHENOMENOLOGICAL APPROACHES TO INTERPRETING
           EXPERIMENTAL DATA OBTAINED ON EHB

CHAPTER 8: THEORETICAL ANALYSIS

CHAPTER 9: SUMMARY

CHAPTER 7

PHENOMENOLOGICAL APPROACHES TO INTERPRETING EXPERIMENTAL
DATA OBTAINED ON EHB

7.1 Temperature dependence of the macroscopic and microscopic properties of EHB

7.1.1 Viscosity-temperature dependence of EHB

The viscosities, self diffusion coefficients and densities of EHB over a 253 to 373K temperature range and a 1bar to 4.5kbar pressure range (except the 253k isotherm which was only measured to a pressure of 3kbar) are shown in Table 7.1. This data was obtained by Walker and co-workers, details of the work is published in reference[77].

The density of EHB varies linearly with temperature at all pressures studied, Fig.7.1 demonstrates this for the 1bar, 1.5kbar and 3kbar isobars. These observations are consistent with data obtained by Barlow and co-workers[24] who studied 10 aromatic hydrocarbon liquids. They observed a linear temperature dependence of density for all the liquids. Their study included measurements on di-(2-ethylhexyl) phthalate (DEHP), a liquid similar to EHB but which is comprised of molecules which have an additional (identical) hydrocarbon chain in the ortho position of the benzene ring.

The variation of the viscosity of EHB with temperature is distinctly non-linear, see Figs.7.2, 7.5, and 7.9. This is consistent with many previous studies on hydrocarbon liquids[24,118], as is demonstrated in Fig.7.2 by the viscosity temperature plots of some aromatic liquids. Viscosity temperature relationships are discussed in Section 1.3.

T. °C	P. bar	η, cP	ρ, g cm⁻¹	$D \times 10^9$, cm² s⁻¹
-20	1	70.3	0.9960	165
	500	250	1.0214	53.8
	1000	945	1.0425	9.36
	1500	2950	1.0605	2.73
	2000	9190	1.0764	1.19
	2500	20800[a]	1.0906	0.455
	3000	88500	1.1035	0.154
0	1	16.9	0.9805	609
	500	44.4	1.0076	244
	1000	119	1.0300	95.2
	1500	293	1.0493	37.5
	2000	714	1.0662	
	2500	1690	1.0814	4.97
	3000	3850	1.0952	1.94
	3500	9800	1.1079	0.937
	4000	24500	1.1197	0.41
	4500	57200	1.1306	0.148
20	1	6.77	0.9650	1540
	500	13.0	0.9940	719
	1000	27.9	1.0175	346
	1500	56.9	1.0376	166
	2000	112	1.0551	89.3
	2500	240	1.0707	42.4
	3000	437	1.0848	
	3500	950	1.0977	
	4000	1790	1.1097	3.08
	4500	3680	1.1208	1.61
40	1	3.62	0.9495	2980
	500	6.60	0.9814	1640
	1000	11.7	1.0066	878
	1500	21.0	1.0277	460
	2000	38.8	1.0459	263
	2500	73.0	1.0620	171
	3000	128	1.0765	91.9
	3500	234	1.0897	45.7
	4000	427	1.1019	
	4500	735	1.1132	
60	1	2.27	0.9340	4230
	500	3.88	0.9687	2740
	1000	5.82	0.9958	1600
	1500	8.94	1.0182	1070
	2000	14.6	1.0375	717
	2500	24.3	1.0545	402
	3000	37.4	1.0698	254
	3500	61.8	1.0837	159
	4000	103	1.0964	96.1
	4500	165	1.1083	61.6
80	1	1.58	0.9185	6500
	500	2.34[a]	0.9562	4310
	1000	3.45[a]	0.9562	2710
	1500	5.20	1.0085	1910
	2000	7.63	1.0286	1280
	2500	11.1	1.0462	882
	3000	16.7	1.0620	582
	3500	24.9	1.0763	381
	4000	36.4	1.0894	255
	4500	54.3	1.1016	172
100	1	1.16	0.9030	9220
	500	1.61[a]	0.9436	6260
	1000	2.23[a]	0.9740	4230
	1500	2.99	0.9987	2900
	2000	4.25	1.0196	2060
	2500	5.81	1.0379	1490
	3000	8.49	1.0542	1080
	3500	11.9	1.0690	795
	4000	15.2	1.0826	530
	4500	20.8	1.0951	387

[a] Extrapolated values   [b] Interpolated values

Table 7.1. Experimental self-diffusion coefficients, viscosities and densities. Reproduced, by permission, from reference 77.

188
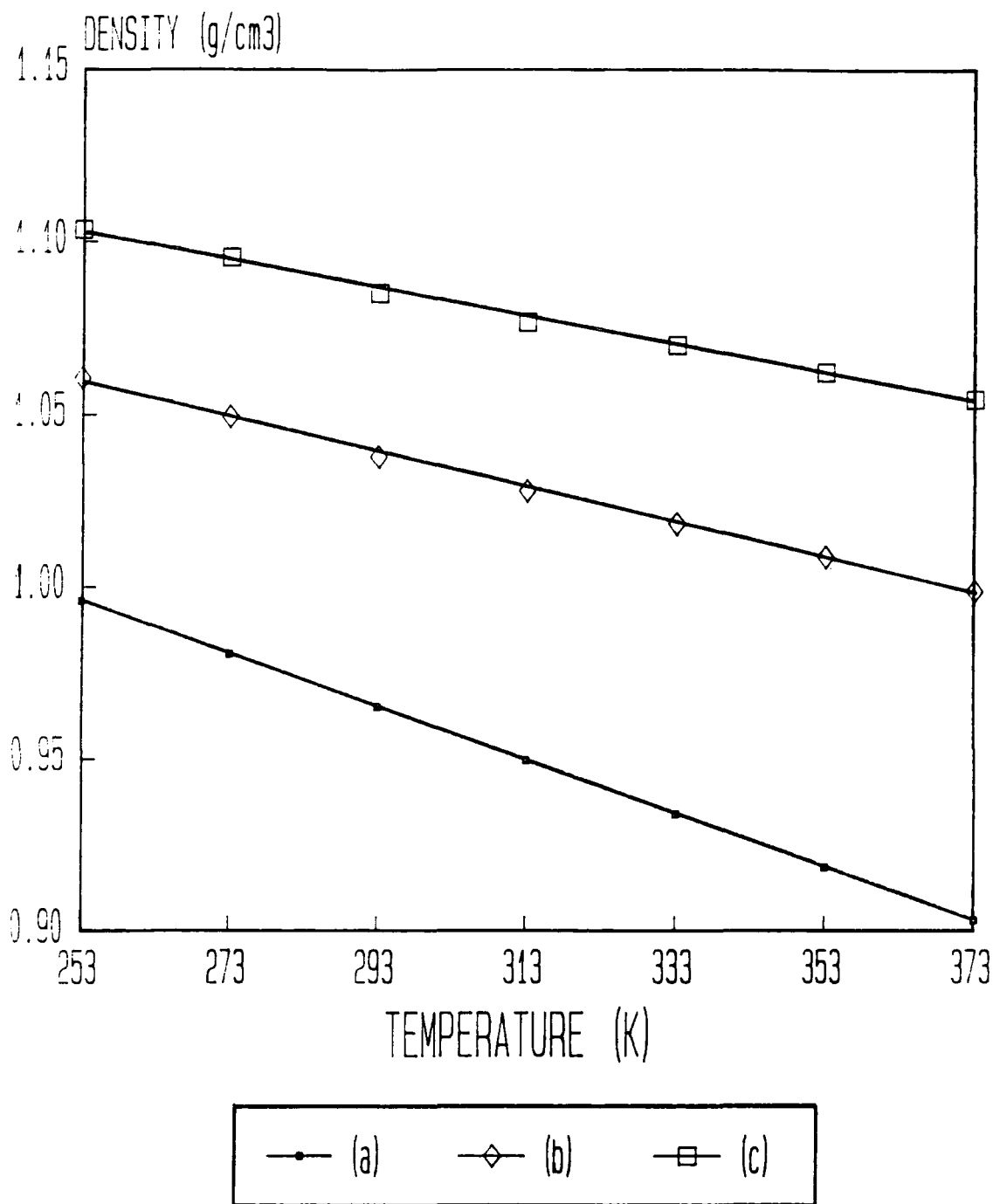
Figure 7.1. The density of EHB as a function of temperature, at (a) 1bar, (b) 1.5kbar, (c) 3.0kbar.
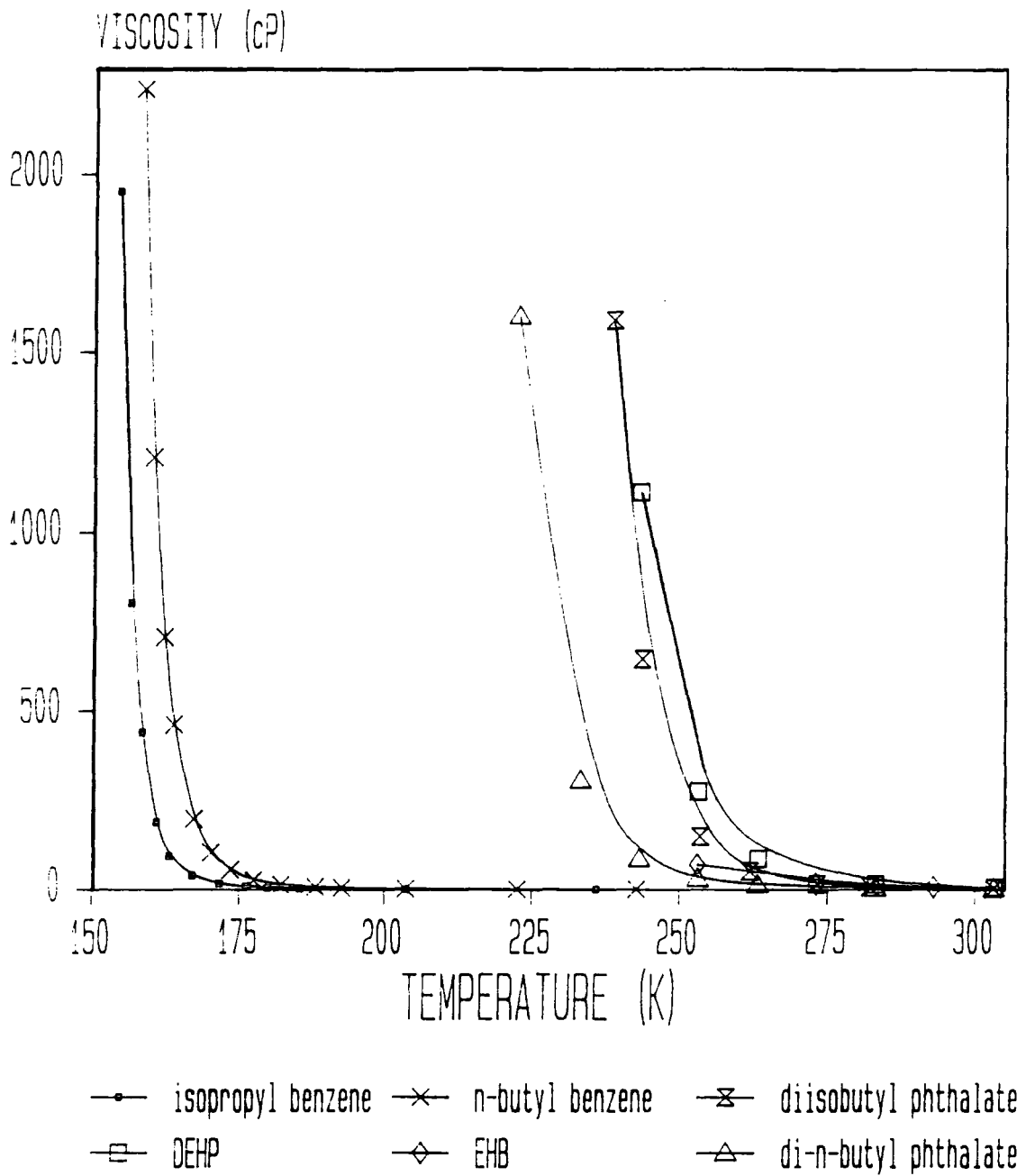
Figure 7.2. Viscosity-temperature plots of some aromatic hydrocarbons.

Barlow[24] et al observed that the Arrhenius viscosity-
temperature relationship is obeyed by each of their liquids
from the boiling point down to about 300K, but that it is
not valid at lower temperatures. If $\ln(\eta)$ is plotted
against (1000/T), the points lie on a smooth curve, as shown
by their data for n-butyl benzene plotted in Fig.7.3. The
dashed line is an extrapolation of the Arrhenius viscosity
dependence at temperatures above 303K. This viscosity-
temperature behaviour makes it difficult to design a
lubricant that is thick enough to provide effective
lubrication at high temperatures but which is not too thick
for efficient machine running at low temperature.

The viscosity data for EHB shows a similar trend when
plotting $\ln(\eta)$ against (1000/T), see Fig.7.4. The data
above 373K were obtained by extrapolation, so there is some
uncertainty about these values.
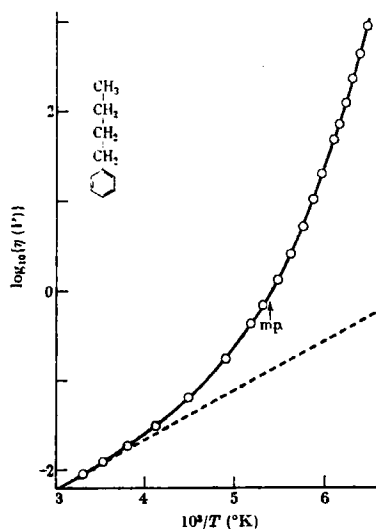
Figure 7.3. log(η) as a function of (1000/T) for n-butyl
benzene. Reproduced, by permission, from reference 24.
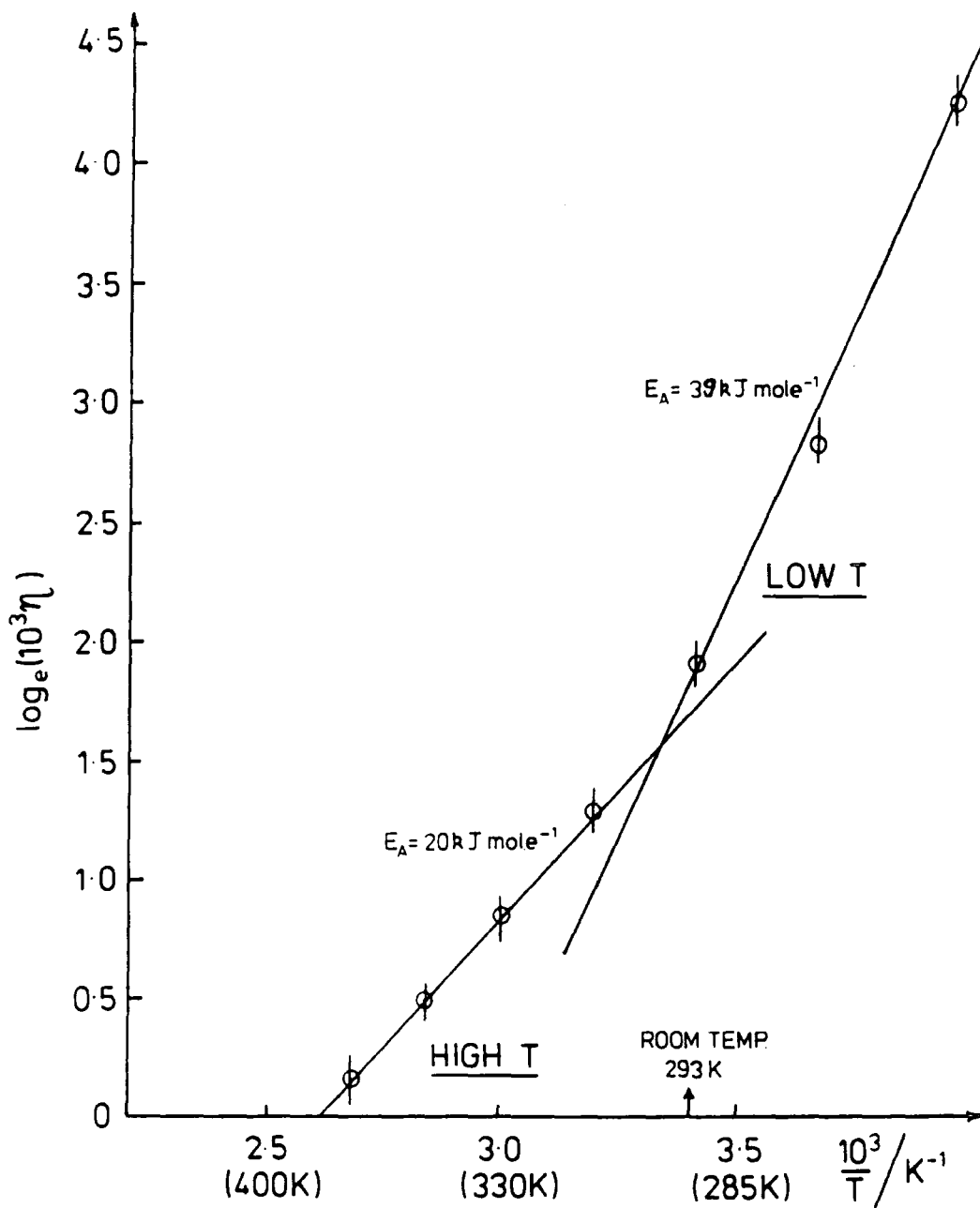
Figure 7.4. $\ln(10^3\eta)$ as a function of $(1000/T)$ for EHB.

The data falls on a distinct curve it does not fit the Arrhenius equation, in common with other complex fluids[24,118]. If the viscosity data is considered to fall into two fairly distinct regimes associated with high and low temperature respectively two values for the activation energy (E_a) for viscous flow can be calculated. The values are 39 and 20kJ/mol at low and high temperatures respectively. An uncertainty of about ±10% must be attached to these parameters. It would appear that the molecular processes which give rise to macroscopic viscometric behaviour are different at high and low temperatures. The transition point between the two regimes appears to be near 300K - not far from ambient temperature. Even if the data are not divided into two distinct temperature regimes there is clearly a change of slope in the 300-320K region.

If the viscosity data for DEHP is analysed in the same way as EHB, the activation energies obtained are 28 and 42kJ/mol at high and low temperatures respectively. The transition temperature is around 315K. The additional chain present in DEHP molecules is likely to cause an increase in intermolecular chain interactions in the fluid compared with EHB. This explains the larger viscosity of DEHP, over EHB at all temperatures, and the greater temperature viscosity dependence. This greater viscosity temperature dependence is brought out in the increased energy barrier to viscous flow, as is observed by the larger values for E_a in both temperature regimes. If the transition temperature is associated with the "locking up" of part of the molecule it might also be expected that the transition temperature for DEHP should be higher than for EHB, as is seen.

The viscosity data can also be considered in terms of the modified free volume (MFV) equation (Section 1.2.5). A value for T_0 of 167K is obtained by solving simultaneous equations set up using the ambient pressure viscosity data for EHB and Eqn.1.8. The values of A' and B' are then obtained by plotting $\ln(\eta)$ against $[1000/(T-T_0)]$. The slope and calculated intercept give values of B' = 611K and A' = -2.903 (or -7.508 if the viscosity is measured in P and not cP) respectively. Using these constants the MFV equation predicts the viscosity of EHB to within 5% for all temperatures, see Table 7.2 and Fig.7.5, except for the two highest temperatures of 353 and 373K where the errors are 7 and 8% respectively. The calculated viscosity data all lies within experimental error of the measured data.

TEMPERATURE (K)	η_{obs} (cP)	η_{MFV} (cP)
253	70.3	66.8
273	16.9	17.5
293	6.77	7.00
313	3.62	3.60
333	2.27	2.18
353	1.58	1.47
373	1.16	1.07

Table 7.2. A comparison of experimental viscosities of EHB, with those calculated by the modified free volume equation.
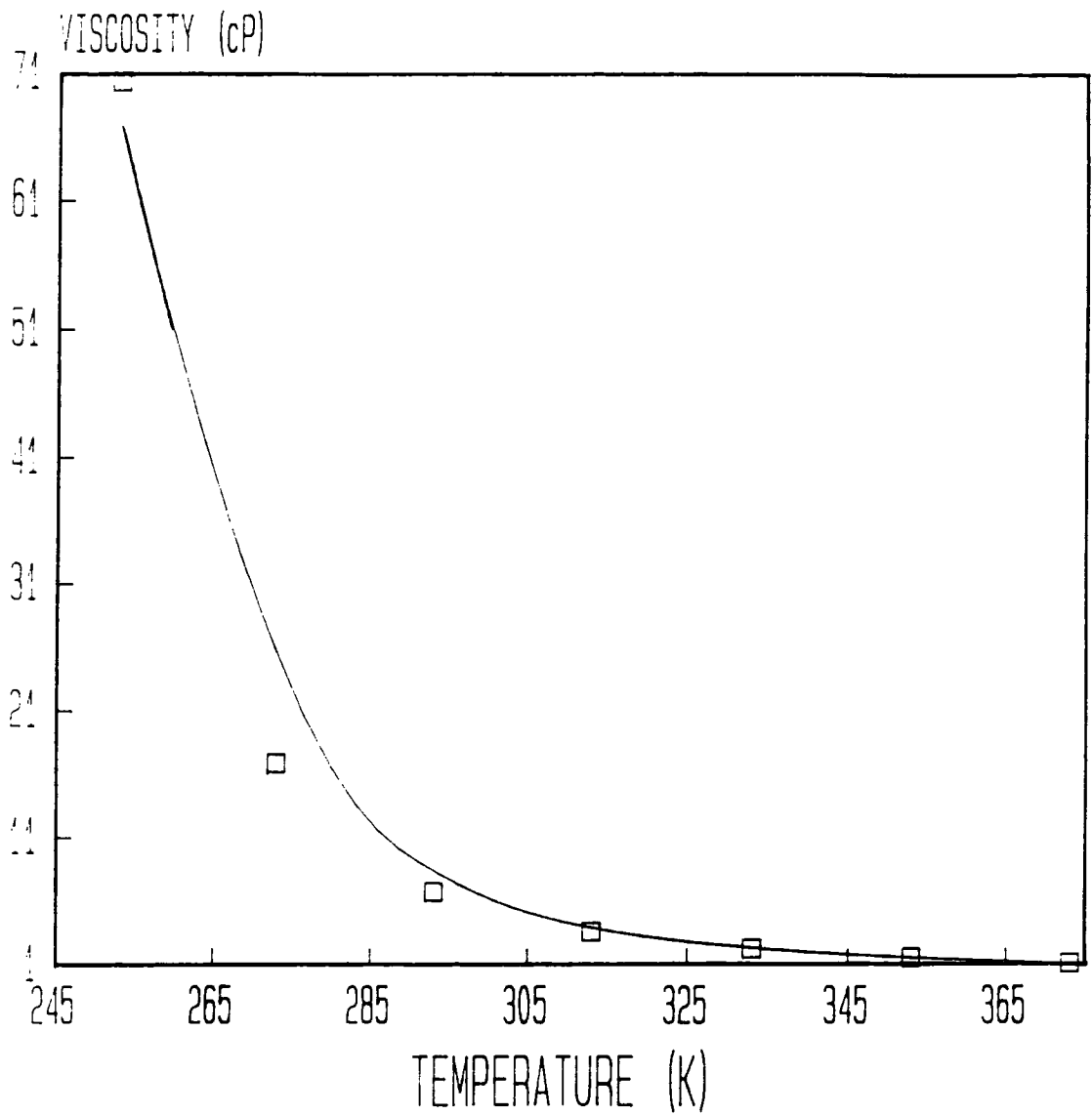
Figure 7.5. Experimental viscosity (□) and modified free volume (——) viscosity data as function of temperature.

Barlow et al also considered their data in terms of the MFV equation. They found that except in the high temperature "Arrhenius" region, the equation adequately described the temperature variation of the viscosity of four of the ten liquids over the whole of the temperature range, including DEHP. For the other six liquids it was found that two sets of constants were required, one set applying to high temperatures (Arrhenius region excluded) the other to low temperatures. The transition temperature T_k for the two regimes was found to always occur within 10K of the liquids melting point. They suggested that the transition from Arrhenius to non-Arrhenius viscosity behaviour occurs when rotation about two molecular axes is restricted on the translational time scale, by a decreasing free volume available to the molecule. They showed that the Arrhenius temperature (temperature at which liquid no longer shows Arrhenius behaviour) occured, for their liquids, when the average volume available to a molecule becomes too small to permit overall rotation about more than one axis. The discontinuity in the non-Arrhenius regime occurs when the volume available to the molecule will not allow free rotation about any axis. The liquids which show no discontinuity in the non-Arrhenius regime have one rotational mode which remains unrestricted even at the melting point. Alternately rotation about all the axes become restricted at the Arrhenius temperature.

The viscosity data for EHB suggests that between the temperatures 253 and 373K the volume available to EHB is insufficient to allow Arrhenius behavior, except maybe towards the high temperatures in the range, and this is why

196

a non linear $\ln(\eta)$ vs 1000/T plot is observed. This is supported by the MFV equation which gives a good describtion of the viscosity data. If the range of viscosities is extended to higher temperature, an Arrhenius region may be observed, as at higher temperatures the EHB molecules should be able to rotate more freely, in the larger free volume available to them. The distinct change in the slope of the Arrhenius plot for EHB at about 300K may be associated with a change in internal flexibility which is modifying the viscosity temperature behaviour of the molecule.

7.1.2 NMR reorientational correlation times for EHB

It has been shown (Section 5.1.1) that the Raman
reorientational correlation times, obtained from the
difference in Raman anisotropic and isotropic bandwidths,
for the v(C-C) ring deformation mode of EHB as a function of
temperature, give excellent agreement with those obtained
for the para-carbon of the ring using NMR ^{13}C spin lattice
relaxation times (T_1's). In order to consider why this is,
it is necessary to understand how the NMR reorientational
correlation times are obtained from the measured T_1 values.

To understand what T_1 values measure consider a
symmetry of isolated spins I = 1/2 suddenly exposed to a
strong external magnetic field B_0. After switching off the
field the spins will be found with equal probability in the
two Zeeman states E_+ and E_-. As time passes a
redistribution over the levels takes place. The spin
redistribution is combined with a build up of nuclear
magnetization $M_z(t)$ which for most liquids follows the
simple Bloch equations[100] to an equilibrium level M_0
according to a Boltzmann distribution

$$dM_z/dt = (-M_z - M_0)/T_1 \qquad \text{Eqn.7.1}$$

which can be integrated to give

$$M_0 - M_z = -k.\exp(-t/T_1) \qquad \text{Eqn.7.2}$$

k is a constant and depends on the initial experimental
conditions, and T_1 is the spin lattice relaxation time.

Several interactions can contribute to the relaxation rate[100] ($R_1=1/T_1$) of a ^{13}C nucleus these include, (1) dipolar relaxation (T_{1-DD}), (2) relaxation by shielding anisotropy, (3) scalar coupling relaxation and (4) spin rotation relaxation. The observed rate is a sum of all four terms. Dipole-dipole relaxation is by far the most important relaxation mechanism, this arises primarily from interaction with nearby nuclei with large magnetic moments, usually ^1H, and is a result of molecular motion. The ^{13}C nucleus is subjected to an additional randomly varying magnetic field from the neighbouring hydrogen nuclei by which it can transfer energy to the lattice. It can be shown[100] that providing the spectra are motionally narrowed ($\tau\omega \ll 1$) relaxation will be purely dipolar. Under these conditions the maximum nuclear Overhauser enhancement[119] (NOE) is obtained and proton decoupling increases the intensities of the ^{13}C resonances by a factor of three. It can be shown[120,121] that

$$1/T_{1-DD} = (N \cdot \gamma_H^2 \cdot \gamma_C^2 \cdot \hbar^2 / r_{C-H}^6)\tau_{eff} \qquad \text{Eqn.7.3}$$

where N is the number of directly bonded protons, r_{C-H} is the C-H bond length taken as being 0.108nm for aromatic carbons[122] and 0.109nm for aliphatic carbons[120], τ_{eff} is the effective correlation time for reorientational motion of the C-H vector, γ_H and γ_C are the gyromagnetic ratios for ^{13}C and ^1H. When $T_1 = T_{1-DD}$, the motionally narrowed region, a value for τ_{eff} can be obtained from the measured T_1.

All the protonated carbons for EHB were found[117], from NOE measurements, to be within the motionally narrowed

region between the temperatures 270K and 376K. Values for τ_{eff} , see Table 5.3, were then obtained using the measured T_1 values and Eqn.7.3.

If the molecules execute purely isotropic reorientation then from Eqn.7.3 one would expect all the carbons to give the same correlation time. However apart for simple rigid molecules this is not observed. Molecular motion for most molecules, including EHB, is highly anisotropic. It can be seen, from Table 5.3, that for EHB both the chain and ring carbons have a distribution of different correlation times. Correlation times for carbons undergoing anisotropic reorientation are, in fact, a product[100] of three rotational diffusion constants R1, R2, and R3 and the direction cosines λ, μ and υ of the appropriate CH vectors in relation to the principal axes of the rotational diffusion tensor

$$1/T_1 = f(R_1, R_2, R_3, \lambda, \mu, \upsilon) \qquad \text{Eqn.7.4}$$

There is an added complication for flexible molecules, such as EHB, that because of their flexibility there is the possibility for internal molecular motions which will contribute to the modulation of the ^{13}C-H vector and thus the observed relaxation time. The observed or effective correlation time must be considered as a weighted average of all the individual motions[123,124] which reorientate the ^{13}C-H vector of concern, i.e. $\tau_{eff} = \sum_k C_k \cdot \tau_k$ where the C_k is a probability dependent coefficient. The effective correlation time is a function of the correlation time for overall reorientation and for the internal motions of the molecule

$$1/\tau_{eff} = 1/\tau_o + 1/\tau_i \qquad\qquad \text{Eqn.7.5}$$

There is also the possibility for a third term arising from coupling of the two types of motion, however for simplicity this is not included here. If one type of motion is much faster than others then, from Eqn.7.5, it can be seen that it will dominate the τ_{eff} term.

As a result of steric constraints and concerted motions the dynamics of macromolecules are extremely complicated. Due to intramolecular and intermolecular interactions the ^{13}C-H vectors will not assume all possible orientations, that is the motion is not isotropic but restricted. The rate of motion of this ^{13}C-H vector cannot be described by a single parameter (i.e. the correlation function is not a single exponential). The time dependence of the correlation functions differ from vector to vector, that is they move at different speeds, the correlation function or time for each carbon depends on all the effective contributions from all the possible motions.

The para carbon of the ring, of EHB, is seen to have a correlation time which is considerably longer than that of the ortho and meta carbons which have similar times to each other. This has been observed for a number of monosubstituted aromatic liquids[99,121,125]. These observations can be explained considering the reorientational motion of the EHB molecules. Preferential reorientation, both intra and intermolecular occurs about the long axis (C_2 molecular symmetry axis) of the molecule, as represented by R3 in Fig.7.6. This results from two effects, the moment of inertia around the R3 axis is lower (inertial effect), and

fewer solvent molecules are disturbed by rotation about this axis. The size, polarity and symmetry of the ring substituent determines the degree of anisotropy in the motion. Rotation about the long axis leads to modulation of the ortho and meta ^{13}C-H vectors and thus causes relaxation of these carbon nuclei. However this motion does not alter the local field which the para-carbon nucleus experiences from the bonded proton, so does not contribute to the relaxation of this nuclei[121]. Molecular rotations about axes perpendicular to the long axes, R1 and R2, are much slower because these motions require the displacement of more solvent molecules, and involve a larger moment of inertia. It was suggested, in 7.1.1, from observations of the viscosity data as a function of temperature, that rotation about the axes R1 and R2 is restricted on the translational time scale, due to insufficient free volume
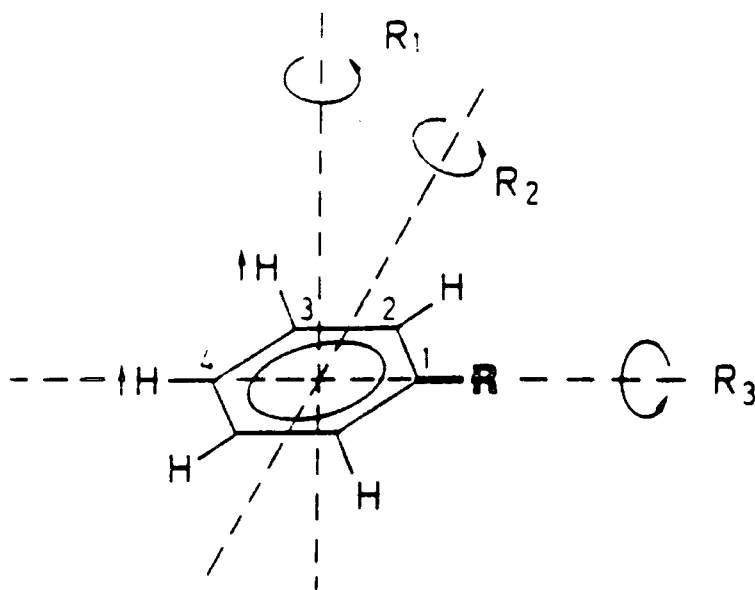
Figure 7.6. Anisotropic reorientational motion in monosubstituted benzenes. (Reproduced, by permission, from reference 100).

202

available to the EHB molecules, within the temperature range studied. These slow motions, perpendicular to the long axes, will give rise to relaxation of the para-carbon nuclei, but the corresponding relaxation times can be expected to be long.

It is also necessary to consider the contribution of internal motions, of EHB, to the observed correlation times for the ring carbons. It will be shown (in Section 8.3) that the energy barrier to rotation of the benzene ring of EHB about the C1-C3 bond is not excessive. Rotation of the ring about this axis, like overall rotation about the long axis, will modulate the ortho and meta ^{13}C-H vectors but it does not modulate the para ^{13}C-H vector. However, it appears, see Section 8.3, that internal rotation about either carbon oxygen single bond will occur more rapidly than rotation of the ring alone. This will modulate the para ^{13}C-H vector, but not to as great an extent as the ortho and meta ^{13}C-H vectors. Therefore rotation about the C-O single bonds will also lead to shorter correlation times for the ortho and meta carbons compared with the para carbon. Other internal reorientational motions will modulate the para ^{13}C-H vector, as well as those of the ortho and meta carbons, and therefore contribute to the relaxation of all three ^{13}C nuclei. The faster the rate of an internal motion the greater is the contribution to the effective correlation time.

The motions which cause the reorientational relaxation of the para ^{13}C nuclei could either be overall rotation about the axes perpendicular to the long axis or internal

motions of the molecule. Considering the length of the EHB molecule it is probable that, on the time scales of observation used here, overall molecular rotation, other than that about the long axis, cannot occur. This is further supported by the viscosity data. It might even be questioned if overall rotation about the long axis is possible on this time scale. Williams[126], however, carried out a similar analysis on octyl benzene and came to a different conclusion. He assumed that the reorientational correlation time for the para carbon of the benzene ring (τ_{eff}^{298K} = 32.8 ± 1.5ps) was dependent on the overall reorientation of the molecule with no contributions from internal motions. Work on simple, rigid monosubstituted benzenes[127], which are not capable of internal motion, has yielded correlation times for overall molecular rotation about axes perpendicular to the long axis of the molecule. However, EHB is more complicated than octyl benzene and simple rigid monosubstituted benzenes, EHB has a side chain and the ester functional group, as well as a significant degree of flexibility.

Whether or not EHB is capable of any significant molecular rotation, perpendicular to the long axis of the molecule is dependent on the shape and interactions of the molecules. Discussions in this section have assumed that EHB has a long axis (i.e. it is non spherical) molecular graphics studies on EHB (which only take into account intramolecular interactions) suggest that the molecule does possess a long axis (see Section 8.3). However there remains a small probability that intermolecular forces in the liquid may contribute to give the molecules a shape

where all the axes are nearly equal in length. Considering the results in this section it is likely that relaxation of the para carbon nuclei is dependent mainly on internal reorientational motion. It is extremely unlikely considering the viscosity data, correlation time behaviour and molecular graphics calculations, that there is any significant contribution from overall molecular motion about axes perpendicular to the long axis of the EHB molecule.

For the effective correlation times of the ortho and meta carbons it is impossible to separate the contributions of internal ring rotation from overall rotation of the molecule around the long axis. It is a distinct possibility, considering the molecular graphics calculations, that internal rotation of the benzene ring end of the molecule about the C-O single bonds will dominate the correlation times of the ortho and meta carbons.

7.1.3 Agreement of Raman reorientational correlation times for the v(C-C) ring deformation vibration of EHB with those for the para carbon of the EHB ring obtained using NMR.

It is now possible to discuss the reasons for the good agreement between the correlation times obtained using the Raman anisotropic and isotropic bandwidth difference for the v(C-C) ring deformation mode and those obtained from ^{13}C spin lattice relaxation times for the para carbon of the ring. The reorientational motion that has the greatest influence on the reorientational relaxation rate of a Raman vibrational mode is that which <u>modulates the particular</u>

<u>transition polarizability tensor</u> of the vibration at the fastest rate. This will not always be around an axis about which reorientation of the molecule is the quickest. For example in the case of a molecule that has the shape of a symmetric top (e.g. CH_3I) the reorientational relaxation of the A_1 vibrational modes arises from the slowest reorientational motion. about the axes perpendicular to the C-I axis. The NMR spin lattice relaxation time is most strongly weighted by the motion about the axis which <u>modulates the ^{13}C-H vector</u> the quickest. In general, this will be the axis around which the molecule reorientates most rapidly. In many cases reorientational relaxation times determined by NMR will be shorter than that determined by Raman spectroscopy. when the motion that modulates the ^{13}C-H vector most quickly does not modulate the transition polarizability tensor. In the case of EHB, for the para carbon of the ring, it is thought that the relaxation of the ^{13}C nuclei has little contribution from overall reorientation about the long axis of the molecule. It is felt that the rotation of the ring about the C1-C3 axis results in little relaxation of the para ^{13}C nuclei. and there is a smaller contribution to the relaxation of the para carbon from internal rotation about the C-0 single bonds compared to the contribution from this motion to the relaxation of the ortho and meta ^{13}C nuclei. If this were not so then there would be no agreement with the Raman reorientational correlation times, see below. It is probable that relaxation of the para carbon nuclei is dependent, mainly, upon internal motions that modulate the ^{13}C-H vector most strongly. If the agreement of the Raman

206

reorientational relaxation times for the v(C-C) ring
deformation mode with the values for the para carbon from
NMR does not occur by chance, it is an indication that the
motions that contribute to the reorientational relaxation of
the ring v(C-C) deformation mode are closely related to
those that cause relaxation of the para ^{13}C nuclei. If this
is the case then their is little contribution to the
reorientational relaxtion of the v(C-C) ring deformation
vibration from the faster molecular rotations about the long
axis. In order for this to be so, it is necessary for the
direction of the transition polarizability, associated with
this mode, to be located parallel to the direction of the
para C-H vector. Considering the description of this mode
by Miller[128], for benzene it has B_{1u} symmetry. If the
symmetry is assumed to be the same in EHB and each carbon
atom of the ring is considered in turn, as in Fig.7.7, it is
found that the transition polarizability is parallel to the
long axis of the EHB molecule. It is important that it is
understood that the rest of the molecule, particularly the
ester functional group, may amend the predicted transition
polarisability. The effect should not alter the overall
direction by much. Consequently the explanation for the
agreement of the reorientational relaxation rates is
complete, and is a consequence of the direction of the
transition polarizabilty for the ring deformation mode being
parallel to the para C-H vector.
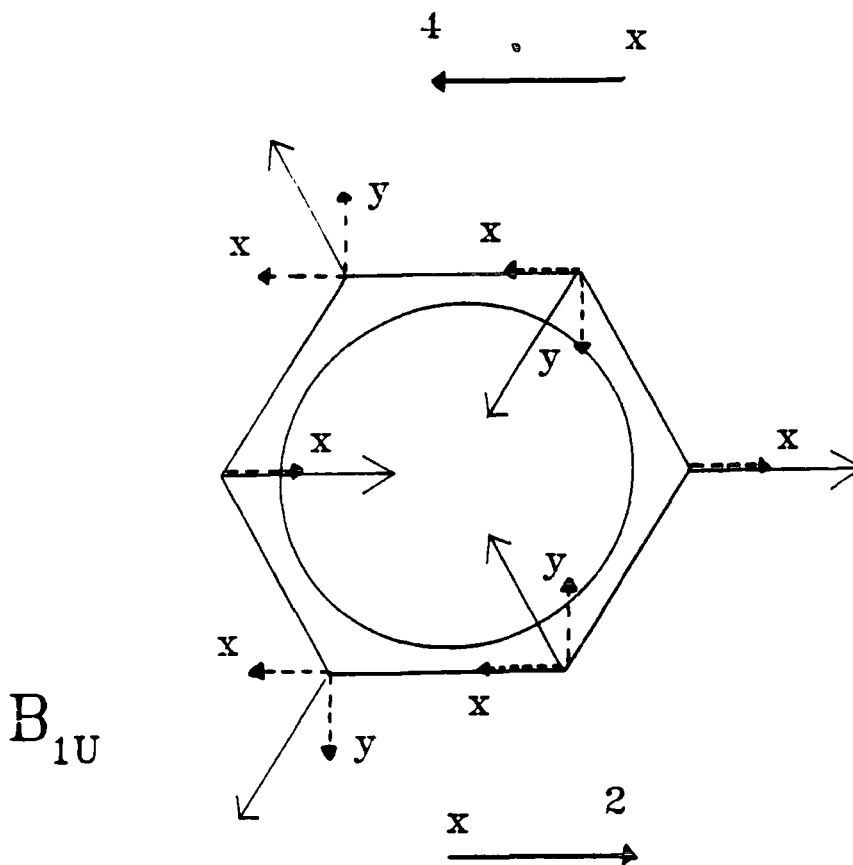
Figure 7.7. Determination of the direction of the transition polarizability of EHB for the ring v(C-C) deformation mode.

7.1.4 NMR reorientational correlation times for the chain carbons of EHB

If the branch point of EHB (i.e. C7) is taken as a reference, it is apparent, comparing the effective correlation times, that the rates of motion increase as the length of the chain and side-chain is progressed. This is observed at all temperatures. The decreasing values for τ_{eff} towards the end of the chains indicates that internal motions are increasingly modifying τ_{eff}. Flexibility increases along the chain. on going from C7 to C12 and C13,

and thus the rate of internal motion gets higher. These internal motions probably involve a combination of cooperative internal flexing motions involving short segments of the chain[97], and rotational motion about individual C-C bonds. The latter rotational motion only occurs at a significant rate for carbons near the chain ends[97] (i.e. C12 to C8, and C13 and C10) as the barrier to rotation becomes too great further in from the end of the molecule. Internal rotation becomes easier the closer to the chain end a carbon is, as the barrier to rotation decreases (see molecular graphics calculation, Section 8.3). Levine and co-workers[129] calculated that the decay of the correlation function for end chain carbons should be virtually independent of overall reorientation, this has been observed for a number of systems, and is probably being seen with the values of τ_{eff} measured for EHB.

The relatively large value of τ_{eff} for C7 can be rationalized as due to a decrease in internal motion. There is a much reduced probability of rotation about C-C bonds, in this portion of the molecule, due to the increased barrier to rotation, see Section 8.3, due to steric effects. There is also a smaller likelihood of co-operative internal motion due to the reduced probability of forming a "kink" in the chain at the branch point[97]. The large value of τ_{eff} for C6 compared to C8 probably reflects restriction of co-operative motion by the mass of the aromatic ring.

7.1.5 The temperature dependence of the reorientational correlation times of EHB.

Comparison of the relative correlation times of the methylene carbons as a function of temperature reveals that the relative rates of motion for all this type of carbon are not significantly temperature dependent. The ratio, however, of the correlation times of the methyl groups to the methylene groups decreases by around 30% on going from 270.7 to 376K. Such behaviour has also been observed in isopropyl benzene[122] and reflects overall reorientation becoming more prominent at high temperatures.

If the data is now considered in terms of the Arrhenius equation $(\tau_{eff} = A.\exp(E/RT))$, by plotting $\ln(\tau_{eff})$ against 1/T, as is shown for some of the carbon atoms in Fig.7.8, the data for EHB is found to be linear for each carbon over the temperature range 270.7 to 376K. The plots thus yield activation energies for reorientational motion for each carbon, see Table 7.3.

ACTIVATION ENERGY (KJ/MOL) CARBON NUMBER										
2	4	5	6	7	8	9	10	11	12	13
19.4	19.7	19.7	19.5	19.0	21.0	18.6	18.8	17.5	12.9	14.3

Table 7.3. Activation energies for reorientational motion for the carbons of EHB, obtained as in Fig.7.8.
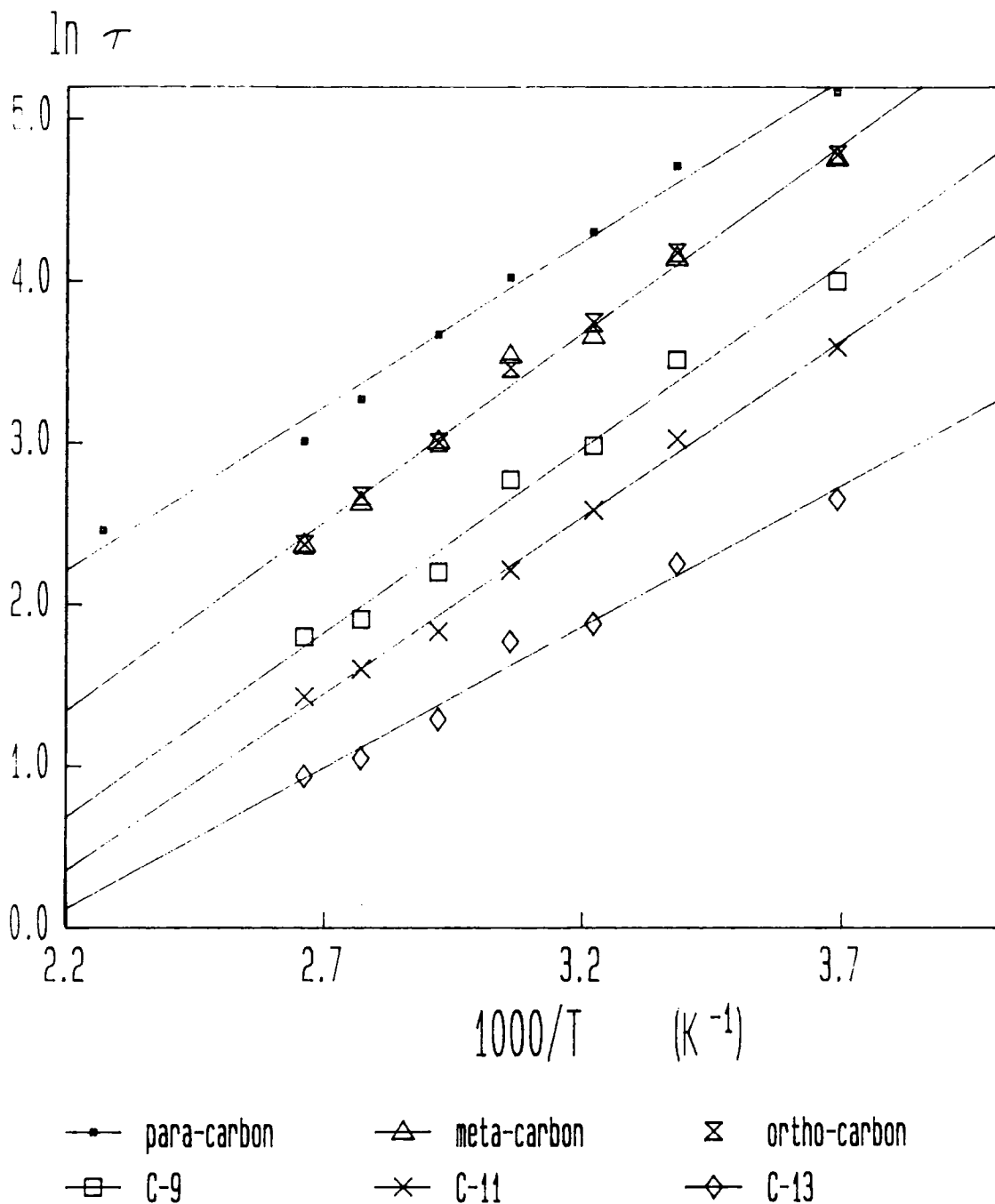
Figure 7.8. Arrhenius plots for the reorientational correlation times of the carbons of EHB.

As is shown by the nearly parallel plots for the methylene and methine carbons, in Fig.7.8, the activation energies are all found to be very similar with values around $20kJmol^{-1}$. The two methyl carbons, however, were found to follow a temperature dependence governed by activation energies of 12.9 and $14.3kJmol^{-1}$ for C12 and C13 respectively. The different temperature dependence of the methyl carbons relative to the methylene carbons presumably arises from the fact that internal rotation of the methyl groups can take place within the molecular volume, such behaviour of methyl groups has been observed many times before[97,100].

If the facility for internal motion decreased to a great extent from the first methylene group inward (into the chain) one might expect to see differing activation energies along the chain. The activation energy for C11 is lowest of all the methylene carbons, as is the trend with most long chain hydrocarbons[97], but the difference is not great. It might also be expected that the ring carbon atoms would show a different temperature dependence from the chain carbons, particularly the ortho and meta carbons for which it has been deduced have correlation times dependent on overall rotation about the long axis and internal rotation of the ring. The chain carbons are influenced to a varying degree by internal and overall motions. It is surprising that the τ_{eff} data for all the carbons, except the methyl carbons, follow a temperature profile defined by a single activation parameter, since it would seem unlikely that the activation energy for overall motion and internal motion would be approximately equivalent. If the temperature range of the

measurements was extended, deviations from linearity may then occur.

7.1.6 Comparison of viscosity data and reorientational correlation times

The variation with temperature of the shear viscosity. and the measured reorientational correlation times for the ring carbons of EHB are shown together in Fig.7.9. It appears that they show different behaviour with temperature, especially in the low temperature regime where the viscosity data is nearly exponential, whereas the τ_{eff} data varies roughly linearly with temperature.

If the temperature variation of the τ_{eff} data are compared with that of viscosity in the high temperature region, it is interesting that the two sets of data yield activation energies which are comparable in magnitude. If this observation is considered with the similarity of the activation energies for all the methylene and ring carbons it suggests that internal and overall reorientational modes of motion in EHB have similar thermal behaviour. This is consistent with observations by Lyerla and co-workers[97], and studies by Heatley[130] on the molecular motion of the polymers polyisobutylene and poly(propyleneoxide), dilution effects on the T_1 values for these molecules indicate that segmental reorientation is not entirely intramolecular but depends on the local environment. These observations on the thermal behaviour of the reorientational motions and viscosity of EHB imply that the motional changes with

213

temperature are ones of degree rather than fundamental difference. These results also suggest that the activation energy for viscous flow. measured in this temperature regime. is related to the activation energy for reorientational motion. Therefore it is likely that the viscosity/temperature behaviour is strongly dependent on the reorientational motion of the molecules, as they manouver to make motion relative to one another possible. This assumption is supported in Section 7.1.7.
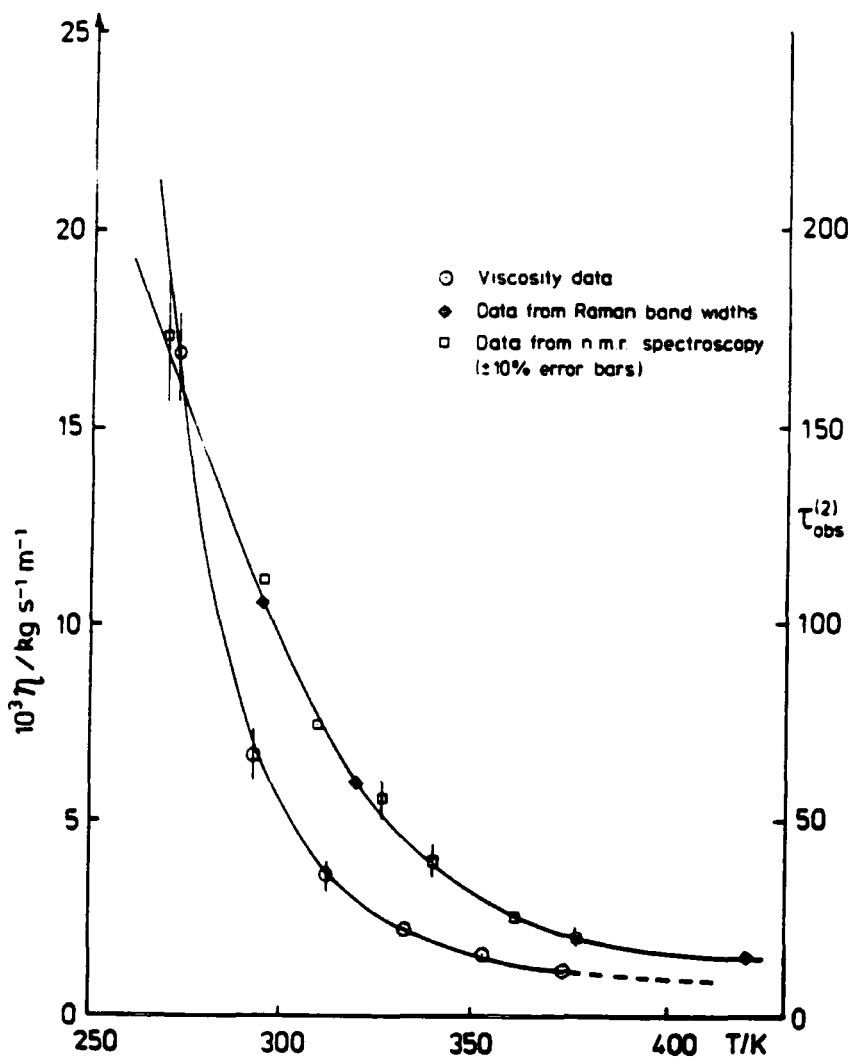
Figure 7.9. Variation of viscosity and the reorientational correlation times of the para carbon as a function of temperature.

7.1.7 The Kivelson model for molecular rotation

Further analysis of the relationship between the viscosity of EHB and the reorientational correlation times is possible by applying the modified hydrodynamic model, for reorientational correlation times, of Kivelson and co-workers[131,132]

$$\tau_1 = \tau_1^0 + V_h \eta K_1 / [1(1+1)k_B T] \qquad \text{Eqn.7.6}$$

where V_h is the effective hydrodynamic volume swept out by the reorientational motion under consideration, η is the viscosity, T is temperature, the subscript 1 indicates the order of the rotational correlation function (it is equal to 2 for light scattering and NMR spectroscopy). K_1 is a "torque/force" ratio parameter (a dimensionless interaction parameter) which measures the coupling of the rotational motions of the molecule to the translational (shear) modes of the fluid. It is included to account for the fact that the effective hydrodynamic volume V_h is often much less than that expected from simple Debye[63,133] considerations. It is found that, for a given molecule, K_1 appears to be independent of pressure and temperature[134]. It also appears that K_1 increases with increased solute solvent interaction and with increasing anisotropy of solvent molecules, the value of K_1 decreases with increasing size of solvent molecules relative to that of the solute molecules. In the Debye "stick" approximation $K_1=1$ and in the "slip" limit $K_1=0$. Debye assumed that the rotational relaxation of molecules in liquids was similar to that of macroscopic

215

bodies in a continuous homogeneous fluid. To a rotating molecule the surrounding fluid does not appear continuous and homogeneous, since on a molecular scale the molecular shape introduces discontinuities and inhomogeneity. This is particularly true for large irregularly shaped molecules such as EHB. Nevertheless Debye based theories have in the past had considerable success describing molecular motions[132,134].

A plot of τ, the reorientational correlation time, against η/T should be a straight line the slope of which enables an estimate of V_h to be obtained. It should be noted that it is not intended to obtain absolute values of V_h, this is impossible without a sure value for K_1, but analysis is an attempt to gain an insight into the relative values of V_h for the motions which cause relaxation of the ortho and meta carbons of the ring compared to value of V_h for the motions of the para carbon. Any change in type of reorientational motion contributing to the relaxation process will be observable by change in the slope of the plots.

It was considered acceptable to use the Kivelson equation to analyse the ring motions as it is felt that these motions involve a considerable reorientational volume. However with chain motions it is less clear as to the volume involved with the motion and also the value of K_1 would be difficult to estimate for such motions.

The τ_{eff} values for the ortho, meta and para carbons were analysed using a value of $K_1=1$, corresponding to the "stick" limit. The fit of the available data on EHB to

216

τ_{obs} /psec
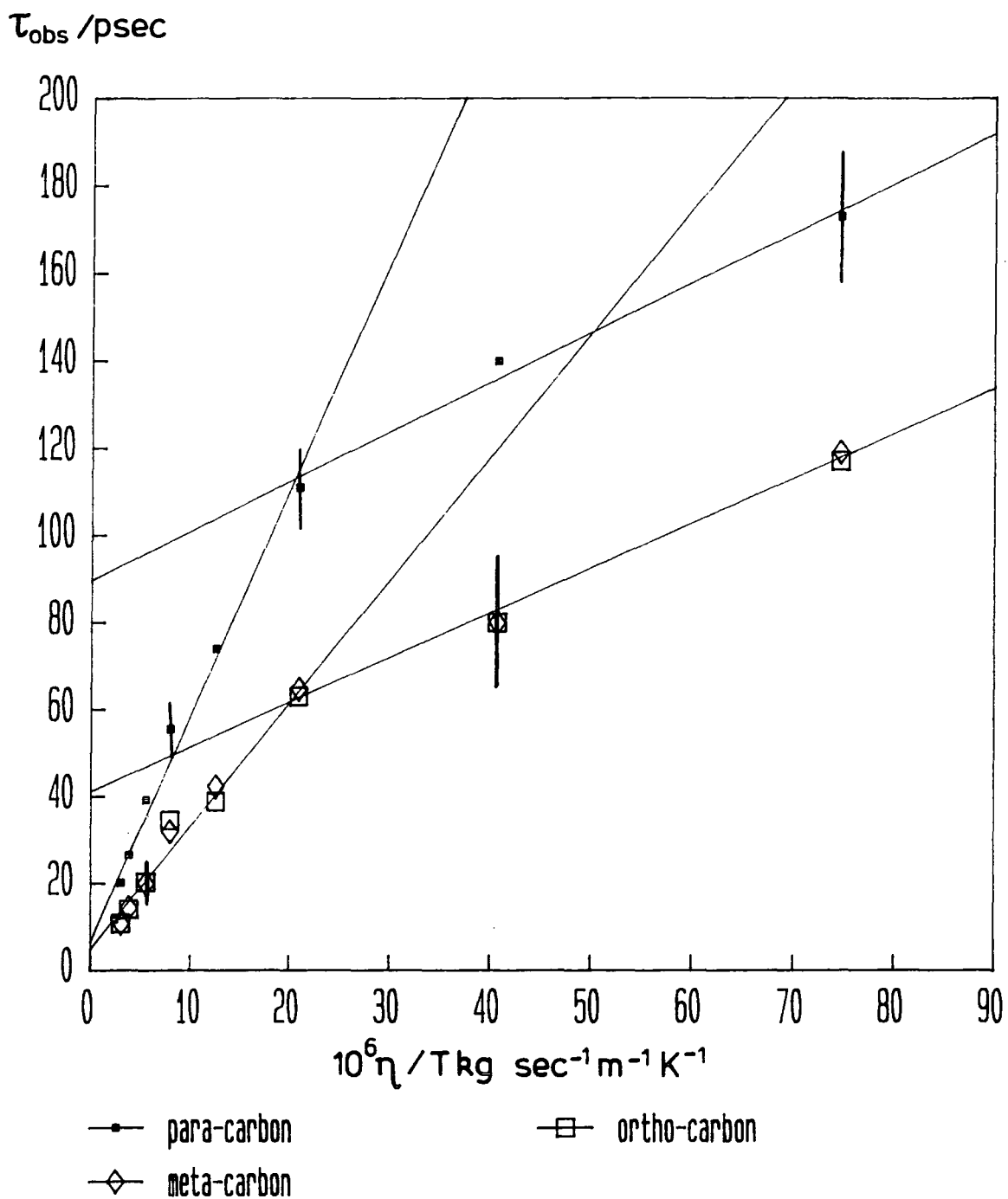
Figure 7.10. Variation of observed reorientational correlation times (psec) for ortho meta and para carbon atoms of EHB with η/T, according to the Kivelson equation.

Eqn.7.6 is shown in Fig.7.10. It should be noted that as the available τ_{eff} values do not correspond to the same temperatures as the experimental viscosity values, the viscosity data for use in Eqn.7.6 was therefore obtained by interpolation of Fig.7.9. It can be seen from Fig.7.10 that, as with the viscosity/temperature data, there is evidence for two regimes from the data for both the para carbon and the ortho and meta carbons.

The effective V_h values, at high and low temperatures respectively are 71 $\overset{\circ}{A}{}^3$ and 16 $\overset{\circ}{A}{}^3$ for the para carbon, and 40 $\overset{\circ}{A}{}^3$ and 14 $\overset{\circ}{A}{}^3$ for the meta/ortho carbons. Evidently the motion which is probed via the NMR ^{13}C spin lattice relaxation times (or Raman band shapes, in the case of the para carbon) involves a larger effective molecular volume at higher temperature than at lower temperatures, for both the para carbon and the meta/ortho carbons. Again the transition point is around 290-300K, near to the change of slope of the η data. One obvious interpretation of this data would involve a model with a change of "flexibility" (internal motional freedom) at about this temperature. The molecule could be envisaged to "lock" into a particular internal configuration below about 300K.

The associated values for V_h^{eff} are small compared with the total molecular volume of approximately 240 $\overset{\circ}{A}{}^3$, obtained by Walker et al using both the fluidity analysis method of Hildebrand et al[77,135] and Bondi's method of additive molecular group volume increments[136]. At about 300K it is thought that the molecule becomes more flexible internally and motions involving larger parts of the molecule contribute to the measured correlation times. It is

218

feasible that this change in internal flexibility is the reason for the change in viscosity behaviour which also occurs around 300K, as the flow of molecules past one another must be mediated by the flexibility of the molecules.

The V_h^{eff} obtained from data for the para carbons in the high temperature regime is approximately twice that of the V_h^{eff} obtained for the ortho/meta carbons in the same regime. This implies that there is a significant contribution to the relaxation of the para carbon from motions that involve a larger effective molecular volume than the motions that dominate the relaxation of the ortho/meta carbons. This is probably a consequence of internal rotation of the benzene ring end of the EHB molecule about the long axis having a major contribution to the relaxation of the ortho/meta carbons, but (as has been explained) not the para carbons. It has been suggested, see Section 7.1.3, that relaxtion of the para carbons involves some other internal motions. As a point of interest the molecular volume of benzene obtained using the Hilderbrand analysis[137] is 70 $\mathring{A}^3$.

If on the other hand the torque/force ratio parmeter K_1 is calculated from Eqn.7.6. taking V_h^{eff} as the calculated molecular volume obtained by Walker then values of 0.3 and 0.07 $\mathring{A}^3$ are obtained, for motion of the para carbom, at high and low temperatures respectively. It is difficult to explain why such a large anisotropic molecule should have K_1 values which approach the "slip" limit. Furthermore, it is impossible to explain why the K_1 value should decrease at lower temperatures. Therefore the model which explains the data in terms of a much reduced V_h^{eff} at low temperatures is

219

preferred.

Transition from low to high flexibility is not of course expected to occur at a particular critical point (this phenomenon is not a phase transition as such). Indeed there may be evidence (see Section 7.3.4) that at ambient temperature (~295K) there are molecules with different degrees of "flexibility" present in liquid EHB. The far-infrared spectrum of liquid EHB shows two dipole librational bands at $\sim 70 \text{cm}^{-1}$ and $\sim 150 \text{cm}^{-1}$, see Fig.II.4. From Fig.7.10. it can be seen that the molecules in the low temperature "flexibility state" are expected to dominate. Such molecules would have a lower "librational" frequency, and the low frequency band does dominate the spectrum.

7.1.8 The dependence of viscosity on the rotational and translational motions of EHB

In order to strengthen the correlation between microscopic rotational motion and viscometric behaviour the reported translational self diffusion coefficients as a function of temperature can be examined. Walker and co-workers[77] reported that the Stokes-Einstein theory could be applied to describe the translational self-diffusion coefficients of EHB, as a function of temperature, at the molecular level. Hydrodynamic theory relates the diffusion coefficient to the viscosity (η) and molecular volume (a) according to

$$D = k_B.T/(C\pi a\eta) \qquad \text{Eqn.7.7}$$

where C is a constant equal to 4 in the "slip" limit and 6 in the "stick" limit. Walker found that for their different isotherms, using the average hard sphere molecular radius obtained from their fluidity analysis, Eqn.7.7 adequately predicted the value of the self diffusion coefficient at the pressures they studied, see Fig.7.11 and Table 7.4. It should be noted that this covers data over five orders of magnitude. For the -20, 0, 20 and 40°C isotherms the values of C fall slightly below the C=4 limit, low values of C have been for observed before for molecules including methylcyclohexane[138] and pyridine[139]. For the 60 and 80°C isotherms the values of C are close to (within error) of the

PRESSURE (kBAR)	$C = kT/(\pi a D \eta)$						
	-20°C	0°C	20°C	40°C	60°C	80°C	100°C
10^{-3}	2.6	3.2	3.4	3.5	4.2	4.2	4.2
0.5	2.3	3.1	3.8	3.5	3.8	4.2	4.5
1.0	3.5	2.9	3.7	3.7	4.3	4.6	4.8
1.5	3.8	3.0	3.8	3.9	4.2	4.3	5.2
2.0	2.8	——	3.5	3.7	3.8	4.4	5.2
2.5	3.2	3.9	3.5	3.0	4.1	4.4	5.2
3.0	2.2	4.4	——	3.2	4.2	4.4	4.9
3.5	——	3.6	——	3.6	4.1	4.5	4.8
4.0	——	3.3	6.4	——	4.1	4.6	5.6
4.5	——	3.9	6.0	——	4.0	4.6	5.6

Table 7.4. Stokes-Einstein constants from Eqn.7.7.
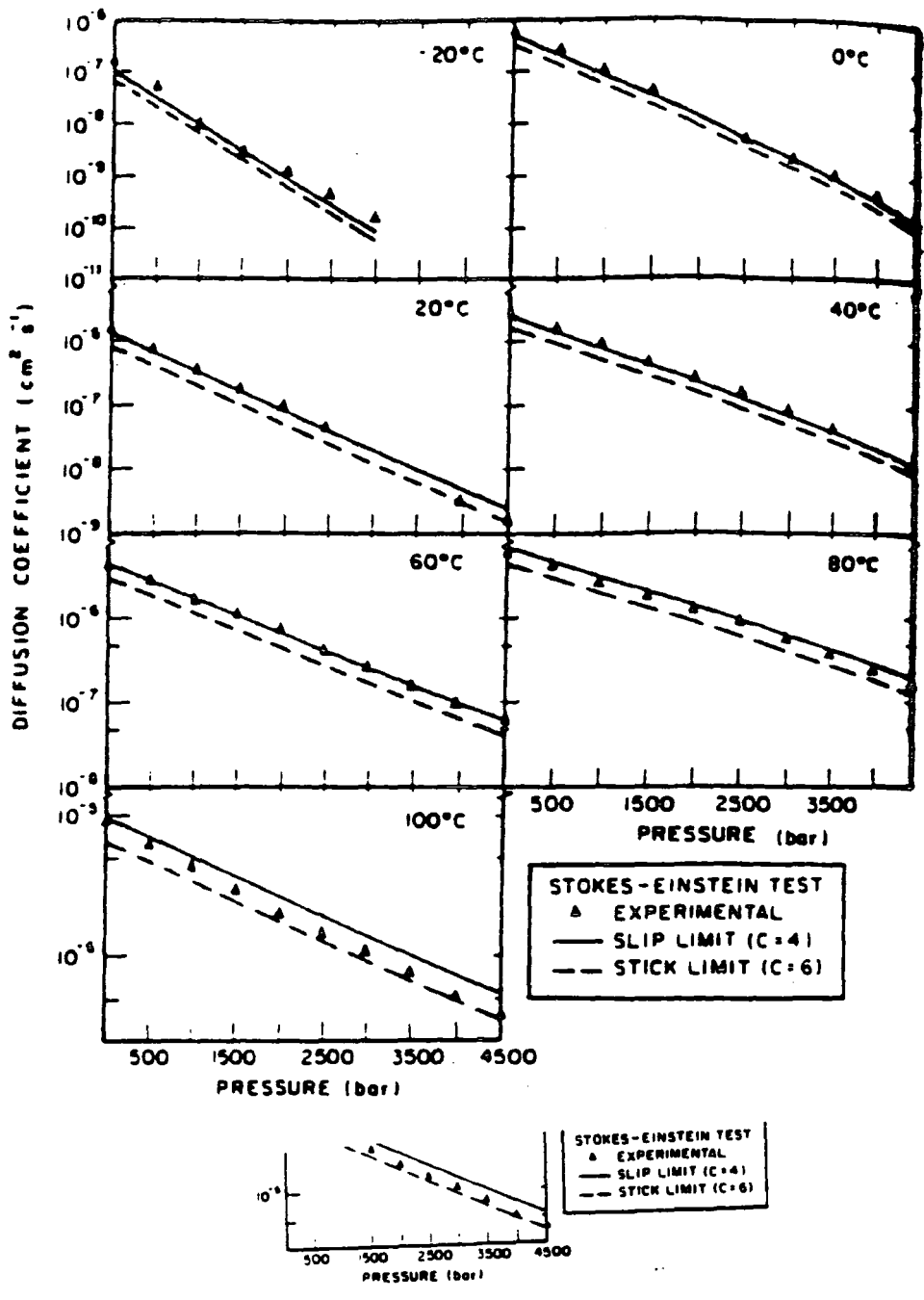
Figure 7.11. Comparison of the experimental and predicted (Stokes-Einstein) self-diffusion coefficients. The symbols Δ represent the experimental data; the solid and broken lines represent the slip (C=4) and stick (C=6) limits respectively. Reproduced, by permission, from reference 77.

slip limit. At 100°C the values of C all lie within the stick-slip boundary conditions.

As may be seen from Fig.7.12 if $1/D_t$ (equivalent to τ_{trans}) is plotted against η/T a perfect straight line is observed. The equivalent molecular volume a, obtained from Eqn.7.7, is 300 $\mathring{A}^3$ in the "slip" limit and 200 $\mathring{A}^3$ in the "stick" limit. Clearly the break in viscometric behaviour shown in Fig.7.4. is associated with the rotational or internal "flexing" motions of the molecule (or is at least dominated by such phenomena). Similar proposals, linking the macroscopic properties of fluids containing flexible molecules to internal reorientational motion, have been made based on molecular dynamic calculations[6,32].

In order to achieve a lubricant with low temperature-viscosity coefficient over the working temperature regime (200-400°C) one presumably needs to drive the transition point to lower temperatures. This presents a problem in chemical design which can, however, now be undertaken with the knowledge of what parameter (i.e. internal flexibility) needs to be changed.
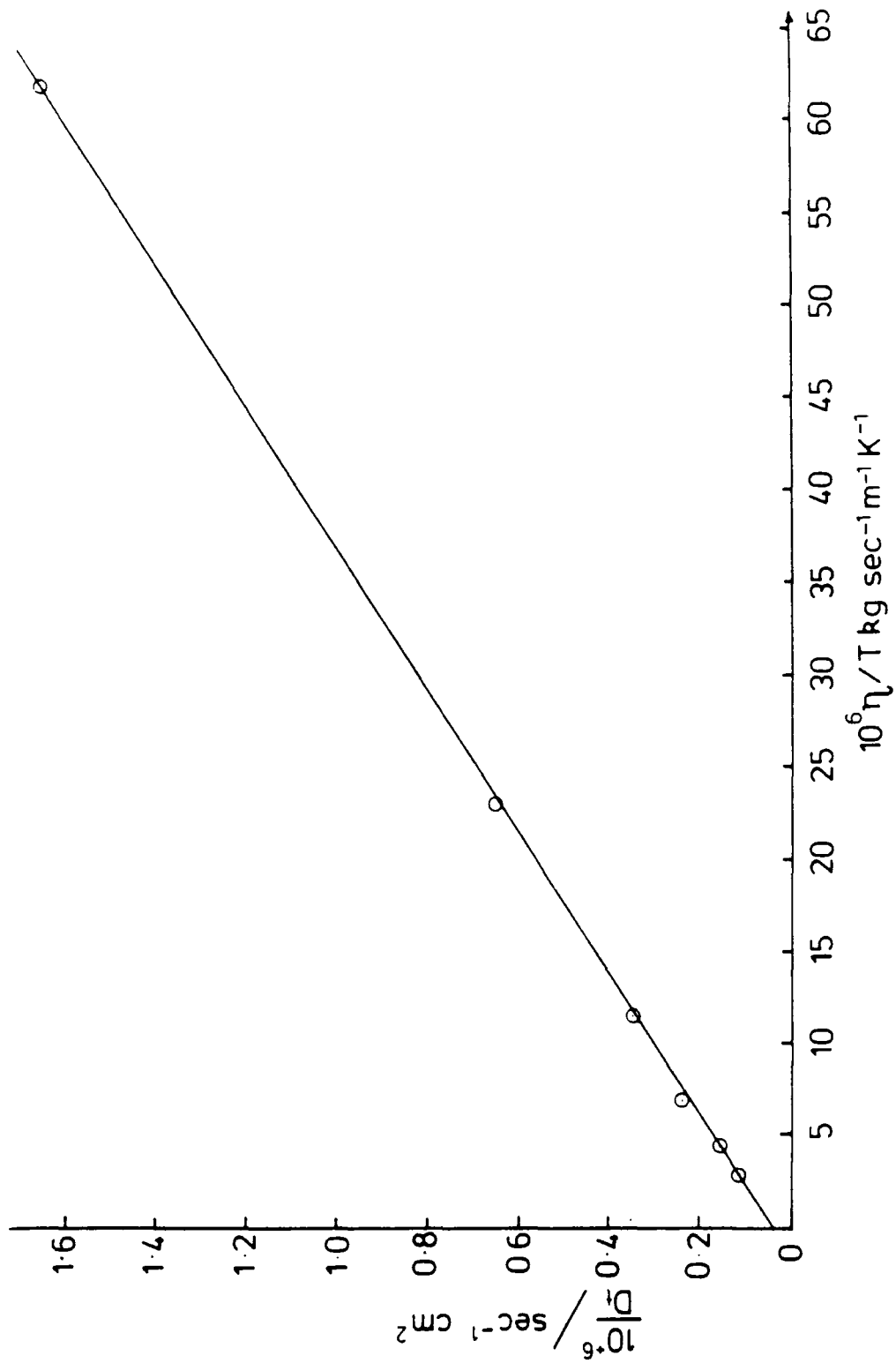
Figure 7.12. Variation of $1/D_t$ with η/T for EHB

7.2 The noncoincidence effect observed in the Raman spectra of the carbonyl $v(C=O)$ stretching mode of EHB

7.2.1 Resonance energy transfer (RET)

The peak frequencies of the isotropic and anisotropic Raman spectra of the carbonyl $v(C=O)$ stretching mode, see Table 6.3 and Fig.II.3 of EHB do not coincide. The frequency difference between the two bands is $3.3cm^{-1}$ in the pure liquid at 298K. This observation is known as the Raman noncoincidence effect and in recent years has been the subject of extensive investigations, both experimentally[140-148] and theoretically[39,149-156]. The effect is commonly associated with symmetric vibrational modes of polar molecules, and is most pronounced for Raman active modes which are also strongly infrared active. The noncoincidence effect has been widely observed for a variety of vibrational modes, for example the $v(C=O)$ mode of carbonyls[144,147,150,157], the $v(S=O)$ mode of sulphoxides and sulphones[145], the $v(N-H)$ mode of amines[158], the $v(C\equiv N)$ mode of nitriles[145], the $v(O-H)$ mode of alcohols[158], the $v(C-H)$ mode of chloroform[159,160] and others.

It is generally found that the peak frequency of the band is higher in the infrared than in the Raman spectrum, and that the peak frequency of the anisotropic Raman spectrum is higher than that of the isotropic Raman spectrum (the noncoincidence effect), and nearly coincides with the infrared peak frequency. This is indeed seen with the carbonyl $v(C=O)$ stretching mode of EHB, at 298K the infrared

band and Raman anisotropic spectrum have peak frequencies of 1721.0 and 1722.1cm^{-1} respectively whilst the Raman isotropic spectrum occurs at 1718.8cm^{-1}.

The noncoincidence effect has been attributed to the resonant transfer of vibrational excitation (resonant energy transfer or RET). and arises because intermolecular interactions of appropriate symmetry (usually but not necessarily those due to permanent dipolar interactions[144.157]) preferentially weight the relative allignment of a pair of active solute molecules. between which a resonant transfer of excitation can occur. The most common source of RET (but not necessarily the only source[149]) is due to transition dipole-dipole coupling induced by strong dipole-dipole intermolecular coupling.
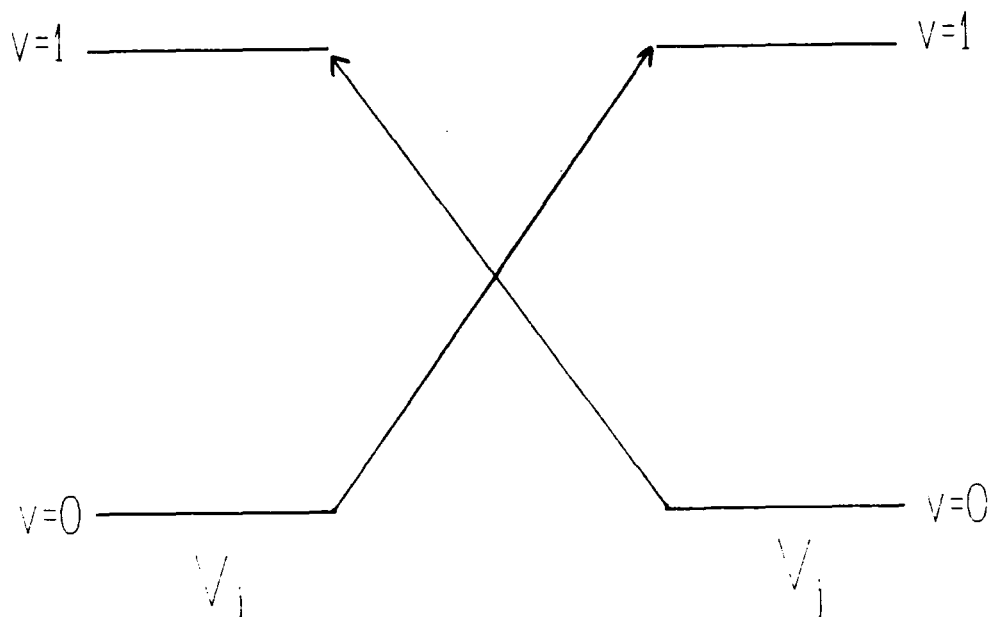
Figure 7.13. Schematic representation of RET

Due to the nature of RET it can only occur between identical oscillators on separate identical molecules. An oscillator is excited to an upper level by the incident radiation field. The oscillator returns subsequently from the excited to its ground level by giving its vibrational energy to an adjacent oscillator in its ground vibrational level, thereby inducing that oscillator to perform the upward transition ("flip-flop"). For a schematic representation of the process of RET see Fig.7.13.

The differences between the excitation frequencies (ω) of the liquid sample and ω_0 the vibrational frequency of the unperturbed molecule (i.e. dilute gas), due to "bath" perturbations, are eigenvalues of an interaction matrix. To calculate the matrix elements for a particular mode the interaction operator can be expanded in a Taylor series as function of the normal co-ordinates of the interacting molecules[140,161], as in Eqn.7.8.

$$V_{ij} = [V_{ij}]_0 + (\delta V_{ij}/\delta Q_i)_0 \cdot Q_i + 1/2(\delta^2 V_{ij}/\delta Q_i^2)_0 \cdot Q_i^2$$
$$+ 1/2(\delta^2 V_{ij}/\delta Q_i \delta Q_j)_0 \cdot Q_i Q_j$$

$$\text{Eqn.7.8}$$

followed by a perturbation calculation for the frequency difference between the ground and first excited state, leading to the expression[140],

$$V_{add} = [(\delta V_{ij}/\delta Q_i)_0(\langle 1|Q|1\rangle - \langle 0|Q|0\rangle) \qquad \text{Eqn.7.9}$$
$$+ 1/2(\delta^2 V_{ij}/\delta Q_i^2)_0(\langle 1|Q^2|1\rangle - \langle 0|Q^2|0\rangle)$$
$$+ (\delta V_{ij}/\delta Q_i)(\delta V_{ij}/\delta Q_j)_0(\langle 1|Q|0\rangle)]$$

There are different mechanisms which can contribute to this coupling potential, for example, dispersion interactions, dipole and multipole interactions which decrease the frequency, and repulsive forces which increase it (see Section 7.3). In the case of EHB, because of the large permanent dipole moment (ethyl benzoate has a dipole moment of $2D^{162}$), dipole-dipole interactions might be expected to dominate. If dipole interactions are responsible for the intermolecular coupling[140,142,143,163-5], in the point dipole approximation, the interaction potential can be represented by

$$V_{ij} = \mu_i \mu_j R_{ij}^{-3} K_{ij} \qquad\qquad \text{Eqn.7.10}$$

where R_{ij} is the intermolecular distance and K_{ij} describes the mutual orientation of two dipole vectors[143,164,166]. Inserting this value for V_{ij} into Eqn.7.9. one gets for the additional energy difference between the vibrational groundstate and the first excited state caused by the dipole interaction

$$V_{add} = K_{ij}/R_{ij}^3 \, [\, (\delta\mu_i/\delta Q_i)_o \mu_j (<1|Q|1> - <0|Q|0>)$$
$$+ \, 1/2 (\delta^2\mu_i/\delta Q_i^2)_o \mu_j (<1|Q^2|1> - <0|Q^2|0>)$$
$$+ \, (\delta\mu_i/\delta Q_i)(\delta\mu_j/\delta Q_j)_o (<1|Q|0>)\,]$$

$$\text{Eqn.7.11}$$

Fig.7.14 shows how the frequency of a vibrational mode, for a dipole molecule i, varies from the molecule being in isolation (gas phase) to being under the influence of identical neighbours (liquid or solid phase).

The first two terms in Eqn.7.11 describe the
interaction of the oscillator with the permanent dipole
field. This leads to the first shift of the frequency, as
seen in Fig.7.14. The first two terms are related to the
diagonal matrix elements and do not depend on the excitation
of molecule j. The third term in Eqn.7.11 describes the
interaction of the transition dipole moments, RET. and leads
to the noncoincidence splitting. The third term is related
to the off-diagonal matrix elements, and does lead to the
excitation of molecule j.
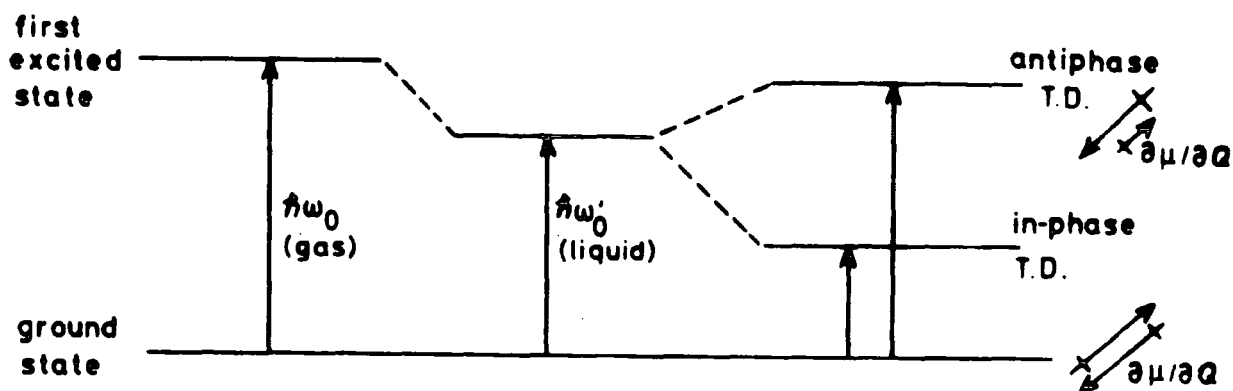
Figure 7.14. The shift and splitting of the vibrational
frequency of an isolated dipole molecule under the influence
of identical neighbours.

The amount of splitting caused by RET depends on the intermolecular distance and the relative orientation of the molecules. The splitting also depends on the magnitude of $(\delta\mu/\delta Q)_0$ which also controls IR absorption intensities. This is the reason that vibrations which are very intense in the infrared and with R_{ij} sufficiently low exhibit the noncoincidence effect or at least show vibration coupling contributions to the vibrational relaxation[38]. It should be noted that the RET process depends on the size of the transition dipole and not that of the permanent dipole. However the permanent dipole coupling does preferentially weight the alignment of a pair of oscillators between which the transition dipole - transition dipole coupling can occur.

The splitting occurs because during the exchange of vibrational energy the dipoles can oscillate both in-phase or with anti-phase (a relative phase shift of 180°) with each other. The intensity of the two frequencies in the spectrum, is due to the contributions of both molecules to the transition polarizability of the coupling system. Because the Raman tensor for the isotropic part of the band is spherically symmetrical, the relative orientation of the molecules are not important for the intensity. For the in-phase vibration the whole transition polarizability of the coupled pair is the sum of the isolated Raman tensors. For the anti-phase vibration, the transition polarizability of the coupled pair is the difference in the isolated Raman tensors and thus for both molecules having the same tensor equal to zero. Therefore only the in-phase vibration of the system is visible in the isotropic part of the spectrum.

However this is not true for the anisotropic part as the intensity depends on the relative orientations of the molecules. The sum (in-phase) and difference (anti-phase) contributions to the intensity of the anisotropic band. depend on the angle between the main axis of the two Raman tensors. Fig.7.15 shows how the contribution from both varies with the angle between the axis. It can be seen from Fig.7.15 that in-phase coupling always contributes some intensity to the anisotropic band, whilst at an angle of 0 and 180° the anti-phase contribution is zero.
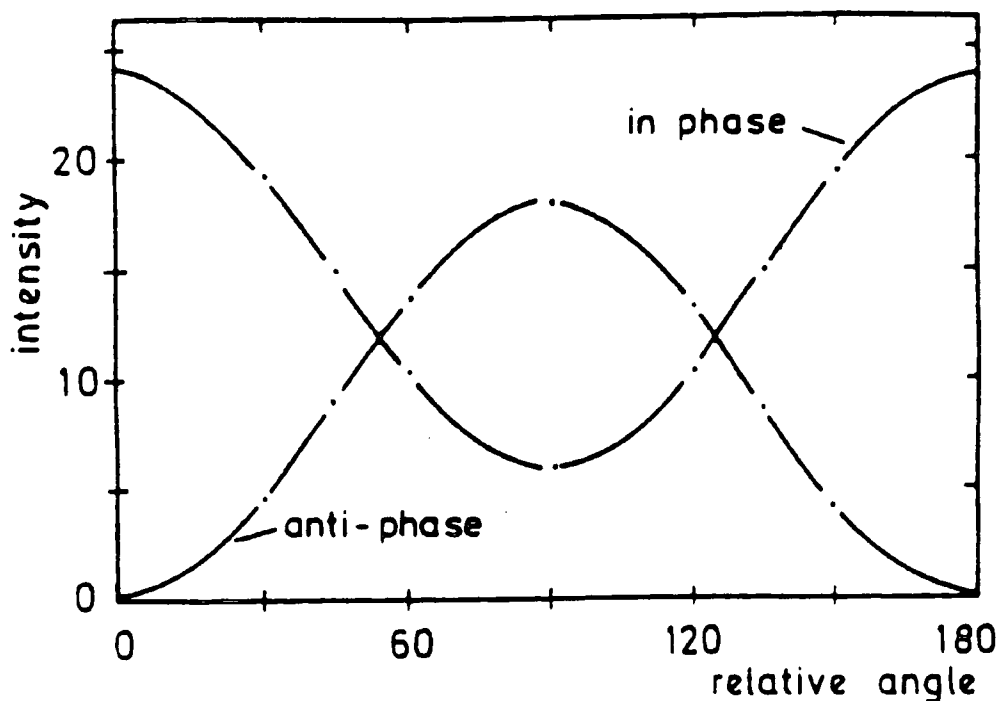
Figure 7.15. Calculated intensities (arbitrary) of the two vibration modes of a resonant coupling pair of linear molecules in anisotropic Raman scattering as a function of their relative angles (degrees). Reproduced, by permission. from reference 140.

231

Both the in-phase and anti-phase modes contribute to the anisotropic band and so this band occurs at higher frequency than the isotropic band. The shape and frequency position of the anisotropic band depend on the relative contributions from the two modes.

RET leads to inhomogeneous broadening, because the disordered liquid results in a distribution of coupling strengths. The resonant effect (third term in Eqn.7.11) then causes a distribution of excitation energies, which results in inhomogeneous broadening (see Chapter 2).

7.2.2 Anomalous behaviour of the band widths of the Raman isotropic and anisotropic spectra of the $v(C=O)$ mode of EHB

At ambient temperature and pressure the Raman anisotropic band of the $v(C=O)$ stretching mode of EHB is observed to be narrower than the isotropic band. The anisotropic FWHM is $14.6cm^{-1}$ compared with $15.8cm^{-1}$ for the isotropic band, see Table 6.3. This difference is removed as EHB is gradually diluted in hexane, see Fig.6.14, and Table 6.6. At 10% m.f. there is no difference at all and as the concentration is lowered even further it appears that the anisotropic band is becoming broader than the isotropic band. The difference in band width is not present for EHB at 10% m.f. in benzene or in CS2. At 373K and 443K the difference in band widths has been reduced, see Table.5.2.

As has been explained previously (Chapter 2) anisotropic bands are found to be broader than isotropic bands if they contain contributions from reorientational

relaxation. The observation that the anisotropic band is actually narrower than the isotropic band suggests that reorientational motion of the carbonyl group is negligable on this time scale (picosecond).

The possibility of the isotropic vibrational width being greater than the anisotropic width, for modes that exhibit RET, has been predicted by both Lynden-Bell[39] and Logan[154]. However as far as can be ascertained observation of such a phenomena has not been previously reported. Studies of RET have tended to be on relatively small molecules that show considerable reorientational motion. Therefore even if the isotropic band does show additional broadening compared to the anisotropic band, due to RET, the difference is obscured by the reorientational broadening of the anisotropic band. It was suggested, as a consequence of the correlation time measurements, in Section 7.1 that EHB exhibits only very slow reorientational motion at room temperature. Therefore there should be little if any contribution to the anisotropic band width of the $\nu(C=O)$ mode from reorientation. Consequently the band width difference predicted by Lynden-Bell and Logan can be observed.

The difference in band width arises because cross terms can occur in Eqn.7.9 between the self and exchange terms, these can contribute to the isotropic relaxation but not to the infrared and negligibly to the anisotropic relaxation[39]. The cross terms may have either sign, giving (in the absence of reorientation) either a greater or lesser vibrational line width for the isotropic band compared to that of the anisotropic band. The cross term only becomes important if

the self and exchange processes are of comparable magnitude[39]. This suggests that the self and exchange terms of the $v(C=O)$ mode of EHB are comparable in magnitude, and the cross term must have positive sign.

In solution pair interactions between molecules of different type give self terms, but the exchange terms are no longer resonant. The vibrational relaxation of the isotropic band will therefore have a smaller contribution from the cross term as the concentration of the active species, and thus the exchange terms, are reduced. Dilution will therefore gradually remove the difference in band width. Increased temperature reduces the interoscillator coupling because of the increased mobility of the molecules. This reduces the contribution from RET to the vibrational relaxation and therefore reduces the difference between the isotropic and anisotropic band width, see Fig.5.6. Increased temperature also increases the contribution from the reorientational relaxation to the anisotropic band width.

If vibrational dephasing resulting from attractive force frequency fluctuations is a dominant relaxation process for the $v(C=O)$ mode of EHB, then exchange terms will contribute significantly to the vibrational relaxation and consequently to the band width of this mode. This has been supported by the results of the solution experiments carried out on EHB, see Section 7.3.

7.2.3 The effect of temperature on the RET process

Considering the effect of temperature on the RET process, clearly the greater the relative mobility of the adjacent molecules bearing the oscillators, the less efficient the resonance transfer process. The coupling is reduced and thereby the contribution from RET to the vibrational relaxation is diminished. The band width therefore decreases, assuming the molecules find no other effective means to relax. In addition the band width is also decreased through motional narrowing[53,57,164]. A reduction in the RET process also leads to a reduction in the observed splitting between the Raman isotropic and anisotropic bands.

The results for the variable temperature Raman study of the $v(C=O)$ band are in agreement with the above statements. Both the anisotropic and isotropic bands show an approximately linear increase in frequency with temperature over the range 190 to 440K, see Fig.5.5. There is a "kink" in this plot between 298 and 190K, it is possible that this "kink" is related to the change of flexibility discussed in Section 7.1. However without further data between 190 and 373K it is impossible to determine whether a transition in the frequency behaviour of the $v(C=O)$ mode has really occured. The splitting, as expected, also diminishes. at 440K it is down to $1.0cm^{-1}$. It is interesting to observe that the splitting does not change on going from 298K to 190 or 77K. At a lower temperature it might be expected to observe an increase in RET (as is seen from 440 down to 298K) but this does not appear to occur for the two lowest

temperatures observed. It seems unlikely that at 298K the interoscillator coupling is at a maximum. A possible explanation for observing no increase in RET at these low temperatures is that some other relaxation process becomes dominant and thus suppresses any increase in RET. It is important to note again that inhomogeneous broadening through RET is by no means the only process that contributes to the band width for this vibrational mode.

There is very little change in the Raman band width of both bands over the whole temperature range studied (see Table 5.2). With increasing temperature the contribution of RET to the vibrational relaxation of this mode will go down. The relative mobility of the molecules increases and the density decreases. The effects of these changes on vibrational dephasing are complicated. In the rapid modulation limit FWHM α τ_v^{-1} = M2$_v \tau_m$ (see Chapter 2). In the slow modulation limit the band width is proportional to the vibrational second moment (M2$_v$). The vibrational second moments may increase as energetically less favorable conformations become populated. However with the reduction in RET, the contribution to the second moment from the exchange terms in Eqn.7.11 will decrease. It is unclear therefore as how the second moment will change with temperature. The value of the environmental modulation time should decrease with increased mobility/ kinetic energy, thus decreasing the band width (motional narrowing). However the contribution from processes such as collision induced dephasing[165] and intramolecular dephasing (see later) may increase, thus increasing the bandwidth. Even for these processes the competing effects of increase in

kinetic energy and decrease in density[53], on the collision rate, make any prediction of the effect of temperature difficult. If it were known which dephasing process was dominant, the overall picture would still be complicated. It may not be so surprising, therefore, that little change in band width is seen upon varying the temperature.

7.2.4 The effect of concentration on RET

Lowering the concentration of the species between which RET occurs, by dissolving the compound (solute) in some solvent reduces the number density of the active species. Also, upon dilution, the permanent dipole-dipole coupling (or whatever intermolecular interaction is responsible), which preferentially wieghts the relative alignment of a pair of molecules between which RET can occur, is progressively removed. Both of these effects contribute to a reduction in RET, the extent of the change depends on the solvent and concentration of the solute. In recent years there have been a number of attempts to quantitatively predict the effect of concentration on the observed splitting[145,153-155] (see Section 8.2).

With EHB it is observed that the splitting between the Raman anisotropic and isotropic bands of the $v(C=O)$ stretching mode is gradually removed as EHB is diluted in hexane. The two bands become coincident at about 10% mole fraction (m.f.), see Fig.6.5. On dilution from 100% to 1% m.f. the two bands exhibit a non linear blue frequency shift of 10.8 and 7.3cm^{-1}, for the isotropic and anisotropic bands

respectively, see Fig.6.13. At 10% m.f. in benzene and CS2 the two bands show a much smaller increase in frequency, however the splitting has again been removed, see Figs.6.6 and 6.7, and Table 6.3.

These observations demonstrate the removal of RET by dilution. The increase in frequency occurs because the attractive coupling interactions between the EHB molecules are reduced upon dilution, thus reducing the contribution from both the self and exchange terms in Eqn.7.9 and increasing the frequency. The size of this increase in frequency, compared to the change in frequency of the other modes (see Chapter 6 and 7.3), confirms that dipole-dipole coupling of the carbonyls is strong. This is further evidence that it is dipole-dipole interactions which preferentially weight the alignment of the dipoles between which transition dipole-dipole coupling and thus RET can occur. The isotropic Raman band[153-5] of this mode has an additional shift, compared to the other vibrational modes, due to removal of the exchange interactions which contribute to the vibrational frequency and give rise to the RET effect.

The relatively large blue frequency shift in hexane, compared with that in benzene and CS2, is due to the reduction of the permanent dipole-dipole coupling between EHB molecules by the hexane molecules. The smaller frequency shift of the $v(C=O)$ mode for EHB in benzene or CS2 is due either to less efficient removal of dipole-dipole coupling. Or because of other contributions to the attractive part of the intermolecular potential for EHB in benzene or CS2, which may result from solvent-solute

interactions. If so Eqn.7.9. would need to be modified to take into account the contribution from solvent-solute interactions.

The band widths of the two peaks are narrowed as the concentration is reduced, see Figs.6.12 and 6.14. This is consistent with lowering the vibrational relaxation rate, some of which can be attributed to loss of RET.

At 10% m.f. in all three solvents, the isotropic band has become narrower than the anisotropic band implying that reorientational motion of the carbonyl group is now possible on the picosecond time scale. This may be a consequence of the reduction in the dipole-dipole coupling of the EHB molecules. However it might be that a small contribution from reorientational relaxation was always present in the anisotropic band width but was obscured by the phenomena described in Section 7.2.2.

7.3 Effects on the vibrational modes of EHB on dissolving EHB in the solvents hexane, benzene and CS2

The Raman and infrared spectra of EHB in solution, discussed in this section, are contained in Chapter 6 along with tables summarising the observed frequency shifts and band widths.

7.3.1 Frequency Shifts

When molecules are placed in solution the intermolecular forces on the solute molecules change with respect to those felt by the molecules in pure solute. This change in forces, felt by the bonds of the molecules, causes a change in frequency of the vibrational modes of the molecule.

Intermolecular forces are expressed as the interaction of two molecules in terms of the intermolecular potential energy, $U(r)$, which results from their separation at a distance r. Several different types of interaction contribute to the intermolecular potential energy. The major types of interaction are dipole-dipole (and/or higher multipole interactions), dispersive, inductive and repulsive interactions. The first three types of interaction, above, involve attractive forces, these are long range and slowly varying. Whilst repulsive interactions are short range and rapidly varying.

Drickamer and co-workers have studied the influence of different types of intermolecular interactions on

240

vibrational frequencies[167,168]. They found that repulsive forces give a blue frequency shift, whilst attractive forces produce a red shift. This has since been further supported by molecular dynamics simulations[169].

According to Drickamer[167,168], the frequency shift Δv_2 on going from isolated molecule to liquid phase is given by,

$$\Delta v_2 = A(\gamma \cdot e'_{12} + e''_{12})$$ Eqn.7.12

where $A = (8\pi^2 c^2 m v^g)^{-1}$, m is the reduced mass of the classical oscillator and v^g is the frequency of the dilute gas or isolated molecule. The symbol γ stands for $(-3f_{111}/f_{11})$, where f_{111} is the anharmonic force constant and f_{11} the harmonic force constant in the vibration potential of the isolated molecule. The e'_{12} is the first and e''_{12} the second derivative of the intermolecular interaction energies, with respect to a displacement from the equilibrium position (δr). The index 2 is used for solute molecules, while i denotes the solvent.

The presence of the term γ (= $-3f_{111}/f_{11}$) allows for the variation in the magnitude of the frequency shift for each different vibrational mode of a molecule. Essentially it is a measure of how much a vibration modifies the intermolecular potential. For example ring v(C-C) deformation vibrations have a very small anharmonicity constant. Therefore it should be expected that these vibrations show relatively little change in frequency upon varying the attractive intermolecular potential felt by the molecule. This has been shown to be the case for EHB, varying the intermolecular interactions, by changing the

241

temperature or dissolving EHB in hexane or CS2, has only a very small effect on the frequency of vibration of the ring v(C-C) deformation of EHB. However the v(C=O) stretching vibration greatly modifies the large attractive intermolecular potential localized at the carbonyl. Therefore a relatively large frequency shift, for v(C=O) stretching mode, can be expected to occur when EHB is diluted or the temperature is varied, as has been seen with EHB.

It was shown in Chapter 6 that when EHB is dissolved in hexane, at 10% m.f. the frequencies of all the vibrational modes, except the ring v(C-C) deformation mode, studied increase, both in the infrared and Raman spectra. However, compared to the hexane spectra, their is little if any change in frequency of any of the modes when EHB is dissolved in benzene or CS2.

Because EHB has a relatively large dipole moment (ethyl benzoate has a dipole moment of 2.0 D[162]) it might be expected that attractive interactions will dominate in the pure liquid and probably in solution. By dissolving EHB in various solvents the intermolecular potential, felt by the EHB molecules, is modified. Attractive interactions between the EHB molecules are reduced causing a blue frequency shift. Whilst new solvent-solute interactions occur.

For EHB in benzene and CS2 it is possible that attractive interactions dominate the solvent-solute interactions. The observation of little overall change in vibrational frequency, for all the modes, for EHB in benzene or CS2, could therefore be due to the solvent-solute interactions causing a large enough red frequency shift to

offset the blue frequency shift caused by separation of the
EHB molecules. In hexane the interactions of EHB with the
hexane molecules does not alter the intermolecular potential
in a manner which cancels the shift due to the reduction in
EHB-EHB attractive interactions. Therefore the overall
effect seen for EHB in hexane is a blue frequency shift. It
is also possible that the repulsive interactions in hexane
are more significant than in benzene or CS2. However there
is no reason to expect that the EHB-hexane repulsive
interactions are any greater than EHB-EHB repulsive
interactions.

To gain an insight into the reasons for the observed
variation in frequency shifts, in the three solvents, an
attempt was made to estimate the relative strengths of the
intermolecular interactions in the three solvents.
Expressions for the attractive interaction energies have
been known for a long time[142-3]. The dispersive energy is
given by

$$U_{disp} = e_{i2}^{disp} = -3/4 \ [I_2 I_i / (I_2 + I_i)] \cdot \alpha_i \alpha_2 / R_{12}^6 \qquad \text{Eqn.7.13}$$

where the I's are the ionization energies of the molecules,
α the polarizabilities and R_{i2} is the bond-bond distances.
The inductive interaction energy can be represented by

$$U_{ind} = e_{i2}^{ind} = (-1/\epsilon^2) \cdot [\alpha_i \mu_j^2 + \alpha_j \mu_i^2] / R_{i2}^6 \qquad \text{Eqn.7.14}$$

the μ's are the permanent dipole moments and ϵ is the
dielectric permittivity of the medium. Finally the dipolar
interaction energy is

$$U_{dip} = e_{i2}^{dip} = (-1/\epsilon^2) \cdot [2\mu_i^2\mu_2^2/3k_bT]/R_{i2}^6 \qquad \text{Eqn.7.15}$$

Both U_{ind} and U_{dip} are dependent on the orientation of the molecules relative to one another, and Eqns.7.14 and 7.15 should strictly contain orientation dependent factors. However for the purpose of obtaining a quantitative estimate of the relative contributions from each type of interaction this can be ignored. The above expressions for interaction energy were used to obtain an estimate of relative contribution from each mechanism in the three solvents, in a hope that this would correlate with the observed frequency shifts. Table.7.5 summarises the parameters used for each solvent and EHB. Table.7.6 shows the values obtained for U_{int}/R_{i2}^6 (for each type of interaction), this is a measure of the relative magnitudes of the different interaction energies in the three solvents. Assuming that R_{i2} does not change significantly in the different solvents.

It can be seen from Table.7.6 that in all three solvents the dispersion energy is significantly greater than the dipole and induction energy. Even in the pure liquid the calculated dipole interaction energy is much less than the calculated dispersion energy. It has long been thought that dispersion interactions should dominate the attractive interactions for non-polar molecules[142]. Similar such calculations as the above have been carried out by other workers[142,143,164], they also found that the dispersion energies dominated. These workers managed to correlate the observed frequency shifts with the dispersion energies. For EHB there appears to be no correlation of the observed frequency shifts with the calculated dispersion energies.

Table 7.5. Molecular parameters used for calculating the attractive interaction energies of EHB in solution

MOLECULE	α $(10^{-24}cm^3)$	I (eV)	ϵ (erg.cm)	μ (D)
EHB	$16.9^{\dagger}$	$9.35^{\ddagger}$	6.02^{*}	2.0^{+}
n-hexane	11.90	10.18	1.89	0.0
benzene	10.74	9.24	2.28	0.0
CS_2	8.86	10.08	2.64	0.0

All data obtained from Ref.162.

$\dagger$ the polarisability of EHB was taken to be that of ethylbenzoate.

$\ddagger$ the ionization potential of methyl benzoate, this should be acceptable considering the small variation in I across a homologous series.

* the dielectric constant of EHB was taken to be that of ethyl benzoate.

+ the dipole moment of EHB was taken to be that of ethyl benzoate.

Table 7.6. Estimates of the different attractive interaction energies for EHB liquid and EHB in solution. Using Eqns.7.13-15.

SOLUTION	$\dfrac{10^{-60}.U_{\mu\mu}}{R^6_{ij}}$ $(ergs.cm^6)$	$\dfrac{10^{-60}.U_{ind}}{R^6_{ij}}$ $(ergs.cm^6)$	$\dfrac{10^{-60}.U_{disp}}{R^6_{ij}}$ $(ergs.cm^6)$
EHB-EHB	7.15	22.5	1602.3
EHB-hexane	0.0	13.3	1176.2
EHB-Bz	0.0	18.3	1012.2
EHB-CS_2	0.0	13.4	871.6

$T = 298K$

$1D = 1 \times 10^{-8}$ erg.cm

$1eV = 1.6 \times 10^{-12}$ ergs

$k_b = 1.381 \times 10^{23}$ J $K^{-1} = 1.381 \times 10^{-16}$ erg.K^{-1}

It was expected that attractive interactions would dominate the frequency shifts on going from liquid EHB to EHB in solution. However the estimates of the attractive interaction energies have not been able to support this, though neither have they refuted it. To obtain a clearer picture it would be necessary to be able to estimate the size of the repulsive energies involved with EHB in solution. Estimating repulsive interactions has always been more difficult than estimating attractive interactions[53,161,170], consequently no attempt has been made to estimate a value for the repulsive interaction energies for EHB in solution.

The models employed to estimate the attractive interactions are non-specific. That is they are only concerned with interactions of the vibrational modes with a continuous intermolecular potential. These models do not allow for specific interactions between the various functional groups of the molecules, for example in the case of EHB strong dipolar coupling localised at the carbonyl groups. This should not create too much of a problem for simple, rigid quasispherical molecules, in solvents made up of molecules of similar shape and size (such systems that tend to have been concentrated on previously). However for non-rigid more complicated molecules such as EHB it would seem that these expressions for interaction energies are not sufficient to accurately model the solvent-solute interactions.

If it is assumed that attractive interactions do dominate the frequency shifts observed for EHB in solution. Then it appears that hexane is showing a greater tendency to

separate the EHB molecules than Benzene or CS2. Thus producing the difference in behaviour of the vibrational modes for EHB in hexane compared with EHB in benzene and CS2. In dealing with dispersion forces between large polyfunctional molecules, geometrical averaging of dispersion force interactions cause interactions between like groups to be somewhat larger than those between unlike groups. Molecules such as EHB are never expected to be packed randomly even in the liquid state. Bearing this in mind, hexane being more "like" the hydrocarbon chain of EHB might, because of this, find it easier to associate with EHB and separate the EHB molecules. This would be particularly true if the hydrocarbon chains of EHB interacted strongly. If the chains of EHB do interact strongly, in hexane the aliphatic v(C-H) stretching modes of EHB would not alter their frequency much compared to the other modes. Unfortunately it is not possible to study the aliphatic v(C-H) stretching modes for EHB in hexane, because the aliphatic v(C-H) stretching modes of hexane interfere too strongly with the EHB spectra in this region.

In addition to the above, of the three solvents hexane has the greater molecular volume (M/ρL) $128cm^3mol^{-1}$, compared with 89 and $60cm^3mol^{-1}$ for benzene and CS2 respectively. So it might be expected, considering the size alone, that hexane would be better at separating the EHB molecules, for EHB at the same mole fraction concentration in the three solvents. However even at 20% m.f. in hexane (which is a greater equivalent volume fraction than is 10% m.f. EHB in benzene or CS2) the frequency of the v(C=O) stretching mode is still considerably higher than for 10%

248

m.f. EHB in benzene or CS2, see Table 6.6. This confirms
that the observed variation in frequency shifts for EHB in
solution is not just a consequence of size of solvent
molecule.

An additional explanation for the difference in
behaviour of the vibrational modes for EHB in hexane than
for EHB in benzene and CS2, could be that solvent molecules
in benzene and CS2 are interacting in some specific manner
with the functional groups of EHB. For instance the
carbonyl group. Interactions which are not allowed for in
the expressions used for the interaction energies, and which
may cause a significant red shift.

The removal of the noncoincidence of the Raman
isotropic and anisotropic bands of the $v(C=O)$ stretching
mode of EHB in all three solvents. As well as the
observation of a much larger blue frequency shift, compared
to the other modes, of the $v(C=O)$ stretching mode for EHB,
in all three solvents, is indication that there are much
stronger attractive interactions localized at the carbonyl
groups. This further confirms that the noncoincidence
effect shown by the Raman bands of this mode is caused by
RET which is allowed because of the dipole-dipole coupling
of this group. It also further points out the need for
models for intermolecular interactions which allow for
specific interactions localized at functional groups of the
molecules.

Finally in this section it is necessary to consider the
dependence of the frequency shifts on the intramolecular
interactions. For rigid molecules the frequency shift
compared to the gas phase depends solely on the changes in

intermolecular potential. For larger flexible molecules, such as EHB, there may also be significant contributions from changes in the intramolecular potential. If the intramolecular interactions of EHB change, for instance because of a shape change or change in molecular flexibility, then this can significantly effect the frequencies of the vibrational modes. This may be occuring for EHB in hexane, explaining the large frequency shifts compared to those seen for EHB in the other two solvents.

7.3.2 Band width changes

The large decrease in bandwidth of the Raman and infrared bands arising from the υ(C=O) stretching mode for EHB, compared to the other vibrational bands, suggests that the vibrational relaxation process for this mode depends on a different type of interaction than the other modes. It has already been shown that the υ(C=O) stretching mode undergoes RET, and that upon dilution this RET is removed. The large fall in band width with dilution and the removal of the isotropic-anisotropic band width difference indicates that inhomogeneous broadening, as a result of RET, has a significant contribution to the vibrational dephasing of this mode.

The decrease in band widths of the other modes indicate that EHB-EHB interactions provide more efficient vibrational relaxation than EHB-solvent interactions. If inhomogeneous broadening is assumed to be the major cause of vibrational relaxation (see Chapter 2), and applying the Kubo line formalism[57] in the rapid modulation limit (FWHM α τ_v^{-1} = M2$_v\tau_m$), then to observe a decrease in band width either the vibrational second moment or the environmental modulation time, or both, must decrease. A decrease in attractive interactions by solvation is predicted, from vibrational dephasing theory[37,53], to decrease both the second moment and τ_m. The environmental modulation time decreases because removal of attractive interactions between EHB molecules will allow for greater molecular mobility. Removal of attractive interactions should also allow for greater molecular flexibility, which will have the effect of

motionally narrowing any broadening due to intramolecular
inhomogeneous dephasing.

As with the frequency changes the greatest band width
changes are seen for EHB in hexane. This provides evidence
that the changes in molecular interactions which cause the
frequency shifts also modulate the relaxation processes. It
has been proposed that the change in attractive
interactions, particularly the dispersive interactions, on
going from liquid to solution are mainly responsible for the
observed frequency shifts. Therefore it is probable that
the band width changes in solution arise from modulations
to the relaxation processes caused by the changes in the
attractive intermolecular potential.

It can be seen from Tables 6.1 and 6.7 that dilution of
EHB in hexane or CS_2 allows reorientational relaxtion of the
ring $v(C\text{-}C)$ deformation mode, on the picosecond time scale.
It would appear from this observation and considering the
previous discussion, that the reorientational motion of EHB
becomes easier as the EHB molecules are separated.
Reorientation is not prevented by interaction with the
solvent molecules, so it is probable that it is the
attractive intermolecular interactions between the EHB
molecules that prevents reorientation of the ring, on the
picosecond time scale, in the pure fluid. It is interesting
to summise that it is the dipole-dipole coupling localised
at the carbonyl groups that prevents the reorientation.
Certainly this is a distinct possibility if the motions that
are being probed, through observation of the reorientational
correlation times of the ring $v(C\text{-}C)$ deformation mode, are

rotations and/or flexing of the benzene ring end of the molecule about either C-O single bond. As has been suggested by the molecular graphics studies on EHB, see Section 8.3.

7.3.3. Hexane dilution of EHB

The results of the Raman and infrared study of EHB in hexane solution at different concentrations varying from 100% m.f. to 0.5% m.f. are summarised in Sections 6.1.2 and 6.2.2 respectively. Both Raman and infrared bands of the $v(C=O)$ stretching mode show a non linear blue frequency shift, see Figs.6.12-13 and 6.18-19, and decrease in band width with concentration, see Figs.6.14 and 6.19.

Both the Raman and infrared bands of the $v(C=O)$ stretching modes exhibit a "concentration threshold", at about 1% m.f.,beyond which further dilution does not appear to alter either the frequency or band width of this mode. It is felt that at this "concentration threshold" the EHB have become completely separated from each other and only feel the influence of the surrounding hexane molecules. Further dilution does not, therefore, alter the potential the EHB molecules "see", and so results in no change in vibrational frequency or band width.

The low value for this "concentration threshold" point suggests that EHB-EHB interactions are extremely strong. The ratio of hexane molecules to EHB molecules required to effectively separate the EHB molecules is 100. The results of this experiment have been supported by an investigation

into the heats of solution generated during the addition of EHB to hexane. The results are summarised in Section 6.4. The results indicate that as EHB in hexane (at sufficiently high concentration that the EHB molecules are associated) is added to pure hexane the EHB molecules become solvated and heat of solvation is generated. At first the heat generated is relatively large, see Table.6.9, as the EHB molecules become completely separated. However when the concentration of bulk solution reaches about 0.3% m.f. the enthalpy change for each addition of an aliquot of EHB/hexane solution reaches a minimum and becomes roughly constant, see Fig.6.21. At this point a distinct change in the slope of the plot of enthalpy change against mole fraction of bulk solution can be seen. The process which is occuring when each aliquot is added has changed, the hexane can now no longer separate all the EHB molecules but can only solvate the groups of associated EHB molecules. This indicates that EHB can only exist as non-associated EHB molecules, in a significant amount, below about 0.3% m.f. This transition point was very reproducable and the only one found up to 2.9% m.f.

Within experimental error the "concentration threshold" obtained from the infrared experiment agrees with the concentration for non-association obtained from the enthalpy experiment. Both experiments indicate that the concentration of EHB needs to be extremely low before EHB molecules become completely separated.

The non-linear frequency and band width changes of the $v(C=O)$ stretching mode of EHB, and the gradual removal of the Raman noncoincidence splitting, with increased dilution

in hexane are discussed further in the next chapter. In
Chapter 8 attempts are made to predict the splitting and
frequency shifts as a function of concentration, solvent and
temperature using theoretical models to describe the
intermolecular interactions.

7.4 The far infrared spectra of EHB

7.4.1 Sources of far infrared spectral bands in liquids

For liquids, infrared bands in the region 1-400cm^{-1},
far infrared (FIR), may arise from a number of molecular
processes, the following section describes some of these.
Vibrational modes will produce bands in the far infrared
providing that - (a) one or more of the atoms involved in
the vibration is sufficiently heavy to ensure the reduced
mass of the vibration is large enough to give a low
vibrational frequency, and/or - (b) the atoms involved in
the vibrations are held together only weakly, when a small
force constant compared to that of a normal "chemical" bond,
will ensure that the vibrational frequency is low[171-2].
Typical examples of type (a) are vibrations involving
metal-metal or metal-ligand bonds[171]. Low-frequency
stretching modes in some hydrogen-bonded systems provide an
example of type (b) vibrations[172]. In addition, for some
systems, bending or similar modes (such as ring puckering)
may occur in the FIR region[173].

Torsional vibrations are often the only bands to be
observed in the 1-400cm^{-1} region, these occur because,
unless there is free rotation about a given bond, there must
exist a potential barrier which hinders the rotation[171] (see
the molecular graphics work in Section 8.3). In general the
potential barrier depends on the orientation of the parts of
the molecule that can rotate, the minimum in the energy
corresponds to the more stable configuration of the

256

molecule. The difference in potential energy between neighbouring maxima and minima are known as <u>barrier heights</u>, while the difference in the potential energy between various minima are termed <u>energy differences</u> between isomers. The torsional frequency is dependent upon the barrier height. If the barrier is sufficiently high there can be several energy levels corresponding to various torsional states in the molecule. It is the transition from the ground state (most stable isomer) to the first or second of these levels that is usually observed. Providing that two conformational isomers have similar energies, so that each has sufficient population to be observed, see Eqn.7.16, and the barrier height is high enough to ensure that the two isomers can exist separately i.e. conversion between the two is not too rapid, then it is possible that two bands with slightly different torsional frequencies can occur.

$$\frac{N(\text{stable})}{N(\text{metastable})} = \exp(V_1/RT) \qquad \text{Eqn.7.16}$$

V_1 = energy difference between two conformers

Miller observed two low-frequency absorption bands, for the halogen meta-substituted benzaldehydes[174], separated by $6\text{-}16\text{cm}^{-1}$. These were considered to most likely represent two rotational isomers co-existing in appreciable concentrations and having slightly different torsional frequencies, see Fig.7.16.

Another class of bands that occur in the FIR region are known as "lattice" modes, these involve motions of a

molecule within the temporary "liquid lattice", formed by neighbouring molecules. The motion may involve motion of the molecule as a whole or part of the molecule, the latter type of motion is known as an external "libration" (similar to a torsional mode). The molecules are considered to be oscillating in a van der Waal's force field which is changing rapidly as the environment of the molecule is undergoing change. The forces between molecules are usually an order of magnitude weaker than the inter-atomic forces. and since a lattice mode involves a molecular grouping the mass will be relatively high. Hence, modes associated with the motions described above are expected in the FIR region.
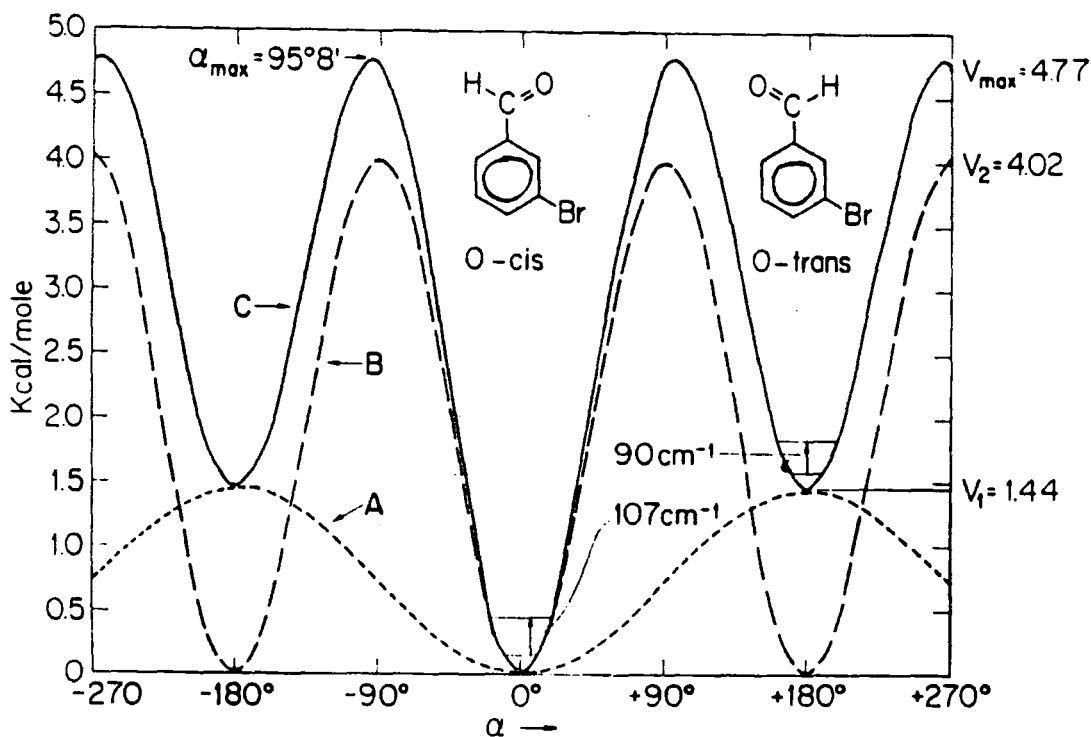
Figure 7.16. Potential curve for the torsion in m-Br-benzaldehde (to scale). $V(\alpha)$ (kcal/mole)$=1.44(1-\cos\alpha)/2 + 4.02(1-\cos2\alpha)/2$. (a) First term. (b) Second term. (c) Sum. V_3 is assumed to be zero. Reproduced, by permission, from reference 171.

The infrared selection rules require that only motions
that produce a change in the magnitude or direction of the
dipole moment relative to the normal coordinates may
contribute to the spectrum. From this it might be expected
that only motion of polar molecules would produce a FIR
spectrum. This however is not the case, many non-polar
molecules such as carbon tetrachloride[175], benzene[176] and
carbon disulphide[177] show significant absorption. This is
explained by considering the presence of fluctuating induced
dipoles, and it is known as collision or interaction-induced
absorption. It should also be expected that the FIR
absorption profile for a polar liquid will have a
contribution from collision induced absorption as well as
the absorptions allowed by the infrared selection rules[177].

Transitions starting from vibrational levels other than
the ground state are more likely to occur in the FIR region
than in regions of higher frequency. This is because the
difference between the energy levels, in the FIR, is much
smaller and consequently closer to kT. From Eqn.2.6 it can
be seen then that the higher energy states have a
significant occupation for modes below $100cm^{-1}$. Thus "hot
bands" are an expected feature of low frequency spectra
observed at room temperature. These bands can usually be
distinguished from others by changing the liquid temperature
which should change their intensity significantly.

7.4.2 The far infrared spectrum of liquid EHB

It is now possible to consider the source of the FIR bands given by liquid EHB. As shown in the introduction to Section II, EHB gives rise to two bands between 4 and $250cm^{-1}$. The low frequency band at $74cm^{-1}$ is seen to be the dominant band with an intensity that is roughly two times that of the higher frequency band found at about $150cm^{-1}$. It is unlikely that the bands arise from vibrational stretching modes as there are no heavy atoms involved with EHB, and both bands appear to be too broad to be characterised by vibrational or difference bands.

The low frequency band is almost certainly connected with the libration of the ester/carbonyl group of EHB. However, is not clear whether the band arises from rapid "librational" motion (it could just as easily be an internal "torsional" mode), or whether it represents the short time part of the overall rotational motion about the long axis. The high frequency component could be associated with an out-of-plane bending mode[178] of the substituted benzene ring. Although, as suggested above, the band appears to be too broad to arise from a vibrational mode. Further possibilities for the origin of these two bands, based on previous FIR studies, are discussed below.

Grosse and Hufnagel[93] studied the FIR spectra between 1 and $350cm^{-1}$, of a number of aromatic aldehydes. They also observed two absorption bands. The low frequency band was assigned to the internal torsional oscillations of the aldehyde group (broad band). The higher frequency band (which tends to occur as a doublet or triplet) was more

intense than the low frequency band and was said to arise from the flexing motions of the aldehyde group about the C-C bond that links it to the aromatic ring. As discussed previously (Section 2.4), for non-rigid aliphatic ketones Vij and Hufnagel[95] saw two absorption profiles in this region, see Fig.2.11. The low frequency band, at about $55cm^{-1}$, was assigned to overall rotation of the molecule. Whilst the second weaker band, at the higher frequency of about $300cm^{-1}$, was said to arise from intramolecular librational motion of the -CO and CH3CO about the alkyl backbone to which they are attached. Such an argument could be applicable to the two far infrared bands of EHB. It is also plausible that <u>both</u> of these bands for EHB are due to intramolecular librations, involving internal rotation about different bonds, if so, the lower frequency mode would most likely involve the rotation of a bigger portion of the molecule than the higher frequency mode. Certainly, from observations made on the Raman bands of the v(C-C) ring deformation mode as a function of temperature, it would appear that a change of flexibilty occurs near 298K, so rotations about different bonds do appear to occur. This will be discussed further in Section 8.3. It might be expected that an increase in temperature would change the relative intensities of the two bands, as the flexibility of the molecule increases. Indeed, Vij saw with the work on alkyl ketones, that the intensity of the band arising from the intramolecular libration increases at the expense of the intermolecular libration, as the chain length of the alkyl ketones is increased. The increased chain length facilitates an increase in intramolecular motion. However

with EHB. as can be seen from Fig.5.7, the increase in flexibility that appears to occur with increased temperature does not change the relative intensities of the two bands.

Reid and Vij observed a band centred at about 60cm^{-1} for diphenyl ether[179]. They derived model parameters for a variety of molecular motions that could give rise to the band, and attempted to reproduce the band theoretically by using a statistical-mechanical approach based on the Mori continued fraction approximation to the general Langevin equation of motion[38,46,180]. They found that the best model parameters to reproduce their experimental data are derived for <u>coupled</u> motions of internal and overall rotation. It is possible that, for EHB, the low frequency band arises from a similar type of motion, whilst the higher frequency band is due to intramolecular libration.

Finally, the two bands could arise from the same libration or torsional mode of two different conformational isomers. However if this is the case, then the barrier height for conversion from one isomer to the other and vice-versa (see Fig.7.16) would need to be significantly different for the isomers to give rise to bands separated by over 70cm^{-1}. In addition, the energy difference between the two isomers would need to be relatively small, so that both isomers exist in an appreciable amount. From the molecular graphics work (see Section 8.3) it would seem that it is extremely unlikely that both these criteria could be satisfied. It might be expected that the relative intensities of the two bands would change with temperature, which does not occur, see Fig.5.7. Also, providing that the interaction of other modes with the surrounding potential

give rise to a vibrational energy difference due to the two
conformers, then doublets in other regions of the Raman or
infrared spectrum should be observed, which they are not.
It is unlikely, then, that these two bands are due to two
different conformers of EHB.

There can be no reasonable certainty about the
assignment of the infrared bands of EHB at 74 and $150cm^{-1}$,
without an attempt to theoretically reproduce the spectrum.
A model is required that is capable of reproducing the basic
features of the spectrum, which allows for different input
parameters to test which type of motion gives the best
correlation with the actual spectrum. Such models,
described by Doge and Yarwood[38,181] (and discussed in
Section 2.3.2), attempt to derive expressions for the far
infrared absorption profile or the corresponding correlation
function. They take into account the dependency of the
motion (and consequently the band shape and CF) on the
intermolecular interactions of the molecule. The
procedures, used successfully by previous workers in
Durham[181] are the Mori truncated fraction approach and the
Oxtoby cell model. These attempt to reproduce the
experimental absorption profile by varying up to four
parameters that are related to the properties of the
molecule and libration. However it is difficult to know
precisely what the parameters mean physically, so their
absolute values may not be too meaningful, especially for
molecules as complex as EHB. On the other hand, observation
of the changes in such parameters with experimental
conditions (e.g. concentration, temperature etc) can reveal
how the intermolecular interactions in the system under

study are changing, for example whether the torque involved with the motion increases or decreases with the change in environment. For EHB it was felt that there was insufficient reliable data in the FIR region to justify such an approach. The overlap of the two bands would make any attempt to fit the data difficult. Also there is no data available for EHB from $10cm^{-1}$ down to the microwave region. Finally the spectra obtained for EHB in this region are limited to two temperatures (25 and $100^{o}C$) and only one concentration in the three solvents (hexane, benzene and CS2). Therefore there would be a considerable amount of uncertainty involved with any conclussion drawn from a three or four parameter fit of the limited experimental data for EHB to theory.

To summarise this section then, it is <u>likely</u>, considering previous studies and the shape of these bands. that the FIR bands at 74 and $150cm^{-1}$ arise from librational motions of EHB involving either the whole of or part of the molecules. Though the exact nature of the libration is uncertain. It was decided that to try and fit the data to any of the models for librational motion (discussed in Section 2.3.2) would not be worthwhile for a molecule as complex as EHB. Therefore interpretations of spectral changes, in this region, as a function of concentration. solvent and temperature, will concentrate on how the molecular torque changes with the surrounding environment.

7.4.3 The far infrared spectra of EHB as function of concentration, solvent and temperature.

It was seen in Section 7.3 that dilution of EHB in hexane had a greater effect on the shape and vibrational frequency of the infrared and Raman bands, particularly those of the $v(C=O)$ mode, than in benzene or CS2. The librational motions that give rise to the two FIR bands of EHB involve rotation of the ester group. It might therefore be expected that dilution in hexane, rather than in benzene or CS2, would give the greater change in the FIR spectra of EHB. In fact this is the case as can be seen from Fig.6.20, the main band has a peak frequency of $67cm^{-1}$ in hexane, a difference of $7cm^{-1}$ over the frequency in pure EHB. It is somewhat surprising that there is very little change in the band shape or relative intensity of the two bands for EHB in solution compared to pure EHB.

It has recently been shown[182-3] that librational frequency depends directly upon the torque effective upon the active molecule. Torques are the anisotropic intermolecular forces exerted on molecules in a fluid as they try to move. The torque depends on both the "surrounding" structure of the liquid and the motions of these "surrounding" molecules. Intermolecular forces between molecules, in particular dipolar forces, give rise to torques on the molecules. In addition there is the collision dependent torque[183]. An increase in torque will increase the librational frequency and a decrease in torque will decrease it. Consequently, observation of change in librational frequency, when a macroscopic variable is

altered, gives information on how the intermolecular interactions are effected. Therefore, from the decrease in frequency of the 74cm^{-1} FIR band of EHB, when EHB is diluted in hexane, it would appear that the torque exerted on the molecule, when undergoing the librational motion that gives rise to this band, is decreased by dilution in hexane. It has been determined that dipole-dipole coupling is reduced as the EHB molecules are separated in hexane. This is also true for EHB in benzene or CS2, however for these solvents the results suggested that EHB-EHB attractive interactions are replaced to some extent by EHB-solvent interactions, and/or that these solvent molecules do not separate EHB molecules as efficiently as hexane molecules. It is therefore not surprising that no shift of the 74cm^{-1} FIR band is seen for EHB in benzene or CS2. Decrease in the dipole-dipole coupling, and separation, of EHB molecules in hexane reduces the torque on the molecules causing a reduction in the librational frequency. The shift is comparable with the shift in the vibrational frequency of the v(C=O) mode for EHB in hexane, see Table 6.8.

The results of the solution study of the FIR spectra of EHB have supported the findings from the similar study of the Raman and mid-infrared spectra, see Section 7.3. It would appear, from the frequency shift observed for the FIR spectra of EHB in hexane, that the torque active on the motion responsible for this band is strongly dependent on the intermolecular dipole-dipole coupling. For this reason it is probable that the 74cm^{-1} FIR band is a consequence of external "librational" motion.

The effect of a 75K increase in temperature, from 298

to 373K, see Fig.5.7, is to decrease the librational frequency, indicating a decrease in effective torque on the molecule. The shift of 3.5cm^{-1} is comparable to the Raman bands of the v(C=O) mode of EHB which showed a shift, over the same temperature range, of 4 and 2cm^{-1} for the isotropic and anisotropic bands respectively. The effect of temperature is to decrease the density and dipolar dependent torque. The lack of any change in either intensity or relative intensity of the two FIR bands, with increased temperature, supports the proposal that both the bands arise from librational modes.

In conclusion to this section, the shape and behaviour of the FIR spectra of EHB are consistent with bands that arise from librational motion. The frequency shifts of the 74cm^{-1} band, for EHB in solution and upon increasing temperature, further support conclusions made in previous sections about the microscopic response of EHB to macroscopic changes. Finally the librations of the ester group of EHB appear to be equally as sensitive to environmental changes as the v(C=O) stretching vibration of EHB.

7.5 Variation of the infrared spectra of EHB with increased pressure

The application of pressure to molecules in the condensed phase can lead to red frequency shifts, blue frequency shifts or nonmonatonic behaviour[167-8,184-5]. There is a delicate balance between the opposing effects of repulsive and attractive interactions which is altered by the increased pressure.

The relaxation processes occuring in the liquid phase are dependent on the intermolecular and intramolecular interactions and so increased pressure also affects the band widths. The change in intermolecular and intramolecular interactions when increasing the pressure can also cause conformational changes. This can result in the suppression or enhancement of any bands dependent on the conformation of the molecule[186]. If the magnitude of the transition dipole moment of a vibrational mode is altered by increased pressure this will also affect the absolute intensity of a band.

The results of the infrared high pressure experiments on EHB are summarised in Chapter 4. Unfortunately because of the closeness of many of the bands a reliable quantification of the relative band intensities or band widths was not possible for many of the bands. Especially at the higher pressures where band overlap becomes significant.

7.5.1 The pressure induced frequency shift of the $v(C=O)$ stretching mode

Unlike the rest of the infrared bands of the vibrational modes of EHB, the carbonyl $v(C=O)$ stretching vibrational band does not show a linear frequency increase with increasing pressure. It can be seen from Fig.4.4 that initially, from 1bar to 6.5kbar, this band shows an approximately linear decrease in frequency of 2.6cm^{-1}. This shift is then reversed so that when the pressure has reached 30.3kbar the frequency has increased by 2.9cm^{-1}, from 1720.5 to 1723.4cm^{-1}, see Table 4.1. Over the whole of the pressure range studied the peak <u>height</u> intensity is not affected significantly, see Fig.4.3, therefore because the band width increases with pressure the integrated band intensity is increasing. Similar observations were made on the carbonyl $v(C=O)$ stretching mode of acetone[184] and the ester 1,2 dioleoyl phosphatidylethanolamine (DOPE)[187].

It was stated earlier that a negative frequency shift is due to attractive forces, whilst repulsive forces result in a shift to higher frequency. The sum of the forces can result in a positive or negative frequency shift. Both types of forces should increase with increasing density in bulk fluid, because the intermolecular distance decreases. Repulsive interaction energies are usually[53] assumed to vary proportionally with R_{12}^{-12}. The attractive interaction energies, discussed in Section 7.3.1, are proportional to R_{12}^{-6}, see Eqns.7.13-15. It is therefore more usual to see increased vibrational frequencies with increased density, indicating that the repulsive interactions increase more

rapidly than the attractive. However if there is an additional variable that affects the attractive interaction energy which is altered by increased density, for example rotational alignment, then the attractive interactions can increase more rapidly with pressure than the repulsive, because the dipoles are more effectively aligned.

It is already known that attractive interactions, most probably dipole-dipole, localised at the carbonyl groups play an important role in determining the spectroscopic properties of the carbonyl v(C=O) stretching mode of EHB. From observations of an initial decrease in frequency with increased pressure it would appear that the dipolar interactions for this group increase rapidly with pressure. This indicates increased alignment of the dipoles and a consequently large increase in interaction energy with decreasing intermolecular distance. Up to 6.5kbar this increase in dipolar interaction energy must be greater than the increase in repulsive interaction energy, for this mode. At 22.7kbar the repulsive forces have become dominant. It should be noted, that as the pressure is increased up to 30.3kbar, it is possible EHB goes through one or more phase transitions. This would make the interpretation of the spectral changes additionally complicated.

Schindler and co-workers[184] saw a linear decrease in frequency, of 4.2cm^{-1}, for the Raman bands of the same mode of acetone, up to 4kbar. This band of acetone, like EHB, shows the noncoincidence effect. Wong and co-workers observed that the frequency of their ester carbonyl decreased by 3cm^{-1} to 8kbar, after which the frequency

increased linearly to 50kbar. Wong pointed out that the change from decreasing to increasing frequency coincided with a phase transition for their ester.

The observation of this decrease in frequency for the carbonyl v(C=O) stretching mode of EHB, contrasts with the other modes which all show an increase in frequency with increased pressure. Or in the case of the symmetric CH vibrational modes exhibit little change in frequency at all. This again indicates the care that must be taken when applying expressions for interaction energies, as employed in Section 7.3.1. in attempts to estimate frequency shifts. These expressions do not allow for specific interactions like the dipolar interaction of the carbonyl groups of EHB.

7.5.2 The effect of increased pressure on vibrational modes of EHB other than the carbonyl v(C=O) stretching mode

It can be seen from Figs.4.4-4.19 and Tables 4.1 and 4.2 that other than the carbonyl v(C=O) stretching mode, and the symmetric CH vibrational modes, all the vibrational modes of EHB show a linear increase in frequency with increased pressure. The frequency/pressure coefficient (dv/dP) varies from mode to mode.

This observation of a linear increase in frequency demonstrates that interactions of the vibrational modes of EHB with the repulsive potential dominates the frequency shift. The extent of the frequency shift is dependent on how much a vibration interacts with the changing potential. Modes involving a large volume change should therefore show a greater increase in frequency over modes involving a smaller amplitude of vibration. For this reason symmetric modes should exhibit a larger frequency increase with increasing density than do assymetric modes. This has been observed by a number of workers[185,187].

However Schweizer and Chandler[161] showed that even when a monotonically increasing frequency shift or dephasing rate are observed with increased density/pressure the role of the slowly varying attractive forces is non-negligible. That is to say that the attractive interaction forces still vary with pressure and contribute to the observed shift. Therefore the extent of any shift will also be affected by the change in attractive interactions, which like the repulsive interactions varies from mode to mode.

7.5.2.1 Pressure induced changes in the vibrational modes involving the CH's of the alkyl chain of EHB

By far the greatest frequency increase with pressure, observed with EHB, is that of the $\nu_{as}(CH_3)$ and $\nu_{as}(CH_2)$ stretching modes, 0.85 and 0.75cm^{-1}kbar^{-1} respectively, see Figs.4.9 and 4.10. The frequency increase of the antisymmetric modes is much more than that seen for the corresponding symmetric stretching modes, see Table 4.2. In fact up to 6.5kbar the $\nu_s(CH_3)$ stretching mode does not appear to change in frequency at all, a phenomena that is mirrored by the $\delta_s(CH_3)$ and $\delta(CH_2)$ bending modes. Similar such observations have been reported for the same modes of n-hexadecane with increased pressure[188]. At first these findings appear to contradict the predictions made in the introduction to this section. However if the vibrations are considered in more detail the observed shifts do agree with those proposals.

Considering first the CH_2 vibrations. The normal modes of each methylene group can couple with the corresponding modes of the neighbouring methylene groups, according to various phase angles. However most of these coupled modes for each normal mode are weak in the infrared and Raman spectra[188], except for those with $\phi = 0$ (which are Raman active) and those with $\phi = \pi$ (which are infrared active). To understand the effect of pressure on the $\nu_s(CH_2)$ mode the volume change during the stretching cycle with $\phi = 0$ and $\phi = \pi$ needs to be assessed. For $\nu_s(CH_2)$ with $\phi = 0$, all the CH_2 groups are stretching symmetrically in phase, which induces a large volume change between the maximum and minimum

stretches of the CH bonds during each stretching cycle. On the other hand for $v_s(CH_2)$ with $\phi = \pi$, any of the CH_2 groups increases its volume by the maximum stretching of the CH bonds within each half of the stretching cycle, while the neighbouring CH_2 group decreases its volume at the same time by the maximum contraction of the CH stretch. Thus the net volume change of the EHB chain associated with the $v_s(CH_2)$ mode for $\phi = \pi$ is significantly smaller. However for the $v_{as}(CH_2)$ mode the volume change during each CH_2 stretch is about the same for both $\phi = 0$ and $\phi = \pi$. Consequently for the Raman spectra of the $v_s(CH_2)$ it would be expected that a relatively large frequency shift is observed with increased pressure and that the shift would be greater than for the $v_{as}(CH_2)$ stretching band. Whilst the infrared band of the $v_s(CH_2)$ mode should show a relatively small frequency shift with increased pressure, which should not be expected to be greater than the frequency shift for the $v_{as}(CH_2)$ mode. Wong and co-workers have shown that this is true for n-hexadecane. They also explained the difference in shifts between the Raman and infrared bands of the $\delta(CH_2)$ bending mode of n-hexadecane in the same way as for the $v_s(CH_2)$ mode. Consequently the relatively small increase in frequency with increased pressure observed for the infrared bands of the $v_s(CH_2)$ and $\delta(CH_2)$ modes of EHB can be readily explained as due to the effect of the intramolecular vibrational coupling of these modes with the corresponding modes on adjacent methylene groups.

Pressure is known to enhance interchain interactions [188-191]. There will therefore be further complications to frequency shifts caused by increased intermolecular CH

coupling. Such changes effect both the CH_3 and CH_2 stretching and bending modes.

The $\delta_s(CH_3)$ bending mode of EHB exhibits no frequency change between 1bar and 6.5kbar (see Table 4.2). This anomalous behaviour was also observed for the same mode in n-hexadecane. Wong explained this in terms of increased interchain coupling between methyl groups as the pressure is increased. For EHB the increased coupling balances the pressure enhanced repulsive intermolecular interactions up to 6.5kbar, after which the repulsive forces dominate. It is probable that this is also the reason for the lack of frequency shift observed for the $\nu_s(CH_3)$ stretching mode up to 6.5kbar.

Wong showed that n-hexadecane undergoes a liquid-solid phase transition at about 1.5kbar. There are few changes in the infrared spectra of n-hexadecane at 1.5kbar to indicate that such a change occurs. Changes that do occur are a significant fall in the peak height intensity of the $\nu_s(CH_2)$ band at $2853cm^{-1}$, which becomes more dramatic as the pressure is increased on the solid. In the solid the peak height of the $\nu_{as}(CH_2)$ band at $2935cm^{-1}$ increases significantly relative to that of the $\nu_{as}(CH_3)$ stretching band at $2960cm^{-1}$. And the $\delta(CH_3)$ band at $1455cm^{-1}$ has a discontinuity in its frequency/pressure dependence, at the liquid/solid transition pressure. To a lesser extent these effects are also seen for EHB, see Figs.4.9 and 4.14. As well as many other observations of similar changes in spectral detail for EHB compared with n-hexadecane (see previous and later paragraphs). Many of the pressure induced spectral changes for the CH vibrational modes of EHB

and n-hexadecane also occur for other molecules that contain alkyl chains[191]. Molecules for which it is known that the pressure increases the interchain interactions. It is possible therefore that EHB undergoes a pressure induced phase change similar to n-hexadecane, or at least to some extent the alkyl chain of EHB is experiencing very similar changes in intrachain and interchain interactions as in n-hexadecane as the pressure is increased.

If, for EHB, a phase change does occur, or there are significant conformational changes, with increased pressure, it is known from previous studies[191-2] on molecules with long alkyl chains (for example polymethylene[191], n-hexadecane, DPPC and DMPC[192]) that the chains prefer to pack in the all trans stucture. Lateral compression of the chains causes a full extension of the alkyl chains, moving towards the all trans structure. It has been shown[193,194] that on going from alkyl chains containing predominantly trans bonds, to chains with gauche structures, or vice versa, that the intramolecular coupling of C-H stretching modes changes. The CH units in the different structures will thus exhibit differing stretching frequencies. Snyder[193] showed that, due to changes in the intrachain CH coupling, the transition from the all trans structure to the disordered chain increases the frequency of the infrared $v_{s}(CH_2)$ mode by about $1cm^{-1}$ and decreases the frequency of the $v_{as}(CH_2)$ mode by approximately $3cm^{-1}$. If EHB does increase its concentration of trans bonds with increased pressure, as is suggested with the close agreement of the spectral details of EHB with n-hexadecane (which is known to have the all trans structure at pressures greater than

1.5kbar)[188], then in addition to the frequency increase induced by changes in the intramolecular and intermolecular potential, there will be further modifications to the frequency due to changes in conformation. According to Snyder these additional changes will result in a further increase in the frequency of the $\nu_{as}(CH_2)$ stretching frequency, whilst slightly decreasing the frequency of the $\nu_s(CH_2)$ stretching mode. Therefore this is an additional reason, besides the volume effect already discussed, that might explain the greater pressure/frequency shift observed for the $\nu_{as}(CH_2)$ mode compared with that of the $\nu_{as}(CH_2)$ mode of EHB.

Apart from the complications involved with interpreting the frequency shifts of the CH stretching region considered so far, there are also significant contributions from Fermi resonance (FR) effects. These arise largely from the FR interaction between the symmetric C-H stretching fundamentals and a dispersion of overtones of the δ_s CH bending fundamentals. Increasing the pressure changes the contributions from FR to the CH stretching region, due to changes in the frequency range of the CH bending overtones $(2\delta_s)^{188}$. Such changes will effect the intensities and band widths of the symmetric CH stretching bands and CH bending overtones, and to a lesser extent the frequencies of these bands. Changes in the dispersion of the CH bending overtones are caused by conformational changes which effect both the intermolecular and intramolecular CH coupling. Observations of these changes in FR with increased pressure are more noticeable with the Raman spectra of the CH stretching region because the overtone bands are more

intense than in the infrared. However the changes in FR are reflected in the infrared spectra of the region. The loss of intensity of the $\nu_s(CH_2)$ stretching band is possibly a direct consequence of changes in FR with increased interchain interaction. This causes a redistribution of intensity between the $\nu_s(CH_2)$ stretching mode and the $2\delta CH_2$ states (at $\simeq 2930 cm^{-1}$ clearly seen in the Raman spectra of EHB, see Fig.II.1a), brought about by increased lateral (interchain) FR.

The observation that the $\nu_{as}(CH_3)$ stretching mode of n-hexadecane exhibits the largest pressure/frequency shift of all the modes, was made by Wong, this is in agreement with obsevations on the same mode of EHB ($1.5cm^{-1}kbar^{-1}$ for n-hexadecane c.f. $0.85cm^{-1}$ for EHB). However the $\nu_{as}(CH_3)$ band of n-hexadecane also splits into two bands associated with the out-of-plane and in-plane antisymmetric CH stretching of the methyl groups, which becomes degenerate with loss of hindered rotation of the methyl groups with respect to the methylene chain[195]. Lack of such an observation for EHB may indicate that the methyl groups do not become as restricted by the neighbouring molecules as they do in n-hexadecane. Thus preventing the degeneracy of the mode, seen with n-hexadecane. Otherwise it may be that because of considerable band overlap and broadening the splitting is not observable for the $\nu_{as}(CH_3)$ band of EHB at this spectral resolution.

The $\nu_{as}(CH_2)$ stretching mode of n-hexadecane exhibits a linear frequency shift of $0.75cm^{-1}kbar^{-1}$ the same as that observed for the $\nu_{as}(CH_2)$ mode of EHB. The greater frequency shift of the $\nu_{as}(CH_3)$ mode compared to the

278

$v_{as}(CH_2)$ mode, is probably a consequence of the
antisymmetric methyl stretching vibration being more
sensitive to changes in the potential and conformation.
because of its position at the end of the chains.

In conclusion, the observed frequency shifts of the CH
modes of EHB can, to a large extent, be explained in terms
of the change in intrachain and interchain coupling of the
CH modes further modifying the frequency shifts arising from
the increase in repulsive interactions. Such coupling
interactions are seen to be most effective for the symmetric
CH modes, which consequently do not show as large frequency
shifts as might have been initially expected. The symmetric
CH stretching modes are further complicated by FR effects.

7.5.2.2 The pressure induced frequency shift of the ring $v(C-C)$ stretching modes of EHB

It is clear from Figs.4.16 and 4.18 that both bands of the doublet of the $v(C-C)$ ring stretching modes at 1603 and 1585cm^{-1} increase in frequency and intensity as the pressure is increased. Both increases in frequency are linear. From observations of blue frequency shifts for these two modes it is clear that the repulsive forces that are dominating the shift with increased density.

This doublet band arises from vibrations in which the main dipole moment change is produced by movements of the substituents on opposite sides of the ring acting in mechanical opposition[113]. Therefore if the substituents are the same for the whole ring, e.g. benzene or para dimethyl benzene, then the vibrations involve no change in dipole moment and the bands do not occur in the infrared. With mono-substituted benzenes there will always be a change of dipole for this mode, so the bands are infrared allowed. It has been determined empirically that in general the more polar the substituent the larger the dipole moment change and as a consequence the bands intensify[113]. Considerable intensification can result from conjugation, as can occur with EHB, because electron delocalisation allows a considerable dipole moment change to occur during the vibration.

As a consequence of this vibration involving motion of opposite substituents against each other then the vibration of this mode will involve a relatively large volume change. Therefore the frequency will be sensitive to an increase in

density and a relatively large frequency shift should occur. as is seen. The increase in intensity seen in Fig.4.16 could in part be a consequence of a conformational change of the alkyl chain (discussed in previous section). If the molecule becomes more elongated at higher density the dipole moment change with this vibration would increase, thus increasing the intensity of the bands.

7.5.2.3 The pressure induced frequency shift of the $v(C-O)$ stretching mode

The infrared band of the $v(C-O)$ stretching mode of EHB exhibits one of the largest frequency shifts, $0.6cm^{-1}kbar^{-1}$. of all the bands studied, see Fig.4.7 and Tables 4.1 and 4.2. Such a large frequency increase with pressure may indicate that the C-O vibration is strongly influenced by the change in the repulsive potential. However the close proximity of the carbonyl group may also influence the frequency shift. If the increase in density causes a conformational change, then it may also effect the intramolecular coupling between the C-O and the carbonyl group. A decrease in dipolar coupling would also cause a blue frequency shift. Such a change in coupling would also effect the $v(C=O)$ stretching mode, however as has already been seen, this mode is dominated, at low pressures, by an increase in intermolecular dipole coupling. Indeed it may be this significant increase in coupling between the carbonyl groups that causes a change in the repulsive potential felt by the $v(C-O)$ stretching mode.

7.5.2.4 Pressure induced frequency shift of the vibrational band found at $712cm^{-1}$

As was explained in Chapter 4 the infrared band found at $712cm^{-1}$, shown in Fig.4.17, could be due to one of two modes. It is either the result of the methylene rocking mode, which usually occurs around $720cm^{-1}$, or it is due to the out-of-plane aromatic C-H bending mode. It is likely that it is due to the latter mode, which tends to be strong[113], obscuring the the former mode, although there appears to be no shoulder to suggest the presence of the CH_2 rocking mode.

The band exhibits a linear increase in frequency with pressure of $0.28cm^{-1}$, see Fig.4.19, unlike the CH bending modes which are complicated by the increased interchain interactions. The linearity of the pressure induced shift may therefore be an indication that it is due to the o-o-p aromatic CH bending mode. However this is by no means certain as the v_{as}(C-H) stretching modes also show a linear increase in frequency with pressure.

The frequency shift indicates that the repulsive forces are dominating the change in intermolecular and intramolecular potential.

7.5.3 Vibrational relaxation of EHB as function of pressure

In such a relatively complicated molecule as EHB it can be expected that many different relaxation processes contribute to the observed relaxation times of the vibrational modes. Provided that these are statistically uncorrelated then each of these processes contribute a band width increment to the overall band width. The vibrational relaxation time τ_v can be represented by

$$\tau_v^{-1} = \tau_1^{-1} + \tau_2^{-1} + \tau_3^{-1} + \ldots\ldots \qquad \text{Eqn.7.17}$$

where τ_1, τ_2 and τ_3 represent the contributions from the separate relaxation processes.

It is usual[53,196-198] to assume that vibrational dissipative energy transfer contributes a negligible amount to the overall vibrational relaxation. Both experiment and theory have shown that $\tau' \gg \tau_{ph}$ sometimes by many orders of magnitude. It is reasonable to discount vibrational population relaxation since the vibrational energy in the process is transferred to the rotational and translational energy of the molecules, this is an inefficient mechanism, since the Fourier frequency components of the effective motions match poorly with the vibrational frequencies involved in infrared and Raman spectroscopy ($\hbar\omega \gg k_b T$). Only molecular collisions of particularly high energy are able to cause vibrational de-excitation. The probability of such high energy events is low[199]. It can be concluded that even in a regime of short-range rapidly fluctuating intermolecular forces vibrational energy dissipation should

contribute considerably less to vibrational relaxation than vibrational dephasing.

The study of the Raman bands of the ring v(C-C) deformation mode showed that reorientational motion of EHB, at ambient temperature, does not contribute significantly to the vibrational band widths of EHB. Only $0.1cm^{-1}$ for the relatively fast motions of the benzene ring end of the molecule. Assuming that the reorientational motions will become even more restricted at higher densities ($\tau_{rot} \propto \eta$)[39,53,203], then any contribution to the band widths from reorientational motion can be ignored without bringing any errors into the interpretation.

In discussing the results of the high pressure band width studies on EHB it is assumed that the bands are broadened by vibrational dephasing alone. This vibrational dephasing includes contributions from both inhomogeneous and homogeneous broadening processes. The vibrational dephasing of the carbonyl v(C=O) mode of EHB also includes a contribution due to inhomogeneous broadening caused by resonance vibrational energy transfer. However dephasing caused by resonance vibrational energy transfer can be described formally by the same theory as inhomogeneous broadening[167,200]. Both give rise to broadening due to a certain distribution of frequencies around a mean value, which is a consequence of the interaction of the individual molecules with the surrounding "bath". The more common type of inhomogeneous vibrational dephasing is dependent on the self terms in Eqn.7.9, whilst inhomogeneous broadening caused by resonance vibrational energy transfer is dependent

on the exchange terms.

The homogeneous broadening contribution to the dephasing is caused by the short range rapidly varying dynamical processes. It is a consequence of loss of phase due to "collisions". It is important to understand that this process is completely different to vibrational energy transfer. The difference arises in that a phase change accompanies every molecular collision, whereas vibrational energy transfer occurs only for relatively very few molecular collisions.

Both homogeneous and inhomogeneous dephasing mechanisms can be considered in terms of the Kubo stochastic line shape theory, Eqn.2.33. Unless the case of rapid or slow (see Chapter 2) modulation occurs then the line shape will be neither Lorentzian nor Gaussian but an intermediate or so-called Voigt line shape.

Before continuing it is necessary to clear up any confusion that may arise from nomenclature when referring to vibrational dephasing. Vibrational dephasing arising from a distribution of frequencies that are modulated by translational or reorientational motion are referred to as inhomogeneous broadening. Whilst if the modulation process is very rapid i.e. due to collisions, the dephasing process is considered to be homogeneous. Since, for very fast modulation the effects of the (inhomogeneous) environment are diminished and the process is mainly dependent on the modulation rate. Homogeneous broadening is therefore in the rapid modulation limit. Whilst inhomogeneous broadening can, depending on the conditions, be in the fast or rapid modulation limit, or be intermediate between the two.

7.5.3.1 The vibrational dephasing of the $v(C=O)$ stretching mode

It can be seen from Fig.4.5 that the infrared band of the $v(C=O)$ stretching mode of EHB exhibits a non-linear increase in band width with increased pressure. This increased band width indicates an increase in vibrational relaxation rate (FWHM $\propto \tau_v^{-1}$). It was seen in Sections 7.2 and 7.3 that this mode is effected strongly by an increase in attractive interaction with increased pressure, most probably due to a significant increase in alignment of the dipoles. There is a significant contribution to the relaxation rate of this mode by resonance vibrational energy transfer. This assumption was made from the observations that the width of the Raman I_{iso} band of this mode is broader than the I_{aniso} band, and that the difference is removed on removal of RET (see Section 7.2). The relatively large decrease of band width upon dilution also supports that resonance vibrational energy transfer contributes significantly to the band width of this mode.

If the inhomogeneous broadening, due to the attractive force frequency fluctuations, of this mode is considered to be in the fast modulation regime. Then, in accordance with the Kubo model FWHM $\propto \tau_v^{-1} = M2_v \tau_m$, and the product $M2_v \tau_m$ must be increasing with pressure. In contrast, if the dephasing is assumed to be in the slow modulation limit, then FWHM $\propto \tau_v^{-1} = 2(2\ln 2)^{1/2} \cdot (M2_v)^{1/2}$, and $M2_v$ must be increasing.

In order to interpret the changes in band width seen with increasing pressure, it is necessary to consider the

effect of pressure on the vibrational first (frequency shift) and second moment ($M2_v$). It has been shown[166,201-2] that in the Kubo model for vibrational dephasing the first moment, arising from dipole-dipole interactions (which appear to dominate the interactions of the carbonyl, see Section 7.2) may be written as

$$\langle \Delta\omega \rangle_{dd} = (NM_{tt}/R_0^3) \cdot \langle K_{ij} \rangle \qquad \text{Eqn.7.18}$$

where N is the mean number of nearest neighbours (within the first solvation shell), M_{tt} is related to the transition dipole, $(\delta\mu/\delta Q)$, and K_{ij} is an orientation function, given in the binary point dipole approximation[201-2] by

$$K_{ij} = -2\text{Cos}\theta_i\text{Cos}\theta_j + \text{Sin}\theta_i\text{Sin}\theta_j\text{Cos}\phi_{ij} \qquad \text{Eqn.7.19}$$

(θ_i and θ_j are the angles made by the two dipoles i and j with an axis through their centres and ϕ_{ij} is the dihedral angle between them, see Fig.7.17). R_0 is the distance to the first peak in the radial distribution function. Clearly, the first moment or frequency shift is related to the orientational ordering in the first solvation shell. In particular K_{ij} becomes more negative, for example, as θ_i and θ_j approach zero and the two dipoles become aligned with each other $\longrightarrow \longrightarrow$. The contribution to the first moment from dipole-dipole interactions vanishes in the absence of orientational order. It is therefore expected that there should be a negative frequency shift induced by increased alignment. On the other hand, the second moment given by

$$\langle \Delta \omega^2 \rangle_{dd} = (NM_{tt}^2 / R_o^6) \cdot \langle K_{ij}^2 \rangle \qquad \text{Eqn.7.20}$$

is related to the <u>distribution</u> of dipoles (oscillators) in
the first solvation shell. It is largely determined by the
width of the first peak in the radial distribution function.
It is therefore expected to decrease as the local order
increases and vice versa. In Section 7.5.1, the decrease in
frequency of the $v(C=O)$ mode with increased pressure to
6.5kbar was taken to indicate an increase in attractive
interactions due to improved orientational order of the
carbonyl dipoles, in agreement with Eqn.7.18. However the
half bandwidth, and therefore the dephasing rate, increases
as the pressure increases, see Fig.4.5, this is in contrast
with observations made on the $v(C=O)$ mode of acetone[184] and
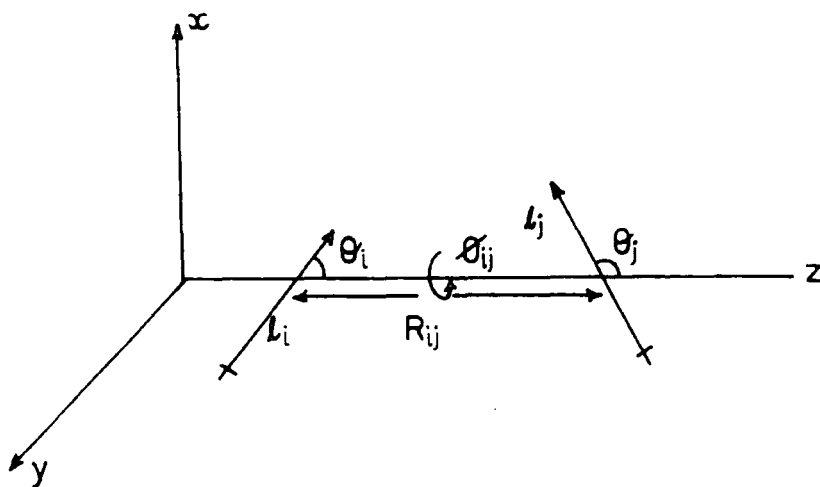
**Figure 7.17 Geometrical configuration of the pair of
transition dipoles μ_i and μ_j which defines the parameter K_{ij}**

the $v(C=CH_2)$ mode of isobutylene[185] which similar to the $(v(C=O))$ mode of EHB show a decrease in frequency with increased pressure, but unlike EHB exhibit a decrease in band width. Schindler and Jonas[184] measured the vibrational second moment of the $v(C=O)$ stretching mode of acetone and found that it decreased with increased pressure, as might be expected (see above) if the distribution of dipoles is decreasing, as suggested from the frequency shift.

If we are in the fast modulation limit then, because $M2_v \tau_m$ ($\propto$ FWHM) increases with pressure for EHB, τ_m must be increasing at a faster rate than the rate of decrease of $M2_v$. There are good reasons to expect that τ_m would increase significantly with pressure for this molecule. For long-ranged attractive potentials, τ_m may be identified with a rotational or translational "correlation time" and as such would follow[39,203]

$$\tau_m \; (\equiv \tau_{rot} \; \text{or} \; \tau_{trans}) \; \propto \; \eta/T \qquad \text{Eqn.7.21}$$

Since provided that the system is in the rapid modulation limit[39,161,203] $M2_v \propto \rho$

$$\tau_v^{-1} \; \propto \; \rho\eta/T \qquad \text{Eqn.7.22}$$

For short range potentials τ_m may be identified with a "time between collisions" and homogeneous broadening, Fischer and Laubereau[165] show that

$$(\tau_{ph})^{-1} = \frac{9}{2} \cdot \frac{\mu\gamma^2}{M^2} \frac{kT}{\omega^2 L^2} \frac{1}{\tau_c} \qquad \text{Eqn.7.23}$$

where M is the reduced mass of the oscillator with frequency ω, L measures the range of the interaction[204], γ is a mass factor, and μ is the reduced mass of the system involved in the collision (e.g. A-B$\cdots$C). The parameter τ_c may be identified with a "time between collisions"[37-39]. Many workers have argued using an isolated binary collision (IBC) model that τ_c should be approximated to an Enskog time (τ_E) for the rate of binary collision of hard spheres[205,206],

$$\tau_E = \{ \frac{8}{3} (k_b T/\pi m)^{1/2} \pi\rho\sigma^2 g(\sigma) \}^{-1} \qquad \text{Eqn.7.24}$$

$g(\sigma)$ is the radial distribution function equal to

$$g(\sigma) = (Z-1)/4\eta_p \qquad \text{Eqn.7.25}$$

and

$$Z = 1 + \eta_p + \eta_p^2 + \eta_p^3/(1-\eta_p)^3 \qquad \text{Eqn.7.26}$$

η_p is the solvent packing fraction and is equal to $\pi\rho\sigma^3/6$. The collision frequency can also be approximated using a "cell" model[204,206-7]

$$\tau_c = \rho d^2/6\eta \qquad \text{Eqn.7.27}$$

where d is the distance between the molecules and can be estimated from the molecular volume. A further method used

to obtain τ_c is to use the Gordon J diffusion (collision-interrupted free rotation) model[37]. In all three methods used to approximate τ_c the collision rate increases with increased density, resulting in an increase in the dephasing rate as estimated using an IBC model. Approximately, the time between collisions is proportional to the inverse of viscosity[206,208], so the increase in vibrational dephasing with density is proportional to the increase in viscosity. It can be seen therefore that τ_v^{-1} values, in the rapid modulation limit, should show the same viscosity dependence, regardless of whether the model employed is one for inhomogeneous or homogeneous dephasing. It can be seen from Fig.7.18 and Table 7.1. that the viscosity goes up very rapidly with pressure, compared to the simpler molecules considered in Fig.7.19, so τ_m should increase rapidly with pressure for EHB.
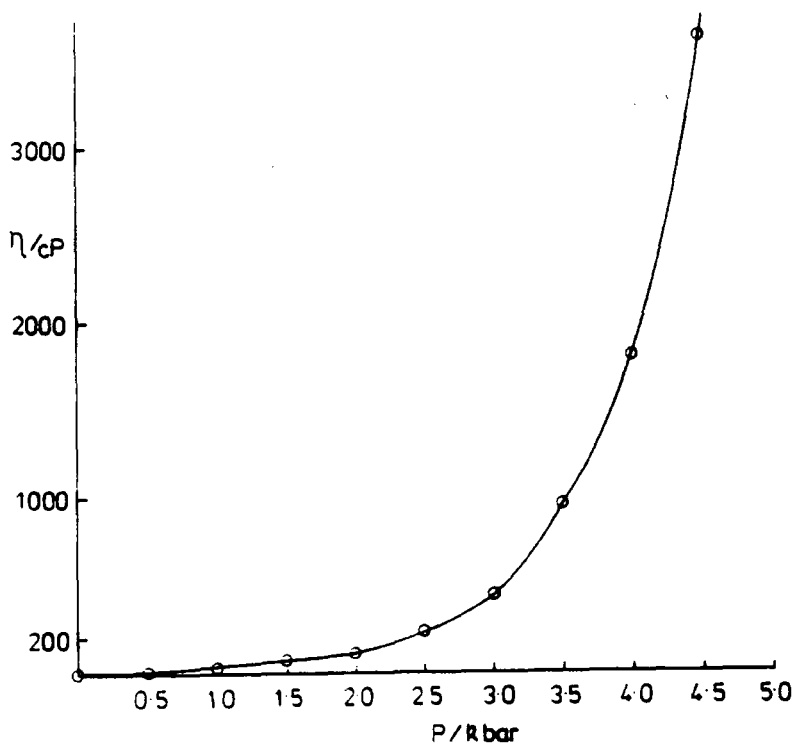
Figure 7.18. Variation of viscosity, η (cP), with pressure, P (kbar), for EHB up to 5.0 kbar.

Furthermore Table 7.1 also shows that the translational diffusion coefficient drops dramatically with pressure, as expected. These factors would probably lead to an increasing band width (FWHM $\propto \tau_v^{-1} = M2_v \tau_m$), even if as predicted[161,202] the vibrational second moment, Eqn.7.17, were to decrease as the local order increases. By applying the Kubo formalism Schindler and Jonas showed[184], that for the same mode in acetone, τ_m does increase with pressure. However their observed increase in τ_m is not enough to offset the decrease in $M2_v$, so overall they see a decrease in band width for this mode of acetone. However it is unlikely that acetone would, being a much simpler molecule compared to EHB, show an increase in τ_m as dramatic as is expected in EHB.
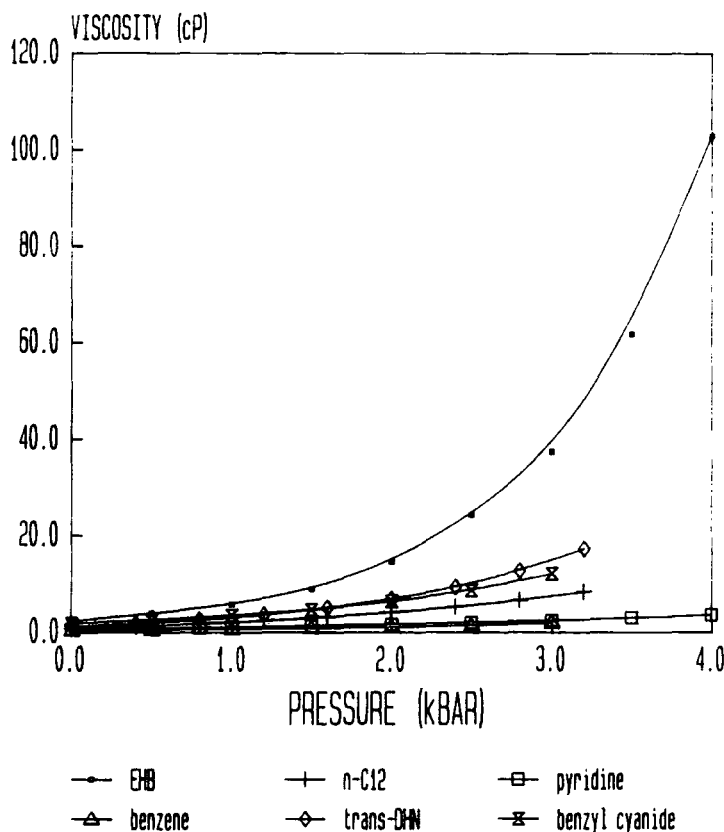
Figure 7.19. A comparison of the pressure-viscosity variation of EHB with some less complicated molecules.

However, it is clear from the figures shown in Table.7.1, and from the previous rotational correlation times (Section 7.1, measured at 1bar over a wide range of temperature) that modulation of the <u>attractive forces</u> in EHB at room temperature are very slow indeed (compared with an observed τ_v^{-1} of about 0.6psec, i.e. for a full band width of $\simeq 16\text{-}20\text{cm}^{-1}$). It is therefore highly likely that this band is formed in the slow modulation limit if dipolar interactions dominate the potential. It is a strong possibility that dipole interactions are important for this molecule because of the observation of the Raman noncoincidence effect caused by RET (discussed in Section 7.2), which is usually only observed in the presence of significant ordering in the liquid phase.

Assumption of being in the slow modulation regime is an approach utilised by Chandler et al[161] to interpret the acetone data of Scindler and Jonas[184]. It was argued that for polyatomic molecules the dephasing time is short compared to the attractive force relaxation time (T_a),

$$T_a = \sigma^2/\pi^2 D \qquad\qquad \text{Eqn.7.28}$$

where σ is the molecular diameter and D is the translational diffusion constant (which decreases with molecular size). Consequently, the attractive forces will generally relax more slowly as the polyatomic molecule becomes increasingly complex. In this same limit the dephasing time often decreases because the perturbation effectively lasts for a long time and the phase of the oscillators is rapidly lost. The contribution from inhomogeneous broadening, arising from

the attractive force fluctuations, should therefore increase
with the complexity of the molecule, compared to that of
simpler molecules. Chandler thus argued that, for
polyatomic molecules, inhomogeneous broadening arising from
the slowly varying attractive forces should be considered to
be in the slow modulation regime.

Chandler then showed that the attractive force,
inhomogeneous broadening, contributions dominate the
dephasing of the $v(C=0)$ mode of acetone. Their calculated
line width contributions from attractive forces (LW_A)
decrease with increased density. Thus the overall band
width of the $v(C=0)$ mode of acetone was predicted to
decrease as the density increases, agreeing with the
experimental observations. The experimental and theoretical
values for the band width were in good agreement. During
his discussions Chandler showed that

$$LW_A \propto (\rho \cdot \chi)^{1/2}$$
<div align="right">Eqn.7.29</div>

where ρ is the density and χ is the isothermal
compressibilty (related to the distribution of the local
environments due to solvent number density fluctuation)[208].
From Eqn.7.29 LW_A would normally be expected to decrease
with increasing pressure since χ decreases rapidly with
pressure. However, changes in density must also be
considered.

Table.7.7 compares the attractive force correlation
times and vibrational dephasing times for the $v(C=0)$ mode of
EHB, as a function of pressure. It should be noted that
values for the self diffusion coefficients at pressures

PRESSURE (kBAR)	D $(\times 10^9)$ cm^2s^{-1}	T_a = $\sigma/\pi^2 D$ (ps)
10^{-3}	1540	370
0.7	552	1030
2.5	35.5	16,000
3.6	6.98	82,000
6.5	0.0082	6.5×10^6
22.7	2.2×10^{-12}	2.6×10^{17}
30.3	2.3×10^{-17}	2.4×10^{22}

Table 7.7. The attractive force correlation time (T_a) for EHB

greater than 4.5kbar were obtained by extrapolation using the Barus[25] equation. The comparison in Table 7.7 further suggests that for EHB the vibrational dephasing due to the attractive force frequency distribution should be considered to be in the very slow modulation regime. It is therefore appropriate to explore the band profile in more detail to check for evidence of a particular modulation regime. If the slow modulation regime is appropriate then the obvious comparison is with a Gaussian profile (as FWHM $\propto \tau_v^{-1}$ = $2(2\ln 2)^{1/2}.(M2_v)^{1/2}$). However this is difficult because of base line fluctuations caused by interference within the DAC. However attempts have been made in Section 8.1, to determine whether the slow or fast modulation regime is appropriate to this particular mode of EHB. Section 8.1

suggests that the slow modulation limit is more likely to be valid for this band of EHB, as might be expected. It therefore obvious that a band width increase with pressure reflects an _increasing_ second moment.

There now exists the problem of interpreting a set of first moment data which indicates clearly an increase in the ordering of EHB molecules (in the first solvation shell) and a set of second moment data which show that the width of the distribution of molecular oscillators (in the first solvation shell) is _increasing_ with pressure. It is a possibility that there is short range "disorder" and some longer range "ordering" of the the molecular dipoles. However the short range forces ought to be rapidly modulated, giving rise to a significant spectral "wing" associated with the short time contribution to the band profile. This is not evident in EHB although of course with such a complex molecule as EHB examination of the high frequency wings is precluded by band overlap. Because of the sizeable hydrocarbon tail of EHB it may be that "ordering" in one part of the molecule system is associated with "disordering" of the molecules as a whole, although the results discussed in Section 7.5.2.1 appear to suggest that the hydrocarbon chain interactions become more ordered as the pressure is increased. It should be noted that because EHB is a flexible molecule, changes in the intermolecular potential (with pressure), due to intramolecular conformational changes, may occur. With respect to interactions in the ester group of the molecule the situation is rather complex, it may be possible that changes in the intramolecular interactions here (due to

conformational changes) are responsible for the increase in band width with pressure. Another possibility is that the $\upsilon(C=0)$ normal coordinate is distributed among vibrational displacements other than the ester grouping (as is the case for even simple molecules such as dimethylformamide[209].

This may lead to $\upsilon(C=0)$ band profile which reflects interactions in other parts of the molecule well away from the carbonyl group.

7.5.3.2 The increase in vibrational dephasing rate of the $v(C\text{-}O)$ stretching and vibrational mode at 712cm^{-1}, for EHB at increased pressure

The infrared spectra of both the $v(C\text{-}O)$ stretching mode (at 1274cm^{-1}) and the band at 712cm^{-1} show a non-linear increase in band width with pressure, see Figs.4.8 and 4.20. The increase in FWHM up to 30.3kbar are 11.1 and 8.9cm^{-1} respectively.

The broadening of these bands reflects an increase in vibrational dephasing rates. The linear frequency shifts, with pressure, of these bands are to higher frequency, suggesting that they are dominated by the repulsive part of the potential. This is likely to mean that the vibrational second moment of these two modes increases with density. Therefore it is not unexpected that the vibrational dephasing rate of both these modes increases with pressure. As, was shown in the previous section, in the rapid modulation limit, both vibrational dephasing rates from inhomogeneous and homogeneous broadening are proportional to viscosity. If however the dephasing is occuring in the slow modulation regime, the band width will still increase with pressure proportional to the increase in $M2_V$.

The difference between the increase in band width for the two modes is small, it is however a reflection of the difference between the interactions of the two modes with the intermolecular and intramolecular potential. Further analysis of the two modes in terms of vibrational dephasing is made in Chapter 8.

7.5.4 The intensity and band width of the CH stretching envelope as function of pressure

Due to the complicated nature of the CH stretching region, discussed in Section 7.5.2.1, there will be no extensive attempt to quantitatively explain the observed changes in band width and intensities of these bands. Such observations depend on a complicated mixture of phenomena. These include variations in intramolecular and intermolecular CH coupling due to changes in conformation and packing of the alkyl chains, changes in Fermi resonance contributions and changes in the intermolecular and intramolecular potential. However, as can be seen from Fig.4.15, the envelope does appear to show an increase in width with increased pressure. There appears to be little change in width up to 3.6kbar, then a sharp increase up to 6.5kbar, which is followed by linear increase in band width between 6.5 and 30.3kbar.

In Section 7.5.2.1 it was suggested, from comparison with other alkyl chain molecules, that at higher pressure the alkyl chain interactions of EHB become more ordered, such a change might be expected to result in a decrease in the vibrational second moment. An increase in band width could reflect an increase in the modulation time τ_c , which as explained previously is expected to increase with increased viscosity. If, however the relaxation is in the slow modulation regime, as has been suggested for the $v(C=O)$ mode, the band width is independent of the modulation time and should decrease with a decreasing second moment. Interpretation of the pressure induced band broadening for

the v(C-H) envelope is, therefore, complex. The broadening may be an indication that chain ordering does not occur and the second moment increases. However those workers[82-85,186,188-91] who observed chain ordering with increased pressure have also seen band broadening of the v(C-H) envelope. It has already been suggested that the increased frequency of the v(C-H) stretching modes is, at least partly, dependent on the change in C-H vibrational coupling. The increase in frequency is also a reflection that the repulsive intermolecular potential is dominating the shift. The initial lack of band width change with pressure may be a consequence of the ordering of the alkyl chains. Further increases in pressure force the chains closer together and may cause local disorder of the C-H interactions, producing the increase in band width. To explain the band width behaviour of the v(C-H) envelope it is tempting to invoke the idea of short ranged "disorder" localized at the C-H interactions along the alkyl chains, whilst the chains themselves "pack" in a more ordered form. Such suggestions are extremely speculative, but they will hopefully stimulate additional theoretical and experimental work.

7.5.5 Possibility of a phase change for EHB at increased pressure

It was suggested in Section 7.5.2.1, because of similarities between the spectroscopic pressure behaviour of EHB and n-hexadecane, that EHB may exhibit a phase transition as the pressure is increased. A pressure-induced liquid/solid transition may be being demonstrated by the discontinuities in the pressure dependency of the infrared spectral parameters as demonstrated in Figs.4.4, 4.5, 4.8 and 4.13-4.15. It would appear that if a transition is occurring it is somewhere between 3.6 and 6.5kbar.

If the pressure behaviour of the frequency and band width of the $v(C=0)$ stretching mode are compared with that of the same mode of DOPE in aqueous dispersions[187] the behaviour appears to be the same. Wong proposes that the transition, from decreasing to increasing frequency behaviour and change in slope for the band width/ pressure plot, seen for there molecule (DOPE) at 9.0kbar, occurs after the system has undergone a liquid solid phase change. It is a distinct possibility that the same transitions seen for EHB at about 6.5kbar, are also mediated by a phase change, especially considering the similarities between the pressure induced spectral changes for EHB and n-hexadecane (which also undergoes a phase change) discussed previously.

In order to probe the possibility of a phase change further it is necessary to carry out a detailed study of the pressure behaviour of EHB between 3 and about 10kbar. It is likely that if a liquid/solid transition occurs a hysteresis

301

effect may be observable at the transition, that is as the transition occurs the pressure at the sample will drop due to an associated fall in volume. In addition to this it is necessary to probe the infrared spectra of EHB around 6.5kbar in more detail, at approximately 0.1kbar intervals, in order to more accurately pinpoint the transition pressure.

CHAPTER 8

THEORETICAL ANALYSIS

8.1 Variation of band widths with pressure

8.1.1 The fast modulation approximation

In recent papers by Lynden-Bell[203,206] she considered
the different contributions to vibrational dephasing made by
long range attractive frequency fluctuations and short range
repulsive forces. If the rapid modulation limit
$(<\Delta\omega^2>^{1/2}.\tau_c>>1)$ holds, then $\tau_v^{-1} = <\Delta\omega^2>.\tau_c$ $(\equiv M2_v.\tau_c)$, τ_c
may have different interpretations depending on the nature
of the potentials giving rise to to the frequency
fluctuations.

For long-ranged attractive potentials, τ_c may be
identified with a rotational or translational "correlation"
time[33,203,206]. Since $M2_v \propto \rho$[161], and __providing__ the rapid
modulation limit is assumed, the dephasing rate varies with
density and D, the translational diffusion coefficient,
as[33,203,206]

$$\tau_v^{-1} \propto \rho D^{-1} \qquad\qquad Eqn.8.1$$

In the Stokes model for the diffusion of rigid spheres,
where d is the hard sphere diameter, D is given by

$$D = k_b T/3\pi\eta d \qquad\qquad Eqn.8.2$$

and so $\qquad\qquad\qquad \tau_v^{-1} \propto \rho\eta/T \qquad\qquad Eqn.8.3$

For short ranged potentials τ_c may be identified with a

"time between collisions"[37,44,53]. Assuming an IBC model
and taking the time between collisions to be proportional to
the Enskog collision time gives[206]

$$\tau_v^{-1} \propto D^{-1}(k_bT)^2 \qquad\qquad \text{Eqn.8.4}$$

Therefore we have $\qquad \tau_v^{-1} \propto \eta(k_bT) \qquad\qquad$ Eqn.8.5

If the temperature is kept constant and the density is
varied, then it can be seen that inhomogeneous broadening
will vary with $\rho\eta$ and homogeneous broadening will vary with
η. However if the viscosity varies at a much larger rate
than the density, as it does for EHB (see Table.7.1), then
inhomogeneous broadening can also be seen to vary with η
alone.

As a test for the rapid modulation limit, viscosity has
been plotted against the FWHM for the infrared bands of the
$v(C=0)$ and $v(C-0)$ stretching modes of EHB at various
pressures. It is assumed that FWHM $\propto \tau_v^{-1}$. The values for
the viscosity at the various pressures were obtained from a
plot of $\log_{10}(\eta)$ vs pressure, for the measured viscosity
pressure data[77] of EHB. This plot is linear, so the unknown
pressure viscosity data was calculated using the measured
slope and intercept. It is assumed, questionably, that log
(η) continues to vary linearly with pressure to 30.3kbar.

Table 8.1. summarises the relevant data used for the
plots of η vs FWHM. From Table 8.1 it can be seen that the
viscosity increases dramatically with pressure, it is
therefore necessary to plot $\log(\eta)$ against $\log(\text{FWHM})$. These
plots are shown in Figs.8.1. and 8.2.

It can be seen from Figs.8.1. and 8.2 that the plots
are distinctly non-linear, especially considering that these
are log-log plots. It might be that up to 6.5kbar that both
plots are approximately linear. If this were the case then
there is the possibility that the vibrational dephasing
mechanism of these two modes changes somewhere between
6.5kbar and 22.7kbar. Such a change in dephasing mechanism
could be a move from the fast to the slow modulation regime,
mediated by a liquid solid phase change or some
conformational change. However the plots do not show
distinct linearity and are thus inconclusive. There is a
need for more spectral data especially between 6.5 and
22.7kbar.

P (kBAR)	η (cP)	$\log_{10} (\eta)$	ρ (g/cm^3)	$(\rho)^{1/2}$ (g/cm^3)$^{1/2}$
10^{-3}	0.677	-0.17	0.9650	0.982
0.7	1.82	1.23	1.0039	1.002
2.5	23.13	2.33	1.0707	1.035
3.6	10.94	2.99	1.1002	1.049
6.5	(658.60)	(4.76)	(1.1592)	(1.077)
22.7	(5.75×10^{12})	(14.63)	(1.3346)	(1.155)
30.3	(2.65×10^{17})	(19.26)	(1.3862)	(1.177)

Table 8.1. Experimental variables, used in this section, for
EHB at 298K. (Extrapolated data in brackets).
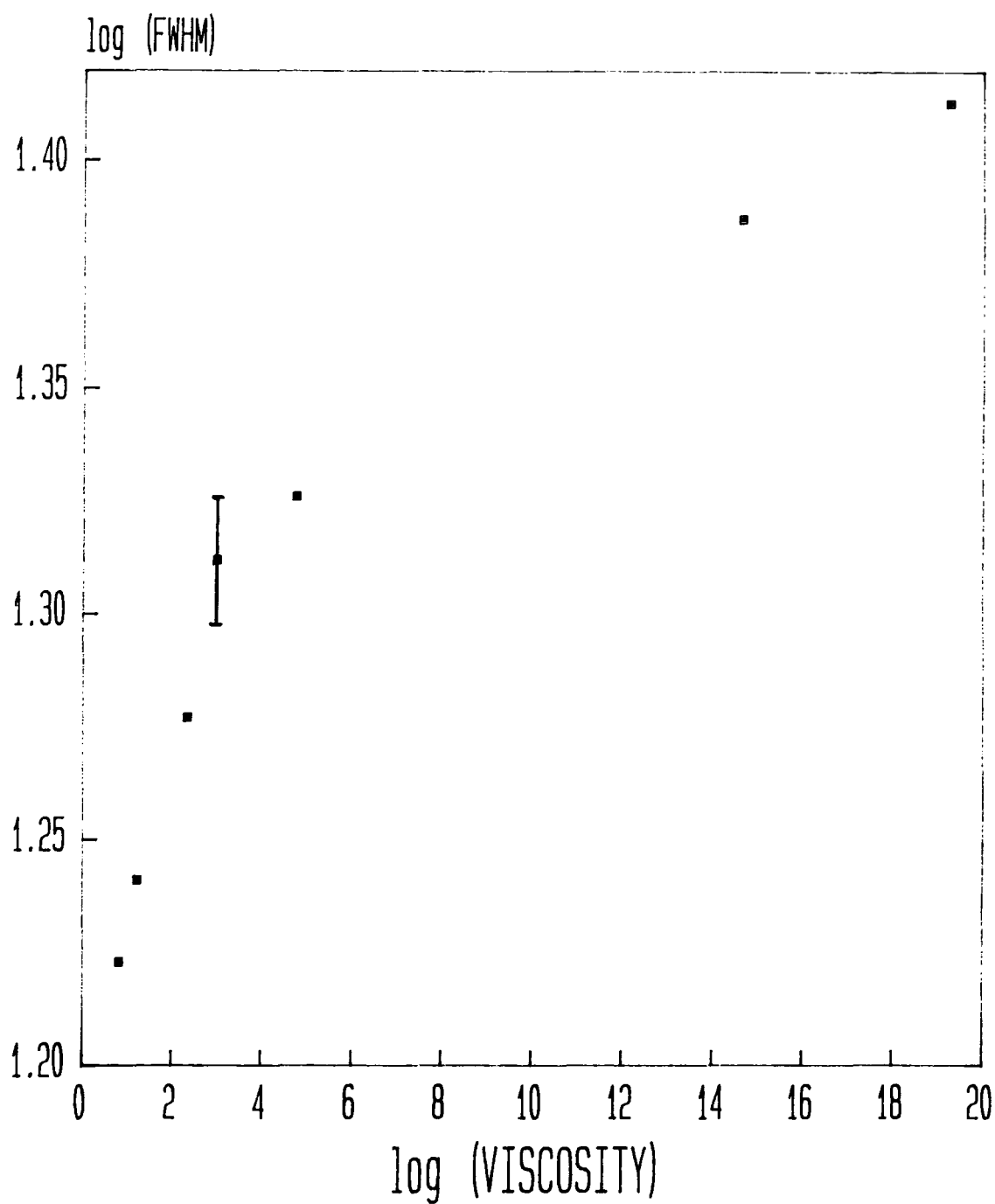
Figure 8.1. Plot of log(FWHM) against log(η) for the v(C=O) stretching mode of EHB as a function of pressure
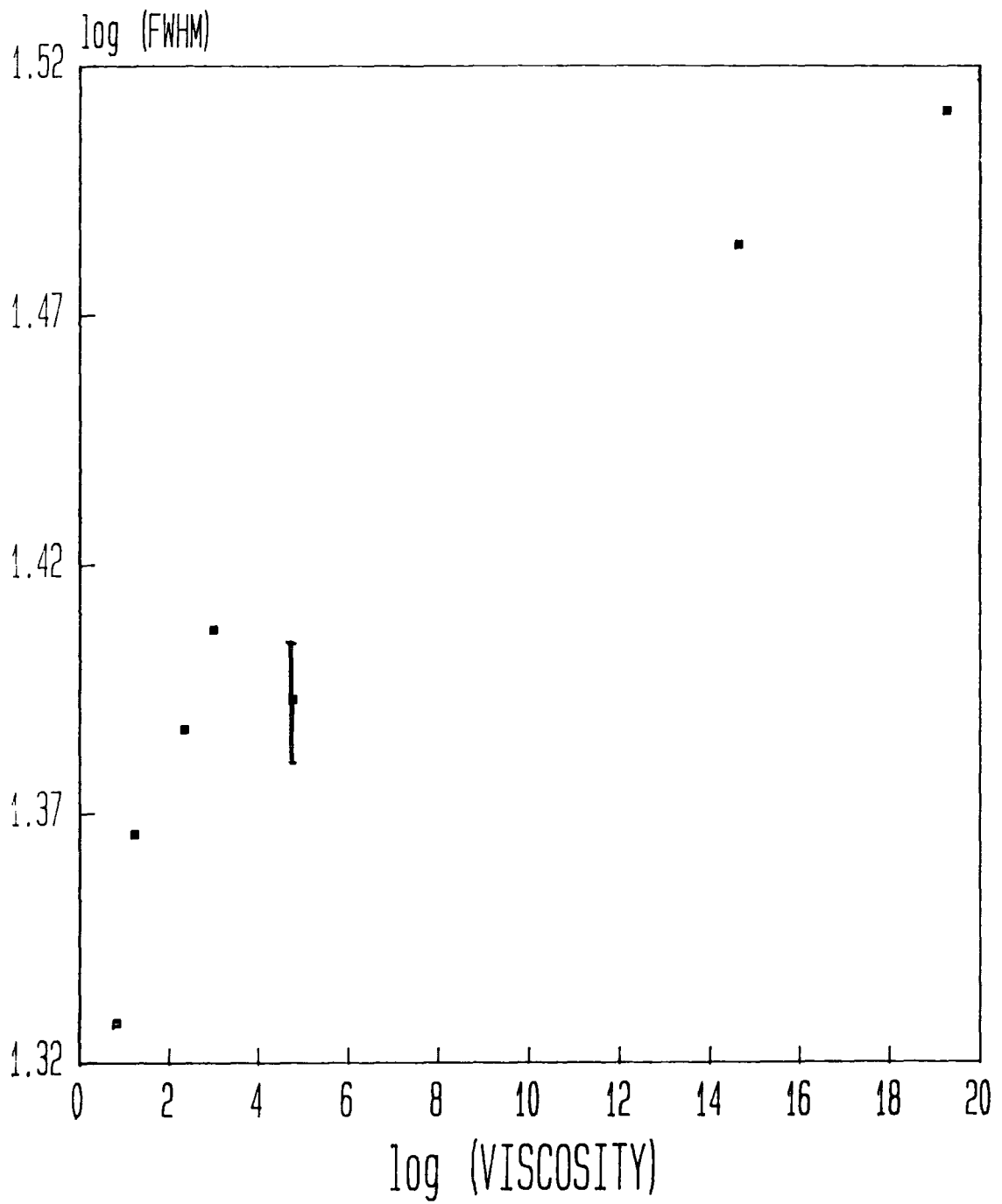
Figure 8.2. Plot of log(FWHM) against log(η) for the v(C-0) stretching mode of EHB as a function of pressure

308

8.1.2 The slow modulation approximation

If a band is formed in the slow modulation limit, that is for slowly varying attractive interactions that lead to inhomogeneous broadening in the slow modulation regime, the dephasing rate is proportional to the vibrational second moment of the mode in question[37,53,196]. It has been shown that[53]

$$FWHM = 2(2\ln2)^{1/2}(M2_v)^{1/2} \qquad \text{Eqn.8.6}$$

Since the vibrational second moment $(M2_v) \propto \rho$ [39,161,203], in such a case the FWHM should vary with the square root of the density. However such an assumption does not fit with a decrease in the vibrational second moment, as may be occurring for the $v(C=O)$ mode of EHB with increased pressure. As was discussed in 7.5.3.1 Chandler assumes $M2_v$ to be proportional to $(\rho\chi)^{1/2}$, where χ is the isothermal compressibility. Without any means of estimating the variation of χ as a function of density, for EHB, there is no way of testing Chandlers approximation for our molecule.

Figs 8.3 and 8.4 show the plots of FWHM vs $\rho^{1/2}$ for the infrared bands of the $v(C=O)$ and $v(C-O)$ stretching modes of EHB. The data at the highest pressures have been obtained by extrapolation using the Tait equation (see Chapter 1). Both plots can be seen to be within good approximation straight lines. It therefore appears that for these modes of EHB the vibrational dephasing is in the slow modulation regime. Such a conclusion is not unexpected considering the
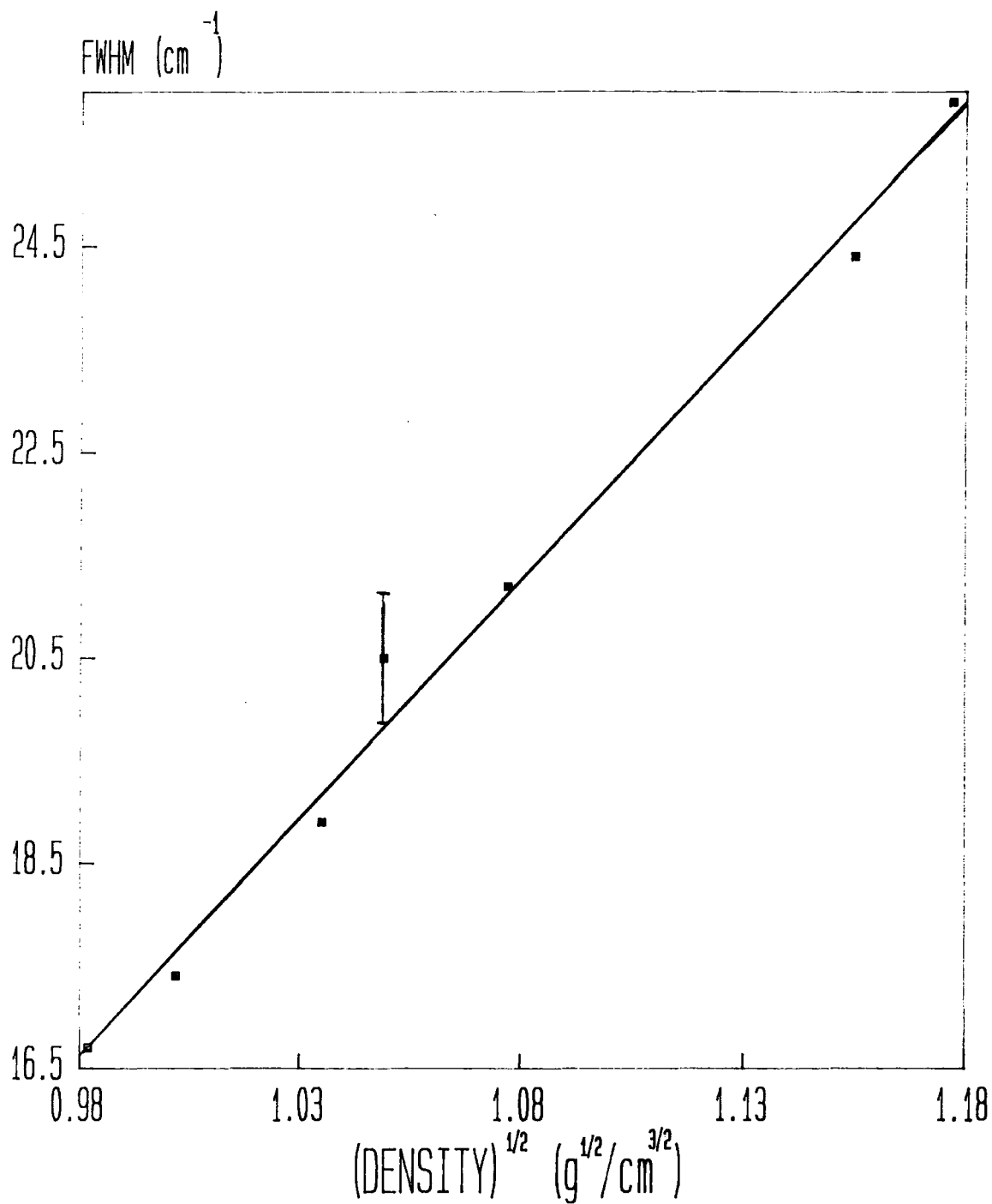
Figure 8.3. Plot of FWHM against $\rho^{1/2}$ for the $v(C=O)$ stretching mode of EHB.
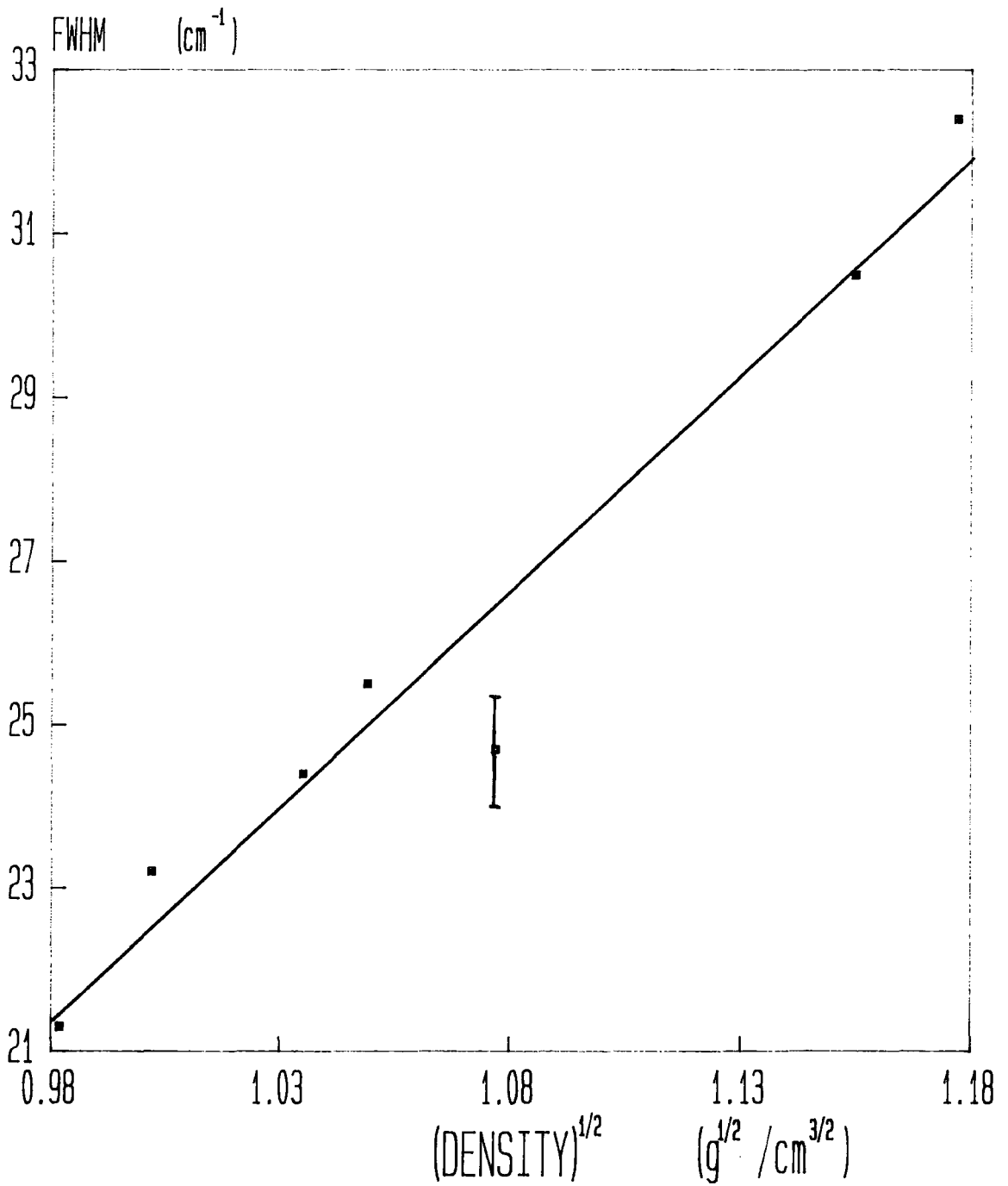
Figure 8.4. Plot of FWHM against $\rho^{1/2}$ for the υ(C-0) stretching mode of EHB.

size of the EHB molecules. This conclusion is also consistent with the previous results (see Section 7.1) that indicate that reorientational motions, even at 1bar, are very slow.

8.2 Theoretical predictions of the Raman noncoincidence effect

It was seen in the preceding chapter that the Raman bands of the carbonyl $v(C=O)$ stretching mode of EHB exhibit the non-coincidence effect, most probably as result of RET due to transition dipole-transition dipole coupling. It is thought that the RET, seen for this mode of EHB, arises from the preferential alignment of a pair of EHB molecules by dipole-dipole interactions.

There have been a number of attempts in recent years to quantitatively predict the Raman noncoincidence effect both as a function of temperature and concentration in binary mixtures[39,149-56,167]. The following section describes attempts to predict the non-coincidence splitting for the $v(C=O)$ stretching mode of EHB as function of concentration in hexane. Two theoretical approaches have been utilised. The first, developed by Fini and Mirone[144-5,150,157], uses simple dielectric continuum theory to scale the alignment effects and thus predict the splitting. This approach does not however consider the role of microscopic liquid structure. The second, more recent model, by Logan[155] attempts to provide an explicit means of estimating the splitting by employing a more detailed molecular model. Logan's approach, unlike Fini and Mirone's, has no recourse to empirical data to arrive at an estimate of the splitting.

313

8.2.1 Fini and Mirone's theory on non-coincidence splitting

Fini and Mirone[150] noted that (1) the splitting, Δv (iso/aniso), becomes zero at a finite concentration which depends on the nature of the solvent, and (2) the shape of the graph of Δv (iso/aniso) depends on the relative values of the dielectric permittivities of the two liquids. The slope increases with increasing concentration when the solvent has a higher dielectric permittivity than the solute, and decreases in the reverse case. Such an observation is made for the $v(C=O)$ stretching mode of EHB, see Fig.8.5, [ϵ(ethyl benzoate) = 6.02, ϵ(hexane) = 1.89]. Fini and Mirone found that in most cases the results are represented quantitatively by the empirical equation

$$v_{soln} = \Delta v_{neat} \{\epsilon_1/(1 - \phi_0)\} \{(\phi - \phi_0)/[\epsilon_1\phi + \epsilon_2(1-\phi)]\}$$

Eqn.8.7

where ϵ_1 and ϵ_2 are the dielectric permittivities of solute and solvent respectively, ϕ is the volume fraction and ϕ_0 is the threshold volume fraction, beyond which no splitting is observed.

The calculated non-coincidence splitting, using Eqn.8.7, compared to the experimentally determined values for Δv (iso/aniso) of the $v(C=O)$ mode of EHB are shown in Fig.8.6, and Table 8.2. The Fini-Mirone function was calculated for EHB with ϕ_0 = 0.1103. It can be seen, from Fig.8.6, that Eqn.8.7 accurately predicts the shape of the $\Delta v_{soln}/\Delta v_{neat}$ vs volume fraction plot. However the predicted values for ($\Delta v_{soln}/\Delta v_{neat}$), and Δv_{soln} see
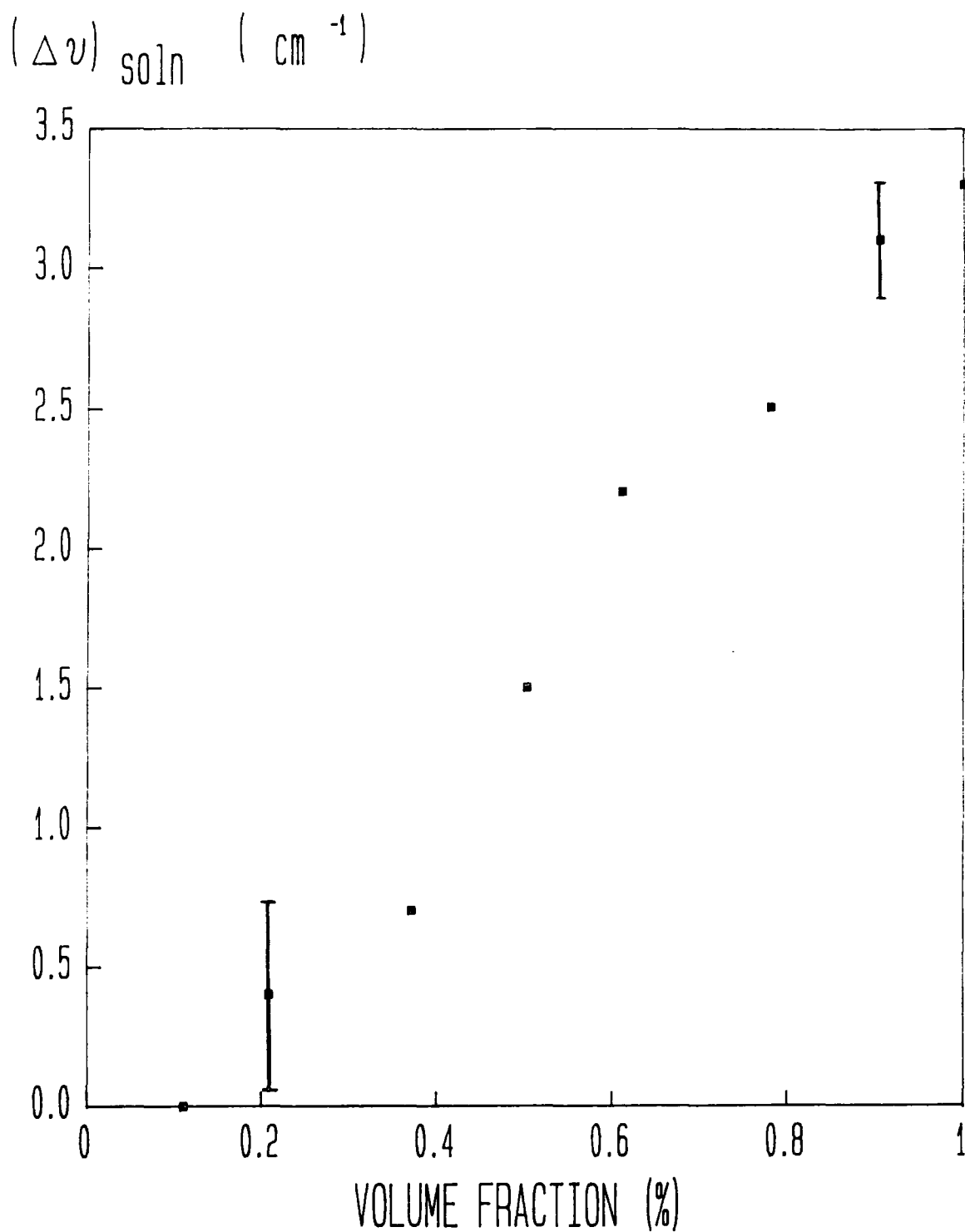
Figure 8.5. The non-coincidence splitting of the $v(C=O)$ stretching mode of EHB as a function of concentration in hexane

volume fraction EHB	$F(\phi)_{exp}$	$F(\phi)_{calc}$ ($\epsilon_0 = 6.02$)		$F(\phi)_{calc}$ ($\epsilon_0 = 4.00$)	
		$\phi_0 = 0.110$	$\phi_0 = 0.208$	$\phi_0 = 0.110$	$\phi_0 = 0.208$
1.000	1.000	1.000	1.000	1.000	1.000
0.904	0.939	0.955	0.941	0.940	0.926
0.780	0.758	0.886	0.851	0.851	0.817
0.611	0.667	0.768	0.694	0.708	0.640
0.503	0.455	0.669	0.565	0.598	0.504
0.371	0.212	0.515	0.361	0.438	0.308
0.208	0.121	0.240	0.000	0.189	0.000
0.110	0.000	0.000	0.000	0.000	0.000
0.000	0.000	0.000	0.000	0.000	0.000

volume fraction EHB	Δv_{soln} (exp)	Δv_{soln}(calc) $\epsilon=6.02$		Δv_{soln}(calc) $\epsilon=4.00$	
		$\phi_0 = 0.110$	$\phi_0 = 0.208$	$\phi_0 = 0.110$	$\phi_0 = 0.208$
1.000	3.3	3.3	3.3	3.3	3.3
0.904	3.1	3.2	3.1	3.1	3.1
0.780	2.5	2.9	2.8	2.8	2.7
0.611	2.2	2.5	2.3	2.3	2.1
0.503	1.5	2.2	1.9	2.0	1.7
0.371	0.7	1.7	1.2	1.4	1.0
0.208	0.4	0.8	0.0	0.6	0.0
0.110	0.0	0.0	0.0	0.0	0.0
0.000	0.0	0.0	0.0	0.0	0.0

Table 8.2. Experimental and calculated (Fini and Mirone's) values for $F(\phi) = \Delta v_{soln}/\Delta v_{neat}$ and Δv_{soln} as a function of volume fraction, for $\phi_0 = 0.110$ and 0.208, and for $\epsilon_1 = 6.02$ and 4.00.
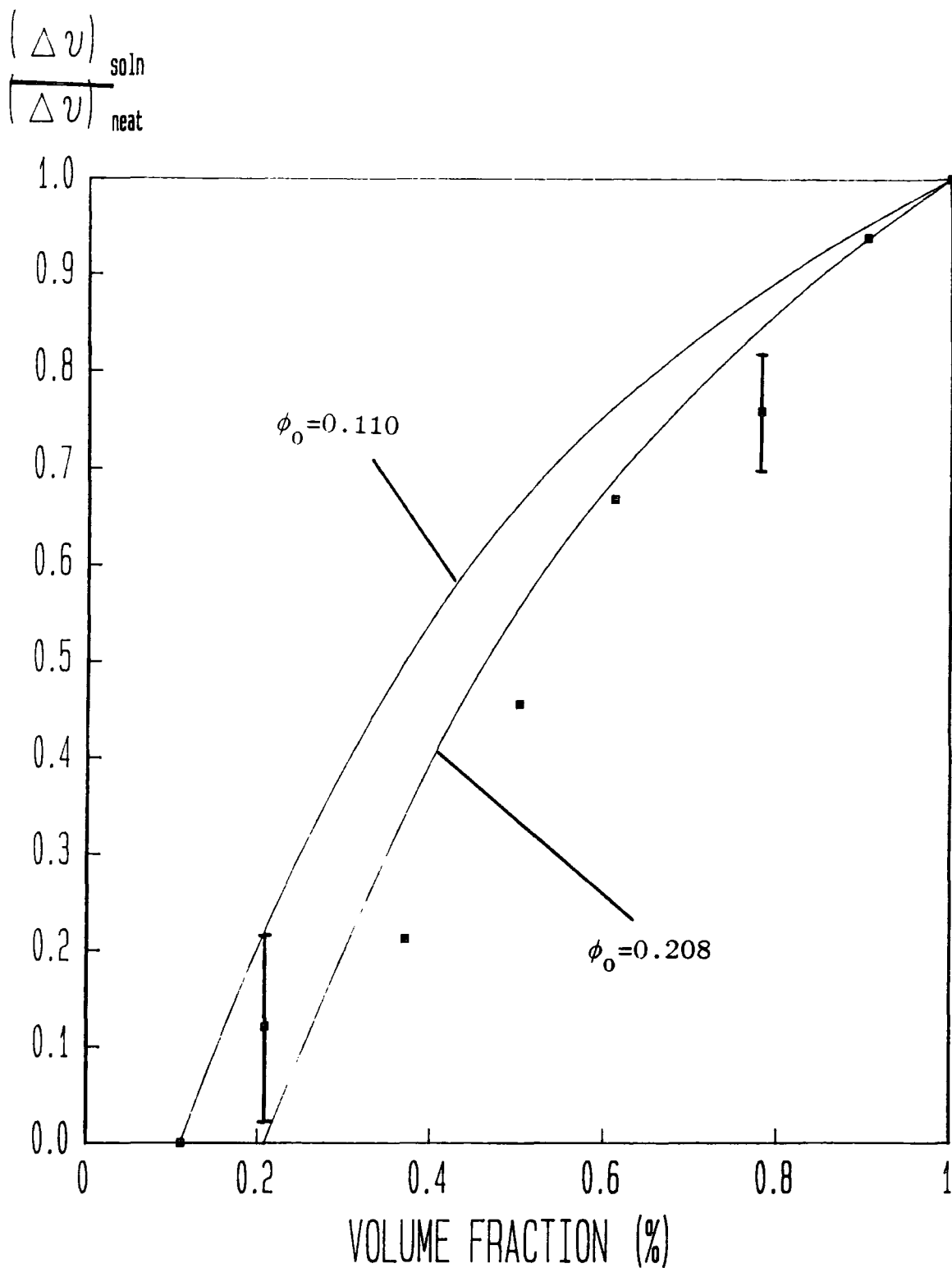
Figure 8.6. The relative noncoincidence splitting for the
v(C=O) stretch of EHB as a function of volume fraction in
hexane. Experimental points (■) compared with splitting
predicted by Fini and Mirone's theory (————), (ϵ_1 = 6.02).

317

Table 8.2, that are too high. As a matter of interest if the value used for ϵ_1 is reduced the theoretical curve, and predictions for Δv_{soln}, move closer to the experimental data. In Fig.8.7 and Table 8.2, it can be seen that if a value of $\epsilon_1 = 4.0$ is used in Eqn.8.7. a much better fit with the experimental data occurs. However, even though the value of ϵ(EHB) can be expected to be lower than ϵ(ethyl benzoate), the values of dielectric permittivity does not vary significantly across a homologous series [ϵ(ethyl benzoate) = 6.02, ϵ(methyl benzoate) = 6.59][162]. If a lower value for ϕ_0 is used the theoretical curve moves even further from the experimental points.

The RET concentration threshold ϕ_0 is not necessarily the same as the concentration threshold discussed in Section 7.3.3, beyond which the EHB molecules are assumed to be completely separated (beyond the range of interaction with other EHB molecules), which occurs at about 2% mole fraction. The RET concentration threshold is a measure of the concentration at which RET ceases to be significant in determining the frequency of the Raman bands of the, in this case, v(C=O) stretching mode. RET depends on the off diagonal (exchange) terms of the intermolecular potential (V_{ij}). These give rise to vibrational excitation of the same mode on identical neighbouring molecules by transfer of a quanta of energy. A reduction in RET occurs by separation (reduction in the solute number density) and loss of alignment of the active molecules between which RET occur. The RET concentration threshold may occur when the contribution to the bands by RET becomes undetectable (i.e. the splitting has become zero within experimental error)
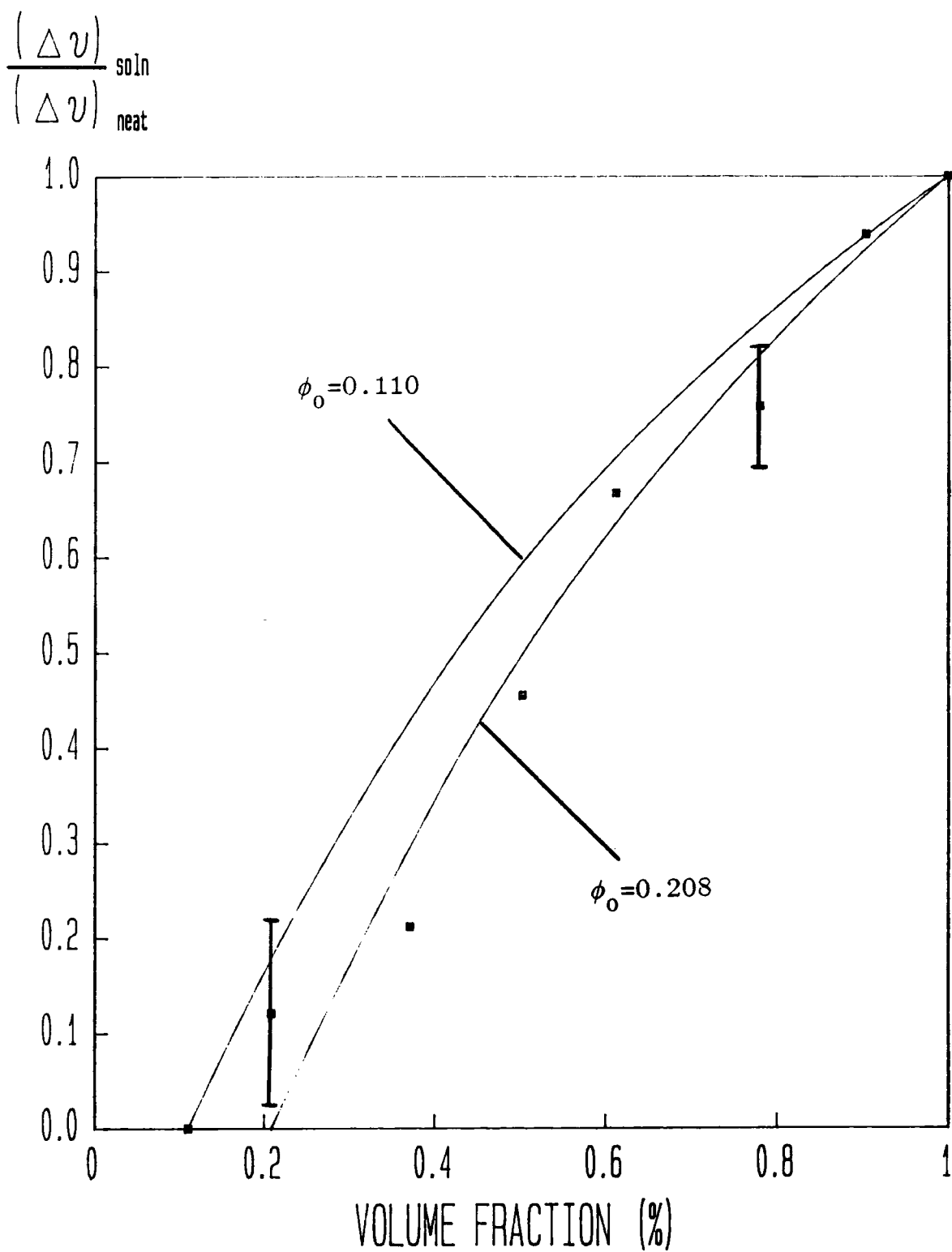
Figure 8.7. The relative noncoincidence splitting for the $v(C=O)$ stretch of EHB as a function of volume fraction in hexane. Experimental points (■) compared with splitting predicted by Fini and Mirone's theory (———), ($\epsilon_1 = 4.00$).

close to zero concentration. In which case ϕ_0 has no real physical meaning. In this case it might be expected that the RET concentration threshold and that discussed in Section 7.3.3 would be very similar. Alternatively because the separation and loss of alignment between the active molecules reduces the efficiency of RET, due to the reduced probability of photon transfer, the correlation time for vibrational relaxation by RET increases. If the correlation time for relaxation by RET becomes long, compared to other vibrational relaxation processes, then it is feasible that relaxation by RET no longer occurs to a significant degree In this circumstance the noncoincidence splitting will disappear at a concentration away from zero, which it appears to do. If this is the case the concentration threshold at which relaxation by RET becomes long will most probably not be the concentration at which the active molecules cease to interact (diagonal terms). It is therefore understandable that ϕ_0 determined by RET is greater than that determined in Section 7.3.3.

The success of the Fini-Mirone empirical equation suggests that, at least to a first approximation the non-coincidence effect is related to the interaction between the permanent dipoles of the dissolved molecules, as was previously suggested. To explain the linear dependence of the splitting on the ratio ϕ/ϵ Fini and Mirone assumed (1) that RET coupling takes place via transition dipoles, implying that every molecule contributes a term to $\Delta v(\text{iso}/\text{aniso})$ proportional to $(\delta\mu/\delta Q)^2/vr^3$, where r is the distance from the reference molecule; and (2) the splitting is directly related to the orientational correlation induced

by static dipolar interactions, which they assume can be represented by $\tanh(\mu^2/\epsilon r^3 kT)$. From these assumptions[150]

$$\Delta v \propto (\delta\mu/\delta Q)^2 \cdot (n/v) \int_d^\infty [\tanh(\mu^2/\epsilon r^3 kT)/r^3] r^2 \delta r \qquad \text{Eqn.8.8}$$

where n is the number of molecules per unit volume and d is the minimum distance of approach between two molecules. Expanding $\tanh(\mu^2/\epsilon r^3 kT)$ to third order followed by integration gives,

$$\Delta v \propto (\delta\mu/\delta Q)^2 \cdot (n/v) \cdot (\mu^2/3\epsilon d^3 kT) \cdot [1 - (\mu^2/3\epsilon d^3 kT)^2] \qquad \text{Eqn.8.9}$$

Fini and Mirone assumed that the second term in square brackets in Eqn.8.9 is small compared to unity. Eqn.8.9. thus explains the proportionality between ϕ/ϵ and the splitting.

Deviations from Eqn.8.7, seen for both EHB and for DMF[148], are likely to be because the theory neglects the role of microscopic liquid structure. Specific interactions are not allowed for, for example short range interactions may contribute to the alignment of the molecules. Contributions from such effects cannot be represented by a bulk property such as dielectric permittivity. There is also the possibility that linearity of the dielectric permittivity of the mixture with volume fraction, which is implied in Eqn.8.7, is not adhered to. However it is unlikely that such deviations would be large enough to explain the overestimation of all the data as occurs for EHB.

8.2.2 Logan's theory of noncoincidence splitting

Logan has developed a theory for the noncoincidence effect applicable to symmetric modes in dipolar isotopic binary mixtures[153-5]. He predicts that there should be a linear relationship between the noncoincidence splitting and mole fraction (X_A) of solute. This linear dependence has been observed experimentally[153-4], through isotopic dilution experiments. The linear dependence on X_A reflects the fact that the permanent dipole-dipole interactions preferentially weight the relative alignment of a pair of active molecules between which resonant transition dipole - transition dipole coupling can occur. Alignment effects are not affected by isotopic dilution, however RET can only occur between identical oscillators. Therefore RET is progressively removed as X_A is decreased in isotopic solution. It depends solely on the total number density (ρ_n) of the active species A so that the splitting is simply proportional to X_A. Non-resonant intermolecular interactions are largely unaffected by isotopic dilution. It is therefore theoretically possible to determine the contribution of RET to the relaxation and frequency of a vibrational mode by comparing the vibrational band in pure liquid with that at low concentration in isotopic solution.

However for non-isotopic dilution, solute and solvent molecules differ in their ability to orientate the solute pair between which RET occurs. As the active species is progressively diluted, alignment effects not involving solely the active species themselves, change from those characteristic of pure solute alignment to those

characteristic of pure solvent. Overall a simple linear dependence of the splitting on X_A is not expected. In addition there is also a variation in ρ_n with dilution, not seen by isotopic dilution, so the dependence of the splitting on X_A and ρ_n become entwined and cannot be isolated from each other.

Recently, however, Logan has extended his theory to the case of dipolar resonant transfer in non-isotopic dipolar binary mixtures[155]. This theory is made within the framework of the mean spherical approximation (MSA) for dipolar hard sphere binary liquids[210]. The dipolar mixture MSA has only been solved analytically for the case where the dipolar constituents have equal hard sphere diameters[210]. Logan has used this solution within his theory, therefore he expects that the theory may only be applicable to binary mixtures with constituents of comparable hard sphere diameters (say within 5-10% of each other). Unfortunately the hard sphere diameter of EHB is approximately[77] 7.4Å, whilst that of hexane can be expected to be considerably less. However, in an attempt to gain more information on the interactions that are important in determining the noncoincidence splitting in EHB, an attempt has been made to apply Logan's theory to EHB in hexane.

Logan's final result embodies all the many body molecular alignment effects and these are calculated explicitly from the chosen molecular model via MSA. Logan's expression for the noncoincidence splitting, relative to that in the pure solute, for the mode α of solute A ($\Delta_{\alpha,A}$), with a volume fraction of ϕ_A, at a temperature T(K) is

$$\frac{\Delta_{\alpha,A}(\phi_A,T)}{\Delta_{\alpha,A}(1,T)} = \frac{\phi_A[1 + (5/4)y_0]}{[1 + (5/2)y_0]^2} \frac{[1 + (5/2)\xi'_{A,0}]^2}{1 + (5/4)\xi'_{A,0}} \qquad \text{Eqn.8.10}$$

where

$$y_0(\phi) \approx \xi'_{A,0} \{\phi_A + [\mu_B/\mu_A]^2[(1-\phi_A)/R]\} \qquad \text{Eqn.8.11}$$

and

$$\xi'_{A,0} = \frac{\mu_A^2 \rho_n(1)}{72\epsilon_0 kT} \qquad \text{Eqn.8.12}$$

where μ_A and μ_B are the dipole moments of solute (A) and solvent (B) respectively, R is the ratio of molar volumes $(=V_{M,B}/V_{M,A})$, $\rho_n(1)$ is the number density of pure solute, ϵ_0 is the permittivity of a vacuum and k is the Boltzmann constant.

The calculated noncoincidence splittings, based on Eqns.8.10-12, are given in Table 8.3, again the dipole moment of EHB is taken to be that of ethyl benzoate. Fig.8.8 shows the predicted relative splittings using Logan's theory, compared with the experimental results. It can be seen that at concentrations above 0.503 v.f. the experimental splitting is predicted reasonably well by Logan's expression. However the experimental points below 0.503 v.f. are less accurately reproduced by the theory. It can be seen by comparing Figs.8.6-8.8 that the shape of Logan's theoretical curve does not mirror the shape of the experimental curve as well as the theory of Fini and Mirone. However it is likely that the microscopic model of Logan

324

volume fraction EHB	$\Delta \nu_{soln}$ (exp)	$F(\phi)$ (exp)	y_o	$F(\phi)$ (calc)	$\Delta \nu_{soln}$ (calc)
1.000	3.3	1.000	0.0421	1.000	3.3
0.904	3.1	0.939	0.381	0.916	3.0
0.780	2.5	0.758	0.0328	0.805	2.7
0.611	2.2	0.667	0.0257	0.646	2.1
0.503	1.5	0.455	0.0212	0.540	1.8
0.371	0.7	0.212	0.0156	0.406	1.3
0.208	0.4	0.121	0.0088	0.234	0.8
0.110	0.0	0.000	0.0046	0.126	0.4
0.000	0.0	0.000	0.0000	0.000	0.0

Table 8.3. Relative noncoincidence splittings for EHB in hexane, as calculated using Eqns.8.10-8.12.

$$\frac{(\triangle \mathcal{V})_{soln}}{(\triangle \mathcal{V})_{neat}}$$
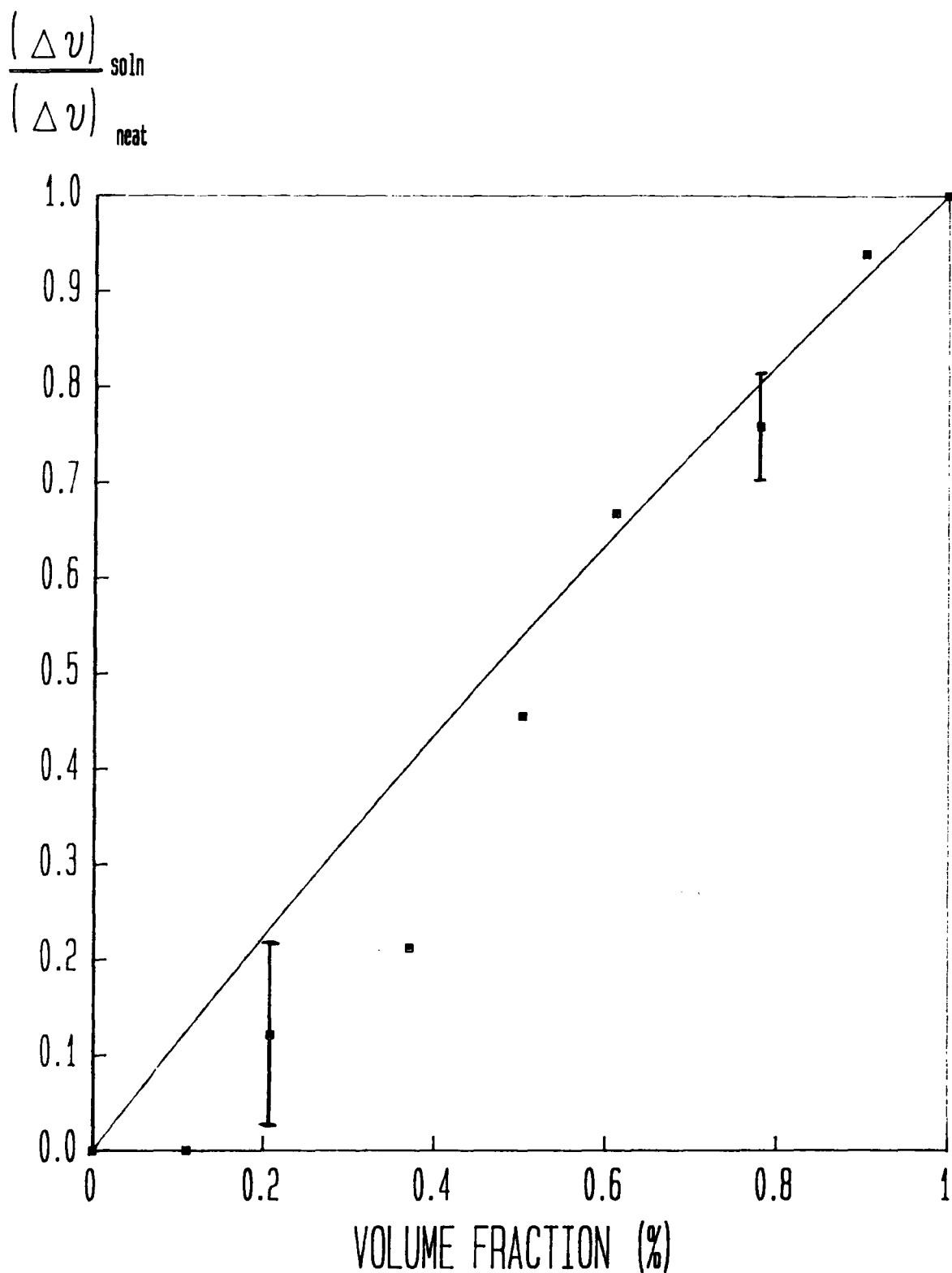
VOLUME FRACTION (%)

Figure 8.8. The relative noncoincidence splitting for the $\mathcal{v}(C{=}O)$ stretch of EHB as a function of volume fraction in hexane. Experimental points (●) compared with splitting predicted by Logan's theory (———).

326

more adequately reflects the origins of the noncoincidence effect, unlike that of Fini-Mirone which does not consider the role of microscopic structure. In fact the experimental data of Fini-Mirone[150] on acetone certainly appear to fit Logan's model, see Fig.8.9. Although at low concentrations, as for EHB in hexane, the theoretical points do appear to stray from the experimental results.

$$\Delta v_{soln}/\Delta v_{neat}$$
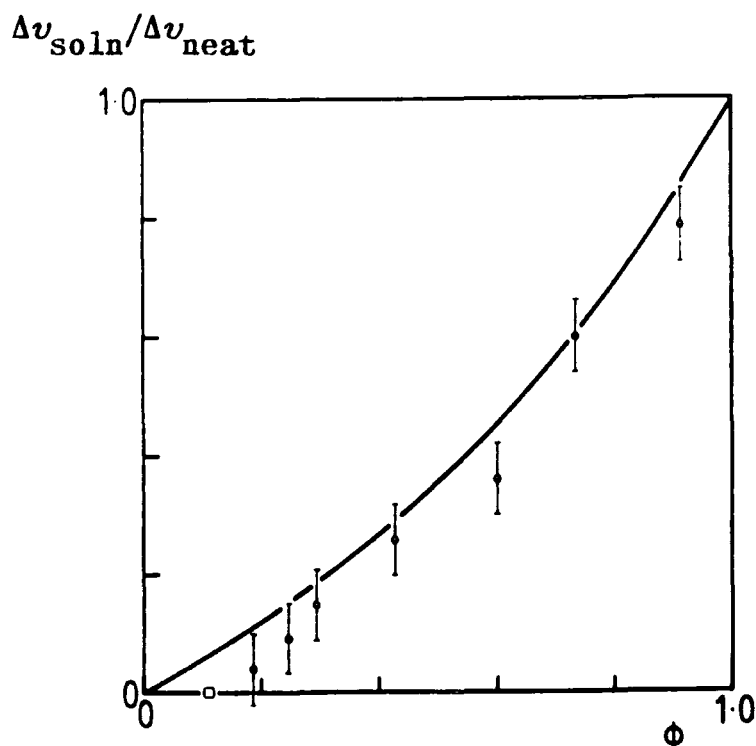
Figure 8.9. The relative noncoincidence splitting for the $v(C=O)$ stretch of acetone as a function of volume fraction in DMSO. Experimental points of Fini and Mirone[150] (●) compared with splitting predicted by Logan's theory (———), (□) is the experimental threshold volume fraction.

Logan's model does not allow for a threshold concentration, this may be the reason for the lack of theoretical fit for his theory at low concentration. Logan himself admits, in an earlier paper[153], that there is no question that a concentration threshold does exist for non-isotopic mixtures. Certainly if it is the point where RET becomes negligible because the correlation time for RET has become relatively long compared to other vibrational relaxation processes, as suggested in Section 8.2.1, then this would cause the experimental data to fall below the theoretical curve of Logan at low concentrations. In order for the phenomena of a concentration threshold to be more readily assessed it is necessary for the splitting at low concentration to be measured to greater accuracy. As at present it is unclear if deviations of experimental data from Logan's theory, as well as deviations from linearity observed for the splitting in isotopic mixtures[148], are within the bounds of experimental error. The powerful technique of Raman difference spectroscopy[211] should, however, be capable of resolving experimentally the uncertainties over the threshold concentration.

It should be remembered that for EHB in hexane the molecules fall outside the solution of the MSA for binary mixtures of molecules of equivalent hard sphere diameter. However if this were to make Logan's theory inapplicable to EHB in hexane then it might be expected that this would make the predictions inaccurate over the whole of the concentration range, which they are not. Apart from the inequivalence of the hard sphere diameters of EHB and hexane, there are a number of other possible explanations,

in addition to those discussed in the previous paragraph, for the discrepancy between the experimental results and the predictions of Logan's theory. These include: (1) The MSA approach is expected to be valid for dipolar mixtures in which the dominant anisotropic intermolecular forces responsible for the necessary alignment effects are due to permanent dipolar interactions. Both EHB and hexane have an effective shape which may lead to "short ranged" (non-hard sphere) anisotropic interactions contributing significantly to the orientational alignment which leads to RET. However this would lead to an additional contribution to the splitting, making the predictions too low (as seen by Shelley[148]). Nor does it explain the agreement of the theory and experiment at high concentration, but lack of agreement at low concentration. (2) The expression for noncoincidence splitting derived by Logan assumes that the number density of the solute varies as in an ideal mixture. Deviation from the ideal mixture, if at all, should be small (as shown for DMF in CCl_4[148]), and therefore not have a significant effect on splitting.

8.2.3 Conclusion to theoretical treatment of the noncoincidence effect

The relative success in predicting the noncoincidence splitting for EHB in hexane using Logan's theory is somewhat surprising considering the discrepancies in the EHB system from the set of constraints that Logan employs. Logan's theory does however fail to predict the shape of the experimental curve at low concentration. It is felt that this is a result of failure to account for the threshold concentration. Fini and Mirone's theory overestimates the splitting at all concentrations, but does more accurately predict the shape of the experimental curve. However this is only achieved by introduction, empirically, of the threshold concentration.

The ability of both theories to predict the splitting reasonably well, with no extreme discrepancies, further supports the idea that it is alignment by the permanent dipoles that is largely responsible for the occurrence of RET and the noncoincidence splitting.

8.3 Computer generated molecular graphic study of the EHB molecule

8.3.1 Introduction

To assist in the interpretation of the vibrational spectra of EHB a computer-aided molecular mechanics system, U-MICRO "CHEMOD", was utilised to provide direct information on the internal rotational rigidity of the EHB molecule. It was hoped that this would allow a closer determination of the molecular motions that contribute to the vibrational and reorientational relaxation processes in EHB. The programme can give valuable data about the energy changes occurring for rotation around chosen bonds, from this information it is possible to surmise which rotations are likely to dominate and which are not. Obviously interpretations have to be made with care as no considerations of the intermolecular interaction energies are made.

"CHEMMOD" carries out a Newton-Raphson energy minimisation procedure to determine the minimum energy conformational state (or states) for the input molecule. For this minimum energy conformer, the rotational rigidity of each significant skeletal bond in the molecule is determined by potential energy calculations as a function of torsion angle (typically at 3° intervals). "CHEMMOD" uses an expression for the overall steric potential energy of the form[212]

$$E(steric) = V(b) + V(a) + V(t) + V(nb) + V(opb) + V(q)$$

<div align="right">Eqn.8.13</div>

where $V(b)$ is the bond stretching potential energy, the sum of the individual bond energies; $V(a)$ is the angle bending potential energy, the sum of all bond angle bending energies; $V(t)$ is the torsional (or dihedral) potential energy; $V(nb)$ is the non-bonded potential energy, the sum of the significant individual non-bonded van der Waal's energies; $V(opb)$ is the out-of-plane bending potential energy, the total energy derived from non-planarity at trigonal atoms (such as $=C$); $V(q)$ is the Coulombic potential energy, the energy due to charged interactions, for EHB this is equal to zero.

The EHB molecule was generated on the "CHEMMOD" computer and the system was allowed to minimise until the minimum energy conformational state was achieved. This conformation is shown in Figs.8.10 and 8.11. It can be seen that, according to "CHEMMOD", the preferred molecular conformation, considering intramolecular interactions alone, is in an elongated form. In this case the molecule has a significant long axis, making overall rotation about the axes perpendicular to the long axis unlikely on the picosecond time scale. This is in agreement with suggestions made as a result of the relaxation rate study on the phenyl ring of EHB (see Section 7.1), which also suggested that EHB possesses a long axis.
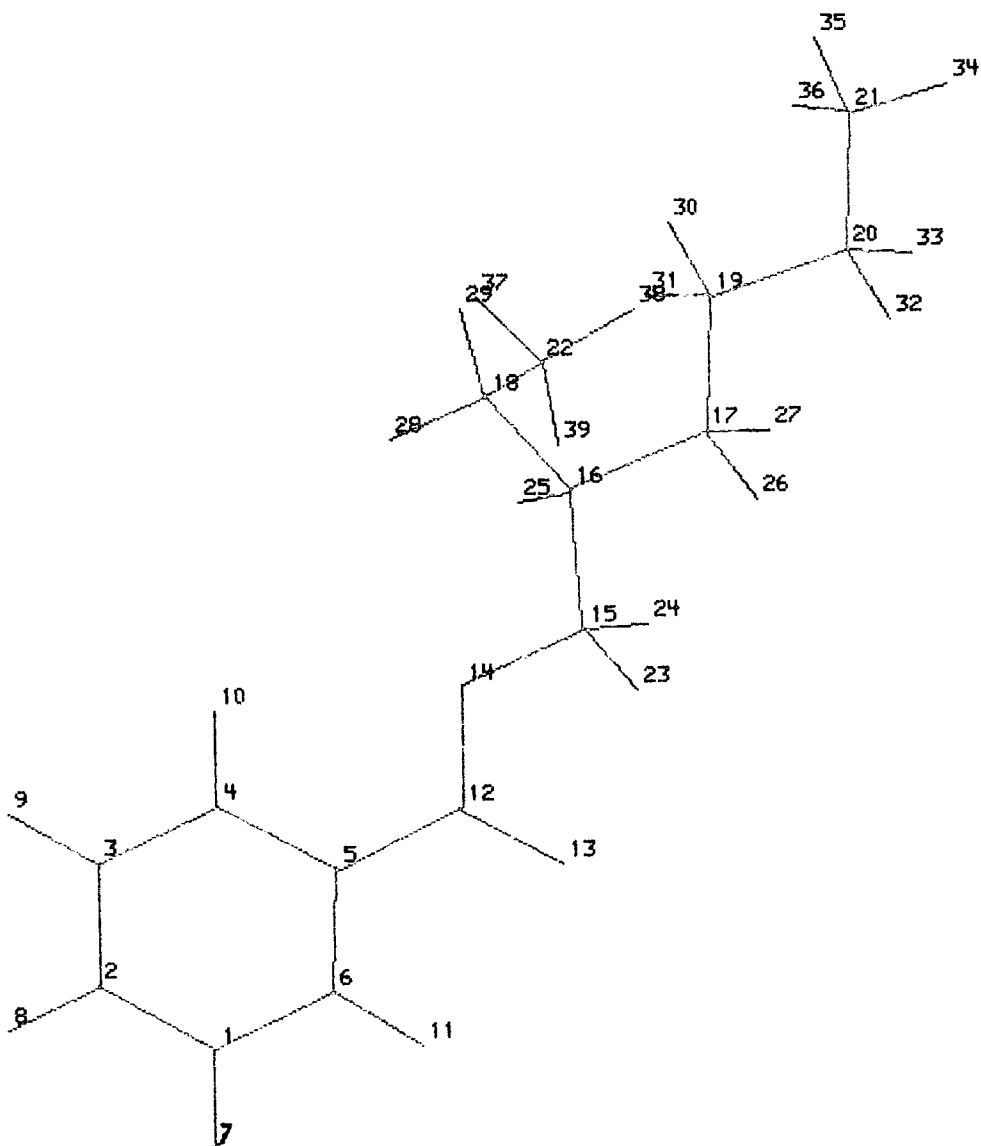
Figure 8.10. Minimum energy conformation of the EHB molecule as calculated by the "CHEMMOD" system. Stick diagram.
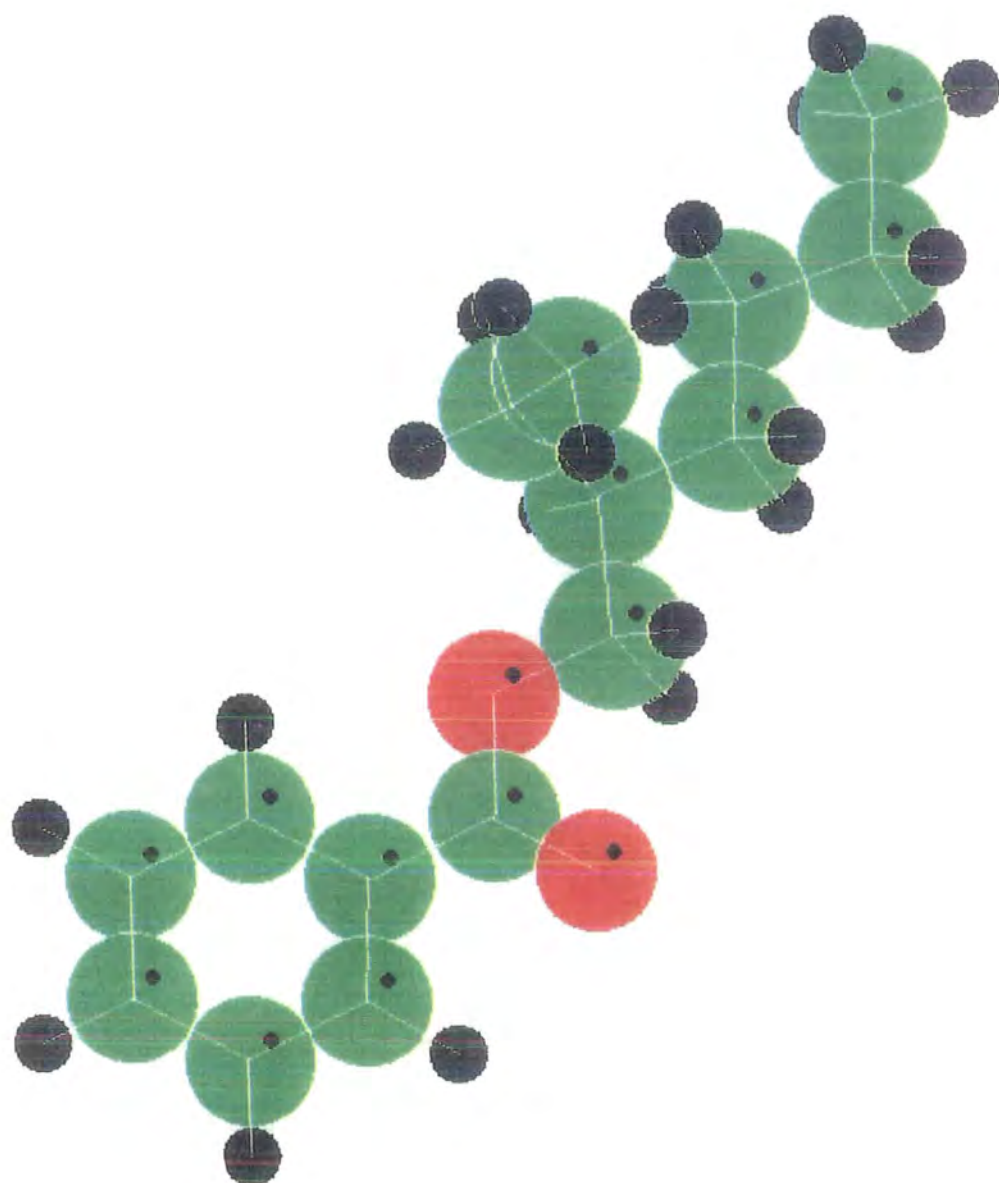
Figure 8.11. Minimum energy conformation of the EHB molecule
as calculated by the "CHEMMOD" system. Van der Waals radii
representation.

8.3.2 Rotation of the phenyl ring of EHB

Separate energy calculations, based on the minimum energy conformation, were made for rotation about individual bonds. The potential energy diagram for rotation of the phenyl ring of EHB and table of the energies at 3° intervals of the torsion angle is shown in Fig.8.12. Atom numbering is as in Fig.8.10. The torsion angle is the dihedral angle between the outer bonds of the three quoted, in the case of Fig.8.12 the angle between the 4,5 and the 12,14-bonds, this angle changes through rotation about the central (5,12) bond. The energy barrier (height), or activation energy (E_a), for rotation of the ring was calculated to be 6.2kcal/mol (25.9kJ/mol). The energy barrier for internal ring rotation of simple mono-substituted benzaldehydes, calculated from their gas phase spectra[212] are of the order of 4-5kcal/mol. It is not particularly surprising that EHB, due to the increased size and complexity of the molecule, has a greater barrier for ring rotation. The barrier to internal rotation[33] about the equivalent bond in phenol is 3.45kcal/mol, for the molecule Ph-CH=CH2 it is 3.06kcal/mol, whilst in ethane the barrier to internal rotation is 2.75kcal/mol and in ethylene (about the double bond) it is 40.0kcal/mol. The energy barrier determines the rate of rotation, that is the time scale over which rotation occurs. The Arrhenius equation, Eqn.8.14, relates the rate of a reaction or process (in this case rotation) to the energy barrier (E_a) for that process

$$k = k_o \cdot \exp[-E_a/RT] \qquad \text{Eqn.8.14}$$
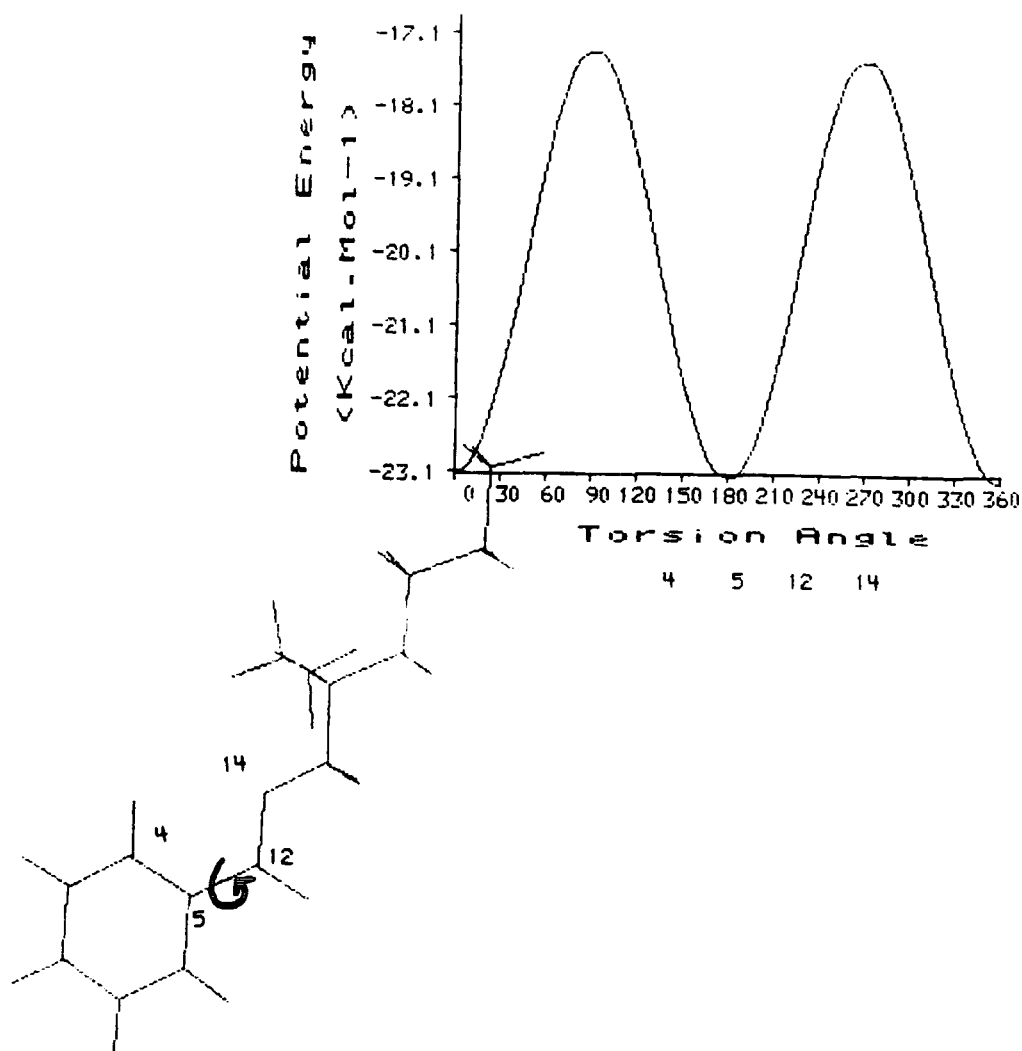
335

Potential Energy (Kcal.Mol⁻¹)

-17.1
-18.1
-19.1
-20.1
-21.1
-22.1
-23.1

0 30 60 90 120 150 180 210 240 270 300 330 360

Torsion Angle

4   5   12   14

Energy values are listed for each step from 0 to 360 degrees
at intervals of 3 degrees

Optimum and Minimum energy values are : -16.9 and -23.1

```
-23.1  -23.1  -23.0  -23.0  -22.8  -22.7  -22.5  -22.3  -22.1  -21.8
-21.6  -21.3  -21.0  -20.7  -20.4  -20.0  -19.7  -19.4  -19.1  -18.7
-18.4  -18.2  -17.9  -17.7  -17.5  -17.3  -17.1  -17.0  -16.9  -16.9
-16.9  -16.9  -17.0  -17.0  -17.2  -17.3  -17.5  -17.7  -18.0  -18.2
-18.5  -18.8  -19.1  -19.5  -19.8  -20.1  -20.5  -20.8  -21.1  -21.4
-21.7  -21.9  -22.2  -22.4  -22.6  -22.7  -22.9  -23.0  -23.0  -23.1
-23.1  -23.1  -23.0  -22.9  -22.8  -22.7  -22.5  -22.3  -22.1  -21.8
-21.6  -21.3  -21.0  -20.7  -20.4  -20.0  -19.7  -19.4  -19.0  -18.7
-18.4  -18.1  -17.9  -17.7  -17.5  -17.3  -17.1  -17.0  -16.9  -16.9
-16.9  -16.9  -17.0  -17.0  -17.2  -17.3  -17.5  -17.7  -18.0  -18.2
-18.5  -18.8  -19.2  -19.5  -19.8  -20.1  -20.5  -20.8  -21.1  -21.4
-21.7  -22.0  -22.2  -22.4  -22.6  -22.8  -22.9  -23.0  -23.1  -23.1
-23.1
```

Figure 8.12. The potential energy diagram for internal rotation of the phenyl ring of EHB, and a listing of the energies at 3° intervals

336

The value of $\exp[-E_a/RT]$ is related to the fraction of molecules with enough energy to react/rotate. To obtain absolute values of the rates of rotation about a particular bond the value of k_0 for that rotation would need to be known. The constant (for a particular molecule(s) and reaction) k_0 is a proportionality factor that relates the number of molecules that possess sufficient energy, to the amount that actually undergo the rotation (or react). For a reaction between two molecules it is dependent on the collision rate. For rotational motions, k_0 is related to the probability that a molecule possessing enough energy to undergo the particular rotation utilises it for that purpose, and not for some other molecular process. In addition k_0 must also contain information about intermolecular interactions in the liquid, as the rotations may be prevented (or even helped) by such interactions. In the study of reaction rates it is usually assumed that for a particular reaction pathway k_0 varies little, compared to E_a, from one molecule to another[213]. If k_0 for reorientational motions in liquids is assumed to be of the same approximate magnitude, then an idea of relative rates of rotation can therefore be made by comparing the values of $\exp[-E_a/RT]$ calculated from the energy barriers for internal rotations in different molecules. Certainly by comparing such values for different bonds in the same molecule the relative rotation rates should be reasonably accurate.

Table 8.4 compares the values of $\exp[-E_a/RT]$, for the internal rotation in the molecules discussed previously in this section, with those for internal rotation about various bonds in EHB. It can be seen that rotation of the phenyl

MOLECULE	T (K)	E_a		MODE OF INTERNAL ROTATION	$\exp[-E_a/RT]$
		kcal/mol	kJ/mol		
ethane	298	2.8	11.5	C-C	9.5×10^{-3}
phenol	298	3.5	14.4	Ph-OH	2.8×10^{-3}
$Ph\text{-}CH=CH_2$	298	3.1	12.8	Ph-C	5.6×10^{-3}
benzald-ehyde	298	4.5	18.8	Ph-C	4.8×10^{-4}
ethylene	298	40.0	167.2	C=C	3.6×10^{-30}
EHB	298	6.2	25.9	Ph-C	2.7×10^{-5}
EHB	373	6.2	25.9	Ph-C	2.3×10^{-4}
EHB	443	6.2	25.9	Ph-C	8.5×10^{-4}
EHB	298	1.7	7.1	$\overset{\text{O}}{\underset{\text{PhCO-C}}{\parallel}}$	5.6×10^{-2}
EHB	373	1.7	7.1	$\overset{\text{O}}{\underset{\text{PhCO-C}}{\parallel}}$	0.10
EHB	443	1.7	7.1	$\overset{\text{O}}{\underset{\text{PhCO-C}}{\parallel}}$	0.70
EHB	298	2.6	10.9	$\overset{\text{O}}{\underset{\text{PhC-OC}}{\parallel}}$	1.2×10^{-2}
EHB	373	2.6	10.9	$\overset{\text{O}}{\underset{\text{PhC-OC}}{\parallel}}$	3.0×10^{-2}
EHB	443	2.6	10.9	$\overset{\text{O}}{\underset{\text{PhC-OC}}{\parallel}}$	5.2×10^{-2}
EHB	298	2.7	11.3	C16-C18	1.0×10^{-2}
EHB	373	2.7	11.3	C16-C18	2.6×10^{-2}
EHB	443	2.7	11.3	C16-C18	4.6×10^{-2}

Table 8.4. Calculated values of $\exp[-E_a/RT]$ for the internal rotation of some simple aromatic compounds, ethane, ethylene and EHB (using results from molecular graphics calculations) at various temperatures.

ring is slower for EHB than in simpler aromatic molecules, as would be expected, but not by many orders of magnitude. In fact for EHB at higher temperatures, Table 8.4 suggests that the rate of rotation of the phenyl ring is approaching the rate of internal rotation for ethane at 298K. Consequently the rate of reorientational relaxation of the ring, discussed in Section 7.1, should have a significant contribution from internal rotation of the ring.

8.3.3 Internal rotations about the C-O bonds of the EHB molecules

Somewhat surprisingly it appears that internal rotation, in EHB, about the single C-O bonds (14,15 and 12,14-bonds) occurs at a faster rate than the rotation of the phenyl ring, see Figs.8.13 and 8.14, and Table 8.4. However it should be noted that overall rotation (on a comparable timescale) about these bonds is not possible, the conformation of the molecule about these two bonds is trapped in a potential well, so that only partial (approximately 180°) rotations are possible. As a consequence of the more rapid rotation about the C-O single bonds, compared with the rotation of the ring, the reorientational relaxation of the ring v(C-C) deformation mode, and of the C13 nuclei of the ring (see Section 7.1), should have a greater contribution from rotation about these C-O bonds. These rotations are still concentrated about the long axis of the molecule and should therefore cause preferential relaxation of the ortho and meta carbon atoms
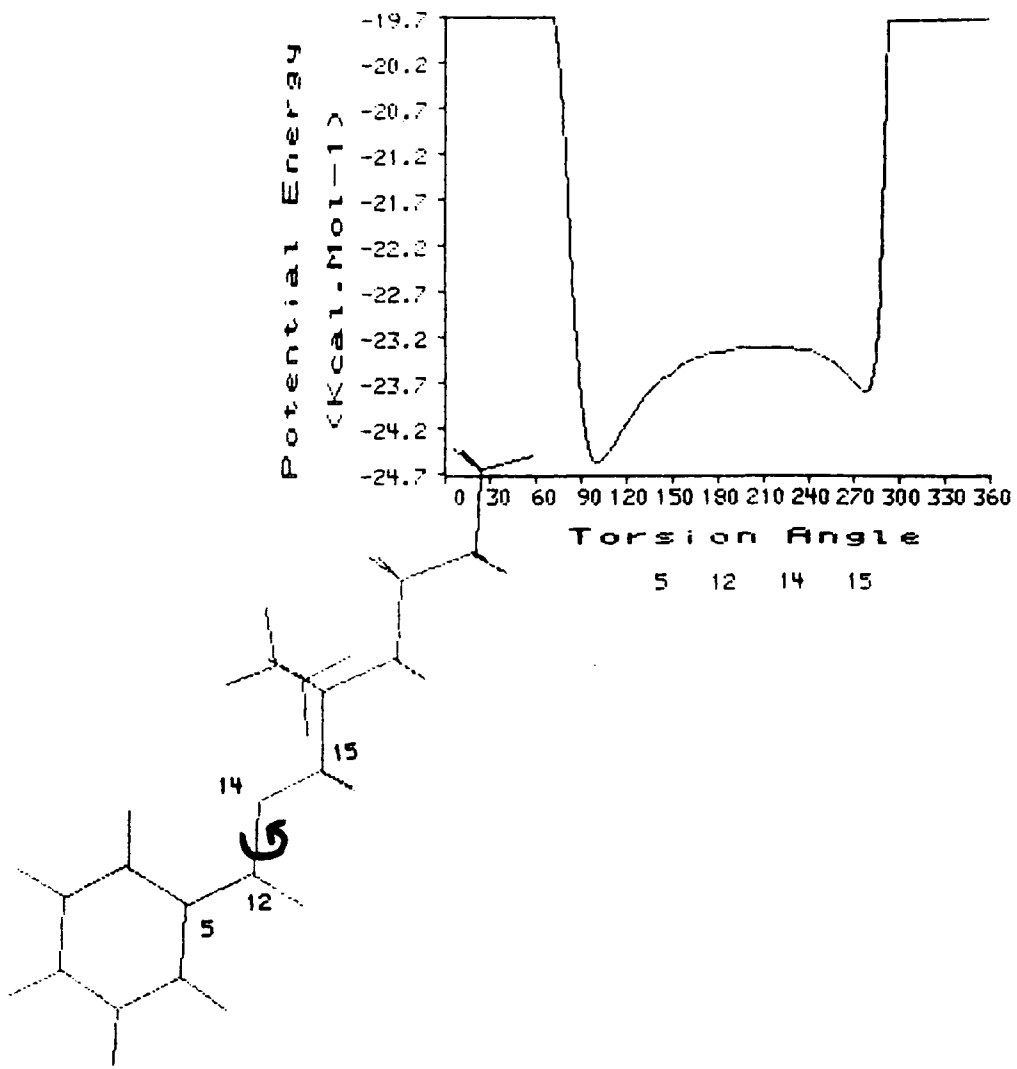
Potential Energy (Kcal.Mol⁻¹)

-19.7
-20.2
-20.7
-21.2
-21.7
-22.2
-22.7
-23.2
-23.7
-24.2
-24.7

0 30 60 90 120 150 180 210 240 270 300 330 360

Torsion Angle

5   12   14   15

Energy values are listed for each step from 0 to 360 degrees
at intervals of 3 degrees

Maximum and Minimum energy values are :   500.0 and -24.7

500.0	500.0	500.0	500.0	500.0	500.0	500.0	500.0	500.0	500.0
500.0	500.0	500.0	500.0	500.0	500.0	308.3	125.0	43.9	7.8
-8.2	-15.1	-17.9	-19.0	-19.5	-20.1	-20.8	-21.7	-22.6	-23.4
-24.0	-24.4	-24.6	-24.7	-24.7	-24.6	-24.5	-24.5	-24.4	-24.2
-24.1	-24.1	-24.0	-23.9	-23.8	-23.7	-23.7	-23.6	-23.5	-23.5
-23.5	-23.4	-23.3	-23.3	-23.3	-23.2	-23.2	-23.2	-23.1	-23.1
-23.1	-23.1	-23.1	-23.1	-23.0	-23.0	-23.0	-23.0	-23.0	-23.1
-23.1	-23.1	-23.1	-23.1	-23.1	-23.2	-23.2	-23.2	-23.2	-23.2
-23.3	-23.3	-23.3	-23.4	-23.4	-23.4	-23.5	-23.5	-23.6	-23.6
-23.7	-23.8	-23.8	-23.8	-23.7	-23.4	-22.7	-21.2	-18.0	-11.3
2.6	32.3	95.7	232.3	500.0	500.0	500.0	500.0	500.0	500.0
500.0	500.0	500.0	500.0	500.0	500.0	500.0	500.0	500.0	500.0
500.0									

Figure 8.13. The potential energy diagram for internal rotation about the first C-O bond (12,14) of EHB, and a listing of the energies at 3° intervals
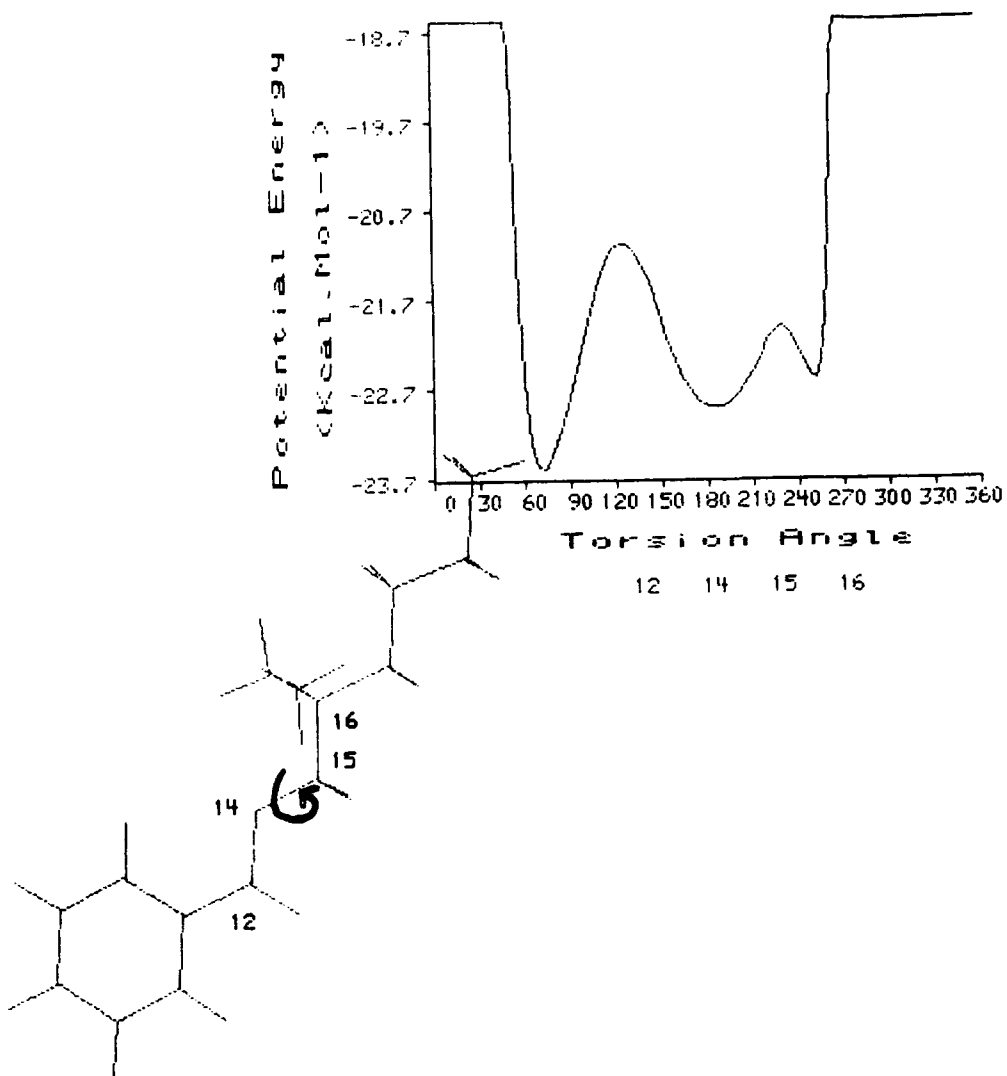
340

Energy values are listed for each step from 0 to 360 degrees
at intervals of 3 degrees

Maximum and Minimum energy values are :   200.0 and -23.7

500.0	500.0	500.0	412.1	168.1	72.2	33.0	16.3	8.7	4.6
1.5	-1.5	-4.7	-8.1	-11.3	-14.3	-16.9	-19.0	-20.7	-21.8
-22.7	-23.2	-23.5	-23.7	-23.7	-23.7	-23.5	-23.4	-23.2	-23.1
-22.9	-22.7	-22.4	-22.2	-22.0	-21.8	-21.6	-21.5	-21.3	-21.2
-21.1	-21.1	-21.1	-21.1	-21.2	-21.3	-21.4	-21.5	-21.7	-21.9
-22.0	-22.3	-22.4	-22.5	-22.7	-22.8	-22.9	-23.0	-23.0	-23.1
-23.1	-23.1	-23.1	-23.1	-23.0	-23.0	-22.9	-22.9	-22.8	-22.7
-22.6	-22.5	-22.4	-22.2	-22.2	-22.1	-22.0	-22.1	-22.1	-22.2
-22.3	-22.4	-22.6	-22.7	-22.7	-22.5	-22.0	-21.0	-19.1	-16.1
-11.5	-5.0	3.3	13.0	23.1	32.5	40.3	46.7	54.8	71.5
112.9	216.8	483.3	500.0	500.0	500.0	500.0	500.0	500.0	500.0
500.0	500.0	500.0	500.0	500.0	500.0	500.0	500.0	500.0	500.0
500.0									

Figure 8.14. The potential energy diagram for internal rotation about the second C-O bond (14,15) of EHB, and a listing of the energies at 3° intervals

compared to the para carbon atom. Explanations made for the faster relaxation times of the ortho and meta carbons, made in Section 7.1 are therefore supported further.

8.3.4 Internal rotations of the alkyl chain of EHB

As was expected the molecular graphics study demonstrates that internal rotation of portions of the alkyl chain of EHB become easier, more rapid, the nearer the rotation bond is to the ends of the chain. This is in agreement with the NMR ^{13}C spin lattice relaxation measurements on EHB, see Section 7.1. Figs.8.15a-d compare the potential energy diagrams for rotation of different portions of the EHB alkyl chain. It should be noted that atom numbering is as in Fig.8.10 for these energy diagrams.
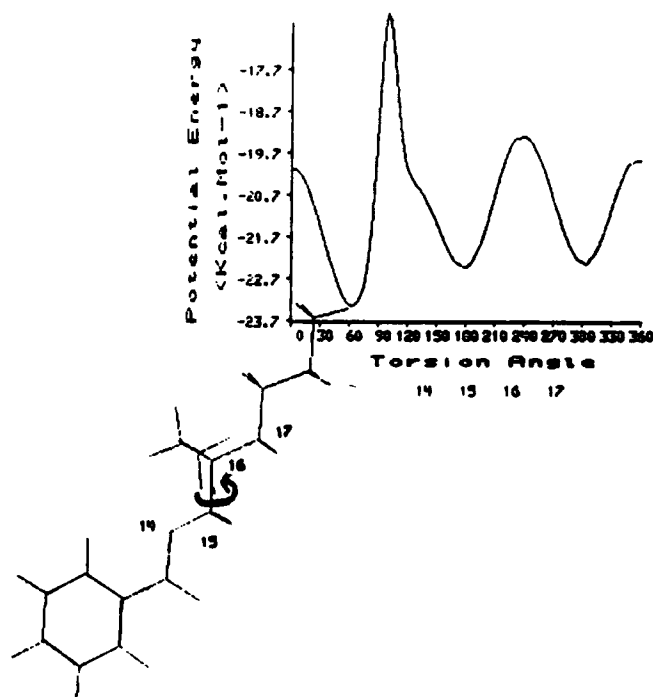
Figure 8.15a. The potential energy diagram for internal rotation of the alkyl chain of EHB about the carbon(15)-carbon(16) bond.
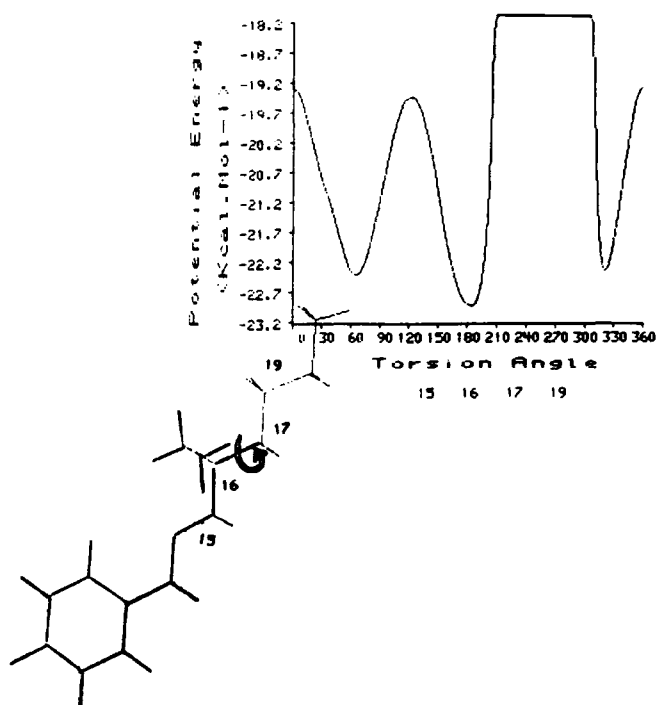
Figure 8.15b. The potential energy diagram for internal rotation of the alkyl chain of EIIB about the carbon(16)-carbon(17) bond.
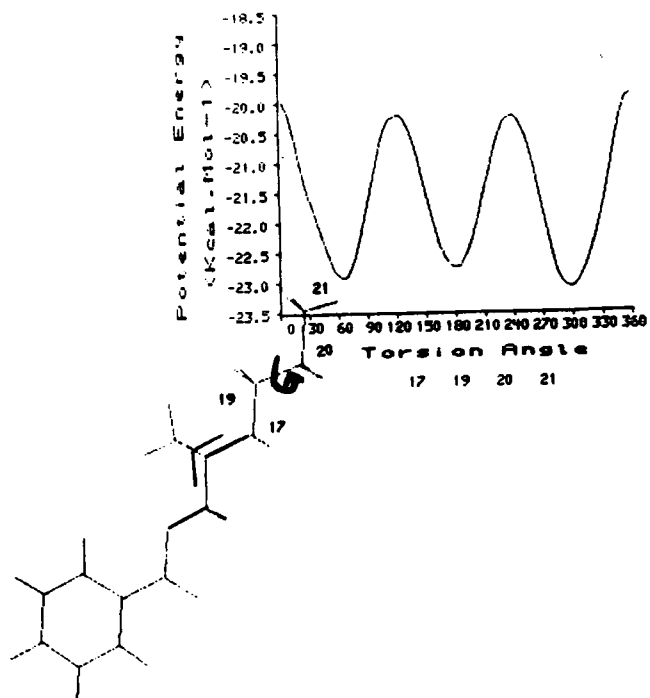
Figure 8.15c. The potential energy diagram for internal rotation of the alkyl chain of EIIB about the carbon(19)-carbon(20) bond.
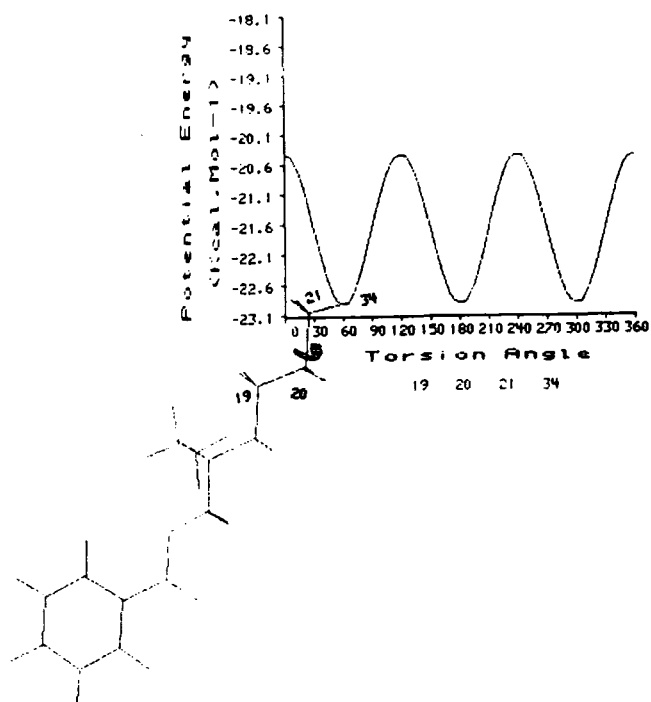
Figure 8.15d. The potential energy diagram for internal rotation of the alkyl chain of EHB about the carbon(20)-carbon(21) bond.

CHAPTER 9

SUMMARY

The aim of this project was to investigate the molecular behaviour of a lubricant like fluid (EHB) under high pressure and variable temperature conditions. The effect of these variables on the vibrational spectra for selected modes along the whole of the molecule have been studied. In addition, in an attempt to learn more about the intermolecular interactions in the fluid, the solution spectra of EHB have been looked at. Vibrational frequency shifts and changes in band widths and intensities have yielded information on the intermolecular and intramolecular dynamics and interactions in EHB. Attempts have been made to link this information with the macroscopic behaviour of the fluid.

Temperature work

The shear viscosity data for EHB at ambient pressure shows a non-exponential behaviour which seems to be well correlated, at high temperatures, with the variation of rotational correlation times for the liquid. The data fall into high and low temperature regimes, the latter being associated with a much lower rotational volume than the former. Clearly these changes in motional freedom are associated with internal degrees of freedom arising from "flexibility" since the translational motion of the molecule does not show similar anomalous behaviour. The viscometric behaviour is thereby correlated with internal motions of the flexible hydrocarbon chain.

Both Raman and infrared bands of the v(C=O) stretching mode of EHB show a non-linear blue frequency shift and band narrowing over the whole of the concentration range (100% to 0.05% mole fraction) in hexane. It appears that the molecules do not become completely separated until below 2% mole fraction. The large increase in frequency for this mode, compared with the other vibrational modes, suggests that strong attractive, most probably dipole-dipole, interactions are localised at the carbonyl group.

All the bands of EHB have a decreased band width in solution, showing that the vibrational relaxation rate is slower. Therefore relaxation arising from EHB-EHB interactions is more efficient than that arising from EHB-solvent (hexane, CS_2 or benzene) interactions.

It was suggested from the solution experiments that hexane is better at separating the EHB molecules than benzene or CS_2. This is possibly a result of significant involvement of the alkyl chains of EHB in the intermolecular interactions. Hexane being more "like" the alkyl chain of EHB is therefore more able to separate the EHB molecules.

The noncoincidence effect

A noncoincidence of the Raman isotropic and anisotropic bands of the υ(C=O) stretching mode of EHB has been observed. This has been explained in terms of a resonance energy transfer (RET) process via transition dipole-transition dipole interactions. Results have suggested that it is dipole-dipole coupling which preferentially weights the alignment of the dipoles, between which RET occurs. The splitting decreases on dilution and when increasing the temperature, as the dipole-dipole coupling is reduced.

The isotropic band width of the υ(C=O) stretching mode is seen to be broader than the corresponding anisotropic band. The difference in band width arises because cross terms can occur between self and exchange terms, these contribute to the isotropic relaxation but not the anisotropic relaxation.

High pressure work

The infrared band of the υ(C=O) stretching mode of EHB shows an unusual red shift with increased pressure, up to 6.5kbar. This is followed by a blue shift as the pressure is further increased. The explanation for these observations is likely to be due to the competing effects of increased alignment of carbonyl dipoles and the the increase in the repulsive interactions. Analysis has shown that this band of EHB is more likely to be formed in the slow modulation regime.

348

All the other bands of EHB show blue frequency shifts, of varying degree, with increasing pressure, indicating that repulsive forces are dominating the observed changes for these bands. The spectral changes have been seen to be consistent with the behaviour of n-hexadecane and other molecules that contain alkyl chains. Molecules which are known to exhibit chain extension and increased interchain interactions with increased pressure.

The band widths of all the vibrational modes increase with pressure, consistent with an increase in vibrational relaxation rate.

The pressure behaviour of some of the vibrational modes of EHB indicate that EHB probably exhibits a phase change close to 6.5kbar

Future work

One of the most important findings in this work is that the viscosity behaviour of EHB is largely dependant on the reorientational motion of the molecule. The sharp increase in viscosity towards low temperature may be a consequence of a loss of flexibility for part of the molecule. To achieve a more desired low temperature viscosity response it is necessary to drive the transition point to lower temperatures. To do this the internal flexibility of the molecule needs to be changed. This problem could be approached through the use of molecular graphics calculations, viscosity measurements, and studies of the behaviour of reorientational motions as a function of

temperature.

In order to investigate the temperature behaviour of EHB further it is necessary to carry out constant density temperature experiments (probably by use of the DAC). This would allow the separation of the effects of decreased density and increased kinetic energy, which tend to compete when the temperature is raised.

A high pressure Raman study is desirable, to see how increased density effects the RET process exhibited by the $v(C=O)$ stretching mode, and the reorientational motions of EHB.

To investigate the possibility of a phase change at increased pressure, more infrared spectral data is required, between 6.5 and 20kbar.

Finally a study of the vibrational and NMR spectra of EHB in the presence of a small amount of Viscosity Index Improver (VII) would hopefully yield information on how these VII's interact with lubricant molecules and improve there viscosity-temperature behaviour.

REFERENCES

1. F.M. Jaeger, Chapter 2 of "Second Report on Viscosity and Plasticity",(1938).

2. R.F. Crouch and A. Cameron, J. Inst. Pet., 47, 307 (1961).

3. A. Bondi, Chapter 1 of "Rheology Theory and Applications", 4Ed. F.R. Eirich, Academic Press, New York (1967).

4. C.J.A. Roelands, J.C. Vlutger and H.I. Waterman, J. Basic. Eng., 11, 601 (1963).

5. H.A. Spikes, "A Thermodynamic Approach to Viscosity", presented as paper at ASME/STLE Tribology Conference Oct 16-19, 1988, STLE Preprint No.88-TC-6C-2.

6. J.H.R. Clarke and D. Brown, J. Chem. Phys., 86(3), 1542-7 (1987).

7. D.M. Heyes, J. Non-Newtonian. Fl. Mech., 27, 47-85 (1988).

8. J. Yarwood, A. Whitley, D.G. Gardiner and M.P. Dare-Edwards, in Proc IV NATO Conf (1988) - "Reactive and Flexible Molecules in Liquids", NATO ASI Series C: Mathematical and Physical Sciences - Vol 291, ed. Th. Dorfmuller, Kluwer Academic Publishers (1989).

9. D. Dowson and G.R. Higginson, "Elasto-Hydrodynamic Lubrication", SI Edition, Permagon Press (1977).

10. F.P. Bowden and D. Tabor, "Friction: An Introduction to Tribology", Science Study Series No.41, Heinemann Educational Books Ltd, London (1974).

11. ASME "Pressure-Viscosity Report. Viscosity and Density of Over 40 Lubricating Fliuds of Known Composition at Pressure to 150,000psi and Temperatures to 425F", ASME, New York (1953).

12. A.G.M. Michell, Chapter 2 of "Lubrication: Its Principles and Practice", Blackie and Sons Ltd, London and Glasgow (1950).

13. C.R. Evans, "Measurement and mapping of rheological properties of elastohydrodynamic lubricants", PhD dissertation, Cambridge University (1985).

14. R.B. Dow, Chapter 8 of "Rheology Theory and Applications", 1Ed. F.R. Eirich, Academic Press, New York (1956).

15. O. Reynolds, Phil. Trans., 177, 157 (1886).

16. S. Glasstone, K.J. Laidler, H. Eyring, "The Theory of Rate Processes", McGraw-Hill Book Co, N.Y. (1941).

17. S. Arrhenius, Z. Physik. Chem., 4, 226 (1889).

18. S.G. Brush, Chem. Rev., 62, 513 (1962).

19. M. Mooney, Trans. Soc. Rheol., 1, 63 (1957).

20. T. Fox and P. Florey, J. Polymer. Sci., 14, 315 (1954).

21. A.K. Doolittle and D.B. Doolittle, J. Appl. Phys., 28, 901 (1957).

22. G.S. Fulcher, J. Am. Ceram. Soc., 8, 339 (1925)

23. D. Tamman, and W.S. Hess., Z. Anorg. Allgem. Chem., 156, 245 (1926).

24. A.J. Barlow, J. Lamb, A.J. Matheson, Proc. Royal. Soc., 4, 322 (1966).

25. P. Barus, Am. J. Sci., 45, 87-96 (1893).

26. D.L. Hogenboom, W. Webb, M. Dixon, J. Chem. Phys., 47, 2587 (1967).

27. P.W. Bridgeman, Proc. Am. Arts Sci., 77, 117 (1949).

28. E. Kuss, Z. Angew. Phys., 7, 372 (1955).

29. G.P. Johari and W. Dannhausser, J. Chem. Phys., 51, 1626 (1969).

30. E. Kuss, Ber. Bunsenges. Phys. Chem., 87, 33 (1983).

31. S.P. Kempsell, J.R. Barnes, C.J. Craven, M.P. Dare-Edwards and F.D. Wayne, in Proc. VI International Colloquium on Tribology, Esslingen, FDR 12-14 January (1987).

32. "Functional Fluids", special issue of "Chemistry in Britain", (Ed. J. Yarwood), April 1990.

33. J.M. Hollas, "Vibrational Spectroscopy", Chapter 6 of "Modern Spectroscopy", John Wiley and Sons (1988).

34. C.V. Raman and K.S. Krishnan, Indian. J. Phys. 2, 399 (1928).

35. A. Messiah, "Quantum Mechanics I", John Wiley and Sons, New York (1957).

36. K.A. Valiev, Opt and Spektrosk., 11, 465 (1960).

37. J. Yarwood and R. Arndt, "Study of Intermolecular Interactions in the Liquid Phase", Chapter 4 of "Molecular Association",Vol. 2, ed. R. Foster, Academic Press (1979).

38. J. Yarwood and G. Doge, "Infrared and Raman Studies on Molecular Dynamics in Liquids", Chapter 6 of "Spectroscopy and Dynamics of Molecular Liquids", Ed. D. Steele and J. Yarwood, Elseveir Publishers (to be published).

39. R.M. Lynden-Bell, Mol. Phys., 33, 907 (1977); Faraday Symp. Chem. Soc., 11, 167 (1978).

40. R.T. Bailey in "Molecular Spectroscopy" (Specialist Periodical Reports), The Chemical Society, London, Vol. 2, p. 173-261 (1974).

41. M. Kamoun and P. Mirone, Chem. Phys. Lett., 75, 287 (1980).

42. C. Brot, Mol. Phys., 45, 543 (1982).

43. D. Kivelson and P.A. Madden, J. Phys. Chem., 86, 4244 (1982).

44. J. Yarwood, Ann. Rep. Roy. Soc. Chem., C79, 157 (1982).

45. P.A. Madden and D. Kivelson, Ann. Rev. Phys. Chem., 31, 523 (1980); Adv. Chem. Phys., 56, 467 (1984).

46. M.W. Evans, G.J. Evans, W.T. Coffey and P. Grigolini, Chapter 11 of "Molecular Dynamics", Wiley-Interscience, London (1982).

47. F.J. Bartoli and T.A. Litovitz, J. Chem. Phys., 56, 404 (1972).

48. W.F. Murphy, M.V. Evans and P. Bender, J. Chem. Phys., 47, 1836 (1967).

49. G. Doge, R. Arndt and J. Yarwood, Chem. Phys., 25, 387 (1977).

50. J. Vincent-Geisse, J. Soussen-Jacob, C. Breuillard, J.C. Briquet and T. Nguyen-Tan, Mol. Phys., 34, 145 (1977).

51. P. Van Konynenberg and W.A. Steele, J. Chem. Phys., 56, 4776 (1972).

52. B. Kellar and F. Kneubuhl, Helv. Physica. Acta., 45, 1127 (1972).

53. W.G. Rothschild, "Dynamics of Molecular Liquids", John Wiley and Sons (1984).

54. G. Wyllie, in "Dielectric and Related Processes", Vol. 1, ed. M.M. Davies, The Chemical Society, London (1972).

55. D. Kivelson, J. Chem. Phys., 63, 5034 (1975).

56. S. Bratos and E. Marechal, Phys. Rev., 4, 1078 (1971).

57. R. Kubo, in "Fluctuations, Relaxation and Resonance in Magnetic Systems", (Ed. D.Ter. Haar), Plenum, New York (1962).

58. J.S. Rowlinson and M. Evans, "Annual Reports, A, 1975", The Chemical Society, London (1975).

59. B.J. Berne and R. Pecora, Ann. Rev. Phys. Chem., 26, 233 (1974).

60. S.L. Whittenberg and C.H. Wang, J. Chem. Phys., 66, 4255 (1977).

61. H. Dardy, V. Volterra and T.A. Litovitz, "Faraday Symposium, No. 6", The Chemical Society, London (1972).

62. T.B. MacRury, W.A. Steele and B.J. Berne, J. Chem. Phys., 64, 1288 (1976).

63. W.J. Moore, "Physical Chemistry", 5th Ed., Pub. Longman Group Ltd, London (1972).

64. R.G. Gordon, J. Chem. Phys., 44, 1830, (1966).

65. D. Kivelson and R.E.D. McClung, J. Chem. Phys., 49, 3380 (1968); S. Sunder and R.E.D. McClung, Can. J. Phys., 52, 1209 (1974).

66. G. Levi, J.P. Marsault, F. Marsault-Herail and R.E.D. McClung, J. Chem. Phys., 63, 3543 (1975).

67. M. Evans, J. Chem. Soc., Faraday. Trans. *II*, 71,843 (1975); 2051 (1975).

68. B. Guillot and G. Birnbaum, in Proc IV NATO Conf (1988) - "Reactive and Flexible Molecules in Liquids", NATO ASI Series C: Mathematical and Physical Sciences - Vol 291, ed. Th. Dorfmuller, Kluwer Academic Publishers (1989).

69. P.M. Corcoran, W.T. Coffey and M.W. Evans, Mol. Phys., 61, 1,15 (1987).

70. W.T. Coffey, Chem. Phys. Lett., 123, 416 (1986); W.T. Coffey and P.M. Corcoran, ibid., 144, 172 (1988).

71. W.T. Coffey, P.M. Corcoran and J.K. Vij, Chem. Phys. Lett., 129, 375 (1986).

72. C. Brot and A. Gerschel, Z. Phys. D., 5, 357 (1987).

73. J. Yarwood, NATO ASI Ser. C., 135 (Mol. Liquids), p. 357-82, Reidel (1984).

74. D. Steele, Stud. Phys. Theor. Chem., 20 (Vib. Intensities Infrared Raman Spectrosc.), 398 (1982).

75. W.A. Steele, NATO ASI Ser. C., 135 (Mol. Liquids), p. 357-84, Reidel (1984).

76. W.A. Steele and R.M. Lynden-Bell, J.Phys. Chem., 88, 6514 (1984).

77. N.A. Walker, D.M. Lamb, S.T. Adamy, J. Jonas and M.P. Dare-Edwards, J. Phys. Chem, 92, 3675 (1988).

78. J. Yarwood, A. Whitley, D.J. Gardiner and M.P. Dare-Edwards, in "Reactive and Flexible Molecules in Liquids" (Ed. T. Dorfmuller), Kluwer Academic Publishers, pp.61-82 (1989).

79. R.G. Snyder, J. Chem. Phys., 47, 1316 (1967).

80. D.J. Gardiner, M.P. Dare-Edwards and N.A. Walker, Nature, 316, 614 (1985) and references therein.

81. J. Devaure and J. Lascombe, Nouv. J. Chim., 3, 579 (1979).

82. P.T.T. Wong, H.H. Mantsch and R.G. Snyder, J. Chem. Phys., 79, 2369 (1983).

83. P.T.T. Wong, in "Current Perspective in High Pressure Biology", Ed. R.E. Marquis, Pub. Academic, London (1987).

84. P.T.T. Wong and H.H. Mantsch, J. Chem. Phys., 83, 3268 (1985).

85. P.E. Schoen, R.G. Priest, J.P. Sheriden and J.M. Schaur, J. Chem. Phys., 71, 317 (1979).

86. J. Schroeder, V.H. Schiemann, P.T. Sharko and J. Jonas, J. Chem. Phys., 66, 3215 (1977).

87. K. Tanabe and J. Jonas, Chem. Phys., 38, 131 (1979).

88. K. Tanabe and J. Jonas, J. Chem. Phys., 67, 4222 (1977).

89. P.A. McGregor and M. Schwartz, J. Mol. Struct., 95, 273 (1982).

90. S.L. Wunder, M.I. Bell and G. Zerbi, J. Chem. Phys., 85, 3827 (1986).

91. A.M. Goulay, A. Migdal-Mikuli, E. Mikuli, J. Saussen-Jacob and J. Vincent-Geisse, Chem. Phys., 96 333 (1985).

92. J.T. Hynes, R. Kapral and M. Weinberg, J. Chem. Phys., 67, 3256 (1977).

93. C. Grosse and F. Hufnagel, J. Mol. Liquids., 33, 213 (1987).

94. W. Richter and D. Schiel, I.R. Phys., 24, 227 (1984).

95. J.K. Vij and F. Hufnagel, Chem. Phys. Lett., 139, 77 (1987).

96. J. Poley, J. Chem. Phys., 23, 405 (1955); G.W. Chantry and H.A. Gebbie, Nature., 208, 378 (1965).

97. J.R. Lyeria and T.T. Horikawa, J. Phys. Chem., 80, 1106 (1977).

98. J. Jonas, J. Magn. Reson., 32, 297 (1978).

99. D.G. Gillies, L.P. Blauw, G.R. Hays, R. Huis and A.D.H. Clague, J. Magn. Reson., 42, 420 (1981).

100. H-O. Kalinowski, S. Berger, S. Braun, "Carbon-13 NMR Spectroscopy", John Wiley and Sons (1988), and references therein.

101. R.L. White, Appl. Spectroscopy., 39, 320 (1985).

102. D.M. Adams, S.J. Payne and K. Martin, Appl. Spectroscopy., 27, 377 (1973).

103. Dr. D.M. Adams, Diacell Products, 54 Ash Tree Road, Oadby, Leicester LE2 5TD, England.

104. R.A. Forman, G.J. Piermarini, J.D. Barnett and S. Block, Science., 176, 284 (1972).

105. G.J. Piermarini, S. Block, J.D. Barnett and R.A. Forman, J. Appl. Phys., 46, 2774 (1975).

106. D.M. Adams, R. Appleby and S.K. Sharma, J. Phys E., 9, 1140 (1976).

107. J. Birnie, PhD Thesis, Newcastle Polytechnic, Newcastle-upon-Tyne (1989).

108. R.J. Bell, "Introductory Fourier Transform Spectroscopy", Academic Press, New York (1972).

109. H. Zahl and M. Golay, Rev. Sci. Instr., 17, 511 (1946).

110. M. Golay, Rev. Sci. Instr., 18, 357 (1947).

111. C. Barker, Phd Thesis, Durham University, Durham (1977).

112. R.A. Smith, F.E. Jones, and R.P. Chasmar, "The detection and measurement of I.R. radiation", Oxford University Press (1968).

113. L.J. Bellamy, "The infrared spectra of complex molecules", Third edition, Chapman and Hall, London (1975).

114. R.L. Amey and D. Chapman, "Infrared Spectroscopic Studies of Model and Natural Biomembranes" in "Biomembrane Structure and Function" pp. 199, Macmillan Press (1983).

115. F.S. Parker, "Applications of Infrared and Resonance Raman in Biochemistry", Plenum Press, New York (1983).

116. J.K. Kauppinen, D.J. Moffatt, H.H. Mantsch and D.G. Cameron, Appl. Spectrosc., 35, 271 (1981).

117. N.A. Walker and J. Jonas (personal communication).

118. F.D. Rossini, K.S. Pitzer, R.L. Arnett, R.M. Braun and C.G. Pimentel, "Selected values of physical and thermodynamic properties of hydrocarbon and related compounds", Pittsburgh, Carnegie Press (1953).

119. D.J. Craik, W. Adcock and G.C. Levy, Org. Mag. Res., 783 (1986).

120. F.A. Bovey and L.W. Jelinski, J. Phys. Chem., 89, 571 (1985).

121. R.C. Farrar, S.J. Druck, R.R. Sharp and E.D. Becker, J. Am. Chem. Soc., 94, 699 (1972).

122. I. Artaki and J. Jonas, Mol. Phys., 55, 867 (1985).

123. T. Bluhm, Mol. Phys., 52, 1335 (1984).

124. D.E. Woessner, J. Chem. Phys., 37, 647.

125. G.C. Levy, J. Chem. Soc. Chem Comm., p47, (1972).

126. A.J. Williams, PhD Thesis, Royal Holloway College, London (1989).

127. G.C. Levy, J.D. Cargioli and F.C. Anet, J. Am. Chem. Soc., 95, 1527 (1973).

128. F.A. Miller, J. Raman. Spectr., 19, 219 (1988).

129. Y.K. Levine, J.M. Birdsall, A.G. Lee, J.C. Metcalfe, P. Partington and G.C.K. Roberts., J. Chem. Soc. Chem. Comm., 757 (1973).

130. F. Heatley, Polymer., 16, 493, (1975).

131. D. Kivelson, Faraday Symposium No. 11, The Chemical Society, London, p.7 (1977).

132. G.T. Evans and D. Kivelson, J. Chem. Phys., 84, 385 (1986); D. Kivelson and P.A. Madden, Ann. Rev. Phys. Chem., 31, 523 (1980).

133. P. Debye, "Polar Molecules", Dover (1945).

134. W.F. Pacynko, D.J. Gardiner and J. Yarwood, Chem. Phys., 78, 319 (1983).

135. J.H. Hilderbrand and R.H. Lamoreaux, Proc. Natl. Acad. Sci. USA., 69, 3428 (1972).

136. A. Bondi, "Physical properties of molecular crystals liquids and glasses", p.450, Wiley, New York (1968).

137. J. Jonas, D. Hasha and S.D. Huang, J. Phys. Chem., 84, 109 (1980).

138. J. Jonas, D. Hasha and S.D. Huang, J. Chem. Phys. 71, 3996 (1979).

139. M. Fury, G. Munie and J. Jonas, J. Chem. Phys., 70, 1260 (1979).

140. D. Scheibe and G. Doge, Ber. Buns. Phys. Chem., 85, 520 (1981).

141. G. Fini and P. Mirone, J. Chem. Phys., 79, 639 (1983).

142. J. Jonas, W. Schindler and T.W. Zerda, J. Chem. Phys., 81, 4306 (1984).

143. A. Purkayastha and K. Kumar, Spectrochemica. Acta., 42A, 1379 (1986); J. Raman Spectroscopy., 19, 249 (1988).

144. G. Fini and P. Mirone, J. Chem. Soc. Faraday Trans. II., 70, 1776 (1974).

145. G. Fini and P. Mirone, Spectrochim. Acta., 32A, 625 (1976).

146. W. Schindler, P.T. Sharko and J. Jonas, J. Chem. Phys., 76, 3493 (1982).

147. V.M. Shelley, A. Talintyre, J. Yarwood and R. Buchner, Faraday Disc. Chem. Soc., 85, 211 (1988).

148. V.M. Shelley and J. Yarwood, Chem. Phys., 137, 277 (1989).

149. C.H. Wang and J. McHale, J. Chem. Phys., 72, 4039 (1980).

150. G. Fini and P. Mirone, J. Chem. Phys., 71, 2241 (1979).

151. P. Mirone, J. Chem. Phys., 77, 2704 (1982).

152. G. Doge, A. Khuen and J. Yarwood, Mol. Phys., 52, 399 (1984).

153. D.E. Logan, Chem. Phys., 103, 215 (1986).

154. D.E. Logan, Mol. Phys., 58, 97 (1986).

155. D.E. Logan, Chem. Phys., 131, 199 (1989).

156. M. Kamoun and P. Mirone, Chem. Phys. Letters, 75, 287 (1980).

157. G. Fini and P. Mirone and B. Fortuanato, J. Chem. Soc. Faraday Trans. II., 69, 1243 (1973).

158. C. Perchard and J.P. Perchard, J. Raman. Spectoscopy., 6, 74 (1975), ibid. 3, 277 (1975).

159. V.J. Korsunskii, N.L. Lavrik and Yu.I. Naberukhin, Opt. Spektroskopiya., 41, 468 (1976).

160. J. Schroeder, V.H. Schiemann and J. Jonas, J. Chem. Phys., 69, 5479 (1978).

161. K.S. Schweizer and D. Chandler, J. Chem. Phys., 76, 2296 (1982).

162. Handbook of chemistry and physics, C.R.C., 63rd. edition, Ed. R.C. Weast.

163. W. Schindler and J. Jonas, J. Chem. Phys., 73, 3547 (1980).

164. J. Yarwood, R. Arndt and G. Doge, Chem. Phys., 25, 387 (1977).

165. S.F. Fischer and A. Laubreau, Chem. Phys. Lett., 35, 6 (1975).

166. G. Doge, Z. Naturforsch. Teil., A28, 919 (1973).

167. A.M. Benson,Jr, and H.G. Drickamer, J. Chem. Phys., 27, 1164 (1957).

168. R.R. Wiederkehr and H.G. Drickamer, J. Chem. Phys., 28, 311 (1958).

169. D. Levesque, J.J. Weiss and D. Oxtoby, J. Chem. Phys., 68, 5528 (1978); ibid., 72, 2744 (1980).

170. J. Yarwood, R. Ackroyd, K.E. Arnold, G. Doge and R. Arndt, Chem. Phys. Lett., 77 (1981).

171. A. Finch, P.N. Gates, K. Radcliffe, F.N. Dickson and F.F. Bentley, "Chemical Applications of Far Infrared Spectroscopy", Academic Press Inc., London (1970).

172. G.L. Carbon, R.E. Witkowski and W.G. Fateley, Spectrochemica. Acta., 22, 1117 (1966).

173. T. Ueda and T. Shimanouchi, J. Chem. Phys., 47, 402 (1967); ibid 47, 5018 (1967).

174. F.A. Miller, W.G. Fateley, R.E. Witkowski Spectrochemica. Acta., 23A, 891 (1967).

175. L. Potthast, D. Samois and T. Dorfmuller, Chem. Phys., 102, 147 (1986).

176. J. Michelson and J. Ketalaar, Mol. Phys., 24, 1181, (1972).

177. T.I. Cox and P.A. Madden, Mol. Phys., 39, 1487 (1980).

178. P.R. Griffith and H.W. Thompson, Proc. Roy. Soc., A298, 51 (1967).

179. C.J. Reid and J.K. Vij, J. Chem. Soc., Faraday Trans. II, 78, 1649 (1982).

180. H. Mori, Prog. Theoretical. Phys., 33, 423 (1965); ibid, 34, 399 (1966).

181. B. Catlow and J. Yarwood, J. Chem. Soc. Faraday Disc. II. 83, 1801 (1987).

182. R. Rodriguez and J.L. McHale, J. Chem. Phys., 88, 2264 (1988).

183. A. Gerschel, I. Darmon, C. Brot, Mol. Phys., 23, 317 (1972).

184. W. Schindler, P.T. Sharko and J. Jonas, J. Chem. Phys., 76, 3493 (1982).

185. W. Schindler, and J. Jonas, J. Chem. Phys., 72, 5019 (1980).

186. S.L. Wunder, Macromolecules 14, 1024 (1981).

187. P.T.T. Wong, S.F. Weng and H.H. Mantsch, J. Chem. Phys., 85, 2315 (1986)

188. P.T.T. Wong, T.E. Chagwedera and H.H. Mantsch, J. Chem. Phys., 87, 4487 (1987).

189. P.T.T. Wong, Annu. Rev. Biophys. Bioeng., 13, 1 (1984).

190. P.T.T. Wong, in "Vibrational Spectra and Structure", Vol. 16, pp.357-445, Ed. J.R. Durig, Elsevier, New York (1987).

191. R.G. Snyder, J.R. Scherer and B.P. Guber, Biochim. Biophys. Acta., 601, 47 (1980).

192. P.T.T. Wong, D.J. Siminovitch and H.H. Mantsch, Biochim. Biophys. Acta., 947, 139 (1988).

193. R.G. Snyder, H.L. Strauss and C.A. Ellinger, J. Phys. Chem., 86, 5145 (1982).

194. S. Abbate, S.L. Wunder and G. Zerbi, J. Phys. Chem., 88, 593 (1984).

195. F.L. Boerio and J.L. Koenig, J. Chem. Phys., 52, 3425 (1969).

196. S. Bratos, J. Chem. Phys., 63, 3499 (1975).

197. W.G. Rothschild, G.J. Rosaro and R.C. Livingstone, J. Chem. Phys., 62 2553 (1975).

198. J. Schroeder, V.H. Schiemann, P.T. Sharko and J. Jonas, J. Chem. Phys., 66, 3215 (1977).

199. B. Hartmann and Z.I. Slawsky, J. Chem. Phys., 47, 2491 (1967).

200. D.C.M. van Woerkom, J. de Bleijer, M. de Zwart and J.C. Leyte, Chem. Phys., 4, 236 (1974).

201. A. Khuen and G. Doge (personal communication).

202. A. Khuen, G. Doge and J. Yarwood, Mol. Phys, 52, 399 (1984).

203. G.C. Tabisz and R.M. Lynden-Bell, Chem. Phys. Letts., 46, 175 (1977).

204. K.F. Herzfeld and T.A. Litovitz, "Absorption and Dispersion of Ultrasonic Waves", Acedemic Press, New York (1959).

205. J. Schroeder, V.H. Schiemann and J. Jonas, Mol. Phys., 34, 1501 (1977).

206. R.M. Lynden-Bell and P.-O. Westlund, Mol. Phys., 61, 1541 (1987).

207. S.A. Rice and P. Gray, "Statistical Mechanics of Simple Liquids", Interscience, New York (1965).

208. T.A. Litovitz, J. Chem. Phys., 26, 469 (1957); W.M. Madigosks and T.A. Litovitz, J. Chem. Phys., 34, 489 (1961).

209. D. Steele, T.C. Jao and I. Scott, J. Mol. Spectrosc., 92, 1 (1982).

210. S.A. Adelman and J.M. Deutch, J. Chem. Phys., 59, 3971 (1973).

211. N. Meinder, M.M. Strube, A.N. Johnson and J. Laane, J. Chem. Phys., 86, 4762 (1982).

212. D.N.J. White and M.J. Bovill, J. Chem. Soc. Perkin II., 1610 (1977).

213. J.B. Hendrickson, D.J. Cram and G.S. Hammond, "Organic Chemistry", Third Ed., Pub. McGraw Hill Book Company (1970).

RAMAN ISOTROPIC AND ANISOTROPIC BANDS

In Raman scattering the three dimensional properties of the polarisability determine the magnitude of the induced dipole in all directions. The polarisability must be treated as a second rank tensor. To describe the induced dipole (P_i) three simultaneous equations may be written:-

$$P_x = E_x \alpha_{xx} + E_y \alpha_{xy} + E_z \alpha_{xz}$$

$$P_y = E_x \alpha_{yx} + E_y \alpha_{yy} + E_z \alpha_{yz}$$

$$P_z = E_x \alpha_{zx} + E_y \alpha_{zy} + E_z \alpha_{zz}$$

where α_{ij} relates the polarisation in the ith direction due to the field in the jth. The three equations may also be written in matrix form. The matrix involving the polarisabilities is known as the Raman tensor. It is symmetric in that $\alpha_{xy} = \alpha_{yx}$, $\alpha_{yz} = \alpha_{zy}$ etc. If a vibration is Raman active it will change one of the components of the polarisability tensor, the component which has the same symmetry as itself.

It can be shown[33] that the intensity of Raman lines depend on the derived polarisability tensor $\alpha' = (\delta\alpha/\delta Q)_e$. Each component of the polarisability tensor contributes to α' as $\alpha'_{ij} = [\delta\alpha_{ij}/\delta Q]$.

Observed scattering will be an average over all

orientations of the molecules. Two quantities are invariant under rotation: the mean value of the isotropic part of the derivative polarisability, the mean derivative polarisability $\bar{\alpha}'$; and the anisotropy $\gamma(\alpha)$, a measure of the deviation of the polarisability from a spherical shape.

$$\bar{\alpha}' = 1/3(\alpha'_{xx} + \alpha'_{yy} + \alpha'_{zz})$$

$$\gamma(\alpha) = 1/2 \ [(\alpha'_{xx} - \alpha'_{yy})^2 + (\alpha'_{yy} - \alpha'_{zz})^2 + (\alpha'_{zz} - \alpha'_{xx})^2 + 6(\alpha'^2_{xy} + \alpha'^2_{yz} + \alpha'^2_{zx})]$$

When the incident radiation is plane polarised and by averaging over all orientations of the molecule the mean value of the squares of all the derivative tensor elements can be expressed thus

$$\bar{\alpha}'^2_{ii} = \bar{\alpha}'^2_{xx} = \bar{\alpha}'^2_{yy} = \bar{\alpha}'^2_{zz} = 1/45 \ (45\bar{\alpha}'^2 + 4\gamma^2)$$

$$\bar{\alpha}'^2_{ij} = \bar{\alpha}'^2_{xy} = \bar{\alpha}'^2_{xz} = \bar{\alpha}'^2_{zy} = 1/15 \ (\gamma^2)$$

Observation of Raman light is normally made at 90° to the direction of propagation of the exciting beam. This scattering geometry is illustrated in Fig.A1.

In Fig.A1, I_z and I_x represent scattering originating from dipoles orientated in the same direction and 90° to the electric vector of the exciting beam E_z respectively. As I is proportional to $E^2.(\delta\alpha/\delta Q)^2_e$

$$I_z = k.E^2_z.\bar{\alpha}'^2_{zz} = (K/45).[45\bar{\alpha}'^2 + 4\gamma^2]$$

ii

$$I_x = k.E_z^2.\bar{\alpha}'^2_{xz} = (K/15)\gamma^2$$

where k and K are constants. From this the expression for the depolarisation ratio is

$$\frac{(K/15)\gamma^2}{(K/45).[45\bar{\alpha}'^2 + 4\gamma^2]} = \frac{3\gamma^2}{45\bar{\alpha}'^2 + 4\gamma^2}$$

Measurement of $I_z = I_{VV}$ and $I_x = I_{VH}$ allows separation of $\bar{\alpha}'^2$ and $4\gamma^2$. as

$$I_{VV} = K.\bar{\alpha}'^2 + K(4/45)\gamma^2$$

$$I_{VH} = (K/15)\gamma^2 = I_{anisotropic}$$

and therefore

$$I_{VV} = K\bar{\alpha}'^2 + 4/3.I_{VH}$$

$$K\bar{\alpha}'^2 = I_{VV} - 4/3.I_{VH} = I_{isotropic}$$
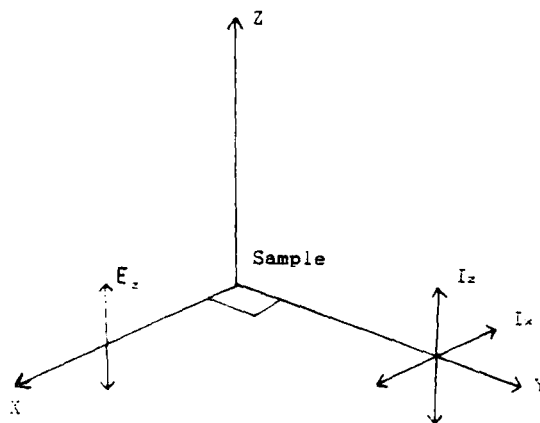
Figure A1. The Raman 90° scattering geometry

APPENDIX II

PUBLICATIONS

Parts of the work contained in this thesis have been report in the following publications:

1. *"Vibrational Spectroscopic Studies on Intermolecular Interactions of the Model Lubricant 2-Ethylhexyl Benzoate (EHB)."* A. Whitley, M.P. Dare-Edwards, D.J. Gardiner and J. Yarwood, in <u>Proc. XI ICORS, 5-9 September 1988, London.</u>, Pub. J. Wiley and Sons Ltd.

2. *"Infrared, Far Infrared and Raman Investigations of the Molecular Dynamics and Interactions of Non-Rigid Molecules in Liquids."* J. Yarwood, A. Whitley, D.J. Gardiner and M.P. Dare-Edwards, in <u>Proc. VI NATO Advanced Study Institute on Reactive and Flexible Molecules in Liquids, Nauplion, Greece, 23 September - 2 October, 1988.</u>, Pub. Kluwer Academic Publishers, the Netherlands.

3. *"Correlation of Viscometric and Molecular Dynamics Behaviour for the Model Lubricant, 2-Ethylhexyl Benzoate (EHB)."* A. Whitley, J. Yarwood and D.J. Gardiner, <u>Ber. Bunsenges. Phys. Chem.</u>, 94, 404 (1990).

4. *"High Pressure Infrared Studies on the Model Lubricant, 2-Ethylhexyl Benzoate (EHB)."* A. Whitley, J. Yarwood, D.J. Gardiner and M.P. Dare-Edwards, <u>J. Mol. Liquids.</u>, to be published (1990).

APPENDIX III

LECTURES, COLLOQUIA AND CONFERENCES

The Board of Studies in Chemistry requires that each postgraduate research thesis contain an appendix listing:

1. All research colloquia, research seminars and lectures arranged by the Department of Chemistry and the Chemical Society during the period of residence as a postgraduate student (* - indicates those Colloquia attended by the author)

2. All research conferences attended, and papers presented by the authors, during the period when the research for the thesis was carried out.

DURING THE PERIOD OCTOBER 1986 - SEPTEMBER 1987

* <u>ALLEN</u>, Prof. Sir G. (Unilever Research)   13th November 1986
     Biotechnology and the Future of the
     Chemical Industry

  <u>BARTSCH</u>, Dr. B. (University of Sussex)   6th May 1987
     Low Co-ordinated Phosphorus Compounds

* <u>BLACKBURN</u>, Dr. M. (University of Sheffield)   27th May 1987
     Phosphonates as Analogues of Biological
     Phosphate Esters

  <u>BORDWELL</u>, Prof. F.G.(Northeastern University,USA)   9th March 1987
     Carbon Anions, Radicals, Radical Anions and
     Radical Cations

* <u>CANNING</u>, Dr. N.D.S. (University of Durham)   26th November 1986
     Surface Adsorption Studies of Relevance to
     Heterogeneous Ammonia Synthesis

  <u>CANNON</u>, Dr. R.D. (University of East Anglia)   11th March 1987
     Electron Transfer in Polynuclear Complexes

  <u>CLEGG</u>, Dr. W. (University of Newcastle-upon-Tyne)   28th January 1987
     Carboxylate Complexes of Zinc;
     Charting a Structural Jungle

  <u>DÖPP</u>, Prof. D. (University of Duisburg)   5th November 1986
     Cyclo-additions and Cyclo-reversions
     Involving Captodative Alkenes

* <u>DORFMÜLLER</u>, Prof. T. (University of Bielefeld)   8th December 1986
     Rotational Dynamics in Liquids and Polymers

* <u>GOODGER</u>, Dr. E.M. (Cranfield Inst.Technology)   12th March 1987
     Alternative Fuels for Transport

* <u>GREENWOOD</u>, Prof. N.N. (University of Leeds)   16th October 1986
     Glorious Gaffes in Chemistry

  <u>HARMER</u>, Dr. M. (I.C.I. Chemicals & Polymer Group)   7th May 1987
     The Role of Organometallics in Advanced
     Materials

  <u>HUBBERSTEY</u>, Dr. P. (University of Nottingham)   5th February 1987
     Demonstration Lecture on Various Aspects of
     Alkali Metal Chemistry

  <u>HUDSON</u>, Prof. R.F. (University of Kent)   17th March 1987
     Aspects of Organophosphorus Chemistry

  <u>HUDSON</u>, Prof. R.F. (University of Kent)   18th March 1987
     Homolytic Rearrangements of Free Radical
     Stability

JARMAN, Dr. M. (Institute of Cancer Research)   19th February 1987
    The Design of Anti Cancer Drugs

KRESPAN, Dr. C. (E.I. Dupont de Nemours)   26th June 1987
    Nickel(O) and Iron(O) as Reagents in
    Organofluorine Chemistry

* KROTO, Prof. H.W. (University of Sussex)   23rd October 1986
    Chemistry in Stars, between Stars and in
    the Laboratory

LEY, Prof. S.V. (Imperial College)   5th March 1987
    Fact and Fantasy in Organic Synthesis

* MILLER, Dr. J. (Dupont Central Research, USA)   3rd December 1986
    Molecular Ferromagnets; Chemistry and
    Physical Properties

MILNE/CHRISTIE, Dr.A./Mr.S.(International Paints)   20th November 1986
    Chemical Serendipity: A Real Life Case Study

* NEWMAN, Dr. R. (University of Oxford)   4th March 1987
    Change and Decay: A Carbon-13 CP/MAS NMR
    Study of humification and Coalification
    Processes

* OTTEWILL, Prof. R.H. (University of Bristol)   22nd January 1987
    Colloid Science a Challenging Subject

PASYNKIEWICZ, Prof. S. (Technical Univ.,Warsaw)   11th May 1987
    Thermal Decomposition of Methyl Copper and
    its Reactions with Trialkylaluminium

ROBERTS, Prof. S.M. (University of Exeter)   24th June 1987
    Synthesis of Novel Antiviral Agents

RODGERS, Dr. P.J. (I.C.I. Billingham)   12th February 1987
    Industrial Polymers from Bacteria

SCROWSTON, Dr. R.M. (University of Hull)   6th November 1986
    From Myth and Magic to Modern Medicine

SHEPHERD, Dr. T. (University of Durham)   11th February 1987
    Pteridine Natural Products; Synthesis and
    Use in Chemotherapy

* THOMSON, Prof. A. (University of East Anglia)   4th February 1987
    Metalloproteins and Magneto-optics

* WILLIAMS, Prof. R.L. (Metropolitan Police   27th November 1987
                        Forensic Science)
    Science and Crime

WONG, Prof.E.H. (University of New Hampshire,USA)   29th October 1986
    Coordination Chemistry of P-O-P Ligands

WONG, Prof.E.H. (University of New Hampshire,USA)   17th February 1987
    Symmetrical Shapes from Molecules to Art and Nature

DURING THE PERIOD OCTOBER 1987 - SEPTEMBER 1988

BAILEY, Dr. P.D. (University of York)   November 1987
 Oncogenes

* BIRCHALL, Prof. D. (I.C.I. Advanced Materials) 25th April 1988
 Environment Chemistry of Aluminium

* BORER, Dr. K. (University of Durham Industrial
       Research Laboratories) 18th February 1988
 The Brighton Bomb - (A Forensic Science View)

BOSSONS, L. (Durham Chemistry Teachers' Centre) 16th March 1988
 GCSE Practical Assessment

* BUTLER, Dr. A.R. (University of St.Andrews) 5th November 1987
 Chinese Alchemy

* CAIRNS-SMITH, Dr. A. (Glasgow University) 28th January 1988
 Clay Minerals and the Origin of Life

DAVIDSON, Dr. J. (Herriot-Watt University) November 1987
 Metal Promoted Oligomerisation Reactions
 of Alkynes

GRAHAM, Prof. W.A.G. (University of Alberta,
         Canada) 3rd March 1988
 Rhodium and Iridium Complexes in the
 Activation of Carbon-Hydrogen Bonds

* GRAY, Prof. G.W. (University of Hull) 22nd October 1987
 Liquid Crystals and their Applications

* HARTSHORN, Prof. M.P. (University of Canterbury,
         New Zealand) 7th April 1988
 Aspects of Ipso-Nitration

* HOWARD, Dr. J. (I.C.I. Wilton) 3rd December 1987
 Chemistry of Non-Equilibrium Processes

JONES, Dr. M.E. (Durham Chemistry Teachers'
       Centre) 29th June 1988
 GCSE Chemistry Post-mortem

JONES, Dr. M.E. (Durham Chemistry Teachers'
       Centre) 6th July 1988
 GCE Chemistry A-Level Post-mortem

KOCH, Prof. H.F. (Ithaca College, U.S.A.) 7th March 1988
 Does the E2 Mechanism Occur in Solution ?

LACEY, Mr. (Durham Chemistry Teacher's Centre) 9th February 1988
 Double Award Science

* LUDMAN, Dr. C.J. (Durham University) 10th December 1987
 Explosives

McDONALD, Dr. W.A. (I.C.I. Wilton) 11th May 1988
 Liquid Crystal Polymers

viii

MAJORAL, Prof. J.-P. (Université Paul Sabatier)   8th June 1988
    Stabilisation by Complexation of Short-Lived
    Phosphorus Species

MAPLETOFT, Mrs. M. (Durham Chemistry Teachers'
                             Centre)   4th November 1987
    Salters' Chemistry

NIETO DE CASTRO, Prof. C.A. (University of Lisbon
                      and Imperial College) 18th April 1988
    Transport Properties of Non-Polar Fluids

* OLAH, Prof. G.A. (University of Southern
                  California)   29th June 1988
    New Aspects of Hydrocarbon Chemistry

* PALMER, Dr. F. (University of Nottingham)   21st January 1988
    Luminescence (Demonstration Lecture)

* PINES, Prof. A. (University of California,
              Berkeley, U.S.A.)   28th April 1988
    Some Magnetic Moments

RICHARDSON, Dr. R. (University of Bristol)   27th April 1988
    X-Ray Diffraction from Spread Monolayers

ROBERTS, Mrs. E. (SATRO Officer for Sunderland)   13th April 1988
    Talk - Durham Chemistry Teachers' Centre -
        "Links between Industry and Schools"

ROBINSON, Dr. J.A. (University of Southampton)   27th April 1988
    Aspects of Antibiotic Biosynthesis

* ROSE, van Mrs. S. (Geological Museum)   29th October 1987
    Chemistry of Volcanoes

* SAMMES, Prof. P.G. (Smith, Kline and French)   19th December 1987
    Chemical Aspects of Drug Development

SEEBACH, Prof. D. (E.T.H. Zurich)   12th November 1987
    From Synthetic Methods to Mechanistic Insight

SODEAU, Dr. J. (University of East Anglia)   11th May 1988
    Durham Chemistry Teachers's Centre: "Spray
    Cans, Smog and Society"

SWART, Mr. R.M. (I.C.I.)   16th December 1987
    The Interaction of Chemicals with
    Lipid Bilayers

TURNER, Prof. J.J. (University of Nottingham)   11th February 1988
    Catching Organometallic Intermediates

UNDERHILL, Prof. A. (University of Bangor)   25th February 1988
    Molecular Electronics

WILLIAMS, Dr. D.H. (University of Cambridge)   26th November 1987
    Molecular Recognition

WINTER, Dr. M.J. (University of Sheffield)   15th October 1987
    Pyrotechnics (Demonstration Lecture)

DURING THE PERIOD OCTOBER 1988 - SEPTEMBER 1989

ASHMAN, Mr. A. (Durham Chemistry Teachers'
                              Centre)   3rd May 1989
    The Chemical Aspects of the National
    Curriculum

* AVEYARD, Dr. R. (University of Hull)   15th March 1989
    Surfactants at your Surface

AYLETT, Prof. B.J. (Queen Mary College, London)   16th February 1989
    Silicon-Based Chips: The Chemists Contribution

BALDWIN, Prof. J.E. (Oxford University)   9th February 1989
    Recent Advances in the Bioorganic Chemistry
    of Penicillin Biosynthesis

* BALDWIN & WALKER, Drs. R.R. and R.W.
                 (Hull University)   24th November 1988
    Combustion: Some Burning Problems

BOLLEN, Mr. F. (Durham Chemistry Teachers'
                           Centre)   18th October 1988
    Lecture about the use of SATIS in
    the classroom

* BUTLER, Dr. A.R. (St. Andrews University)   15th February 1989
    Cancer in Linxiam: The Chemical Dimension

* CADOGAN, Prof. J.I.G., (British Petroleum)   10th November 1988
    From Pure Science to Profit

CASEY, Dr. M. (University of Salford)   20th April 1989
    Sulphoxides in Stereoselective Synthesis

WALTERS & CRESSEY, Mr. D. and T.
        (Durham Chemistry Teachers' Centre)   1st February 1989
    GCSA Chemistry 1988: "A Coroner's Report"

* CRICH, Dr. D. (University College London)   27th April 1989
    Some Novel Uses of Free Radicals
    in Organic Synthesis

* DINGWALL, Dr. J. (Ciba Geigy)   18th October 1988
    Phosphorus-containing Amino Acids:
    Biologically Active Natural and
    Unnatural Products

ERRINGTON, Dr. R.J. (University of Newcastle-
                       upon-Tyne)   1st March 1989
    Polymetalate Assembly in Organic Solvents

* FREY, Dr. J. (Southampton University)   11th May 1989
    Spectroscopy of the Reaction Path:
    Photodissociation Raman Spectra of NOCl

* HALL, Prof. L.D. (Addenbrooke's Hospital,
                     Cambridge)   2nd February 1989
    NMR - A Window to the Human Body

x

HARDGROVE, Dr. G. (St. Olaf College, U.S.A.)   December 1988
    Polymers in the Physical Chemistry Laboratory

HARWOOD, Dr. L. (Oxford University)   25th January 1988
    Synthetic Approaches to Phorbols Via
    Intramolecular Furan Diels-Alder Reactions:
    Chemistry under Pressure

* JÄGER, Dr. C. (Friedrich-Schiller University GDR)   9th December 1988
    NMR Investigations of Fast Ion Conductors
    of the NASICOM Type

JENNINGS, Prof. R.R. (Warwick University)   26th January 1989
    Chemistry of the Masses

* JOHNSON, Dr. B.F.G. (Cambridge University)   23rd February 1989
    The Binary Carbonyls

JONES, Dr. M.E. (Durham Chemistry Teachers'
                           Centre)   14th June 1989
    Discussion Session on the National
    Curriculum

JONES, Dr. M.E. (Durham Chemistry Teachers'
                           Centre)   28th June 1989
    GCSE and A Level Chemistry 1989

LUDMAN, Dr. C.J. (Durham University)   18th October 1988
    The Energetics of Explosives

* MACDOUGALL, Dr. G. (Edinburgh University)   22nd February 1989
    Vibrational Spectroscopy of Model
    Catalytic Systems

MARKO, Dr. I. (Sheffield University)   9th March 1989
    Catalytic Asymmetric Osmylation of Olefins

McLAUCHLAN, Dr. K.A. (University of Oxford)   16th November 1988
    The Effect of Magnetic Fields on
    Chemical Reactions

MOODY, Dr. C.J. (Imperial College)   17th May 1989
    Reactive Intermediates in Heterocyclic
    Synthesis

* MORTIMER, Dr. C. (Durham Chemistry Teachers'
                           Centre)   14th December 1989
    The Hindenberg Disaster - an Excuse
    for Some Experiments

* NICHOLLS, Dr. D. (Durham Chemistry Teachers'
                           Centre)   11th July 1989
    Demo: "Liquid Air"

PAETZOLD, Prof. P. (Aachen)   23rd May 1989
    Iminoboranes $XB\equiv NR$: Inorganic Acetylenes ?

PAGE, Dr. P.C.B. (University of Liverpool)   3rd May 1989
    Stereocontrol of Organic Reactions Using
    1,3-dithiane-1-oxides

* <u>POLA</u>, Prof. J. (Czechoslovak Academy of Sciences)   15th June 1989
        Carbon Dioxide Laser Induced Chemical
        Reactions - New Pathways in Gas-Phase Chemistry

  <u>REES</u>, Prof. C.W. (Imperial College London)   27th October 1988
        Some Very Heterocyclic Compounds

  <u>REVELL</u>, Mr. P. (Durham Chemistry Teachers'
                                        Centre)   14th March 1989
        Implementing Broad and Balanced
        Science 11-16

  <u>SCHMUTZLER</u>, Prof. R. (Technische Universitat
                                        Braunschweig)   6th October 1988
        Fluorophosphines Revisited - New
        Contributions to an Old Theme

  <u>SCHROCK</u>, Prof. R.R. (M.I.T.)   13th February 1989
        Recent Advances in Living Metathesis

  <u>SINGH</u>, Dr. G. (Teeside Polytechnic)   9th November 1988
        Towards Third Generation Anti-Leukaemics

* <u>SNAITH</u>, Dr. R. (Cambridge University)   1st December 1988
        Egyptian Mummies: What, Where, Why and How ?

  <u>STIBR</u>, Dr. R. (Czechoslovak Academy of Sciences)   16th May 1989
        Recent Developments in the Chemistry of
        Intermediate-Sited Carboranes

* <u>VON RAGUE SCHLEYER</u>, Prof. P. (Universitat Erlangen
                                        Nurnberg)   21st October 1988
        The Fruitful Interplay Between
        Calculational and Experimental Chemistry

  <u>WELLS</u>, Prof. P.B. (Hull University)   10th May, 1989
        Catalyst Characterisation and Activity

III.2 Research Conferences Attended by the Author During the Period October 1986 - September 1989.

1. R.S.C. Graduate Symposium, Durham, 27th March, 1987.

2. R.S.C. Faraday Division, General Discussion No.85, "Solvation", Durham, 28-30 March, 1988. A poster was presented entitled "*Vibrational Spectroscopic Studies of the Model Lubricant 2-Ethylhexyl Benzoate*".

3. R.S.C. Graduate Symposium, Durham, 19 April, 1988.

4. R.S.C. XI International Conference on "Raman Spectroscopy", London, 5-9 September, 1988. An abstract was contributed along with a poster entitled "*Vibrational Spectroscopic Studies on Intermolecular Interactions of the Model Lubricant 2-Ethylhexyl Benzoate (EHB)*".

5. NATO-Advanced Studies Institute, VI Annual EMLG Conference on "Reactive and Flexible Molecules in Liquids", Nauplia, Greece, 23 September - 2 October, 1988. A poster was presented entitled "*Vibrational Spectroscopic Studies on Intermolecular Interactions of the Model Lubricant 2-Ethylhexyl Benzoate (EHB)*".

6. Conference on "Functional Fluids", Durham, 12-14 December, 1988.

7. R.S.C. Graduate Symposium, Durham, 12 April, 1989.

8. Shell Research U.K.-meeting of Shell sponsored postgraduates and supervisors, 14-16 September, 1989. A lecture was given entitled "*Vibrational Spectroscopic Studies of the Model Lubricant 2-Ethylhexyl Benzoate*".